

**STUDIES ON SYNTHESIS AND CHARACTERIZATION OF $MnFe_2O_4$
NANOPARTICLES AND THEIR HYPERTHERMIA THERAPY
APPLICATION**

A THESIS SUBMITTED TO

D. Y. PATIL EDUCATION SOCIETY, KOLHAPUR

**Deemed to be University
(Declared u/s 3 of the UGC Act. 1956)**



FOR THE DEGREE OF

**DOCTOR OF PHILOSOPHY IN
CHEMISTRY**

**UNDER THE FACULTY OF INTERDISCIPLINARY STUDIES
BY**

Mrs. PRITI R. GHUTEPATIL
M. Sc.

UNDER THE GUIDANCE OF

Prof. (Dr). S. H. PAWAR Emeritus Scientist (CSIR)
M.Sc. Ph.D., F.I.C.C., F.M.A.Sc.

DISTINGUISHED PROFESSOR
D. Y. PATIL EDUCATION SOCIETY, KOLHAPUR – 416 006 (M.S.) INDIA
AND

DIRECTOR, CENTRE FOR INNOVATIVE AND APPLIED RESEARCH,
ANEKANT EDUCATION SOCIETY, BARAMATI – 413 102 (M.S.) INDIA

CENTRE FOR INTERDISCIPLINARY RESEARCH
D.Y. PATIL EDUCATION SOCIETY,
KOLHAPUR – 416 006 (M.S.), INDIA.

MAY 2019

DECLARATION

I hereby declare that the work presented in this thesis entitled, “**Studies on Synthesis and Characterization of MnFe₂O₄ Nanoparticles and Their Hyperthermia Therapy Application**” is entirely original and was carried out by me independently in the D. Y. Patil Education Society (Deemed to be university), Kolhapur under the supervision of Prof. (Dr.) S. H. Pawar, Emeritus Scientist (CSIR) and Distinguished Professor, D. Y. Patil Education Society, Kolhapur. I further declare that it has not formed the basis for the award of any degree, diploma, fellowship or similar title of any Universities or Institution.

Place: Kolhapur

Date: 16-05-2019

Research Student


Mrs. Priti Ghutepatil

Centre for Interdisciplinary Research
D. Y. Patil Education Society
Kolhapur – 416 006, (M.S.) India

CERTIFICATE

This is to certify that the thesis entitled “STUDIES ON SYNTHESIS AND CHARACTERIZATION OF $MnFe_2O_4$ NANOPARTICLES AND THEIR HYPERTHERMIA THERAPY APPLICATION” which is being submitted herewith for the degree of Doctor of Philosophy in Chemistry to D. Y. Patil Education Society, Kolhapur is the result of original work completed by **Mrs. Priti Ghutepatil** under my supervision and guidance. Neither this thesis nor any part of it has been submitted elsewhere for any degree or diploma of any other academic award anywhere before.

Place: Kolhapur

Date: 16-05-2019

Research Guide


16-05-2019

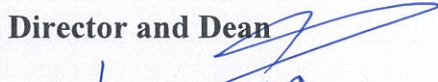
Prof. (Dr.) S. H. PAWAR

Emeritus Scientist (CSIR) &
Distinguished Professor,
D. Y. Patil Education Society,
Kolhapur – 416 006 (M.S.) India.

And

Director,
Centre for Innovative and Applied Research,
Anekant Education Society,
Baramati – 413 102 (M.S.) India.

Research Director and Dean


16/05/2019

Centre for Interdisciplinary Research,
D. Y. Patil Education Society,
Kolhapur-416 006 (M.S.) India.

ACKNOWLEDGEMENT

I wish to express my deep sense of gratitude and profound thanks to my supervisor Prof. Dr. S. H. Pawar, Emeritus Scientist (CISR) and Distinguished Professor, D. Y. Patil Education Society, Kolhapur and Director, Center for Innovative and Applied Research, Anekant Education Society, Baramati for his invaluable guidance, constant encouragement, inspiring and thought provoking discussions throughout my Ph. D. program. I have been able to learn a great deal from him and consider my association with him as a rewarding experience. I greatly appreciate the freedom my supervisor gave me and the opportunity to pursue my research in my own way.

Besides my guide, I would like to acknowledge to Dr. Mrs. Shimpa Sharma Vice Chancellor and Dr. Prakash B. Behere, Ex-Vice Chancellor, D.Y.Patil Education Society, Kolhapur for their encouragement and support.

I also express my gratitude to Prof. Dr. Chandrakant D. Lokhande, Research Director and Dean, D. Y. Patil Education Society, Kolhapur and Principal, Dr. Chandrashekhar Murumkar, T. C. College, Baramati for their guidance, constant encouragement, inspiring and thought provoking discussion throughout my Ph.D. program.

I acknowledge Dr. Vishwanath V. Bhosale, Registrar and Mr. Sham P. Kole, Finance Officer of D. Y. Patil Education Society, Kolhapur and other staff members who have helped me directly or indirectly during my research work.

There is nothing better than encouragement from good friends. My special words of thanks should also go to my friends Dr. Ashwini Salunkhe, Dr. Vishwjeet Khot, Dr. Arpita Tiwari, Ms. Priyanka Patil, Dr. Jagruti Meshram, Mr. Abhinandan Patil, Mr. Nayeem Mulla and Mr. Deepak Sawant, who were always there for me and without them my research work would have been impossible to imagine.

I take this opportunity to convey my hearty admiration to all my teachers from my school days to post graduation level.

I would like to thank my friends and well wishers for their moral support and motivation, which drives me to give my best.

I am grateful to my husband Anant, daughter Aarna and other family members for their constant support, cheering for success, immense patience, unconditional infinite love and belief in my aptitude which have made me to achieve my goal. I sincerely apologize to those who I have failed to mention and thank them.

Finally, I dedicate my entire work and thesis to my beloved late father and mother.



Mrs. Priti Ghutepatil

TABLE OF CONTENTS

Chapter 1

Introduction

Page no.

1.1	Introduction	1
1.2	Nanoparticles	2
1.3	Magnetic nanoparticles	3
1.3.1	Types of magnetic nanoparticles	4
1.3.1.1	Metallic	4
1.3.1.2	Ferrites	5
1.3.1.3	Types of Ferrites	6
1.4	Manganese ferrite (MnFe_2O_4): An example of spinel ferrites	7
1.5	Biomedical applications of MNPs	11
1.5.1	Drug delivery	12
1.5.2	Cell separation	16
1.5.3	Magnetic resonance imaging	16
1.5.4	Magnetic hyperthermia in cancer treatment	19
1.6	Problem statement	24
	References	27-32

Chapter 2

Surface Functionalization of MNPs for Biomedical Applications (Theoretical Background)

2.1	Introduction	33
2.2	Need of surface functionalization	35
2.2.1	Stabilization against aggregation	36
2.2.2	Steric stabilization	36
2.2.3	Electrostatic stabilization	37
2.2.4	Colloidal stability	38
2.2.5	Particle size and distribution	39

2.2.6	Magnetic controllability	39
2.2.7	Biocompatibility	39
2.3	Surface functionalization methods	40
2.3.1	One-step surface functionalization	40
2.3.2	Two-step surface functionalization	41
2.4	Surface functionalization strategies of MNPs	41
2.4.1	Ligand addition	41
2.4.2	Ligand exchange	42
2.4.3	Encapsulation	43
2.5	Materials used for functionalization of MNPs	44
2.5.1	Polymers	45
2.5.1.1	Polyvinylpyrrolidone (PVP)	46
2.5.1.2	Dextran	46
2.5.1.3	Acrypol	47
2.5.1.4	Polyvinyl Alcohol (PVA)	48
2.5.1.5	Polyethylene glycol (PEG)	48
2.5.1.6	Chitosan	49
2.5.2	Monomers	49
2.5.2.1	Phosphates	49
2.5.2.2	Carboxylates	50
2.5.3	Small molecules	50
2.5.3.1	Amines and aminosilanes	50
2.5.3.2	Thiols	51
2.5.4	Inorganic materials	51
2.5.4.1	Gold	51
2.5.4.2	Silica	51
2.5.4.3	Metal oxides or sulphides	52
2.6	Functionalization of MNPs with biological molecules	52
2.7	Tabular representation of materials used for functionalization	54
	References	57-66

Chapter 3

Experimental and Characterization Techniques

3.1	Introduction	67
3.2	Synthesis of magnetic nanoparticles	67
3.3	Characterization techniques	68
3.3.1	X-ray diffraction technique (XRD)	69
3.3.2	Fourier transform infrared spectroscopy (FTIR)	71
3.3.3	Thermogravimetric analysis (TGA)	73
3.3.4	Scanning electron microscopy (SEM)	75
3.3.5	Transmission electron microscopy (TEM)	78
3.3.6	Vibrating sample magnetometer (VSM)	79
3.3.7	Dynamic light scattering (DLS)	82
3.3.8	Induction heating system	83
3.3.9	Biocompatibility study:Cytotoxicity assay	86
	References	88-91

Chapter 4

Synthesis and Characterization of MnFe₂O₄ Nanoparticles

4.1	Introduction	92
4.2	Synthesis methods of MNPs	92
4.3	Chemical methods	93
4.3.1.1	Co-precipitation method	94
4.3.1.2	Polyol method	95
4.3.1.3	Hydrothermal method	97
4.3.1.4	Combustion method	98
4.3.1.5	Sol-Gel method	99
4.3.1.6	Microemulsion method	100
4.3.1.7	Thermal decomposition method	101
4.4	Experimental	102
4.4.1	Synthesis of MnFe ₂ O ₄ nanoparticles by polyol method	102

4.4.2	Characterization of MnFe ₂ O ₄ nanoparticles	104
4.5	Results and discussion	104
4.5.1	Structural analysis	104
4.5.2	Microstructural analysis	106
4.5.3	Chemical bonding study	108
4.5.4	Magnetization study	109
4.5.5	Thermogravimetric analysis	110
4.5.6	Colloidal stability study	111
4.6	Conclusions	112
	References	113-117

Chapter 5

Studies on Functionalization of MnFe₂O₄ Nanoparticles with APTES

5.1	Introduction	118
5.2	Experimental	119
5.2.1	Synthesis of APTES coated MnFe ₂ O ₄ nanoparticles	119
5.2.2	Characterization	121
5.3	Results and discussion	122
5.3.1	Structural analysis	122
5.3.2	Microstructural analysis	123
5.3.3	Chemical bonding study	125
5.3.4	Magnetization study	126
5.3.5	Thermogravimetric analysis	127
5.3.6	Colloidal stability study	128
5.4	Conclusions	129
	References	131-134

Chapter 6

Magnetic hyperthermia study of APTES Functionalized MnFe₂O₄ Nanoparticles

6.1	Introduction	135
6.2	Magnetic hyperthermia of MNPs	135
6.3	Magnetic induction heating	137
6.3.1	Mechanism of magnetic induction heating	138
6.3.2	Heat dissipation processes by MNPs	138
6.3.3	Specific absorption rate	143
6.4	Experimental	144
6.5	Results and discussion	145
6.5.1	Hyperthermia properties of MnFe ₂ O ₄ nanoparticles	145
6.5.2	Hyperthermia properties of APTES functionalized MnFe ₂ O ₄ nanoparticles	148
6.6	Conclusions	153
	References	154-156

Chapter 7

In Situ Surface Functionalization of MnFe₂O₄ Nanoparticles and Their Potential Application in Cancer Hyperthermia Therapy

7.1	Introduction	157
7.2	Experimental	159
7.2.1	Synthesis of EDA functionalized MnFe ₂ O ₄ nanoparticles	159
7.2.2	Synthesis of PVP functionalized MnFe ₂ O ₄ nanoparticles	161
7.2.3	Characterization	163
7.3	Results and discussion	164
7.3.1	Role of ethylenediamine	164
7.3.2	Role of PVP	165
7.3.3	Structural analysis	168
7.3.4	Microstructural analysis	169

7.3.5	Chemical bonding study	172
7.3.6	Magnetization study	174
7.3.7	Thermogravimetric analysis	176
7.3.8	Hyperthermia properties	178
7.3.9	Potential of MnFe ₂ O ₄ nanoparticles in cancer therapy	183
7.4	Conclusions	184
	References	186-187

Chapter 8

Biocompatibility Study of Functionalized MnFe₂O₄ Nanoparticles

8.1	Introduction	188
8.2	Experimental	188
8.2.1	Selection and procurement of cell culture	188
8.2.2	The MTT assay experimental procedure	189
8.3	Results and Discussion	189
8.3.1	Choice of cell type	189
8.3.2	Choice of cytotoxicity assay	190
8.3.3	Physicochemical properties of nanoparticles	191
8.3.4	<i>In vitro</i> cytotoxicity study of bare MnFe ₂ O ₄ nanoparticles	191
8.3.5	<i>In vitro</i> cytotoxicity study of APTES functionalized MnFe ₂ O ₄ nanoparticles	194
8.3.6	<i>In vitro</i> cytotoxicity study of EDA functionalized MnFe ₂ O ₄ nanoparticles	196
8.3.7	<i>In vitro</i> cytotoxicity study of PVP functionalized MnFe ₂ O ₄ nanoparticles	198
8.4	Mechanisms of cytotoxicity of nanoparticles	199
8.6	Conclusions	201
	References	203-204

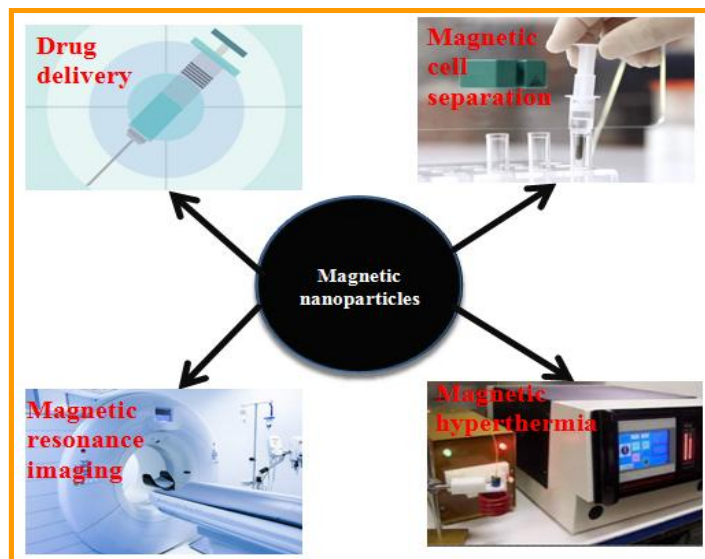
Chapter 9

Summary and Conclusions

9.1	Introduction	205
9.2	Competent components of the thesis	206
9.3	Summary of thesis	208
9.4	Major conclusions	210
9.5	Future scope of the thesis	211

Curriculum Vitae

Introduction



Nanotechnology in medicine is going to have a major impact on the survival of the human race.

-Bernard Marcus

1.1 Introduction

Nanotechnology is nothing but depiction, characterization, manufacturing of structure and systems by fabricating size and configuration at nano-scale. In general term, the study and implementation of immensely very small objects is called nanotechnology. It can be used in several science areas such as chemistry, biology, physics and engineering. Recently discovered revolutionary technology of 21st century is nanotechnology and it already became a commonly used buzzword in everyday life and various fields of science. It is difficult to conceptualize that how much small-scale nanotechnology is. If we try to calculate the size of 1 nanometer then it will be a billionth of 100 cm or 10^{-9} of 100 cm. For e.g. an inch can have 25400000 nanometers. The size of Pin's head is approximately 1 millimeter, which is equal to 1000000 nanometers. Thickness of human hair is 100000 nanometers [1-4].

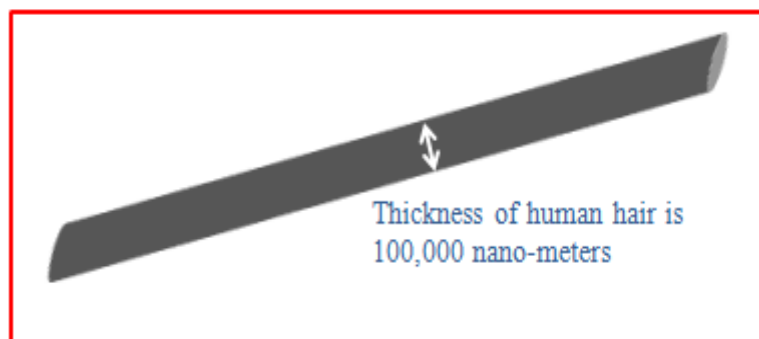


Fig. 1.1 Nanometer

The lecture entitled "There's Plenty of Room at the Bottom" by an American scientist R. Feynman started concept about nanotechnology in 1959 [5, 6]. Norio Taniguchi was a Japanese scientist and he was first to use the nanotechnology word or term in a 1974 conference to explain semiconductor processes. According to him, nanotechnology as mainly consists of the processing of separation, consolidation and deformation of materials by one atom or one molecule [7]. The physicist K. Eric Drexler had conceptually explored the nanotechnology and nanoscale technology in depth in 1980 decade [8].

1.2 Nanoparticles



Fig. 1.2 Structure of nanoparticles [9]

The term nanoparticle is a combined name for both nanospheres and nanocapsules. It can be categorized according to their size and diameters. In recent decade, an interest in nanomaterials is increased in various fields due to their well definite properties. Nanoparticles (NPs) are anticipated to have outspread of implementations in several areas like electronics as well as biological systems. These implementations are based on factors like their physical properties, smaller size with large surface area which offers feasibility for fabrication and scope for multiple functionalities [10-13].

In quasi-zero-dimensional (0D), all the 3 dimensions are in nano scale range. The quasi-zero-dimensional nanomaterials can be contained nanocluster materials and nanodispersions. The nanoparticles isolate from each other. In quasi-one-dimensional (1D), any 1 dimension out of 3 dimensions is in nanoscale range and quasi-one-dimensional are nanotubular and nanofiber materials with fibre like rod or tube and length ranging from 99-110 nm to 10s of microns. In quasi-two-dimensional (2D),

any 2 dimensions out of 3 dimensions are in nano scale range and these nanomaterials are films with nm thickness. Quasi-three-dimensional (3D) can be formed by arrangement of multiple 0D, 1D or 2D materials forming 3D structure. These materials contain powders, multilayer and polycrystalline materials. Interfaces can be formed by contacting each other by these 0D, 1D and 2D structural elements [14, 15].

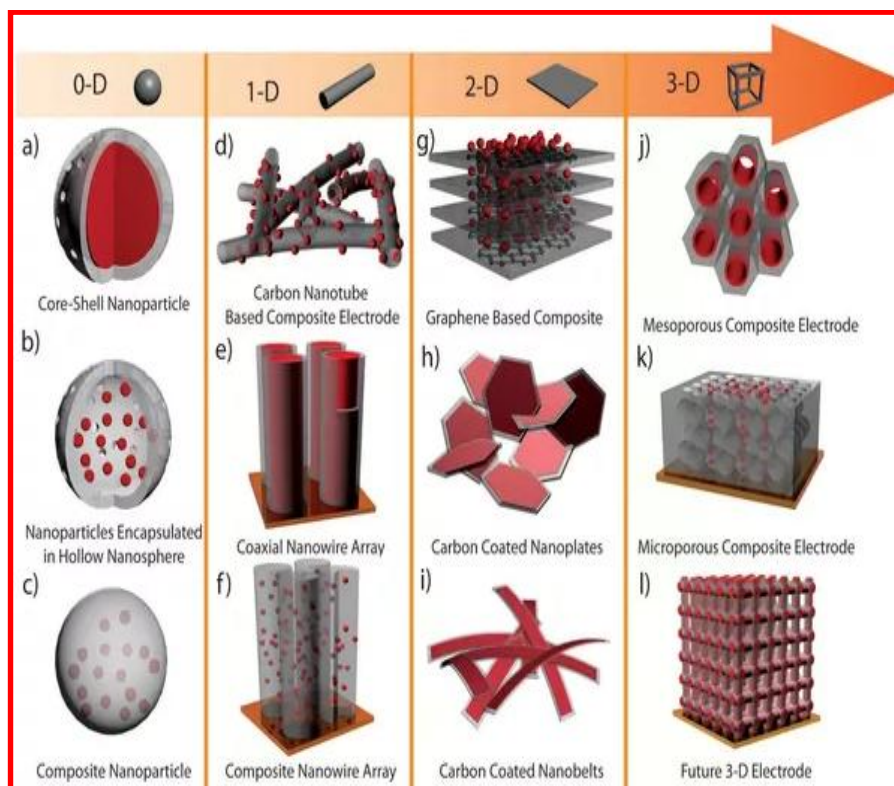


Fig. 1.3 Nanoparticle's classification [16]

1.3 Magnetic nanoparticles

Magnetic nanoparticles (MNPs) have become highly attractive to biomedical applications because they possess excellent chemical and physical properties. Biomedical research field enormously benefited from advancement of nanotechnology. The MNPs are encouraging material for biomedical applications/implementations like drug delivery, magnetofection, cell separation, tissue repairing, magnetic resonance imaging, magnetic fluid hyperthermia (MFH), and tracking agent vectors for gene therapy among different nonmaterial [17-22]. Due

to this, MNPs are most challenging exploration in nanomagnetism. Over the years, spinel ferrites have exhibited captivating properties and these are used in outspread applicatons. These ferrite nanoparticles have been to the forefront of nanoscience and nanotechnology because of their magnificent properties. Ferrite is compound made by iron oxide and one or more additional metallic elements having ferrimagnetic properties. There are 3 types of ferrites namely hexagonal, garnet and spinel ferrites. The formula of hexagonal ferrites is $MFe_{12}O_{19}$ and these are rhombohedral or hexagonal oxides. These ferrites have high coercivity and widely used magnets. The general formula of garnet is $M_3Fe_5O_{12}$ having complex crystallite structure with cubic shape [23]. Spinel ferrites are also called as cubic ferrits and they are used eveywhere. The electrical resistivity of some spinel ferrites is high and eddy current losses are low, which make them appropriate for their usage at microwave frequencies [24].

MNPs can be engineered by applying exterior magnetic field. Magnetic anisotropy and magnetization of nanoscale magnetic particles could be greater than the bulk material. Magnetic properties of materials can be influenced by various factors. The chemical composition, size of particle, shape, morphology and interaction between nanoparticles are main factors among them [25]. One of main advantages of MNPs is that they have controllable sizes and dimensions can be smaller in size as compare to cell (9-99 μm), protein (4-49 nm) or virus (19-451 nm). The foremost characteristics of MNPs that make them appropriate selection for biomedical applications are biocompatibility and highest-level aggregation in wanted tissue. These particles should be sufficient to sustain biological circulation and small in scale [26].

1.3.1 Types of magnetic nanoparticles

The MNPs can be mainly categorized into four types i.e. ferrites, metallic, ferrites with a shell and metallic with a shell.

1.3.1.1 Metallic

Metallic nanoparticles are formed of iron, nickel or cobalt. Metallic nanoparticles are normally protected by layer like gold or silica. Colloid formation is very challenging in case of metallic particles. Metallic nanoparticles may be favorable for some technical applications due to their higher magnetic moment but often ignored for biological applications/implementation because of chemical instability [27]. Metallic nanoparticles required complex synthesis process but still the research on them continues because of their distinctive advantages. The main disadvantage of metallic nanoparticles is that they are reactive to oxidizing agents to several degrees and makes their handling inflexible. Metallic nanoparticles are less appropriate for biomedical applications as they allow unwanted side reactions [28].

The reactivity of the MNPs can be improved by coating a layer of different coating materials onto their surface. The shell of coating material can be easily modified with various surface functional groups. The FePt and FeCo are the examples of such nanoparticles. These nanoparticles are superparamagnetic in nature and which makes them potential contrast agent for MRI or carriers for drug delivery [29].

Metallic with a shell

The surfactants, gentle oxidation, polymers and metals can be used to make metallic core of MNPs passivity. The important feature of these nanoparticles is that they exchange bias effect when 2 magnetic stages come in close proximity. This effect is caused by exchange of coupling over the interface between metallic core as well as shell. Extra source anisotropy can be provided by exchange coupling, which leads to magnetization stabilization [30]. The main advantages of these nanoparticles are that they have higher magnetization, higher stability in acidic and organic solutions.

1.3.1.2 Ferrites

Iron oxide nanoparticles are composed of iron oxide particles with diameters between about 1-100 nm. Ferrite nanoparticles are largely investigated nanoparticles

because of their biocompatibility and simplicity of synthesis. Ferrite nanoparticles normally composed of nano-crystalline magnetite i.e. Fe_3O_4 either maghemite i.e. $\gamma\text{-Fe}_2\text{O}_3$ and possess a spinel crystal structure. In spinels, 32-oxygen atom and cations (24) configures unit cell. The 6-octahedral and 8-tetrahedral sites are held by cations total of 32-octahedral and 64-tetrahedral sites. The extensive scope of magnetic properties is achieved based on various cations holding on crystal positions [31, 32]. Metal ferrites can be tailored with a composition of MFe_2O_4 , where the M is Mn, Fe, Co or Ni value is (+2) cation of by various methods to fine-tune particular magnetic properties. Ferrite particles show their magnetic behavior after applying an exterior magnetic field. Superparamagnetic behavior of nanoparticles prevents self agglomeration. Normally, ferrite particles exhibit superparamagnetic property once they become smaller in size and it averts self aggregation as they show magnetic behavior only after applying exterior magnetic-field [33, 34]. The surfactants like silica, phosphoric or silicones are used to fabricate the surface of ferrite nanoparticles, which increases their stability in aqueous solution [35, 36].

1.3.1.3 Types of ferrites

Ferrites can be normally classified into soft and hard ferrites. Soft ferrites have low-coercivity. It means that magnetization of materials can effortlessly get into opposite directions without dissipating much energy and this is called as hysteresis losses. High resistivity averts eddy current in core. Manganese-zinc-ferrite and Nickel-zinc-ferrite are the examples of soft ferrites. Hard ferrites have high-coercivity and it means ferrites are immune to behaving for demagnetization. These are also called as ceramic magnets because of their high quality of being magnetic permeable. Cobalt ferrite and Strontium ferrite are two examples of hard ferrites.

Ferrite with a shell

The reactivity of the MNPs can be improved by coating a layer of different coating materials onto their surface. The shell of coating material can be easily

modified with various surface functional groups. The binding of amine surfactants and carboxylate can be achieved by surface chemistry and it is used to upgrade aqueous solubility of nanoparticles. In compare to other metallic particles, greater chemical stability can occur because of interactions between two chemical categories. FePt and FeCo are the examples of such nanoparticles. These nanoparticles can show superparamagnetism, which make them potential material for biomedical implementations.

1.4 Manganese ferrite (MnFe_2O_4): An example of spinel ferrites

Spinel ferrites are the most widely used and investigated ferrites. In recent years, research on ferrites (spinel) has been increased owing to their potential in various fields especially in biomedical field. Spinel ferrites are being employed in many biological applications because of their magnetic and electrical properties [37]. Magnetic properties can be engineered according to need of application and it can be modified by several ways. Properties of spinel ferrite can be controlled by pH, stirring time and speed, fuel and preparative parameters used [38]. Another name for spinel ferrites is cubic ferrites as structure of spinel ferrites is closely packed with cubic.

The general formula of spinel ferrites is $\text{Me}^{\text{II}}\text{Fe}_2^{\text{III}}\text{O}_4$, in which, Me^{II} is metal cation like Mn, Co, Fe, Cu, Cd, Mg, which are divalent and Fe^{III} represents iron cation, which are trivalent. The extensive differences in electrical, structural and magnetic properties are because of cations of non-identical valence. Spinel structure is a member of $\text{Fd}3\text{m}$ space group. The constituents of unit cell (cubic) is configured by 56-atoms, out of these 32-oxygen anions, which are scattered in close loaded structure and 24-cations holding 8-tetrahedral sites of available 64-tetrahedral sites and 16-octahedral sites of available 32-octahedral sites. Spinel compound is represented in general formula is as follows:



where, i represents inversion parameter.

Cation distribution can decide whether spinel is inverse, partially inverse or normal. In normal spinel, tetrahedral sites are located by 8-bivalent cations and octahedral sites located by 16-trivalent cations. ZnFe_2O_4 and CdFe_2O_4 are two examples of normal spinel ferrites. In inverse spinel, 8-bivalent cations hold 8-octahedral sites and 16-trivalent cations are scattered between 8-tetrahedral and 8-octahedral sites. MnFe_2O_4 , NiFe_2O_4 and CoFe_2O_4 are 3 examples of inverse spinel ferrites. The value of i is equal to 0 for normal spinel and i is equal to 1 for inverse ferrite. For partially inverted ferrite, the value of i is greater than 0 or less than 1. CuFe_2O_4 and MgFe_2O_4 are two examples of partially inverted ferrite [39-41].

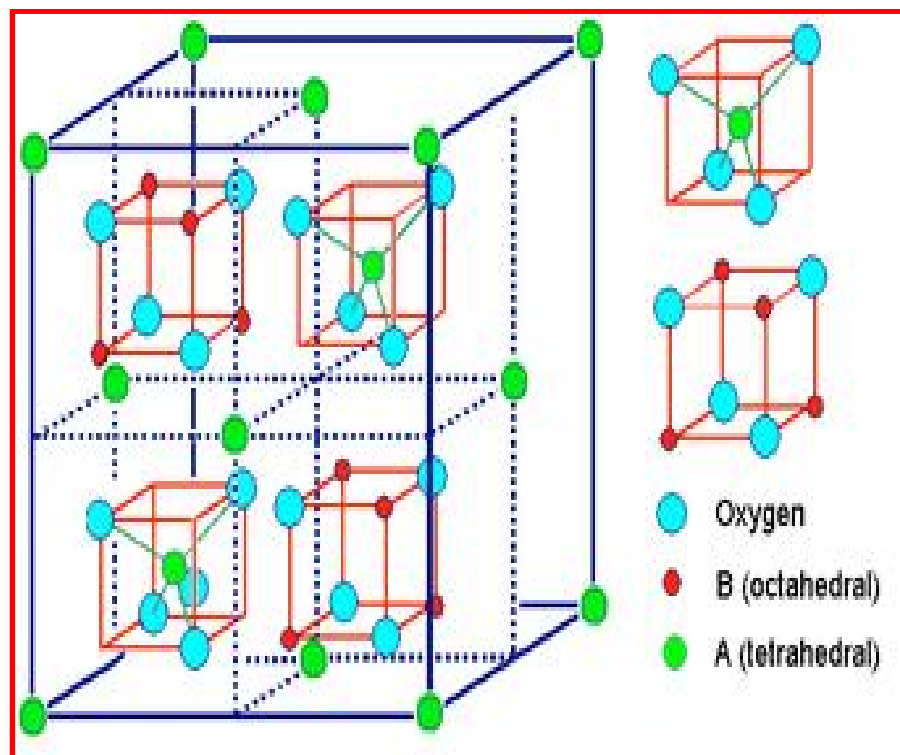


Fig. 1.4 Structure of MFe_2O_4 [42]

Manganese ferrite (MnFe_2O_4) is foremost representative of the spinel ferrite family and it has received great attention of the researchers because of its remarkable properties like coercivity, superparamagnetism, modest saturation magnetization, good mechanical hardness and chemical stability. Manganese ferrite has received great attention because of these properties and it has been widely used in the

several biomedical applications. The properties of manganese ferrite can be controlled by composition, morphology and size of nanoparticles. Among spinel ferrites, manganese ferrite has been foremost due to its highest magnetization, which qualifies them for many biomedical applications.

The type of MnFe_2O_4 is partially inverse spinel and which is having majority of Mn^{2+} ions. In MnFe_2O_4 , ions are situated at tetrahedral site and 20% out of them are situated at octahedral site. The resistivity of MnFe_2O_4 is very less than the resistivity of CoFe_2O_4 and NiFe_2O_4 . The magnetic moment of MnFe_2O_4 is consistent with the Neel coupling scheme [43, 44]. The MnFe_2O_4 prepared at highest temperatures ($> 1,173 \text{ K}$), 20% of the Mn^{2+} ions transfer from the A to B-sites. It means MnFe_2O_4 is a mixture of inverse and normal spinel ferrite. Saturation magnetization of bulk MnFe_2O_4 is 80 emu/g and an anisotropy constant K having value of $2.5 \times 10^3 \text{ J/m}^3$ at room temperature (RT) [45, 46].

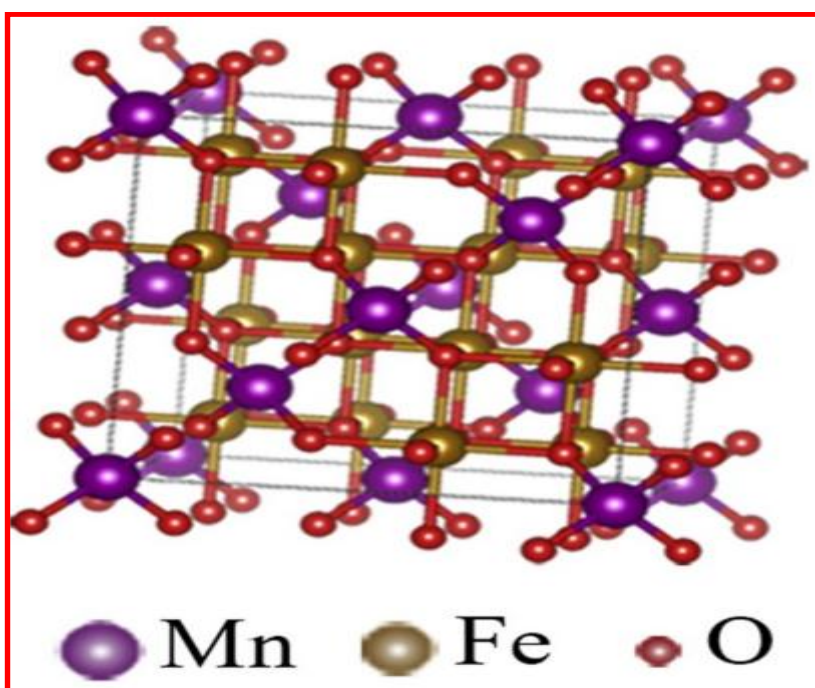


Fig. 1.5 MnFe_2O_4 ferrite structure [47]

A better comprehension of fundamental properties especially the superparamagnetism of MnFe_2O_4 nanoparticles is crucial for biomedical implementations. When E_A i.e. anisotropy energy of MNPs is conquering thermally then superparamagnetism of MNPs occurs [48]. This energy can be expressed by Stoner and Wohlfarth equation (1.2)

$$E_A = KV \sin^2 \theta \dots \dots 1.2$$

where, θ represents easy axis and angle between magnetization of nanoparticles, K is constant for anisotropy energy and V represents volume of nanoparticles.

For temperature above T_B , thermal activation threshold is represented by blocking temperature T_b and is utilized as manifestation for transition to superparamagnetic state. Magnetic moment of every nanoparticle differs quickly with unfavored orientation and clustering of MNPs act as a common paramagnetic material. Past decade, magnetocrystalline anisotropy (K) and effects of size upon magnetic properties is described and crystalline anisotropy contributes to magnetic properties of MNPs. Change in magnetic properties and magnetic anisotropy nanoparticles can be contributed by interparticle interactions of MNPs. Interactions arises in MNPs may take place from dipole dipole interactions as well as exchange interactions arising between the magnetic ions. The increased spacing between nanoparticles can outcome into negligible exchange interaction when capping surfactant like oleic acid is utilized [49-51]. The key interactions are examined from dipole dipole coupling and energy related to their interactions (E_{d-d}) can be expressed as in equation (1.3).

$$E_{d-d} = \frac{-(\mu_0 m_0^2)}{(4\pi l^3)} \dots \dots 1.3$$

where, μ_0 represents permeability, m_0 represents magnetic moment and l presents separation of particles.

1.5 Biomedical applications of MNPs

In recent year, use of MNPs for biomedical applications has been increased tremendously. Research and advances in nanotechnology allow manufacturing of MNPs of specific morphology, their surface modification and manipulation of properties of MNPs for aimed biomedical applications/implementations. MNPs have been explored with great interest due to their intrinsic characteristics to use them in biomedical implementations like as magnetic cell separation, drug delivery, as contrast agent for MRI and magnetic fluid hyperthermia [52-56].

The MNPs have fabricable sizes ranging from few nm (nanometers) to tens of nm (nanometers) and MNPs are magnetic in nature so they can be engineered by applying exterior magnetic field. In 1950, Gilchrist and et al had used MNPs for biomedical application. They had injected metallic particles to treat lymphatic nodes and metastases and then heated using magnetic field [57]. Magnetic fields interact infirmly with biological molecules and easily pierce into body so they are favorable for remote simulation. Electrical methods are challenging to analyze compound networks in human as electrical fields are greatly attenuated by tissues. MNPs can be functionalized using biocompatible surfactants such as APTES, EDA, chitosan, starch, polyethyleneamine, polyethylen oxide, dextran and polyethylene glycol, PVP to utilize them for biomedical implementations. The perfect surface fabrication can be used to intensify water affinity of MNPs in biological fluid and make MNPs biocompatible. Here, fundamental concepts of MNPs and their uses in biomedical applications have been discussed [58, 59].

The nanoparticles should be biocompatible before using them for biomedical applications. *In vitro*, MNPs application can bear less rigorous toxicological properties where as *in vivo* usage of MNPs requires rigorous exploration of kinetic and toxicology of MNPs. *In vitro*, incubation times, various cell lines and colorimetric assays used to perform the cytotoxicity study of MNPs. Cytotoxicity study includes broad range of MNPs concentrations and exposure time, this makes hard to determine that cytotoxicity noticed is physiologically not relevant or relevant [60-62].

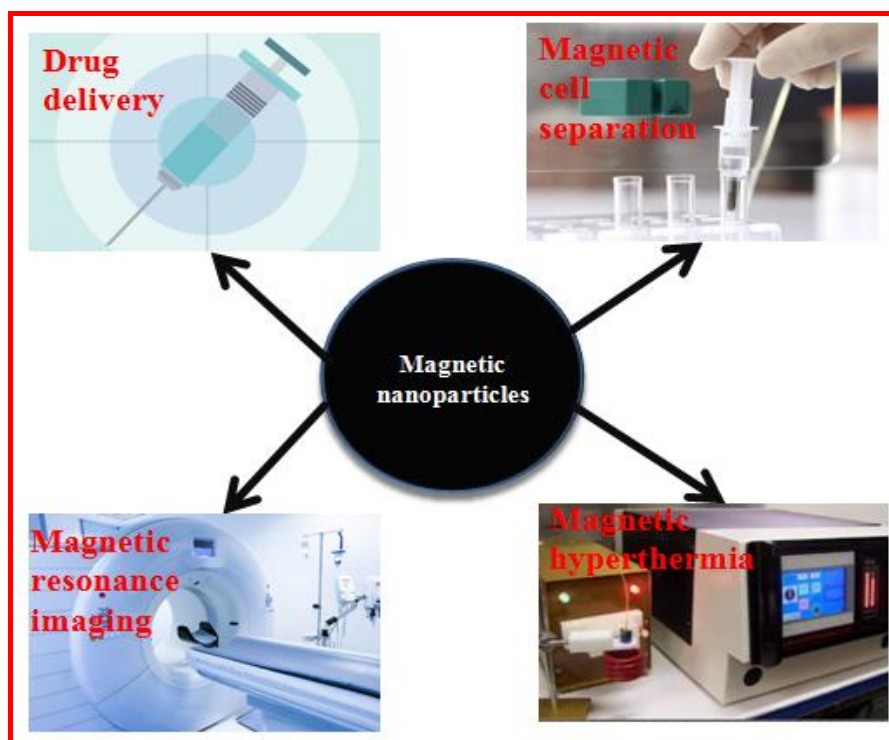


Fig. 1.6 Biomedical application of MNPs

1.5.1 Drug delivery

The therapeutic effects are accomplished in human or animals by administering pharmaceutical compound in drug delivery system (DDS). Many scientists and researchers have provided attention towards the drug delivery area as the important shortcoming of pharmaceutical and biomedical industries is to deliver medicine fluid to its therapeutic action site [63]. Drug delivery optimizes a drug's therapeutic index by localizing its pharmacological activity to organ and this is important distinction from classic targeting systems. A physical, biological and molecular system with high-rise concentrations of the active drug at the physiologically applicable organ is a basic principle for targeted drug delivery. Result of targeting would be remarkable reduction in dose of drug, toxicity and increment in treatment efficacy in case of successful drug delivery [64].

In 1960, Freeman et al. advanced a concept that MNPs can be delivered into a vascular system at specific point into body with help of magnetic field. In delivery

system, bio triggered drug is merged with carrier so that drug is freed in pre-decided modus at persistent rate in cyclic approach. Carrier must be non toxic and should be produced on industrial scale. The most of chemotherapeutic agents provide potential unwanted effects on healthy cells or tissues. The drug delivery system employs attraction of MNPs carrier to an exterior magnetic field to increase site particular delivery to overcome this issue [65].

The contention between forces deployed on nanoparticles by blood bay and magnetic forces produced from applied field are used for drug localization in magnetic delivery system. MNPs are reserved at the target site when magnetic forces overreach the blood flow rates arteries (10 cms^{-1}) or capillaries (0.05 cms^{-1}). The MNPs support the transfer through the capillaries system of site and tissues by avoiding vessel embolism [66]. Fig. 1.7 shows schematic representation of magnetic transport of drugs to a particular region.

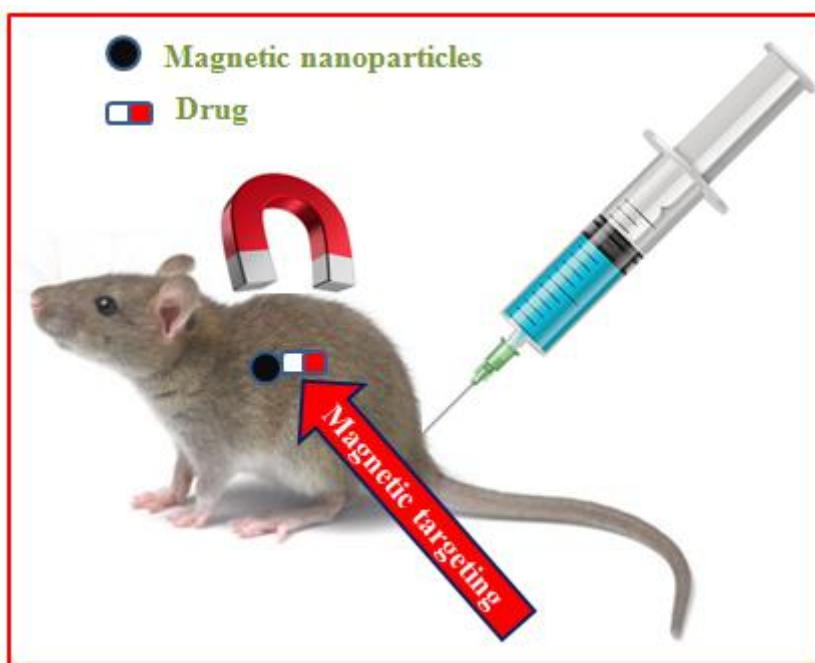


Fig. 1.7 Representation of magnetic driven transport of drugs to particular region

In targeted drug delivery mechanism, cytotoxic drug can be linked to carrier such as biocompatible MNPs. These drug and carrier tangled in ferrofluid form,

which is then injected into affected site or tissue via circulatory system. An exterior high risen magnetic field is utilized to concentrate tangled ferrofluid at particular target part within body when particles enter the bloodstream. Enzymatic activity in physiological conditions is used to release drugs. Liposomes, polymeric micelles or nanoparticle drug carriers can be useful for drug carriers or vehicles in targeted drug delivery system [67]. The main advantages of targeted drug delivery are that it improve efficacy and reduces the side effects.

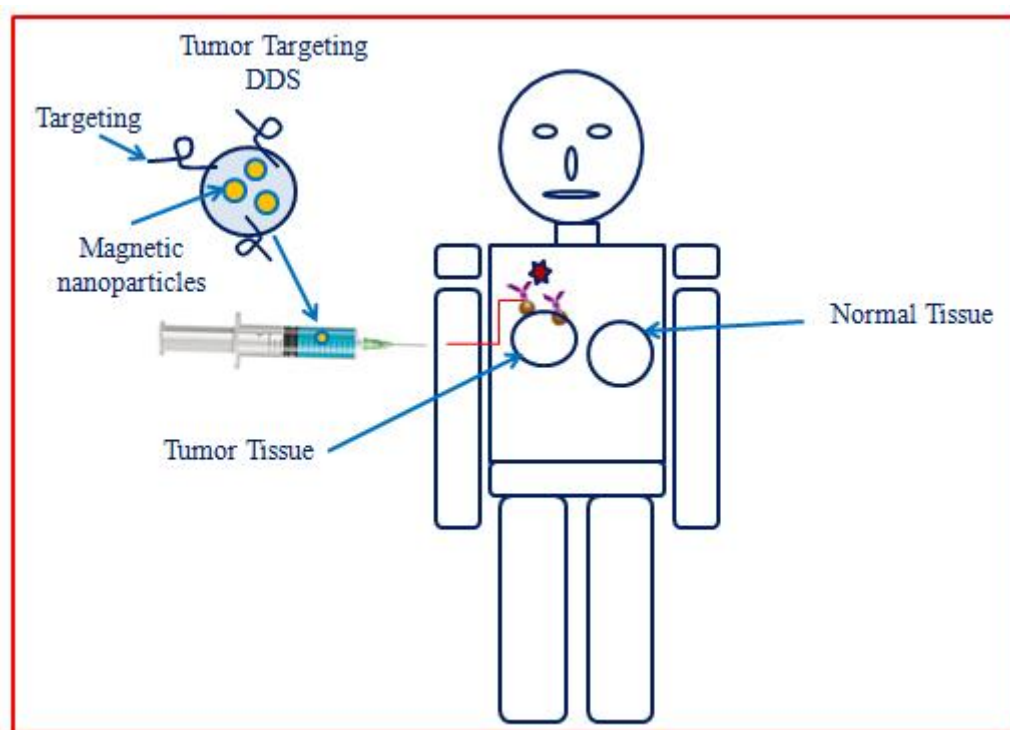


Fig. 1.8 Mechanism of targeted drug delivery system

There are mainly two approaches of drug targeting i.e. passive targeting and active targeting. The potential of nanoparticles to concentrate in affected tissues or areas is accomplished through either one or both target approach.

Passive targeting

Passive targeting utilizes neutral course of bio-distribution of the carrier. Passive targeting makes a use of anatomical deviation between diseased and normal

cells or tissues to dispatch drugs to certain cell or tissue. The injected nanoparticles can assemble more in tumor cells or tissues than normal tissues or cells because of leaky tumor vasculature [69].

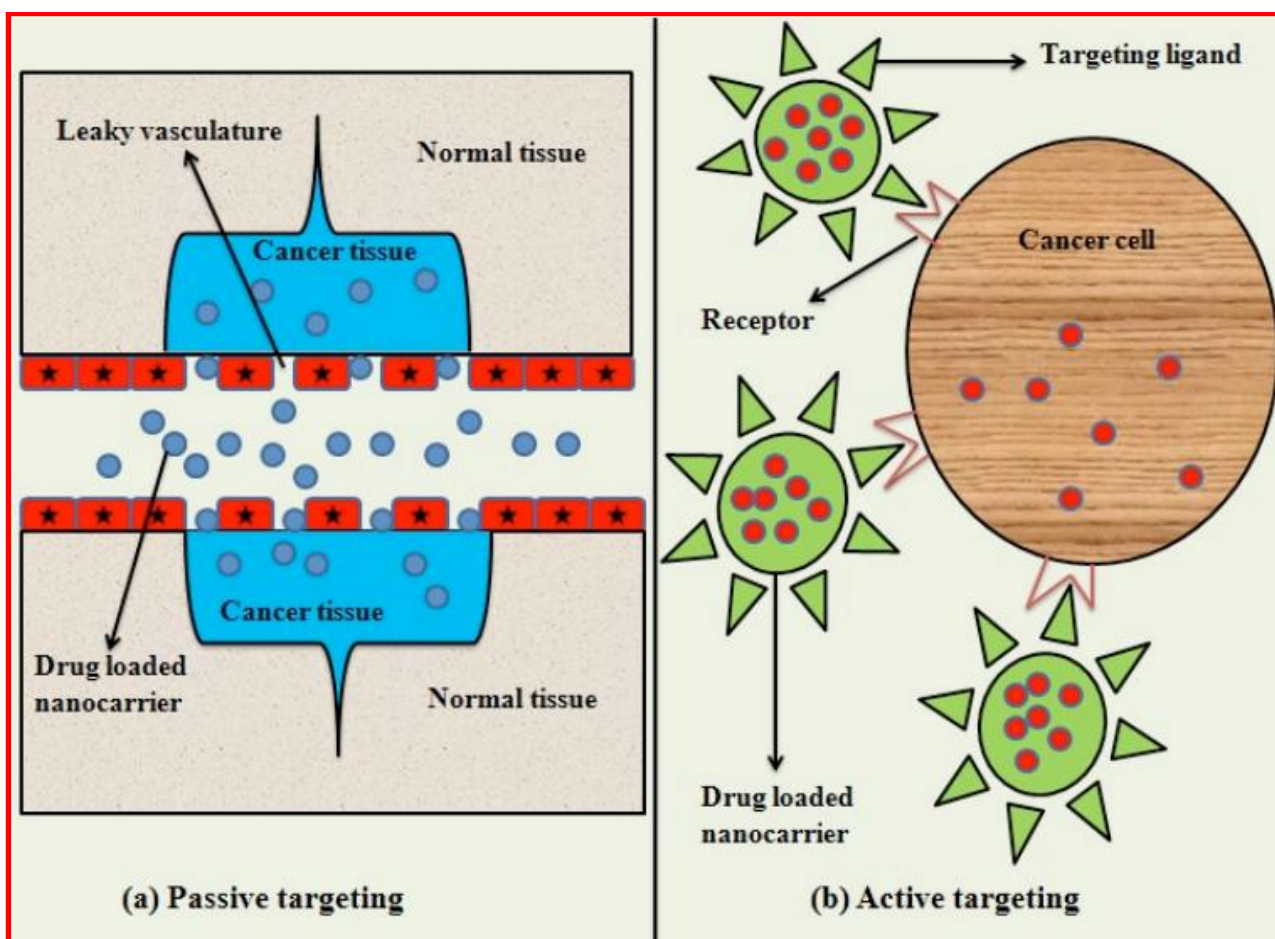


Fig. 1.9 Drug targeting approaches: (A) Passive targeting, (B) Active targeting [68]

Active targeting

Active targeting involves the functionalization or modification of drug carriers so that content can be delivered exclusively to targeted site. Active targeting needs a combination of two molecule ligands that advances targeting to certain site. The selection of targeting moiety is key factor for the success of drug targeting. Active targeting is achieved by identification of the diseased tissues by several signature

molecules over expressed at diseased site. It can be accomplished by targeting diseased tissue to know the nature of receptor on the cell to target the drug [70, 71].

1.5.2 Cell separation

In cell separation, MNPs are used to label the cells, which could be detected by MRI. There are two common approaches of cell labeling. First is attaching the MNPs to cell surface and second is internalizing biocompatible MNPs by receptor mediated endocytosis or phagocytosis. Particular and efficient cell labeling of MNPs can be done by altering the nanoparticles surface with ligand. Functionalized MNPs strongly bind to receptor of surface in such a way that phagocytosis is inhibited [72-74].

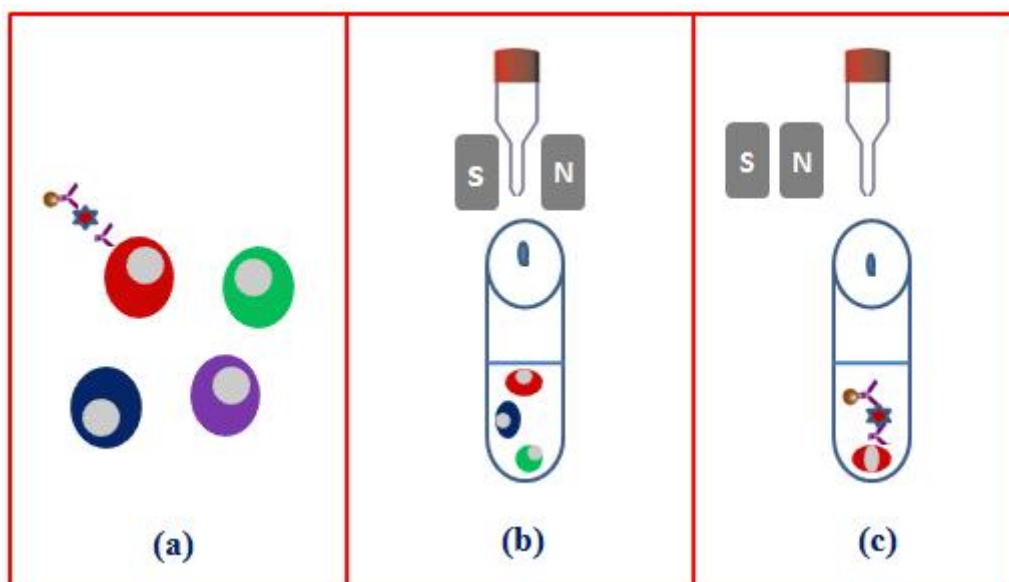


Fig. 1.10 Magnetic cell separation process (a) cell labeling (b) cell separation (c) elution of labeled cells

1.5.3 Magnetic resonance imaging

Any disease can be cured easily only when a disease is diagnosed more accurately as early as possible. There are many modalities available to diagnose a various diseases but still many types of diseases require strenuous effort to diagnose. Magnetic resonance imaging (MRI) is one to most effective technique to diagnose the

disease more accurately at early state. Magnetic resonance imaging technique is based on directional magnetic moment and charged particles in motion associated with it. MNPs have contrast imaging effect, which is used to differentiate between pathogenic targets and normal tissues via magnetic resonance imaging [75].

In 1970s decade, the scientists Peter Mansfield and Paul Lauterbur had developed EPI (echo planar imaging) like MRI approach. After 10 years, first commercial scanning of human body had been performed. Now days, MRI has become one of the most crucial and high powered diagnostic tools in medical field. In 2003, Mansfield and Lauterbur were awarded by Nobel Prize (medicine) for their research and detection concerning MRI [76].

The imaging technique utilize strong magnetic fields to range the relating to nucleus of cell. Many free hydrogen nuclei range themselves with magnetic field direction after placing human body in strong magnetic field. The technique related with nuclei precess of magnetic field direction is like a device consisting of a wheel or gyroscopes and this is called as Larmor precession. From which ‘Frequency of Larmor precession’ (ω) is defined by equation (1.1) and it is directly proportional to the strength of applied magnetic field [77].

$$\omega_o = \gamma B_o \dots \dots 1.1$$

where, B_o is the strength of applied magnetic field and γ is gyromagnetic ratio and it is nuclei specific constant. In case of hydrogen, the value of γ is 42.6 MHz/Tesla. Fig. 1.11(b) shows nuclei of hydrogen atom aligned in applied magnetic field direction.

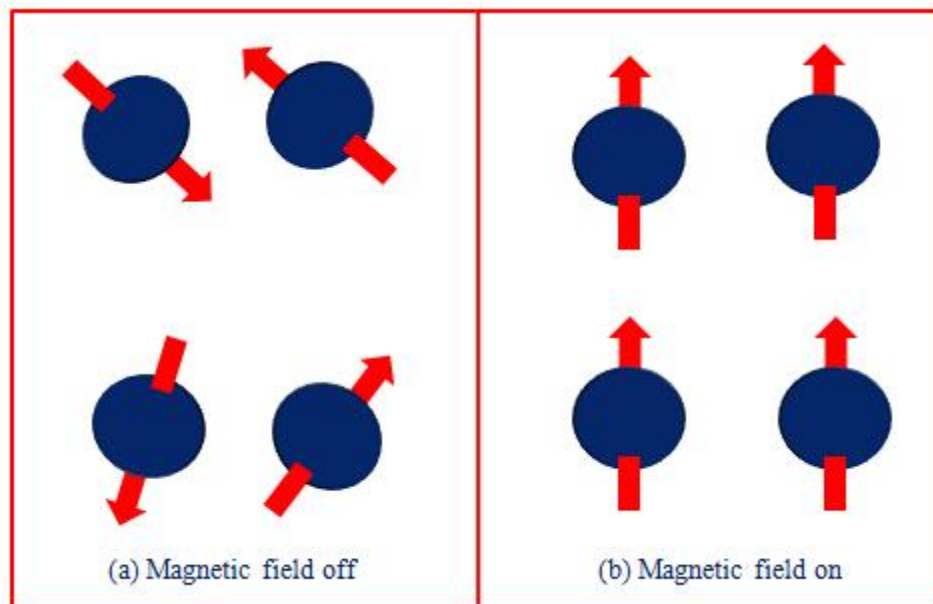


Fig. 1.11 Hydrogen nuclei (a) magnetic field is absent (b) magnetic field is present

Fig.1.12 (a) shows a RF (radio frequency) applied perpendicular to magnetic field (B_0), which causes nuclei tilt away from B_0 . The nuclei returns to equilibrium when radio frequency (RF) pulse get stopped (Fig.1.12 (b)). Measurable RF signal and nuclei lose energy during realignment as shown in Fig.1.12 (c). This is referred as FID i.e. free induction decay response signal.

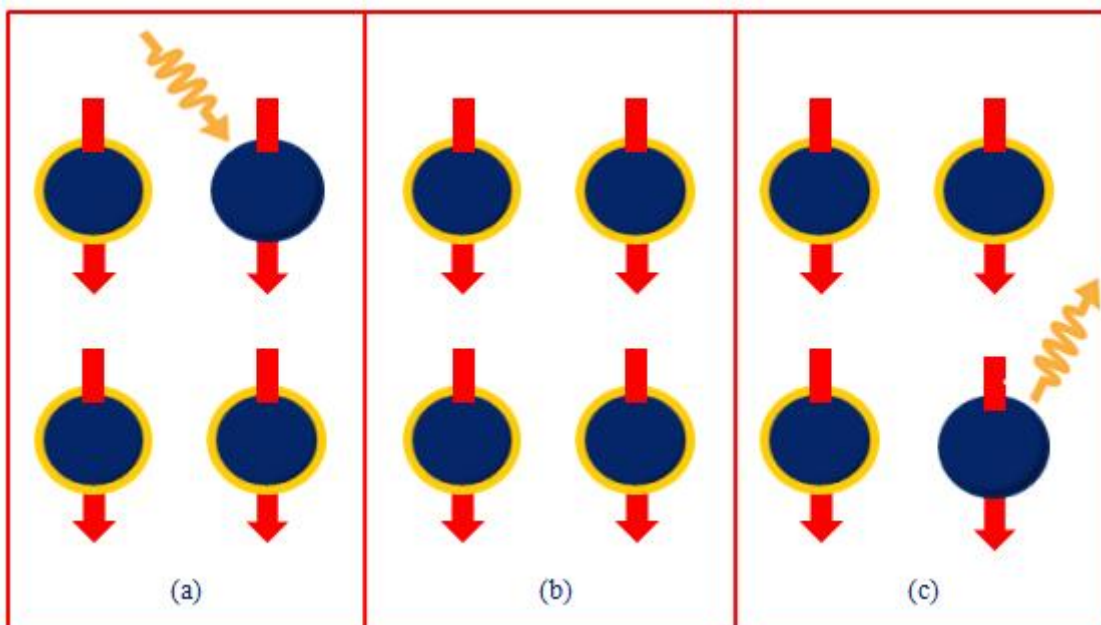


Fig.1.12 (a) Radio frequency applied perpendicularly to magnetic field (b) Radio frequency pulse stopped (c) Realignment

The nuclei reversed to their initial relax state and which is measured by its longitudinal relaxation (T_1) or transverse relaxation (T_2). This is being used to generate magnetic resonance imaging. In T_1 images, the signal are enhanced by Gd based contrast agents, where as iron oxide MNPs gives powerful contrast outcome in T_2 weighted images. It is because of several contrasting methods. The r_2 and r_1 represents transverse and longitudinal relaxation rate/mmol respectively. The higher value of r_2/r_1 ratio guides to good T_2 contrast efficacy [78-80].

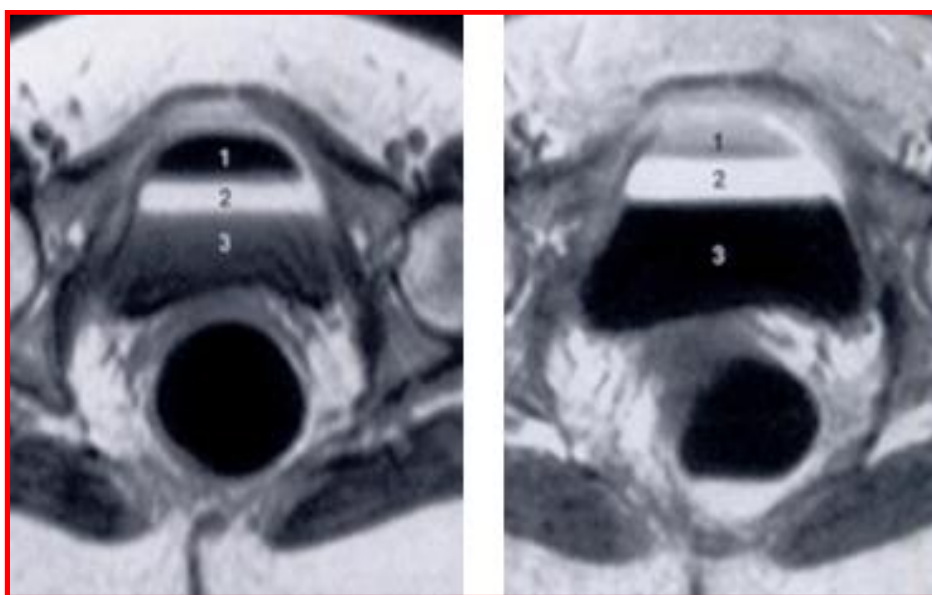


Fig. 1.13 T_1 and T_2 weighted MRI comparison [81]

1.5.4 Magnetic hyperthermia in cancer treatment

There are many therapies available for cancer treatment but some are costly and some have side effects. Hyperthermia therapy is most encouraging therapy for cancer treatment. The concept of applying heat to treat certain condition or tumor is not a new, it has long history. In ancient history, Greeks, Romans and Indians used to apply a heat to treat various tumors. In 1988, Westermark intentionally used

hyperthermia to treat cancer with temperature of 42 to 44 °C. In 1950s decade, hyperthermia therapy using magnetic field and nanoparticles has been started. There are 2 types of heating treatments renowned i.e. hyperthermia and thermoablation. Hyperthermia therapy can be performed between 41 to 46 °C, where as thermoablation can be performed between 46 to 56 °C to destruct the tumors. In thermal therapy, the applied heat should be appropriate and should be applied to correct site or part of body. Also, cancer cells get damaged or killed only when applied temperature is high enough and sustains long enough [82-84].

In hyperthermia thermotherapy, the affected cancer tissues are heated to temperature range of 41°C to 46°C by exposing MNPs to external AC magnetic field. Heat get generated by MNPs due to three different losses i.e. hysteresis, Néel and Brownian relaxation. However, superparamagnetic nanoparticles show only Néel and Brownian losses. The SAR value of MNPs depends on particle size, dipole – dipole interactions, viscosity of the medium, suspension media, magnetic anisotropy, magnetic field amplitude and frequency. Manganese ferrite (MnFe_2O_4) among spinel ferrites is a remarkable magnetic material for hyperthermia applications due to their high resistivity and high saturation magnetization. Relaxivity of manganese ferrite nanoparticles is large due to their large magnetic spin magnitude, which improves heating in AC magnetic field. [85, 86].



Fig. 1.14 Magnetic hyperthermia therapy [85]

There are many ways by which heat is induced for hyperthermia therapy. The most usual ways are direct application of heat, microwave heating, focused ultrasound and magnetic hyperthermia. Magnetic hyperthermia is very popular and effective therapy among hyperthermia therapies. Magnetic hyperthermia produces controllable heat inside patient's body and temperature distribution can be controlled by size of MNPs [86]. In 1999, Jorden et al. was first instigated the magnetic fluid hyperthermia technique. A fluid containing MNPs can be injected into affected tissue and an exterior magnetic field is being applied with frequencies. The MNPs generate heat and destroy tumor cells or tissues [87]. The main principle of MNPs based hyperthermia is a distribution of nanoparticles through targeted tumor area or site accompanied by heat generation using an external alternating magnetic field. Heat generation efficiency due to applied magnetic field of any particle is measured by specific absorption rate (SAR). Heating mechanism of MNPs includes three types of heat losses i.e. hysteresis losses, Neel and Brownian relaxation losses. Diffusion due

to Brownian and Neel relaxation of MNPs magnetic moment control magnetization relaxation with very less hysteresis loss [49, 50].

Hyperthermia can be mainly categorized into four types i.e. regional, local, whole-body and interstitial hyperthermia.

Local hyperthermia

In local hyperthermia, heat is applied exteriorly on small area to treat tumor, which is near to skin or near to openings of body. Here, heat can be created on affected diseased area or site using microwave, ultrasound energy, radiofrequency or magnetic hyperthermia. Heat can be applied to patient's body surface, inside deep in tissue depending on the place of disease or tumor. Normally, local hyperthermia is used for solid tumors [90].



Fig. 1.15 Local hyperthermia treatment [91]

Regional hyperthermia

In regional hyperthermia therapy, the heat is being applied on entire organ or large part of body. Here, cancer cells or tissues are normally killed by radiation and chemotherapeutic medications. Regional hyperthermia is normally used for larger or

multiple tumors and it utilizes microwave lesser or ultrasound energy. Regional hyperthermia may rely on blood perfusion. Patient's blood can be separated from body and heated up. Then, blood is returned to vessels that way through wanted part of patient's body [92].

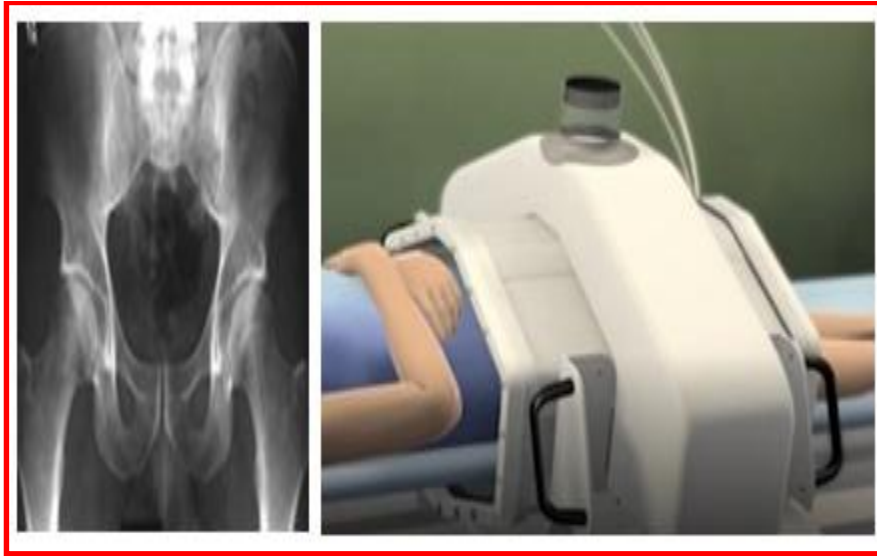


Fig. 1.16 Regional hyperthermia treatment [93]

Whole-body hyperthermia

Whole-body hyperthermia is typically used for cancer treatment grown on multiple parts of body or metastatic cancer. In whole-body hyperthermia, heat is applied on whole body and about temperature of 39 to 43°C. The patient is put in a very chamber, wrap the patient in water tubing suit with infrared domes in whole body hyperthermia technique [94].



Fig. 1.17 Whole-body hyperthermia treatment [95]

Interstitial hyperthermia

In interstitial hyperthermia therapy, heat is generated from inside the tissue or call using metal electrodes or microwave antenna. Low frequency current fields of about 500 kHz can be passed between electrodes embedded into tumors and this forms resistive heating. The tumors which are deep within body can be treated using interstitial hyperthermia [96, 97].



Fig. 1.18 Interstitial hyperthermia [98]

1.6 Problem statement

In recent years, there is huge advancement in medicine field but cancer still remains major source of death in world. About 90.5 million people had been affected world wide by cancer disease and about 14.2 million new patients find every year. By 2030, this number is expected to increase upto 21.1 million by [99]. Cancer is second most leading cause of human deaths. Inappropriate diagnosis and disease detection at later stages are the most common reasons behind deaths. Risk of cancer is getting increased significantly day by day and many cancers cases occur more commonly in developed countries. Detection of the tumor on time and cure it without side effects remains challenge to scientific community. The treatments used for cancer including cancer treatments radiation therapy, chemotherapy, immunotherapy have side effects such as eye irritation, hair loss etc. Hyperthermia therapy reduces serious side effects caused to normal cells or tissues in compare to traditional cancer therapies. In hyperthermia thermotherapy, the affected cancer tissues are heated to temperature range of 41 °C to 46 °C by exposing MNPs to external AC magnetic field. Heat get generated by MNPs due to three different losses i.e. hysteresis, Néel and Brownian relaxation. Magnetic hyperthermia therapy has emerged as potential cancer therapy.

Spinel ferrites have emerged as important material for several of biomedical implementations like drug delivery, magnetofection, cell separation, tissue repairing, MRI and magnetic hyperthermia as nanoparticles offer controlled size and ability to be manipulated externally. MNPs are playing very crucial part in detection and cancer therapy. They can be used to heat specific organ or tumor cells in magnetic hyperthermia therapy. Manganese ferrite (MnFe_2O_4) among spinel ferrites is a remarkable magnetic material for biomedical applications due to their high resistivity and high saturation magnetization. Thermal conductivity of manganese ferrite nanoparticles is lower than NiFe_2O_4 , CoFe_2O_4 . Low heat loss in AC magnetic heating arises due to lower thermal conductivity. Relaxivity of manganese ferrite nanoparticles is large due to their large magnetic spin magnitude, which improves heating in AC magnetic field. Therefore, manganese ferrite nanoparticles over other

spinel ferrites have been selected for magnetic hyperthermia cancer therapy by reviewing literatures.

Preliminary to the use of MNPs for biomedical implementations, nanoparticles should pass specific criteria like biocompatibility, ability to carry payloads and improved colloidal stability. Surface modification of MNPs is required through specific functionalization strategy to satisfy above criteria. Therefore, the different techniques of surface fabrication with various materials were used to manufacture functionalized MNPs.

The MNPs should accomplish following requisites prior to use as material for magnetic hyperthermia therapy.

- Nanosize
- High colloidal stability
- High saturation magnetization
- Superparamagnetic behavior
- High SAR value
- Non-toxicity

Based on the above considerations, present thesis was designed with following objectives:

- Synthesis of MnFe_2O_4 MNPs by one step polyol method.
- Surface functionalization of MnFe_2O_4 nanoparticles with APTES, EDA and PVP for hyperthermia application.
- Structural and Morphological characterization of bare and functionalized MnFe_2O_4 nanoparticles.
- Heat induction studies of MnFe_2O_4 nanoparticles for hyperthermia therapy application.
- *In-vitro* biocompatibility study of functionalized MnFe_2O_4 nanoparticles.

References

1. C. Poole and F. Owens, Introduction to nanotechnology, 2003, 1, 1-7, Wiley, John Wiley & Sons, Inc., Hoboken, New Jersey.
2. K. Chattopadhyay and A. Banerjee, Introduction to Nanoscience and Nanotechnology, 2009, 1-5, 1st Edition, PHI Learning Private Limited, New Delhi.
3. C. Rao and A. Cheetham, J. Mater. Chem., 2001, 11, 2887-2894.
4. J. Jortner and C. Rao, Pure Appl. Chem., 2002, 74, 1491-1506.
5. J. Gribbin, and M. Gribbin, Richard Feynman: A Life in Science, 1997, 1- 13, 1st Edition, Dutton Adult.
6. <http://www.zyvex.com/nanotech/feynman.html>
7. N. Taniguchi, Proc. Intl. Conf. Prod. Eng. Tokyo, Part -II, Japan Society of Precision Engineering, 1974.
8. K. Drexler, PNAS, 1981, 78, 5275-5278.
9. <http://oncologynews.com.au/new-nanoparticle-delivers-and-tracks-cancer-drugs/>
10. J. Ortega-Vinuesa, R. Hidalgo-Álvarez, F. Nieves, C. Davey, D. Newman and C. Price, J. Colloid Interface Sci., 1998, 204, 300-311.
11. A. Bradwell, H. Carr-Smith, G. Mead, L. Tang, P. Showell, M. Drayson and R. Drew, Clin. Chem., 2001, 47, 673-680.
12. E. Stoner and E. Wohlfarth, IEEE Trans. Mag., 1947, 27, 3475-3518.
13. A. Nel, T. Xia, L. Madler and N. Li, Science, 2006, 311, 622-627.
14. N. TK Thanh, Magnetic Nanoparticles: From Fabrication to Clinical Applications, 2012, 3-43, CRC Press, Taylor & Francis Group, New York.
15. E. Duguet, S. Vasseur, S. Mornet and J. Devoisselle, Nanomed., 2006, 1, 157-168.
16. R. Liu, J. Duay and S. Lee, Chem. Commun., 2011, 47, 1384-1404.
17. B. Graziano, E. Collins, N. McCutcheon, C. Griffith, N. Braunscheidel, T. Perrine and B. Wilem, Inorganica Chim. Acta., 2019, 484, 185-196.

18. M. Mahmoudi, A. Simchi, M. Imani and U. Häfeli, *J. Phys. Chem. C*, 2009, 113, 8124-8131
19. R. Hachani, M. Lowdell, M. Birchall, A. Hervault, D. Mertz, S. Begin-Colin and N. Thanh, *Nanoscale*, 2016, 8, 3278-3287.
20. M. Zborowski, J. Chalmers and W. Lowrie, *Microsystems and Nanosystems*, 2016, 15-55.
21. B. Rittich, A. Španová, D. Horák, M. Beneš, L. Klesnilová, K. Petrová and A. Rybníkář, *Colloids Surf. B*, 2006, 52, 143-148.
22. J. Bramhill, S. Ross and G. Ross, *Int. J. Environ. Res. Public Health*, 2017, 14, 66-89.
23. A. Muela, D. Muñoz, R. Martín-Rodríguez, I. Orue, E. Garaio, A. Abad Díaz de Cerio, J. Alonso, J. García and M. Fdez-Gubieda, *J. Phys. Chem. C*, 2016, 120, 24437-24448.
24. D. Shriver, P. Atkins, T. Overton, J. Rouke, M. Weller and F. Armstrong, *Inorganic Chemistry*, 2010, 5th Edition, Oxford University Press.
25. K. Buschow, *Handbook of Magnetic Materials*, 2003, 15, 1-199, Elsevier, Elsevier B.V.
26. L. Katz, A. Burkhalter and W. Dreyer, *J. Nature*, 1984, 310, 498-500.
27. F. Kievit and M. Zhang, *Acc. Chem. Res.*, 2011, 44, 853-862
28. H. Wang, X. Kou, J. Zhang and J. Li, *Bull. Mater. Sci.*, 2008, 31, 97-100.
29. D. Huber, *Small.*, 2005, 5, 482-501.
30. V. Shubayev, T. Pisanic and S. Jin, *Adv. Drug Deliv. Rev.*, 2009, 61, 467-477.
31. L. Zhou, J. Yua and Y. Wei, *J. Mater. Chem.*, 2011, 21, 2823-2840.
32. M. Singh, S. Manikanandan and A. Kumaragaru, *Research journal of nanoscience and nanotechnology*, 2011, 1, 1-11.
33. J. W. Steed and J. L. Atwood, *Supramolecular Chemistry*, 2009, 2nd Edition, Wiley, John Wiley and Sons, Ltd.
34. D. Ho, X. Sun and S. Sun, *Accounts Chem. Res.*, 2011, 44, 875-882.

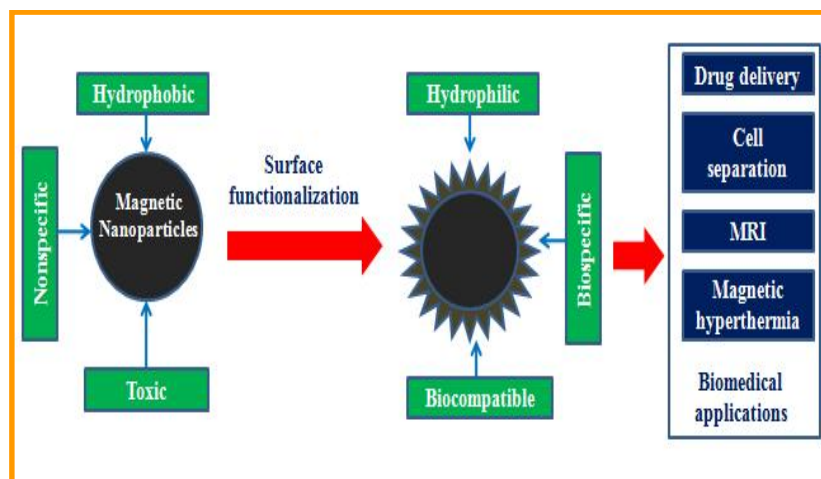
35. J. Salazar, L. Perez, O. Abril, L. Phuoc, D. Ihiawakrim, M. Vazquez, J. Greneche, S. Begin-Colin and G. Pourroy, *J. Chem. Mater.*, 2011, 23, 1379-1386.
36. M. Willard, Y. Nakamura, D. Laughlin and M. McHenry, *J. Am. Ceram. Soc.*, 1999, 82, 3342-3346.
37. S. Amiri and H. Shokrollahi, *Mater. Sci. Eng. C.*, 2013, 33, 1-574.
38. A. Sykes, *Advances in Inorganic Chemistry*, 1994, Volume 41, Academic Press Inc.
39. J. Verwey and E. Heilmann, *J. Chem. Phys.*, 1947, 15, 4
40. K. Sickafus and J. Wills, *J. Am. Ceram. Soc.*, 1999, 82, 12.
41. V. G. Harris, N. C. Koon, C. M. Williams, Q. Zhang, M. Abe and J. P. Kirkland, *Appl. Phys. Lett.*, 1996, 68, 15.
42. https://chem.libretexts.org/Bookshelves/Inorganic_Chemistry
43. X. Zuo, A. Yang, S. Yoon, J. Christodoulides, V. Harris and C. Vittoria, *J. Appl. Phys.*, 2005, 97, 10.
44. F. Lotger, *J. Phys. Chem. Solids*, 1964, 25, 345.
45. K. Buschow, *Handbook of Magnetic Materials*, Amsterdam: Elsevier North-Holland, 1995, 8, 212.
46. J. Adam, L. Chao and Z. Zhang, *J. Phys. Chem. B*, 2001, 105, 7967-7975.
47. M. Ghobadi, M. Gharabaghi, H. Abdollahi, Z. Boroumand and M. Moradian, *J. Hazard. Mater.*, 2018, 351, 308-316.
48. X. Battle and A. Labarta, *J. Phys. D: Appl. Phys.*, 2002, 35, 15-42.
49. C. Liu, B. Zou, J. Rondinone and Z. Zhang, *J. Am. Chem. Soc.*, 2000, 122, 6263-6267.
50. M. Hansen and S. Morup, *J. Magn. Magn. Mater.*, 1998, 184, 262-274.
51. A. Samia, K. Hyzer, J. Schlueter, C. Qin and J. Jiang, *J. Am. Chem. Soc.*, 2005, 127, 4126-4127.
52. H. Pardoe, W. Chua-anusorn, T. Pierre and J. Dobson, *J. Magn. Magn. Mater.*, 2001, 225, 41-45.

53. S. Son, J. Reichel, B. He, M. Schuchman and S. Lee, *J. Am. Chem. Soc.*, 2005, 127, 7316-7317.
54. Y. Jun, Y. Huh, J. Choi, J. Lee, H. Song, S. Kim, S. Yoon, K. Kim, J. Shin, J. Suh and J. Cheon, *J. Am. Chem. Soc.*, 2005, 127, 5732-5733.
55. E. Allard, C. Passirani and J. Benoit, *Biomaterials*, 2009, 30, 2302-2318.
56. R. Gilchrist, R. Medal, W. Shorey, R. Hanselman, J. Parrott and C. Taylor, *Ann. Surg.*, 1957, 146, 596-606.
57. A. Gupta, R. Naregalkar, V. Vaidya and M. Gupta, *Nanomedicine*, 2007, 2, 23-39.
58. R. Misra, *Mater. Sci. Tech.*, 2008, 24, 1011-1019.
59. Y. Wang, S. Hussain and G. Krestin, *Eur. Radiol.*, 2001, 11, 2319-2331.
60. J. McCarthy and R. Weissleder, *Adv. Drug Deliv. Rev.*, 2008, 60, 1241-1251.
61. C. Sun, J. Lee and M. Zhang, *Adv. Drug Deliv. Rev.*, 2008, 60, 1252-1265.
62. A. Jordan, R. Scholz, P. Wust, H. Fahling and R. Felix, *J. Magn. Magn. Mater.*, 1999, 201, 413-419.
63. R. Juliano, *Can. J. Physiol. Pharmacol.*, 1978, 56, 683-690.
64. M. Babincova, D. Leszczynska, P. Sourivong, P. Cicmanec and P. Babinec, *J. Magn. Magn. Mater.*, 2001, 225, 109-112.
65. M. Freeman, A. Arrot and H. Watson, *J. Appl. Phys.*, 1960, 31, 404-405.
66. A. Willis, N. Turro and S. O'Brien, *Chem. Mater.*, 2005, 17, 5970-5975.
67. S. Chandra, K. Barick and D. Bahadur, *Adv. Drug Deliv. Rev.*, 2011, 63, 1267-1281.
68. L. Kumar, A. Baldi, S. Verma, P. Utreja, *Pharmaceutical Nanotechnology*, 2018, 6, 1-17.
69. H. Maeda, G. Bharate and J. Daruwalla, *Eur. J. Pharm. Biopharm.*, 2009, 71, 409-419.
70. M. Babincova, D. Leszczynska, P. Sourivong, P. Cicmanec and P. Babinec, *J. Magn. Magn. Mater.*, 2001, 225, 109-112.

71. P. Cherukuri, E. Glazer and S. Curley, *Adv. Drug Delivery Rev.*, 2010, 62, 339-345.
72. P. Lauterbir, *Nature.*, 1973, 242, 190-193.
73. C. Rivet, H. Lee, A. Hirscha, S. Hamiltona and H. Lu, *Chem. Eng. Sci.*, 2011, 66, 1490-1507.
74. Y. Zhang, N. Kohler and M. Zhang, *Biomaterials*, 2003, 23, 1553-1561.
75. B. Dale, M. Brown and R. Semelka, *MRI: Basic Principles and Applications*, 2015, 39-44, 5th Edition, Wiley Blackwell, John Wiley and Sons, Ltd.
76. C. Brazel, *J. Pharm. Res.*, 2009, 26, 644-656.
77. H. Joshi, Y. Lin, M. Aslam, P. Prasad, E. Schultz-Sikma, R. Edelman, T. Meade and V. Dravid, *J. Phys. Chem. C.*, 2009, 113, 17761-17767.
78. G. Wolf and E. Fobben, *Invest. Radiol.*, 1984, 19, 324-328.
79. H. Weinmann, R. Brasch, W. Press and G. Wesbey, *Ame. J. Roentgenol.*, 1984, 142, 619-624.
80. H. Wu, G. Liu, X. Wang, J. Zhang, Y. Chen, J. Shi, H. Yang, H. Hu and S. Yang., *J. Acta Biomater.*, 2011, 9, 3496-3504.
81. <http://mriquestions.com/does-gd-affect-t2.html>
82. S. Mornet, S. Vasseur, F. Grasset and E. Duguet, *J. Mater. Chem.*, 2004, 14, 2161-2175.
83. R. Hergt and W. Andra, *Magnetism in Medicine: A Handbook*, 2007, 550-565, Wiley, Wiley-VCH Verlag GmbH & Co. KGaA, Weinheim.
84. P. Moroz, S. Jones and B. Gray, *Int. J. Hyperthermia*, 2002, 18, 267-284.
85. <http://www.klinik-bad-trissl.de/en/klinik/hyperthermie/>
86. B. Thiesen and A. Jordan, *Inter. J. Hyperthermia*, 2008, 24, 467-474.
87. P. Wust, B. Hildebrandt, G. Sreenivasa, B. Rau, J. Gellermann, H. Riess, R. Felix and P. Schlag, *Lancet Oncol.*, 2002, 3, 487-497.
88. R. Hergt, W. Andra, C. D'Ambly, I. Hilger, W. Kaiser, U. Richter and H. Schmidt, *IEEE Transactions on Magnetism*, 1998, 34, 3745-3754.

89. M. Latorre and C. Rinaldi, P R Health Sci J., 2009, 28, 227-238.
90. S. Jha, P. Sharma and R. Malviya, Achiev. Life Sci., 2016, 10, 161-167.
91. <https://www.arcadia-praxisklinik.de/en/treatment-options/hyperthermia.html>
92. R. Gilchrist, R. Medal, W. Shorey, R. Hanselman and J. Taylor, Ann. Surg., 1957, 146, 596-606.
93. <https://www.pyrexar.com/how-deep-regional-hyperthermia-works>
94. A. Nemmar, M. Hoylaerts and P. Hoet, Am. J. Respir. Crit. Care Med., 2002, 166, 998-1004.
95. <https://www.heckel-hyperthermia.com/index.php/en05>
96. J. Dormann, D. Fiorani and E. Tronc, J. Magn. Magn. Mater., 1999, 202, 251-267.
97. C. Vestal and Z. Zhang, J. Am. Chem. Soc., 2003, 125, 9828-9833.
98. <https://www.hcioncology.com/hyperthermia-therapy/interstitial-hyperthermia/>
99. T. Vos, Lancet. 2015, 388 (10053): 1545-1602.

Surface Functionalization of MNPs for Biomedical Applications (Theoretical Background)



If we can reduce the cost and improve the quality of medical technology through advances in nanotechnology, we can more widely address the medical conditions that are prevalent and reduce the level of human suffering.

-Ralph Merkle

2.1 Introduction

MNPs have become an impressive material in science as well as medical areas. It is mandatory to study dispersion stability of MNPs in different liquid media, which controls the properties of yielded products. Nanoparticles have highest tendency of adhesion, aggregation as they possess different surface structures with surface interactions. Hence, it is necessary to discover approach to admin dispersion and aggregation of MNPs to use them for biological implementations [1]. Nanoparticles stability under physiological conditions can be determined by achieving surface functionalization of nanoparticles.

The MNPs incline to agglomerate without a hydrophilic coating layer because of robust interparticle magnetic dipole-dipole interactions. Biocompatibility of material and cell adhesion is dependent on surface characteristic of nanoparticles. The overall size of colloid can be established by surface modification type and their subsequent geometric arrangement on MNPs. It is also vital for biodistribution and biokinetics of MNPs in the body. Type of specific surface coating can be selected based on particular application, derivatization and inflammation response [2]. Surface modification prevents liquefaction core materials, which might origin toxicity. Surface tailoring also influence the perputation of in build nanocrystals properties like magnetic behavior and fluorescence. Therefore, surface functionalization is precondition for combining biomolecules to MNPs for biomedical implmentations. MNPs must be dissolved in aqueous medium and it can be attained with surfactant exchange or addition [3].

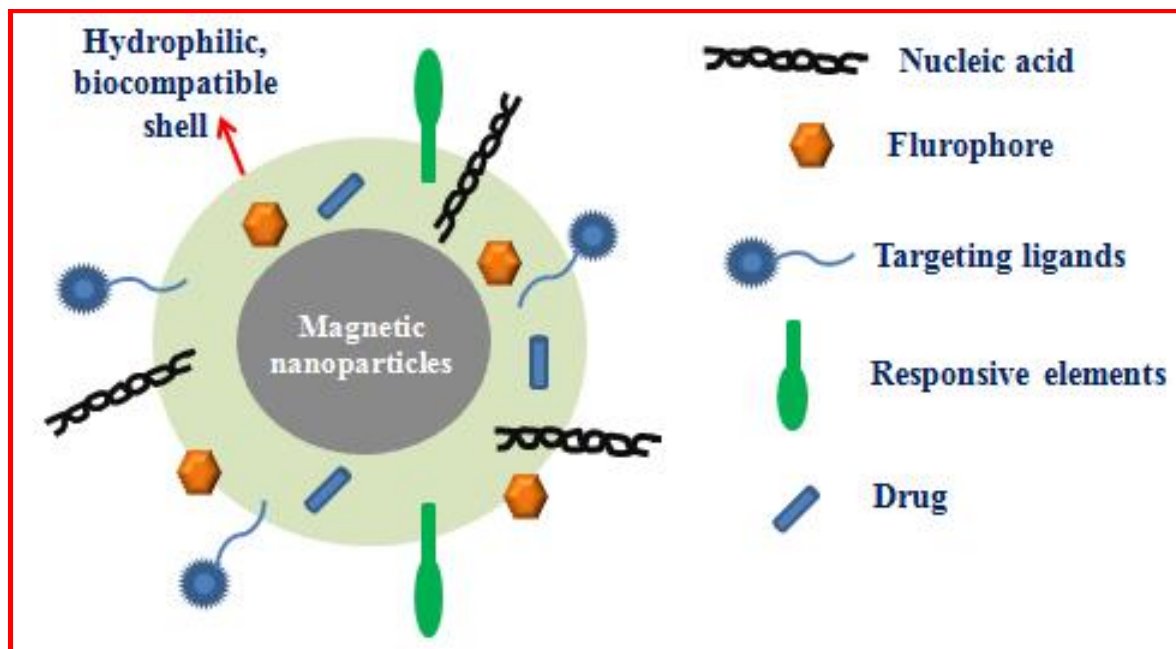


Fig. 2.1 Surface functionalization of MNPs

Addition of surfactant is carried out with the adsorption of molecules having both hydrophobic and hydrophilic parts. The two layer structure with the original hydrocarbon chain is created by hydrophobic segment and hydrophilic assemblies can be exposed to outside of nanoparticles, which turn into water soluble [4]. Original surfactant is replaced with new bi-functional surfactant in case of surfactant exchange process. Bi-functional surfactants can have first functional group ability to bind to MNPs surface through chemical bond. At other end, another functional group can have polar property, which disperses the nanoparticles in water [5, 6]. The different types of materials can be selected for functionalization of MNPs. Surface of MNPs must be stabilized and shielded from the impact of exterior components, which could influence the magnetic properties.

Surface functionalization should report below properties to MNPs for successful usage of MNPs for biomedical applications.

- Surface functionalization must avert MNPs from aggregation and improve colloidal stability.
- Surface functionalization of MNPs must increase water compatibility.

- Surface functionalization must support better magnetic controllability of nanoparticles.
- Surface functionalization must stabilize the surface of MNPs.
- Surface functionalization must require in protection of MNPs surface.
- Surface functionalization should make MNPs nontoxic and biocompatible.
- Surface functionalization should give conventional form of functional groups to couple biologically energetic substances for biomedical implementations.

2.2 Need of surface functionalization

MNPs should be functionalized in order to utilize them successfully for biomedical application and ideal surface functionalization must avert MNPs form aggregation, guide to increase water compatibility, upgrade colloidal stability, stabilize the surface and make nanoparticles biocompatible.

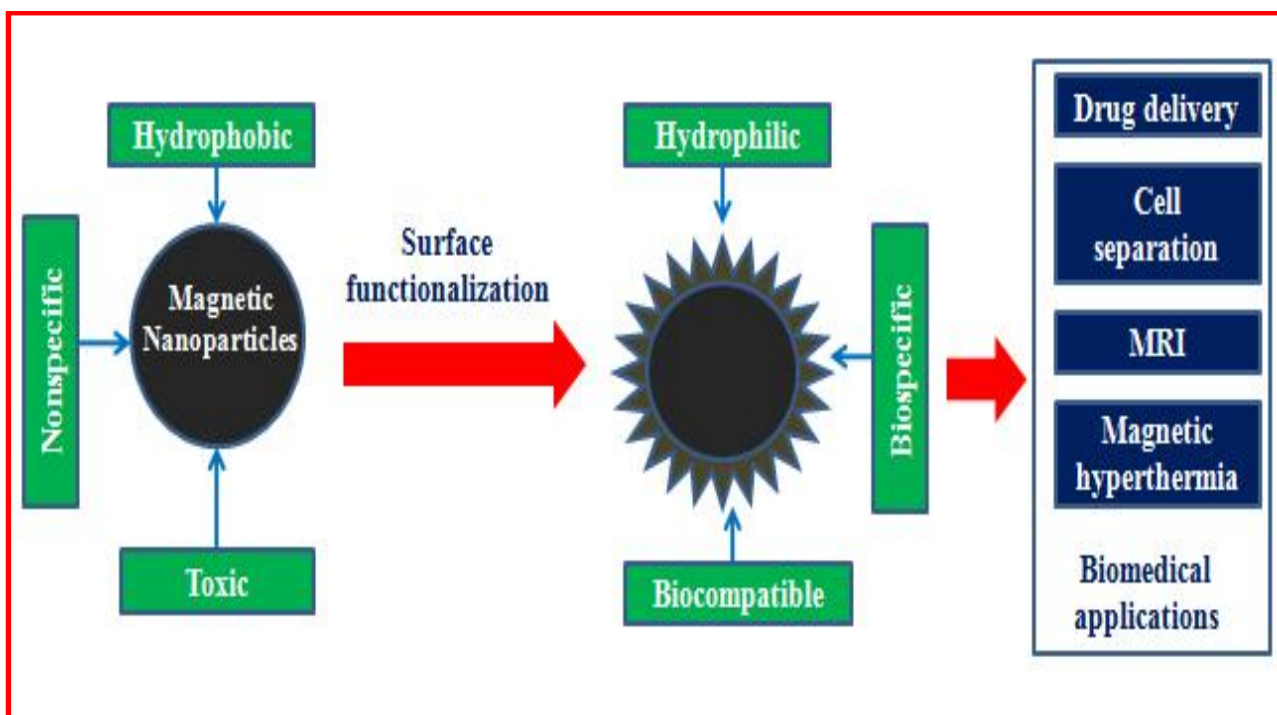


Fig. 2.2 Need of surface functionalization for magnetic hyperthermia application

2.2.1 Stabilization against aggregation

On surface of nanoparticles, capping agents enable magnification of tiny seeds and avert cluster formation. Hydration layer, steric exclusion or electrostatic repulsion can generate repulsive force between MNPs. Particles get dispersed in aqueous media depending on particle system and right selection of surfactants [7]. Chemical groups can have a specific tendency to combine to inorganic surfaces. MNPs surface can be covered by hydrophobic ligand molecules using organic solvents, which prevent aggregation of particles. Interactions between NPs surface and an electron-donating group of a ligand molecule create bond between them which is responsible for dynamic binding and unbinding processes [8, 9]. There are two main strategies (Electrostatic stabilization and steric stabilization) used to decrease nanoparticles agglomeration.

2.2.2 Steric stabilization

MNPs which require colloidal stability under high salt concentrations and over wide pH range should be sterically stabilized. Steric repulsion forces need to be considered for functionalized MNPs. It depends on the polymeric material used in surface fabrication of MNPs and it can be achieved by functionalizing MNPs with ligand shell or embedded polymeric matrix. Resulting repulsive potential can be monitored by polymer density, molar mass of polymer, solvent quality and binding reversibly. When two sterically stable central core of base material are proceed towards each other polymer brushes confinely to MNPs. It increases osmotic pressure between MNPs guiding to stability of colloid and reduces the entropy of polymers [10, 11].

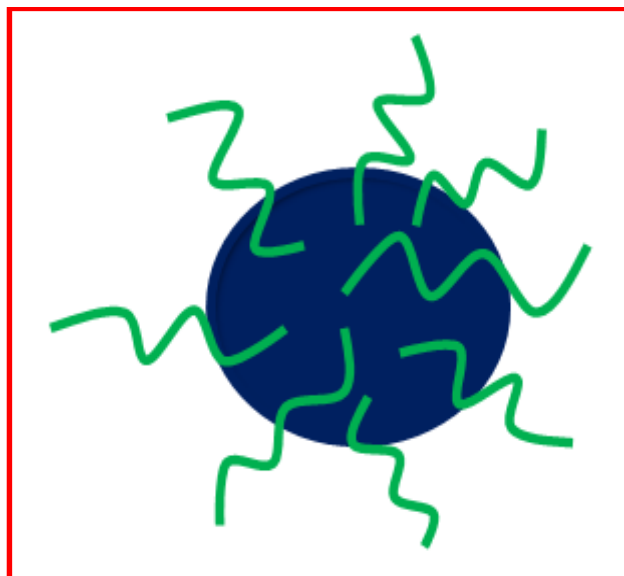


Fig 2.3 Steric stabilization of MNPs

2.2.3 Electrostatic stabilization

The formation of clusters of suspension of colloid can accompanied to experiment and electrostatic stability by modifying the added different concentration of salt. Particles from aggregation can be prevented by reflecting the efficacy of the potential barrier [12]. For this, stability factor W need to be studied. Here, W represent ratio of total number of collisions which results in conglomeration and it is shown in equation (2.1).

$$W = \frac{K_{fast}}{K} \dots \dots 2.1$$

where, K is an conglomeration rate constant for concentration of salt which is used for experiment and K_{fast} is a rate constant explaining rapid aggregation.

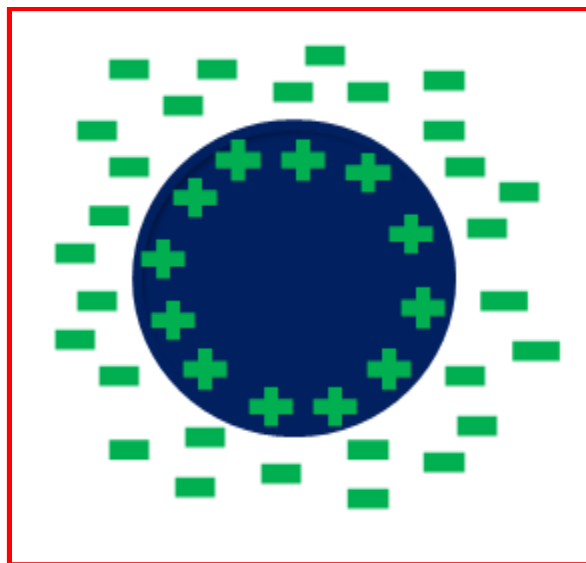


Fig. 2.4 Electrostatic stabilization of MNPs

Stability factor is obtained through turbidimetric measurements or light scattering and factors related with colloidal stability as a function of salt concentration provides access to concentration of salt changing to coagulated form. The two electrostatic layers at this concentration can be suppressed. The interaction between the MNPs can be explained by the DLVO theory absence of steric stabilization layer. DLVO theory states that the aggregation of aqueous dispersions quantitatively and describes the force between charged surfaces interacting through a liquid medium. It combines the effects of the van der Waals attraction and the electrostatic repulsion due to the so-called double layer of counterions. Stabilization is effective at low salt concentrations in electrostatic nanoparticles and at pH above or below to isoelectric point [13, 14].

2.2.4 Colloidal stability

MNPs should be stored in liquid conditions to utilize them for biomedical implementations and corresponding liquid systems are called as ferrofluids or magnetic fluids. MNPs can be functionalized with particular shells of polymers or surfactants for colloidal stabilization of magnetic fluids. It is difficult process to store

MNPs without clustering because of powerful interaction of surfactants with aqueous medium. There are various side effects of formation of aggregates in biomedical context. Aggregated particles are difficult to eliminate from organisms, appearance of blood clots and reduction in therapeutic efficiency [15, 16].

2.2.5 Particle size and distribution

MNPs should have controllable size ranging from small nanometers (nm) to tens of nm (nanometers). MNPs can offer attractive possibilities depending on size of MNPs. Nanoparticles can interact with biological entity and provide adminable size if functionalized with suitable biological molecules [17]. Most of biomedical applications require monodisperse, crystalline, single domain nanoparticles. This ensures that each and every independent nanoparticle owns approximately similar chemical and physical properties for administered bioelimination and contrast effects.

2.2.6 Magnetic controllability

Magnetic response of MNPs can be described using Saturation magnetization (Ms). MNPs are separated and transported magnetically to desired place based on Ms values of MNPs and it becomes easy task if Ms value remains high [18]. Magnetic administraton of MNPs is always higher than that of individual shell particles. Magnetic administraton of nanoparticles is attained by clustering of particles and functionalization of nanoparticles.

2.2.7 Biocompatibility

The toxicity of MNPs is critical point in designing the MNPs for biomedical applications. Surface functionalization ensures averting transfer of toxic ions, which are toxic from base material into biological medium. It also prevent from corrosion. Iron oxide nanoparticles are most commonly engaged for *in vivo* application as iron is physio-logically good tolerated. Free nanoparticles are proved to be toxic and dangerous than their bulky sized particles. Biocompatibility of nanoparticles can be

controlled by size, charge on surface of MNPs and hydrophilicity. It is also controlled by charge and mass of coating molecules [19]. Positively charged nanoparticles show good cooperation with biosystems whereas negatively charged magnetic material can exhibit better biocompatibility.

2.3 Surface functionalization methods

The choice of appropriate base/core material and engineering of surface material are the challenges in designing the MNPs for their usage in biomedical implementations. Functionalization can exist of polymers or organic ligands and these can be initiated by *in situ* (during) or post synthetic (after) synthesis. Precursors of magnetic cores and functionalization materials can be dispersed in same solution during in-site approach. In this, nucleation and coating takes place parallelly. Functionalized materials are added after forming base core in post synthetic approach.

Surface functionalization of MNPs acts a decisive in biomedical implementation. Inorganic or organic surface functionalization is important due to following reasons:

- Surface functionalization prohibits agglomeration of MNPs because of their interactions between each other and provides the colloidal stability of aqua.
- Surface functionalization provides biocompatibility.
- Surface functionalization serves as bed for attachment of further groups like biomolecules.

2.3.1 One-step surface functionalization

One-step surface functionalization is also called as *In situ* surface functionalization. The synthesis and surface modification of MNPs are conducted within single reaction in one-step surface functionalization strategy. The reaction material contains precursors for MNPs and material to be functionalized on surface of MNPs. Functionalization or coating process can start once the nucleation occurs during the reaction and it prevents furthermore growth. The disadvantage of this

strategy is irreconcilability of functional group and main advantage is that size of particle gets reduced and distribution of particle size reduces to narrow range. In synthesis process, functionalization process begins as early as nucleation takes place and furthermore particle extension gets prevented after starting the functionalization process. Phosphates, carboxylates, hydroxyl and thiols are commonly used for direct functionalization.

2.3.2 Two-step surface functionalization

Two-step surface functionalization is also called as post synthesis functionalization. Two-step functionalization process can be classified into 2 categories i.e. synthesis and surface modification of MNPs. Bifunctional molecules or compounds can be used for modification. First, binding ligand groups is gets reacted and after that coupling area group is formed to endmost functional group. From the core-shell it can be confirmed that structure whether the attachment of functional groups with surface is done or not. The disadvantage of two-step functionalization strategy is that functional group should own high attraction for MNPs surfaces and main advantage is that availability of maximum numbers of coupling area. Two step surface functionalization i.e. post synthesis of MNPs normally contains 3 processes i.e. Ligand addition, exchange and Encapsulation.

2.4 Surface functionalization strategies of MNPs

Surface modification of MNPs usually depends or based on three strategies which are helpful for the stability, specificity and biocompatibility point of view. These strategies are:

2.4.1 Ligand addition

In this approach, an incorporation of ligand to the exterior area of surface without eliminating any ligands, which are already present on the surface of MNPs.

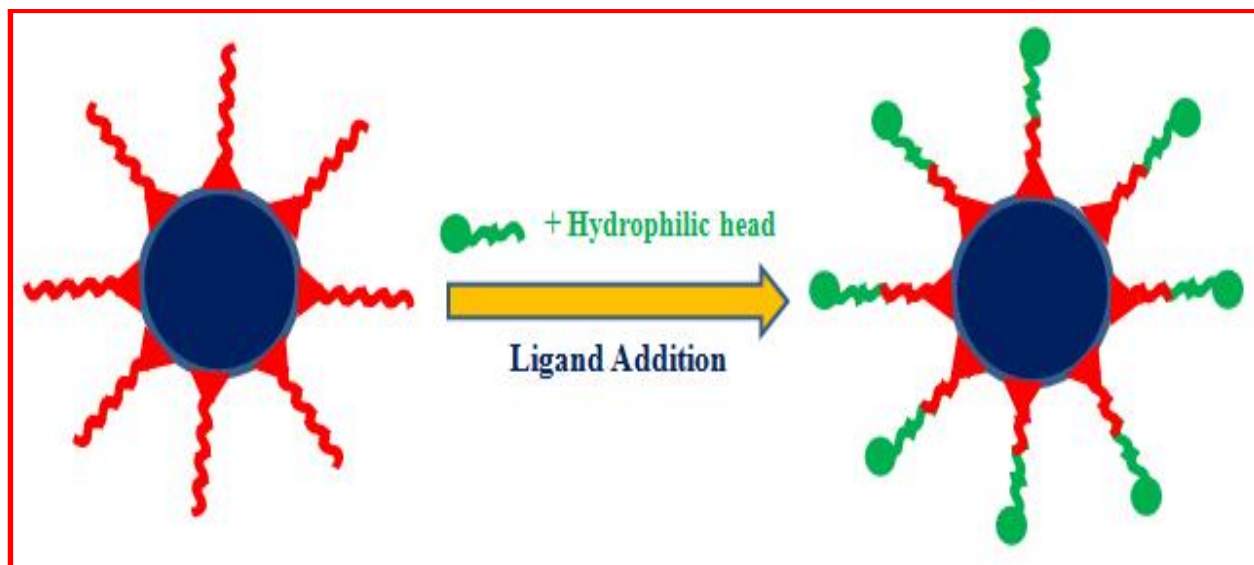


Fig. 2.5 Ligand addition mechanism

There are 4 perspectives for inclusion of ligand as listed below:

- Ligand addition to particles originally fabricated without surfactant.
- Layer growth of inorganic material onto particle's surface with succeeding adsorption straightly on to the surface by ionic. This is indirect ligand addition.
- Manipulation of force of attraction which is hydrophobic in nature to insert between the species. These are also hydrophobic into shell of hydrocarbon covered by ligand molecules.
- Development of a covalent bond in the middle of previous ligand and new ligand.

2.4.2 Ligand exchange

In this process, initial hydrophobic ligands can be substituted by other strongly bonded hydrophilic ligands for use them in implementation of biomedical area. Replaced hydrophilic ligands allow transfer from organic state to aqueous solution for MNPs. In short, we can say change of hydrophobic surface to hydrophilic. This process is very obligatory to bring the nanoparticles solubility in water.

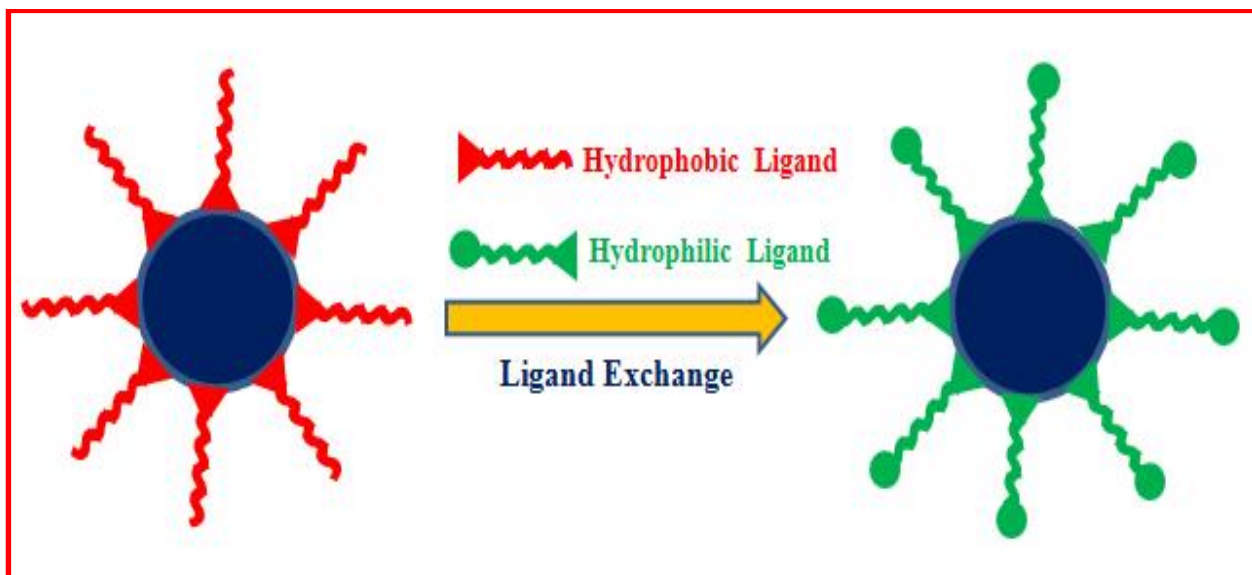


Fig. 2.6 Ligand exchange mechanism

Colloidal stability of MNPs can be enhanced by exchanging ligand molecules on surface so that new properties can be extended to MNPs easily. Several hydrophilic ligands like thiol, phosphine groups or amino etc can be used to replace the ligand present on surface of nanoparticles to transfer into water [20].

2.4.3 Encapsulation

Encapsulation is a modification strategy in which amphiphilic materials is used to over coat encapsulation nanoparticles. The encapsulation reactions is accomplished by inserting in two layers of hydrophobic parts of sample with opening ligand on surface of nanoparticles and provide hydrophilic section in the direction of solution.

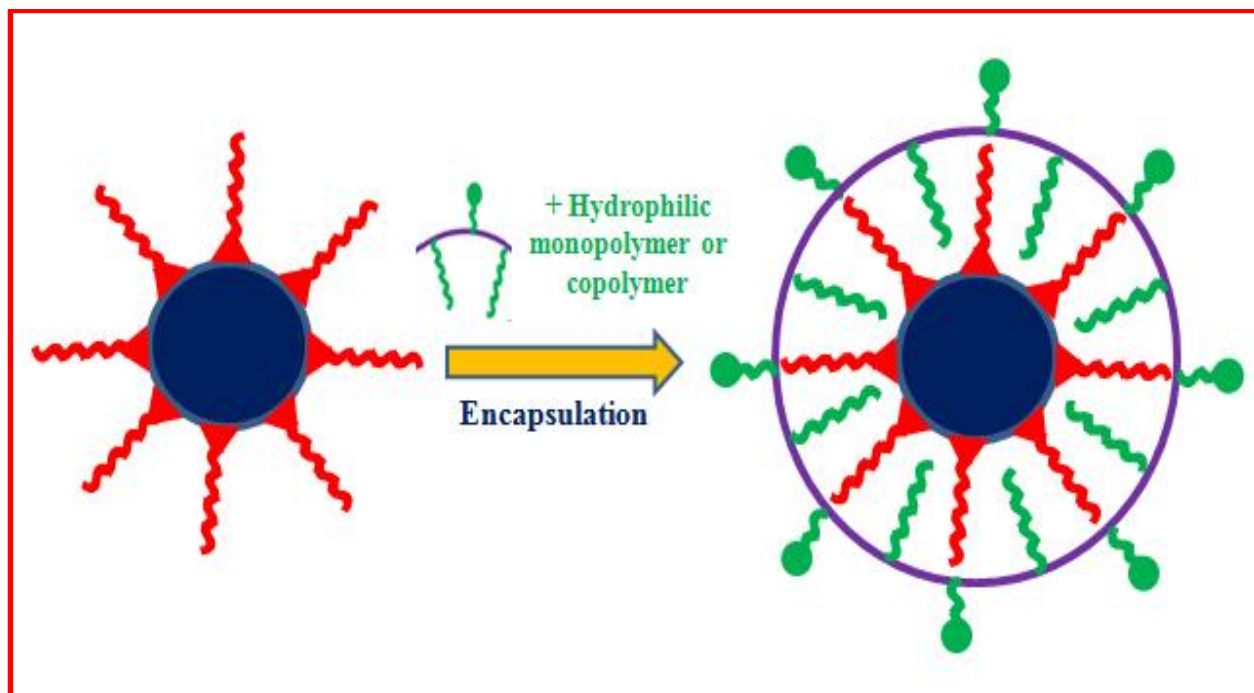


Fig. 2.7 Encapsulation mechanism

The MNPs turn to water compatible because of head inside the hydrophilic section. Furthermore functionalized groups permit for bio modification and bioconjugation of particles [21]. There are various methods of encapsulation which can be classified according the material used for the encapsulation and technique used for encapsulation. Generally the materials used for the encapsulation are hydrophilic polymer, polymer matrix or inorganic compound or material.

2.5 Materials used for functionalization of MNPs

For the use of MNPs in variety of biomedical application they must possess or show stability, specific binding and biocompatibility which can be achieved by functionalization strategy. Variety of materials can be used for the coating of outer surface of nanoparticles to use for biomedical applications. This part gives attention on which materials can be used for the protection, functionalization and stabilization through surface coating. The different stabilizers can attain the criteria and these

stabilizers are polymeric stabilizer, monomeric stabilizer, small molecules, inorganic materials etc.

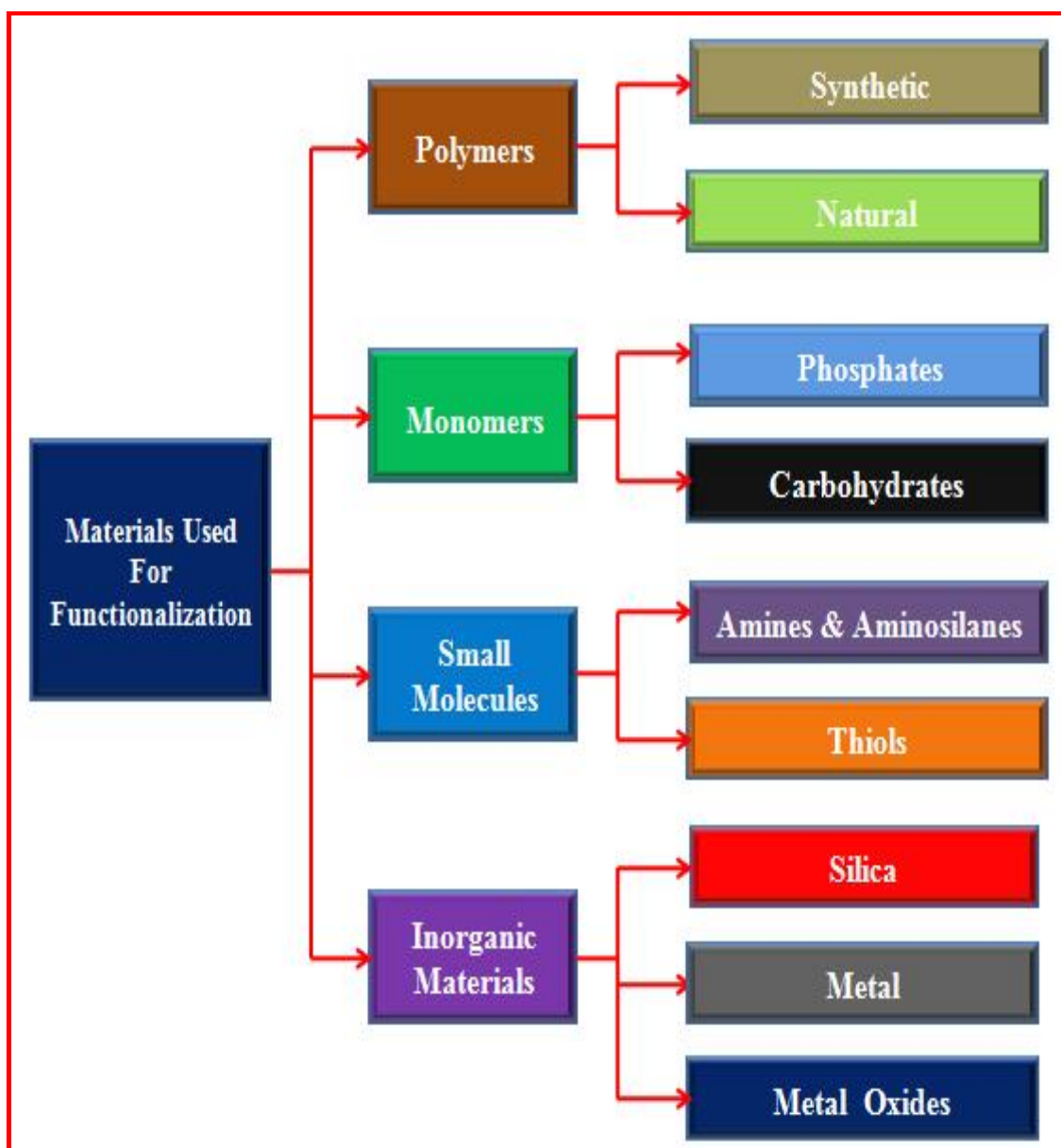


Fig. 2.8 Materials used for surface functionalization of MNPs

2.5.1 Polymers

Polymers have an excellent biocompatibility, colloidal stability and biodegradability over the other materials. Polymer coating provides excellent

colloidal stability of MNPs and polymer coating increases repulsive forces and Van der Waals force of attraction affecting on nanoparticles [22]. MNPs can be anchored mainly using two approaches i.e. ligand adsorption and ligand exchange to generate a more stable structure. Polymers with numerous functional groups are merged with MNPs by adsorbing ligands or exchanging ligands. Active terminal groups help for polymer coating. Monomeric species like alkoxysilanes, DSMA and bisphosphonates can be used to support the fitment of polymer coating on surface of MNPs. Polymer forms a blockade among magnetic particle after functionalization. It prevents agglomeration and provides several surface properties imparting highest potential to nanoparticles for biomedical implementations. MNPs functionalization with polymers provides linking advantage of MNPs with biomolecules. For biomedical application usage, the surface potential of the polymer functionalized nanoparticles can be impacted by complex structures. MNPs can be functionalized with polymers by fabricating the monodispersed nanoparticles with good defined shapes and composition. Synthetic polymers and natural polymers are two types of polymeric materials used for functionalization of magnetic materials [23, 24].

2.5.1.1 Polyvinylpyrrolidone (PVP)

Polyvinylpyrrolidone (PVP) is an amorphous, hygroscopic and available as powder. It is nontoxic and neutral in nature. PVP acts as additive to coating of MNPs and it possesses very good wetting property to form film. Lee et al. [25] have reviewed PVP functionalized ferrite nanoparticles for MRI application. They found depletion of T2 MRI intensity compared to normally used feridex for concentration of ferrite nanoparticles. Jadhav et al. [26] have studied PVP functionalized LSMO nanoparticles and used for hyperthermia. They concluded that such type of combustion synthesized PVP coated LSMO nanoparticles are potential heating agent in hyperthermia.

2.5.1.2 Dextran

Dextran is natural, neutral polymer, branched polysaccharide composed of glucose subunits. Polysaccharide polymer like Dextran composed of exclusively of R (risalfa sign)-D-glucopyranosyl units with varieties of degrees of chain length and branching. Dextran is being useful as a coating material due to its biocompatibility and it shows spontaneous associative properties in aqueous dispersion. Dextran is having a zero (0) net charge and biocompatible in nature. Dextran should be selected for coating of nanoparticles based on dextran chain size. This sanctions bonding of hydrogen with nanoparticles surface [27, 28]. Dextran molecules may be released from nanoparticles surface by dilution or heating and agents like epichlorhydrin can be used to avoid desorption of dextran [29]. The positive trait of dextran is that it can be aminated by ammonia. It enables union with complementary chemical groups. Bautista et al. [30] have studied that Dextran functionalized iron oxide nanoparticles and found that dextran functionalized nanoparticles have great potential for biomedical application like cancer theranostics. Khot et al. [31] have studied Dextran coated $MgFe_2O_4$ nanoparticles having size around 20 nm and used for magnetic particle hyperthermia. Nath et al. [32] have studied the targeting and sensing Novel Dextran-Coated Iron Oxide Nano rods applications with union with antibodies.

2.5.1.3 Acrypol

Acrypol aqua soluble polymer of acrylic acid having high molecular weight is useful applications in cosmetics and pharmaceutical industries. Solubility enhances because of polyol have property to lose proton from a crypolchains (Acrypol is an aqueous soluble polymer with high density of reactive functional groups) and get negative (-) charge in water at neutral pH. Hence acrypol polyelectrolyte has potential to absorb, keep water and expanded in to their initial volume. Acrypol has been used for coating purpose and also used as suspension media. Acrypol became attractive in bio-nano area because of its ability to form polymer chain protein via electrostatic as well as hydrogen bonding [33]. Shete et al. [34] have studied MNPs synthesized by

alkaline precipitation method and observed that these MNPs are suitable for hyperthermia therapy applications.

2.5.1.4 Polyvinyl Alcohol (PVA)

Polyvinyl Alcohol (PVA) is hydrophilic and non toxic polymer, which get transformed into gel of macromolecular network class. PVP coating on surface of nanoparticles provide monodispersed particle and prevents their agglomeration [35]. Surface functionalization of MNPs with PVA enriches the colloidal stability of the ferrofluids. PVA irreversibly binds on the surface of MNPs due to inter connected network with interface. The residual PVA can control MNPs properties like particle sizes and hydrophobic surface. It is proposed that the lower intracellular uptake of MNPs with high amount of residual PVA can be linked to the high hydrophilicity of surface of nanoparticles [36]. Albornoz et al. [37] have performed synthesis of ferric material which is soluble in water and prepared magnetic gel with PVA. Biocompatible film was prepared by drying magnetic gel having great stability. Kayal et al. [38] synthesized Fe_3O_4 nanoparticles and functionalized with PVP to act as promising material for targeted drug delivery. Salunkhe et al. [39] have studied *in vitro* cytotoxicity evaluations of PVA coated cobalt ferrite nanoparticles effectively improved their biocompatibility for biomedical applications.

2.5.1.5 Polyethylene glycol (PEG)

PEG is hydrophilic, linear synthetic and neutral polymer. PEG can be binded to different surfaces by changing the functional groups. PEG functionalized MNPs show excellent stability and solubility in water. Blood circulation time of MNPs gets increased after functionalizing them with PEG and it also enhances their hinderence. Polyethylene glycol (PEG) is broadly utilized surfactant because of its hydrophilicity, biocompatibility, hydrophilicity and non-antigenicity. Water compatibilization and stabilization of MNPs can be improved due to high hydrophilicity of PEG chains [40]. Kim et al. [41] have reported PEG functionalized nanoparticles are incorporated in

cytoplasm due to their highest attraction for phospholipid bilayer membranes. Chen Yue-Jian. [42] have prepared PEG functionalized nanoparticles which can be used in variety of applications like hyperthermia, MRI etc. Khot et al. [43] have synthesized PEG functionalized nanoferrites and concluded that these nanoferrites are potential heating arbitrators for *in vitro* as well as *in vivo* magnetic hyperthermia. Nikam et al. [44] have synthesized PEG functionalized CZF MNPs and studied their colloidal stability for magnetic hyperthermia.

2.5.1.6 Chitosan

Natural derivatives and their polymers broadly used for surface functionalization for biomedical implementations because of polymers are inexpensive. Chitosan is a natural polysaccharide cationic polymer and is nontoxic. There are many of studies performed introducing chitosan as MNPs carriers with the focus of use in biomedical implementations. Chitosan functionalized MNPs are getting great attention in biomedical area due to its alkaline, biodegradable, hydrophilic and biocompatible properties. Lee et al. [45] have reported that chitosan has been implanted on to MNPs to synthesize a ferrofluid and they observed that prepared MNPs exhibited a strong enhancement as contrast agent for MRI.

2.5.2 Monomers

The monomeric stabilizers such as phosphates and carboxylates are utilized for functionalizing the surface of nanoparticles. They can be also used for dispersibility in aqueous media.

2.5.2.1 Phosphates

Many researchers have reported that alkane sulphonic and alkane phosphonic acid will be useful as efficient material to provide binding of ligands on the exterior surface of NPs and stabilize particle dispersion in organic solvents [46]. Due to its biocompatibility those groups are helpful to coat MNPs for biomedical

implementations. Yee et al. [47] have proved the ions of phosphates generate bidentate complexes having free sites on MNPs surface. They have proposed two binding schemes for phosphonates ions. Sahoo et al. [48] have observed that derivatization of surface by different surfactant. It has also observed that alkyl phosphonates as well as phosphates can be helpful for dispersions of nanoparticles obtain.

2.5.2.2 Carboxylates

The MNPs surface can be coated by citric acid in aqueous dispersion. Carboxylic acid group is important functionality on the surface of nanoparticles. Growth of MNPs and their properties can affect because of Carboxylates. The coordination process is helpful to absorption of acid by 1 or 2 functionalities of surfactant and it is related to steric hindrance. It leaves minimum one carboxylic group when it reacts with solvent, which gives hydrophilic and negatively charged surface. Liu et al. [49] observed that if the concentration of citric acid is increased then it affects on crystallinity of MNPs and they also studied influence of citric acid on surface of nanoparticles. They observed that presence of citrate is responsible to alter the geometry of surface of yielded nanoparticles [49].

2.5.3 Small molecules

2.5.3.1 Amines and aminosilanes

For production of various types of functionalized MNPs the short chain amines and aminosilanes are commonly used as stabilizing agent. Barick et al. have synthesized the amine-functionalized Fe_3O_4 nanoparticles (Ethylenediamine coated iron oxide nanoparticles) in a one step using thermal decomposition technique. They have refluxed precursors after dissolving in ethylene glycol in presence of surfactant and ethylenediamine. These formed Fe_3O_4 nanoparticles were highly stable in aqueous media and applicable for biological implementation. Another different amine groups are also used for the stabilization which play vital role in during successful functionalization.

2.5.3.2 Thiols

The compounds present with thiol group show higher affinity for binding to the NPs. The compounds like DMSA or organo sulphur consist of carboxylic group along with thiol group and it shows property of stabilizer [50]. Maurizi et al. [51] used post functionalization strategy to stabilize thio groups on nanoparticles surface using methoxypolyethylene glycol. They noticed that after the thiol functionalization particles show high stability and stability is play vital role for implementation. They have also explained that after the addition of DMSA stability of thiol group will be increased.

2.5.4 Inorganic materials

Inorganic compounds are widely being used for surface coating of nanoparticles and inorganic compound coated material can be very promising for biomedical applications. Mostly gold and silica are being used for functionalization of nanoparticles and to protect nanoparticles against agglomeration. They can enhance stability to MNPs in solution as well as help to bind numerous biological ligands to nanoparticles surface.

2.5.4.1 Gold

MNPs can be functionalized using Gold (Au) to protect iron core against oxidation. Gold shell allows facile conjugation with several biomolecules and makes these composites useful for biomedical application. Gold can also form strong bonds with sulfur. Au coated nanoparticles can mask them from intravascular immune system and show absorption band in visible part because of their surface plasmon phenomenon [52]. Gold functionalized nanoparticles are potential material for optical applications in biomedical area.

2.5.4.2 Silica

Silica is usually known for its easy formation and chemical stability. The process of adsorption of ligand is similar with silica functionalization and silica functionalized MNPs form a core shell structure. Silica is largely used as surface coating materials for MNPs. Silica functionalized nanoparticles are colloiddally stable, robust and water-soluble. Agglomeration in liquid is prevented by silica coating for better protection against toxicity. Two ways to stabilize MNPs in which first is to shielding of magnetic dipole interaction with silica shell and another is imparting MNPs with -ve charge and enhance repulsive interactions [53]. There are various advantages of silica coating on magnetic surface such as better biocompatibility, hydrophilicity, ease of surface modification, can be controlled interparticle interaction.

2.5.4.3 Metal oxides or sulphides

Distinct physical and chemical properties can be enhanced after the functionalization of MNPs with metal oxides or metal sulfides. Hong et al. [54] have prepared ZnO-coated Fe₃O₄ nanoparticles by using the precursors like ammonium carbonate and zinc. They observed that coated nanomaterials possess antioxidant properties in compare with bare nanoparticles. When material is coated with ZnO, it shows astonishing properties like magnetization. These materials have been studied by number of scientist and they got fantastic results regarding saturation magnetization [55, 56].

2.6 Functionalization of MNPs with biological molecules

After the primary functionalization of core material another important step is synthesize bioactive material. Functionalization of iron oxide nanoparticles with biomoleule has become effectual approach in variety of bioapplications because of their cytocompatibility. The biomolecules like nucleic acid, proteins, albumin, avidin etc romp on to the iron oxide surface but this task is a not easy task. For the biofunctionalization of iron oxide nanoparticles, they (iron oxide nanoparticles and

biomolecules) must be suitable for each other. There are mainly three types of conjugations of MNPs with biological substance. The first involves a chemical modification of the functional group on the iron oxide nanoparticles. The next one is activation of the moiety of the bioactive substances and third step is based on modification of biomolecules chemically [57-63].

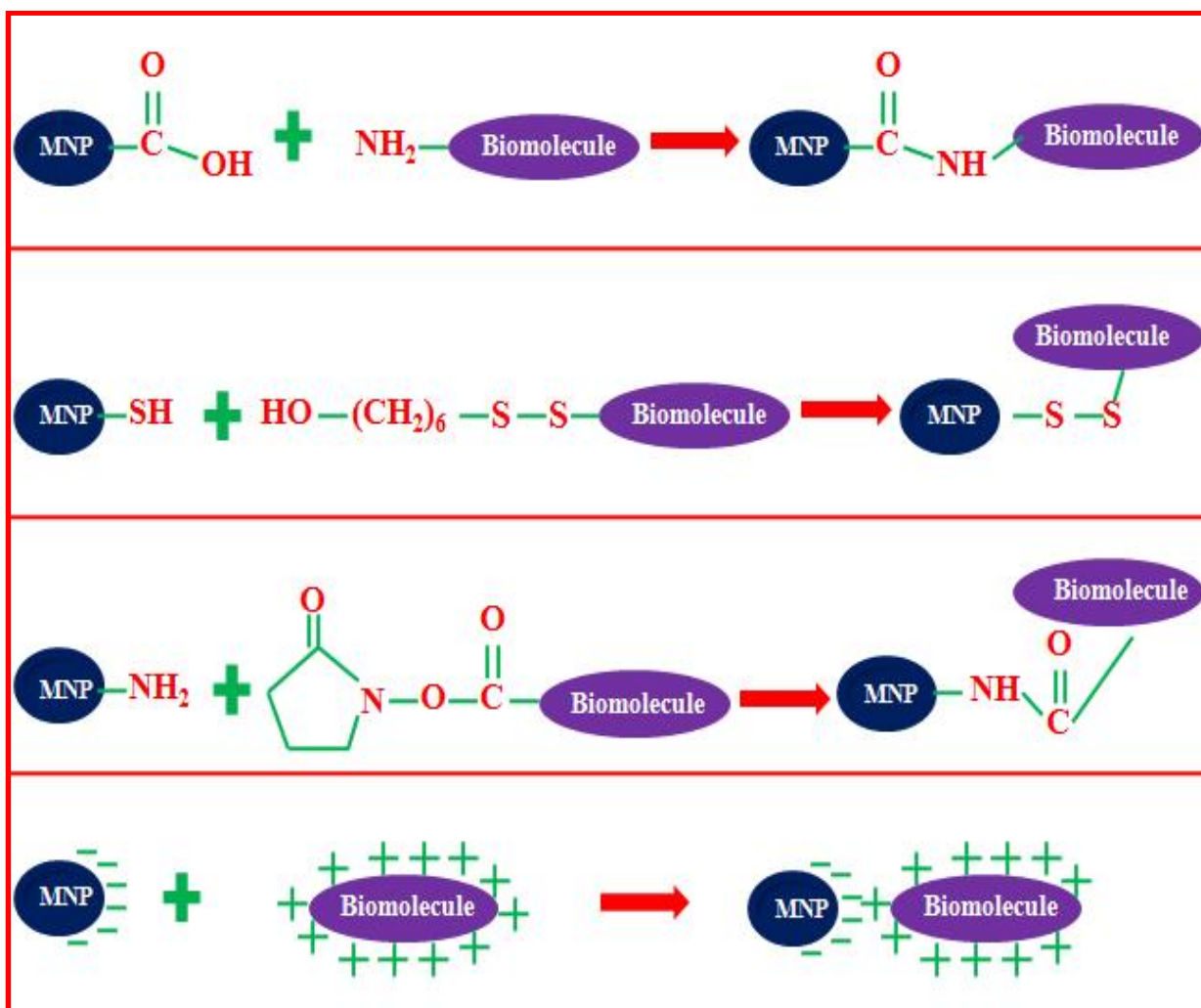


Fig. 2.9 Representative bioconjugation schemes for the attachment of biomolecules on surface of MNPs

Electrostatic interaction is commonly used approach among the various techniques in physical interactions. This electrostatic interaction depends on ionic attractiveness in the opposite charges. The best example is bonding between -vely

charged DNA to +vely charged (catonic) nanoparticles. The covalent linkages are stable and form strong bond between the functional moiety which present on nanoparticles surface and biomolecules. Out of these, some reactions comprise conjugation directly that is click chemistry and coupling reactions of carbodiimide. The functionalization propounds the various functional moieties like aldehyde, sulfhydryl and amino group on nanoparticles surface, promoting the formation of conjugation with biomolecules. This strategy is also applicable for the coupling in amino functionalized nanoparticles and (-COO) group of biomolecule. The click chemistry is another strategy for directly conjugation of biomolecules. The effective and fast reactions which require mild condition gives biocompatible linkage [64-68].

2.7 Tabular representation of materials used for functionalization

Sr. No	Material Used For Functionalization	Properties/Advantages	Application	Reference(s)
Polymers				
1	Dextran	<ul style="list-style-type: none"> Stability Biocompatibility Improves blood circulation time 	<ul style="list-style-type: none"> Hyperthermia MRI of Spinal Cord 	[31, 69-73]
2	Starch	<ul style="list-style-type: none"> Biocompatibility 	<ul style="list-style-type: none"> MRI Drug Delivery Contrasting and imaging 	[7, 74, 75]
3	Chitosan	<ul style="list-style-type: none"> Non toxic Biocompatible Linear Alkaline 	<ul style="list-style-type: none"> Hyperthermia Drug Delivery Tissue Engineering 	[76-80]
4	Pullulan	<ul style="list-style-type: none"> High water solubility Nontoxic Targeting hepatocytes-particle accumulation in the liver 	<ul style="list-style-type: none"> Drug delivery 	[81]

5	Gelatin	<ul style="list-style-type: none"> • Emulsifier • Nontoxic • Natural polymer • Improved bioactivity • Biocompatibility • Excellent carrier capacity for drugs 	<ul style="list-style-type: none"> • Cell Separation 	[82-84]
6	PVP	<ul style="list-style-type: none"> • Stabilizes colloidal solution • Enhances blood circulation time 	<ul style="list-style-type: none"> • Hyperthermia • MRI contrast • Agents 	[26,85,86]
7	Poly (ethyleneglycol) (PEG)	<ul style="list-style-type: none"> • Improves biocompatibility • Water solubility • Blood circulation time 	<ul style="list-style-type: none"> • Hyperthermia • MRI • Gene Transfection • Biosensor 	[43, 44, 87-90]
8	PVA	<ul style="list-style-type: none"> • Prevent conglomeration • Monodispersed 	<ul style="list-style-type: none"> • Hyperthermia • Drug delivery • <i>In vivo</i> imaging • Biosensor 	[39, 91-95]
9	Alginate	<ul style="list-style-type: none"> • Improves stability • Biocompatibility 	<ul style="list-style-type: none"> • Drug delivery 	[81, 96-98]
10	Polymethylmethacrylate (PMMA)	<ul style="list-style-type: none"> • Improves stability • Hydrophilicity 	<ul style="list-style-type: none"> • Drug delivery • Cell separation 	[99, 100]
11	Polyacrylic acid (PAA)	<ul style="list-style-type: none"> • Improves stability • Biocompatibility • Bioconjugation 	<ul style="list-style-type: none"> • Drug delivery 	[101-103]
12	PEI	<ul style="list-style-type: none"> • Hydrophilic • Capable for interactions • Fabrication of stable ferrofluids • Improved cytocompatibility 	<ul style="list-style-type: none"> • Cancer cell separation • Hyperthermia 	[81, 104, 105]
Monomers				
1	Phosphate	<ul style="list-style-type: none"> • Encapsulation of nanoparticles 	<ul style="list-style-type: none"> • Biological applications 	[106]

		<ul style="list-style-type: none"> • Electrostatic stabilization • Sensitive to the pH 		
2	Carboxylate	<ul style="list-style-type: none"> • Affect on the growth of MNPs 	<ul style="list-style-type: none"> • Biological applications. 	[49]
Small molecules				
1	Amines and aminosilanes	<ul style="list-style-type: none"> • Highly water stable • Stabilizer 	<ul style="list-style-type: none"> • Hyperthermia • Separation of DNA 	[107-109]
2	Thiol	<ul style="list-style-type: none"> • Stabilizing agent • Stable under physiological pH 	Drug delivery	[110]
Inorganic material				
1	Silica	<ul style="list-style-type: none"> • Biocompatible • Easily coupled • Stabilized Many prospects for various biological applications 	<ul style="list-style-type: none"> • Sensor • Contrast agents in biomedical • Photoacoustic imaging 	[111, 112]
2	Gold	<ul style="list-style-type: none"> • Completely stable • Magnetic properties of base material remains unchanged 	<ul style="list-style-type: none"> • Drug delivery 	[113]
3	Metal oxides or sulphides	<ul style="list-style-type: none"> • Antioxidant ability 	<ul style="list-style-type: none"> • Hyperthermia • Antibacterial activity 	[55 ,56]
Biological molecules				
1	Enzymes, Antibodies, Protiens, Nucleic Acid	<ul style="list-style-type: none"> • Effective strategy in the biomedical applications 	<ul style="list-style-type: none"> • Targeted drug delivery • Hyperthermia • Mgnetic cell sepperration. 	[114]

References

1. P. Lin, S. Ueng, S. Yu, M. Jan, A. Dak, C. Yu and C. Lin, *Organic lett.*, 2007, 9, 2131-2134.
2. D. Nguyen and K. Kim, *Korean. J. Chem. Eng.*, 2014, 31, 1289-1305.
3. A. Gupta, R. Nalegalkar, V. Vaidya and M. Gupta, *Nanomedicine*, 2007, 2, 23-39.
4. A. Gupta and M. Gupta, *Biomater.*, 2005, 26, 3995-4021.
5. R. Fratila, S. Mitchell, P. Pino, V. Grazu and J. De La Fuente, *Langmuir.*, 2014, 30, 15057-15071.
6. E. Guenin, Y. Lalatonne, J. Bolley, I. Milosevic, C. Platas-Iglesias and L. Motte, *J. Nanoparticle Res.*, 2014, 16, 1-13.
7. R. Hao, R. Xing, Z. Xu, Y. Hou, S. Gao and S. Sun, *Adv. Mater.*, 2010, 22, 2729-2742.
8. C. Weisbecker, M. Merritt and G. Whitesides, *Langmuir.*, 1996, 12, 3763-3772.
9. J. Love, L. Estroff, J. Kriebel, R. Nuzzo and G. Whitesides, *Chem. Rev.*, 2005, 105, 1103-1169.
10. G. Fritz, V. Schadler, N. Willenbacher and N. Wagner, *Langmuir.*, 2002, 18, 6381-6390.
11. D. Napper, *J. Colloid Interface Sci.*, 1970, 32, 106-114.
12. X. Ji, D. Copenhaver, C. Sichmeller and X. Peng, *J. Am. Chem. Soc.*, 2008, 130, 5726-5735.
13. M. Kobayashi, M. Skarba, P. Galletto, D. Cakara and M. Borbovec, *J. Colloid*

- Interface Sci., 2005, 292, 139-147.
14. J. Ortega-Vinusea, A. Martin-Rodriguez and R. Hidalgo-Alvarez, *J. Colloid Interface Sci.*, 1996, 184, 259-267.
 15. B. Hao, R. Xing, Z. Xu, Y. Hou, S. Gao and S. Sun, *Adv. Mater.*, 2010, 22, 2729-2742.
 16. K. Widder, A. Senyei and D. Ranney, *Adv. Pharmacol. Chemother.*, 1979, 16, 213-271.
 17. P. Tartaj, M. Morales, S. Verdaguer and T. Carreno, *J. Phys. D: Appl. phys.*, 2003, 36, 182-197.
 18. J. Cheon, J. Park, J. Choi, Y. Jun, S. Kim, M. Kim. Y. M. Kim and Y. Kim, *Proc. Natl. Acad. Sci. USA*, 2006, 103, 3023-3027.
 19. M. Papisov, A. Bogdanov Jr, B. Schaffer, N. Nossiff, T. Shen, R. Weissleder and T. Brady, *J. Magn. Magn. Mater.*, 1993, 122, 383-386.
 20. B. Graziano, E. Collins, N. McCutcheon, C. Griffith, N. Braunscheidel, T. Perrine and B. Wilem, *Inorganica Chim. Acta.*, 2019, 484, 185-196.
 21. J. Yang, Y. Hu, R. Wang and D. Xie, *Soft Matter.*, 2017, 13, 7840-7847.
 22. S. Pierrat, I. Zins, A. Breivogel and C. Sonnichsen, *Nano Lett.*, 2007, 7, 259-263.
 23. E. Amstad, T. Gillich, I. Bilecka, M. Textor and E. Reimhult, *NanoLett.*, 2009, 9, 4042-4048.
 24. C. Zhang, B. Wangler, B. Morgenstern, H. Zentgraf, M. Eisenhut, H. Untenecker, R. Kruger, R. Huss, C. Seliger, W. Semmler and F. Kiessling, *Langmuir.*, 2007, 23, 1427-1434.

25. H. Lee, S. Lee, C. Xu, J. Xie, J. Lee, B. Wu, A. Koh, X. Wang, R. Sinclair, S. Wang, D. Nishimura, S. Biswal, S. Sun, S. Cho and X. Chen, *Nanotechnol.*, 2008, 19, 165101-165106.
26. S. Jadhav, D. Nikam, V. Khot, N. Thorat, M. Phadatare, R. Ningthoujam, A. Salunkhe and S. Pawar, *New J. Chem.*, 2013, 37, 3121-3130.
27. K. Lee, S. Kim, W. Kim and S. Kim, *Korean. J. Chem. Eng.*, 2002, 19, 480-485.
28. L. Gamarra, G. Brito, W. Pontuschka, E. Amaro, A. Parma and G. Goya., *J. Magn. Magn. Mater.*, 2005, 289, 439-441.
29. N. Thorat, S. Otari, R. Patil, V. Khot, A. Prasad, R. Ningthoujam and S. Pawar, *Colloids Surf. B*, 2013, 111, 264-269.
30. M. Bautista, O. Miguel, M. Morales, C. Serna and S. Verdager, *J. Magn. Magn. Mater.*, 2005, 293, 20-27.
31. V. Khot, A. Salunkhe, N. Thorat, R. Ningthoujam and S. Pawar, *Dalton Trans.*, 2013, 42, 1249-1258.
32. S. Nath, C. Kaittanis, V. Ramachandran, N. Dalal and J. Manuel Perez, *Chem. Mater.*, 2009, 21, 1761-1767.
33. S. Jadhav, D. Nikam, S. Mali, C. Hong and S. Pawar, *New J. Chem.*, 2014, 38, 3678-3687.
34. P. Shete, R. Patil, R. Ningthoujam, S. Ghosh and S. Pawar, *New J. Chem.*, 2013, 37, 3784-3792.
35. T. Neuberger, B. Schopf, H. Hofmann, M. Hofmann and B. Rechenberg, *J. Magn. Magn. Mater.*, 2005, 293, 483-496.

36. J. Lee, T. Isobe and M. Senna, *J. Colloid. Interface. Sci.*, 1996, 177, 490-494.
37. C. Albornoz and S. Jacobo, *J. Magn. Magn. Mater.*, 2006, 305, 12-15.
38. S. Kayal and R. Ramanujan, *Mater. Sci. Eng. C*, 2010, 30, 484-490.
39. A. Salunkhe, V. Khot, N. Thorat, M. Phadatare, C. Sathish, D. Dhawaleb and S. Pawar, *Appl. Surf. Sci.*, 2013, 264, 598-604.
40. V. Thangaraja V. Savitha and S. Jegatheesan, *Int. J. Nanotechnol. Appl.*, 2010, 4, 31-38.
41. E. Kim, K. Lee, Y. Huh and S. Haam, *J. Mater. Chem. B*, 2013, 1, 729-739.
42. C. Yue-Jian, T. Juan, X. Fei, Z. Jia-Bi, G. Ning, Z. Yi-Hua, D. Ye and G. Liang, *Drug Dev. Ind. Pharm.*, 2010, 36, 1235-1244.
43. V. Khot, A. Salunkhe, J. Ruso and S. Pawar, *J. Magn. Magn. Mater.*, 2015, 384, 335-343.
44. D. Nikam, S. Jadhav, V. Khot, R. Ningthoujam, C. Hong, S. Mali and S. Pawar, *RSC Adv.*, 2014, 4, 12662-12671
45. H. Lee, E. Kim, H. Shao, B. Kwak, *J. Magn. Magn. Mater.*, 2005, 293, 102-105.
46. D. Kreller, G. Gibson, W. Novak, G. Van Loon and H. Horton, *J. Colloids Surf. A*, 2003, 212, 249-264.
47. C. Yee, G. Kataby, G. Ulman, T. Prozorov, H. White, A. King, M. Rafailovich, J. Sokolov and A. Gedanken, *Langmuir.*, 1999, 15, 7111-7115.
48. Y. Sahoo, H. Pizem, T. Fried, D. Golodnitsky, L. Burstein, C. Sukenik and G. Markovich, *Langmuir.*, 2001, 17, 7907-7911.

49. C. Liu and P. M. Huang, *Soild Sci. Soc. Am. J.*, 1999, 63, 65-72.
50. K. Gordeyeva, H. Voisin, N. Hedin, L. Bergström and N. Lavoine, *Mater. Chem. Front.*, 2018, 2, 2220-2229.
51. L. Maurizi, A. Papa, L. Dumont, F. Bouyer, P. Walker, D. Vandroux and N. Millot, *J Biomed Nanotechnol.*, 2015, 11, 126-136.
52. S. Banerjee, S. Raja, M. Sardar, N. Gayathri, B. Ghosh, and A. Dasgupta, *J. Appl. Phys.*, 2011, 109, 1-7.
53. C. Bain, E. Troughton, Y. Tao, J. Evall, G. Whitesides and R. Nuzzo, *Am. Chem. Soc.*, 1989, 111, 321-335.
54. S. Hong, H. Son and J. Park, *J. Porphyr. Phthalocyanines*, 2018, 22, 611-618.
55. L. Wang, K. Neoh, E. Kang and B. Shuter, *Biomater.*, 2011, 32, 2166-2173.
56. N.Venkatesha, Y. Qurishi, H. Atreyab and C.Srivastava, *RSC Adv.*, 2016,6,18843-18851.
57. M. Cao, Z. Li, J. Wang, W. Ge, T. Yue, R. Li, V. Colvin and W. Yu, *Trend. Food Sci. Technol.*, 2012, 27, 47-56.
58. B. Samanta, H. Yan, N. Fischer, J. Shi, D. Jerry and V. Rotello, *J Mater Chem.*, 2008, 18, 1204-1208.
59. Y. Iwaki, H. Kawasaki and R. Arakawa, *Anal Sci.*, 2012, 28, 893-900.
60. M. Okuda, J. Eloi, S. Jones, A. Sarua, R. Richardson and W. Schwarzacher, *Nanotechnology.*, 2012, 23, 415601.
61. J. Xie, J. Wang, G. Niu, J. Huang, K. Chen, X. Li and X, Chen, *Chem. Commun.*, 2010, 46, 433-435.

62. S. Laurent, D. Forge, M. Port, A. Roch, C. Robic, L. Elst and R. Muller, *Chem. Rev.*, 2008, 108, 2064-2110.
63. O. Veiseh, J. Gunn and M. Zhang, *Adv. Drug. Deliv. Rev.*, 2010, 62, 284-304.
64. K. Sapsford, W. Algar, L. Berti, K. Gemmill, B. Casey, E. Oh, M. Stewart, I. Medintz, *Chem Rev.*, 2013, 113, 1904-2074.
65. S. McBain, H. Yiu, A. El Haj and J. Dobson, *J. Mater. Chem.*, 2007, 17, 2561-2565.
66. Y. Liu, B. Zhang and B. Yan, *Int. J. Mol. Sci.*, 2011, 12, 4395-4413.
67. J. Gunn, H. Wallen, O. Veiseh, C. Sun, C. Fang, J. Cao, C. Yee and M. Zhang, *Small.*, 2008, 4, 712-715.
68. M. Chastellian, A. Petri and H. Hofman, *J. Colloid. Interface Sci.*, 2004, 278, 353-360.
69. M. Mikhaylova, D. Kim, N. Bobrysheva, M. Osmolowsky, V. Semenov, T. Tsakalacos and M. Muhammed, *Langmuir*, 2004, 20, 2472-2477.
70. M. Bautista, O. Bomati-Miguel, M. Morales, C. Serna and S. Veintemillas-Verdaguer, *J. Magn. Magn. Mater.*, 2005, 293, 20-27.
71. C. Berry, S. Wells, S. Charles and A. Curtis, *Biomaterials*, 2003, 24, 4551-4557.
72. F. Zhao, M. Williams, X. Meng, D. Welsh, A. Coimbra, E. Crown, J. Cook, M. Urban, R. Hargreaves and D. Williams, *Neuroimage*, 2008, 40, 133-147.
73. E. Osborne, T. Atkins, D. Gilbert, S. Kauzlarich, K. Liu and A. Louie, *Nanotechnology*, 2012, 23, 215602.
74. D. Kim, M. Maria, F. Wang, K. Jan, B. Bořrje, Y. Zhang, T. Tsakalacos and M.

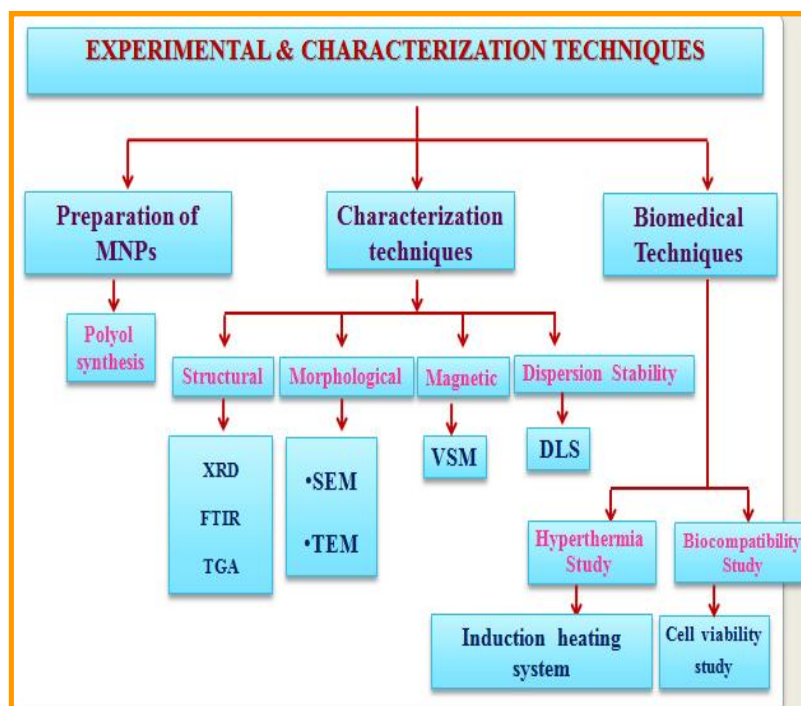
- Muhammed, *Chem. Mater.*, 2003, 15, 4343-4351.
75. W. Wang and Z. Zhang, *J. Disper, Sci. Technol.*, 2007, 28, 557-563.
76. G. Li, K. Huang, Y. Jiang, P. Ding and D. Yang, *Colloids Surf. A Physicochem. Eng. Asp.*, 2008, 320, 11-18.
77. G. Li, Y. Jiang, K. Huang, P. Ding and L. Yao, *Colloid. Surf. A*, 2008, 320, 11-18.
78. E. Kim, H. Lee, B. Kwak and B. Kim, *J. Magn. Magn. Mater.*, 2005, 289, 328-330.
79. P. Shete, R. Patil, N. Thorat, A. Prasad, R. Ningthoujam, S. Ghosh and S. Pawar, *Appl. Surf. Sci.*, 2013, 288, 149-157.
80. A. Javid, S. Ahmadian, A. Saboury, S. Kalantar and S. Rezaei-Zarchi, *Chem. Biol. Drug Des.*, 2013, 82, 296-306.
81. S. Laurent, J. Bridot, L. Vander Elst and R. Muller, *Future Med. Chem.*, 2010, 2, 427-449.
82. D. Olsen, C. Yang, M. Bodo, R. Chang, S. Leigh, J. Baez, D. Carmichael, M. Perala, E. Hamalainen, M. Jarvinen and J. Polarek, *Adv. Drug. Deliv. Rev.*, 2003, 55, 1547-1567.
83. B. Gaihre, M. Khil, D. Lee and H. Kim, *Int. J. Pharm.*, 2009, 365, 180-189.
84. B. Gaihre, M. Khil, H. Kang and H. Kim, *J. Mater.Sci.: Mater. Med.*, 2009, 20, 573-581.
85. P. Rose, P. Praseetha, M. Bhagat, P. Alexander, S. Abdeen and M. Chavali, *Technol. Cancer Res.*, 2013, 12, 463-472.
86. A. D'Souza, R. Schowen and E. Topp, *J Cont. Rel.*, 2004, 94, 91-100.

87. R. Bachmann, R. Conrad, B. Kreft, O. Luzar, W. Block, S. Flacke, D. Pauleit, F. Traiber, J. Gieseke and K. Saebo, *J. Magn. Reson. Imaging*, 2002, 16, 190-195.
88. Z. Stephen, C. Dayringer, J. Lim, R. Revia, M. Halbert, M. Jeon, A. Bakthavatsalam, R. Ellenbogen and M. Zhang, *ACS Appl. Mater. Interfaces*, 2016, 8, 6320-6328.
89. M. Phadatare, V. Khot, A. Salunkhe, N. Thorat and S. Pawar, *J. Magn. Magn. Mater.*, 2012, 324, 770–772.
90. M. Anbarasu, M. Anandan, E. Chinnasamy, V. Gopinath and K. Balamurugan, *Spectrochim. Acta. A*, 2015, 135, 536-539.
91. H. Pardoe, W. Chua-anusorn, T. Pierre, J. Dobson, *J. Magn. Magn. Mater.*, 2001, 225, 41-46.
92. M. Chastellain, A. Petri and H. Hofmann, *Colloid Interface Sci.*, 2004, 278, 353-360.
93. A. D'Souza, R. Schowen, E. Topp, *J. Control. Release*, 2004, 94, 91-100.
94. S. Kayal and R. Ramanujan, *Mater. Sci. Eng. C*, 2010, 30, 484-490.
95. H. Ardiyanti, E. Suharyadi, T. Kato and S. Iwata, *AIP Conf. Proc.*, 2016, 1725, 020007.
96. H. Ma, Y. Xu, X. Qi, Y. Maitani and T. Nagai, *Int. J. Pharm.*, 2006, 354, 217-226.
97. M. Morales, P. Finotelli, J. Coaquira, M. RochaLeaño, C. Diaz-Aguila and E. Baggio-Saitovitch, *Mater. Sci. Eng. C*, 2007, 28, 253-257.
98. H. Ma, Y. Xu, X. Qi, Y. Maitani and T. Nagai, *Int. J. Pharm.*, 2008, 354, 217-

- 226.
99. D. Zhu, F. Wang, M. Han, H. Li and Z. Xu, *Chin. J. Inorg. Chem.*, 2007, 23, 2128-2132.
100. L. An, Z. Li, Y. Wang and B. Yang, *Chem. J. Chin. Univ.*, 2006, 27, 1372-1379.
101. G. Shan, J. Xing, M. Luo and H. Liu, J. Chen, *Biotechnol. Lett.*, 2003, 25, 1977-1981.
102. A. Arbab, L. Bashaw, B. Miller, E. Jordan, B. Lewis, H. Kalish and J. Frank, *Radiology*, 2003, 229, 838-846.
103. K. Burugapalli, V. Koul and A. Dinda, *J. Biomed. Mater. Res.*, 2004, 68, 210-218.
104. M. Calatayud, C. Riggio, V. Raffa, B. Sanz, T. Torres, M. Ibarra, C. Hoskins, A. Cuschieri, L. Wang, J. Pinkernelle, G. Keilhoff and G. Goya, *J. Mater. Chem. B*, 2013, 1, 3607-3616.
105. H. Cai, X. An, J. Cui, J. Li, S. Wen, K. Li, M. Shen, L. Zheng, G. Zhang and X. Shi, *ACS Appl. Mater. Interfaces*, 2013, 5, 1722-1731.
106. S. Mohapatra and P. Pramanik, *S Colloids Surfaces A: Physicochem. Eng. Aspects*, 2009, 339, 35-42.
107. K. Barick, M. Aslam, Y. Lin, D. Bahadur, V. Pottumarthi, V. Prasad, P. Vinayak, Dravid, *J. Mater. Chem.*, 2009, 19, 7023-7029.
108. P. Ghutepatil, A. Salunkhe, V. Khot, B. Thombare and S. Pawar, *Asian J. Chem.*, 2019, 31, 1081-1086.
109. P. Ghutepatil, A. Salunkhe, V. Khot and S. Pawar, *Chem. Pap*, 2019, 1-9.

110. L. Maurizi, H. Bisht, F. Bouyer and N. Millot, *Langmuir.*, 2009, 25, 8857-8859.
111. C. Zhang, B. Wängler and B. Morgenstern, *Langmuir.*, 2007, 23, 1427-1434.
112. R. Alwi, S. Telenkov, A. Mandelis, T. Leshuk, F. Gu, S. Oladepo and K. Michaelian *Biomed. Opt. Express*, 2012, 3, 2500-2509.
113. S. Silva, R. Tavallaie, L. Sandiford, R. Tilley and J. Gooding, *Chem. Commun.*, 2016, 52, 7528-7540.
114. K. Hola, Z. Markova, G. Zoppellaro, J. Tucek and R. Zboril. *Biotechnol. Adv.*, 2015, 33, 1162-1176.

Experimental and Characterization Techniques



Nanotechnology offers vast potential for increasing the performance of products and processes. Moreover, it will enable us to develop completely new products that will improve our quality of life in many respects.

-Paul McEuen

3.1 Introduction

MNPs are fascinating the many researchers and scientists these days because of their in biomedical implementations [1-6]. A synthesis of nanoparticles is needed to upgrade physical as well as chemical properties of nanoparticles and make them appropriate for biomedical implementations [7]. MNPs can be synthesized by using biological, chemical and physical processes.

The characterization of synthesized MNPs is necessary to understand the effect of synthesis and decide a usability of nanoparticles for biomedical applications depending on their characteristics. The MNPs can be characterized by phase and structural analysis, morphological analysis, magnetic properties analysis, dispersion stability analysis, induction heating or hyperthermia analysis and biocompatibility analysis [8]. Here, several characterization techniques have been discussed with their working principle.

3.2 Synthesis of Magnetic nanoparticles

MNPs can be synthesized by physical, chemical and biological approaches. Chemical method supports the manipulation of sample particle at atomic and molecular scale. Chemical methods provide the flexibility in synthesizing and designing new material, which will be converted in purified form. The main benefit of chemical method over other processes is superior chemical homogeneity as it involves mixing at molecular level. Several chemical methods included co-precipitation, polyol, hydrothermal, combustion, microemulsion and thermal decomposition are available to synthesize of magnetic material for biomedical applications. These methods are useful to synthesize nanoparticles in uniform composition and narrow size distribution. Synthesis method should produce controlled particle size, shape, distribution, crystal structure nanoparticles.

Polyol method is very powerful approach for preparation of non agglomerated nanoparticles with required size and shape, which can be obtained by controlling the

kinetic of the precipitation. Polyol like ethylene glycol, diethylene glycol, triethylene glycol etc. acts as solvent, reducing agent and complexing agent for metallic precursor. Metal precursor could be soluble in polyol. The mechanism behind this synthesis process is as: solid metal precursor dissolution used metallic species reduction, extension of nuclei and metallic phase nucleation. Distribution with narrow sized nanoparticles can be obtained by achieving complete separation of nucleation and avoiding aggregation of metal particles during nucleation. Non-aggregated magnetite nanoparticles can be directly produced by using polyols including ethylene glycol (EG), temperature using modified polyol process. Here, only reaction with DEG yields nanoparticles which are non-clustered having uniform shape. Transmission electron microscopy (TEM) analysis confirms that MNPs prepared by polyol methods are monodispersed in nature.

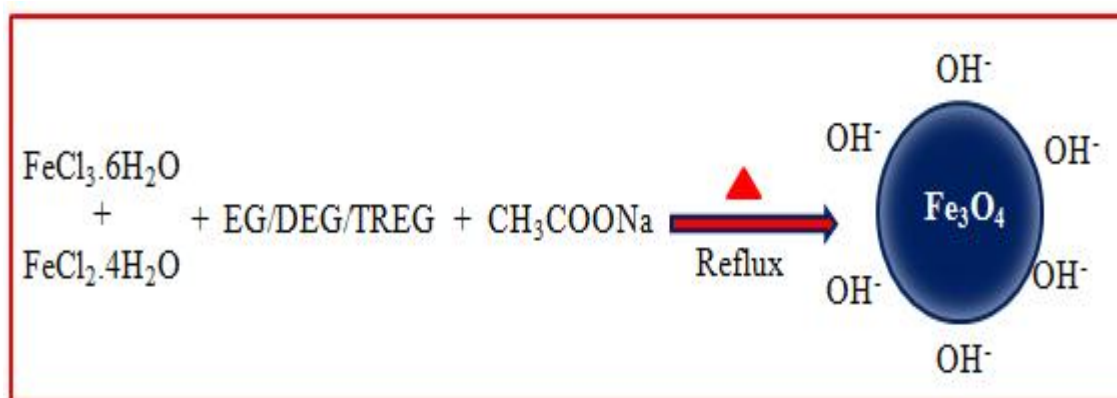


Fig. 3.1 Synthesis of MNPs using polyol method

In advanced polyol method, Sun *et al.* have prepared uniformly sized magnetite nanoparticles in which oleic acid and oleylamine is used and at high-temperature reduction of $\text{Fe}(\text{acac})_3$ (acac=acetylacetonate) by 1, 2-hexadecanediol. Variation of reaction conditions and seed-mediated growth is used to adjust particle diameter up to 20 nm.

3.3 Characterization techniques

3.3.1 X-ray diffraction technique (XRD)

The X-ray Diffraction (XRD) is basic, powerful and non destructive method, which is widely used for characterization of nanoparticles. The XRD analysis is used to get the information about structure, phase, particle size, phase equilibria and structural parameters like lattice parameter, crystal defects and crystallite size. Therefore, XRD pattern is impression of crystalline material [9]. In XRD, diffraction of X-rays occurs exclusively when a wavelength and wave motion is in same order of magnitude as the repeat distance in the midth of scatterings centers. In 1895, Wilhelm Roentgen had discovered the XRD technique [10] and Fig. 3.2 shows the schematics representation of the X-ray diffractometer.

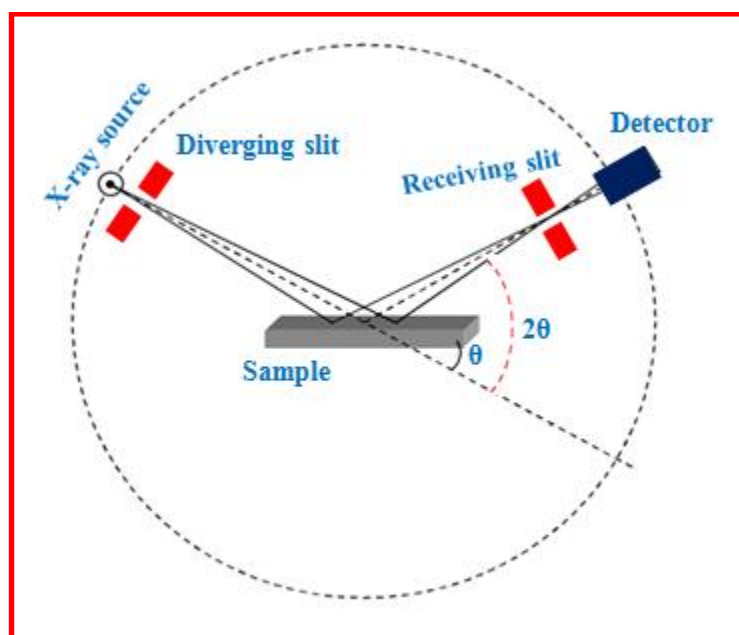


Fig. 3.2 schematics representation of X-ray diffractometer

The diffraction from crystalline material was studied by Bragg and he formulated by mathematical expression as given in equation (3.1). It is also called as Bragg's law [11].

$$2d \sin \theta = n\lambda \dots \dots 3.1$$

Where,

θ = diffraction angle

d = interplanar spacing

n = order of diffraction

λ = wavelength of x-ray

During the experiment, either λ or θ can be continuously varied to satisfy the Bragg's condition. There are mainly three types of diffraction methods distinguished based on the different quantities are the Laue method, Rotating crystal method and Powder method. In Laue diffraction method, λ value is varied continuously and θ value is fixed during the experiment. In powder method, crystal fine powder is situated in the monochromatic X-ray beam. Powder particles are aggregated and oriented randomly with incident beam. Rotation is required as materials having micro crystals and arranged impossible orientations like (100) planes and (110) reflections and so on. According to Bragg's law we get constructive interference of x-rays can occur only at particle Bragg's angle θ for particular d value. There should be destructive interference for constructive interference of x-ray and intensity of diffracted beam should be less [12].

Fig. 3.3 shows the typical X-ray diffractometer and designed as the Bragg-Brentano geometry. A diffractometer detect diffracted X-rays using source of X-ray. For crystalline solid, crystal structure and phase formation is confirmation takes place by x-ray diffraction studies using diffracted x-rays direction, which give information about atomic level arrangements. The X-rays reflect from a series of parallel planes in which three indices h , k and l are used define the orientation as well as interplanar spacing of planes. Set of planes with these indices cut a -axis in h sections, the b axis in k sections and the c axis in l sections in unit cell. The planes parallel to corresponding axis can be indicated by zero.

Obtained whole destructive interference at $\theta \pm d\theta$ if size of diffracting tiny crystal is small, which widens the peak which corresponds with diffracted beam in direct proportion with size of the tiny crystal. Calculation of the particle size carried out by Scherrer equation (3.2).

$$D = \frac{0.9 \lambda}{\beta \cos \theta_B} \dots \dots 3.2$$

Where, D represents particle size, θ_B represents diffraction angle, λ represents the wavelength of X-rays and β line broadening at Full Width at Half Maxima (FWHM).



Fig. 3.3 XRD instrument

3.3.2 Fourier transform infrared spectroscopy (FTIR)

FTIR gives details about appearance of particular chemistry and is used for qualitative analysis of organic material and inorganic substances. Fourier-transform infrared spectroscopy is originated from reality that Fourier transform is necessary to

transmute the raw data to definite spectrum. FTIR technique is depended on molecular spectroscopy principle, where specific molecules engross light energy of particular wavelengths. It provides phase confirmation based on presence octahedral and tetrahedral molecular vibrations [13]. The successful anchoring of coating material on surface of MNPs is confirmed by FTIR technique. Fig. 3.4 shows the typical FTIR instrument.



Fig. 3.4 FTIR instrument

Fig. 3.5 shows the basic working principle of FTIR technique. Relying on pattern of bond and elements, molecular bonds vibrate at various frequencies and there are various particular frequencies at which it can vibrate for any given bond. The bond can be excited by having absorbed light energy to increase frequency of molecular vibrations. The light energy resolved by wavelength should be precisely same the difference in energy between lower state and higher state for any transition between two states [14]. The band intensities can be exhibited either as transmittance (T) or absorbance (A) and also IR encloses a spectral region from visible spectrum to the microwave in the electromagnetic spectrum. FTIR is mainly based on Michelson interferometer. Fig.3.5 is of typical spectrophotometer which is having three main

components i.e. Radiation source (Nernst filament ($\text{ZrO}_2 + \text{Y}_2\text{O}_3$) or Globar (SiC), Optical path means Monochromator and Detectors.

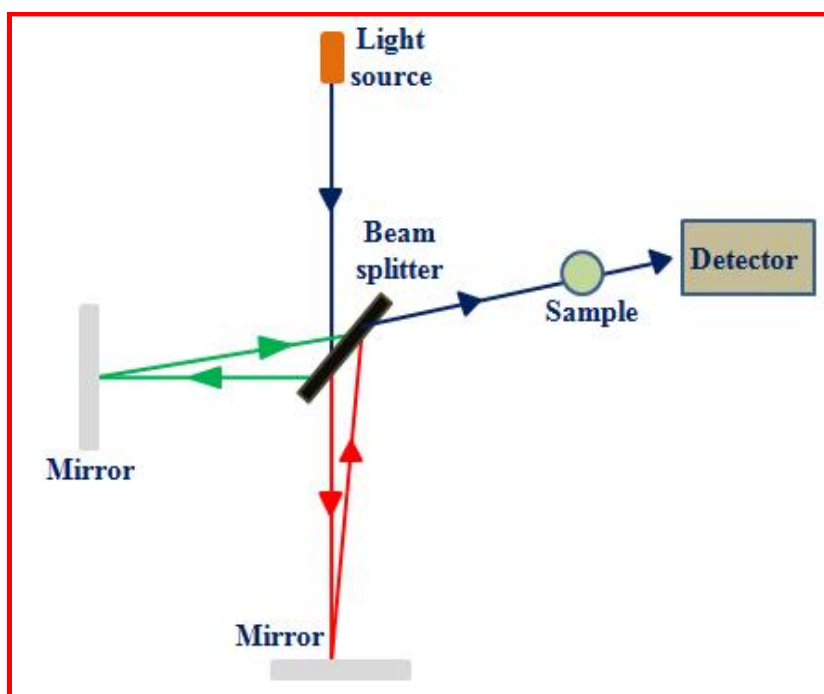


Fig. 3.5 Basic working principle of FTIR system

3.3.3 Thermogravimetric analysis (TGA)

TGA is used to measure a weight loss or gain of material as function of time or function of increasing temperature in an atmosphere of various gases or in vacuum. This analysis is also used to discover composition of material and to confirm stability of the material at high temperature. TGA can be applied in forensic work or for examination of water. Inorganic materials, metals, polymers plastics, ceramics, glasses and composite materials are analyzed using TGA. Powder form of sample used for analysis so that internal sample temperature remains adjacent to measured gas temperature [10]. Isothermal Thermogravimetry, Quasistatic Thermogravimetry, Dynamic Thermogravimetry these are the three types of thermogravimetry. Fig. 3.6 shows the schematic representation of TGA instrument.

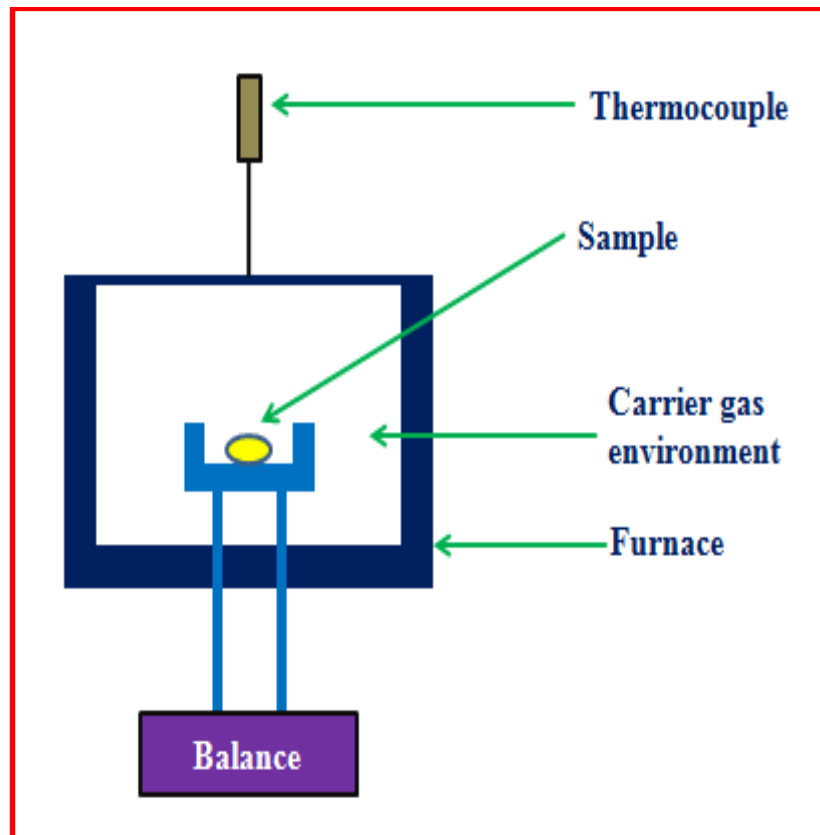


Fig. 3.6 Schematic representation of TGA

In the TGA analysis testing specimen can be placed in pan and this pan is attached to micro balance and then it is heated for a specific time in a control manner. Air or inert gases can be used as atmosphere to avert oxidation of material. Plot of weight change verses temperature is used to present result of experiment. Specifications of the instrument are Transanalytical instrument mode (SDT 2960) was used for thermal study.

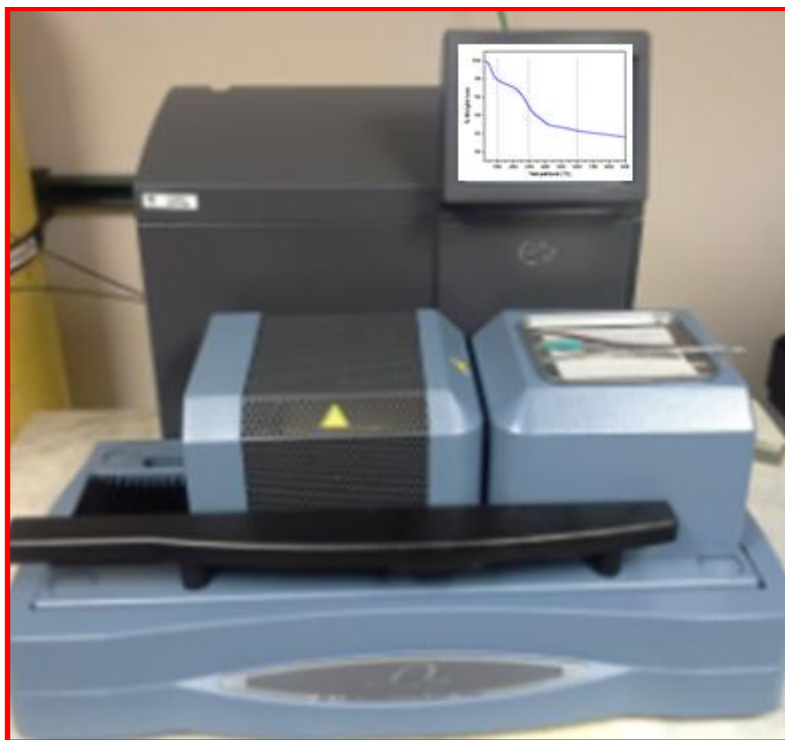


Fig. 3.7 Thermogravimetric analysis measurement unit

In Differential thermal analysis techniques, sample material is subjected to a programmed temperature change to study how it affects on the sample material. The difference in behavior between the sample material and static reference material is examined. The latent heat of phase transition is absorbed as soon as the material changes state, crystal form and temperature of material lags behind that of reference material. In Differential scanning calorimetry, the variation in energy inputs into a substance and a reference material is constantly recorded as a function of temperature and the substance and reference material are subjected to a controlled temperature program [9].

3.3.4 Scanning electron microscopy (SEM)

Surface of topography and morphology of specimen can be studied SEM. SEM is also used to conduct the analysis of point locations selected. This technique can be

convenient in semi quantitatively or qualitatively to discover chemical compositions, crystal orientations and crystalline structure.

SEM is based on principle that material to be analyzed is focused on a beam of electron. The elastic and inelastic scattering is generated when a beam of electrons interconnect with material atoms. The images are formed when signals transmit to the detector and cathode ray tube through an amplifier [15].



Fig. 3.8 Scanning electron microscopy instrument

Field Emission Scanning Electron Microscopy (FE-SEM) is a very powerful technique in the field of material science. For the investigation of molecular structure of surface as well as their electronic properties this technique is very useful. The electrons are triggered by source are accelerated in field gradient under vacuum and these accelerated electron beam get across electromagnetic lenses, which focuses on sample. The several types of electrons are emitted from specimen because of the bombardment. The detector grasp secondary electron and surface sample image is collected by measuring secondary electron intensity to scan primary electron beam.

The image gets displayed on a screen of monitor after the construction. The specification of the instrument used for our investigation is FESEM (Hitachi S-4800).

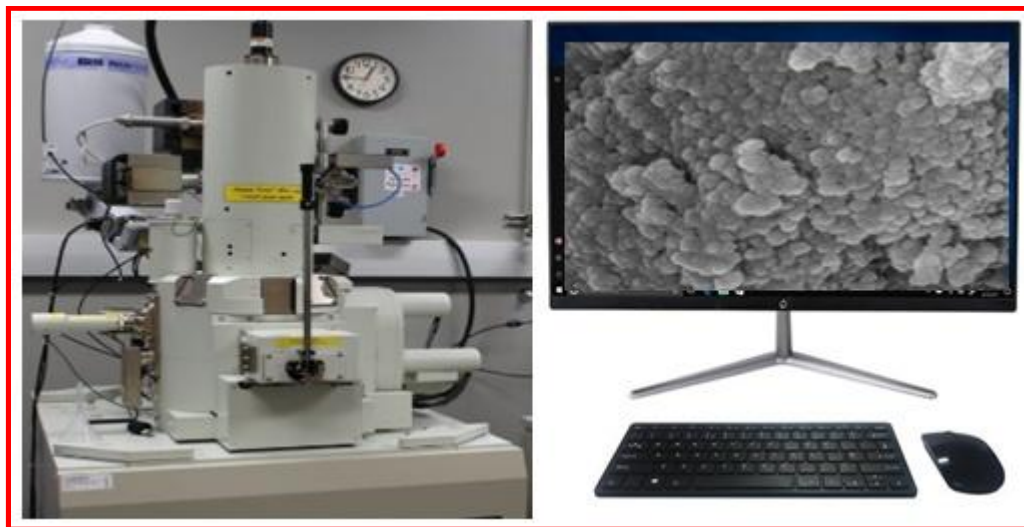


Fig. 3.9 FE-SEM Instrument

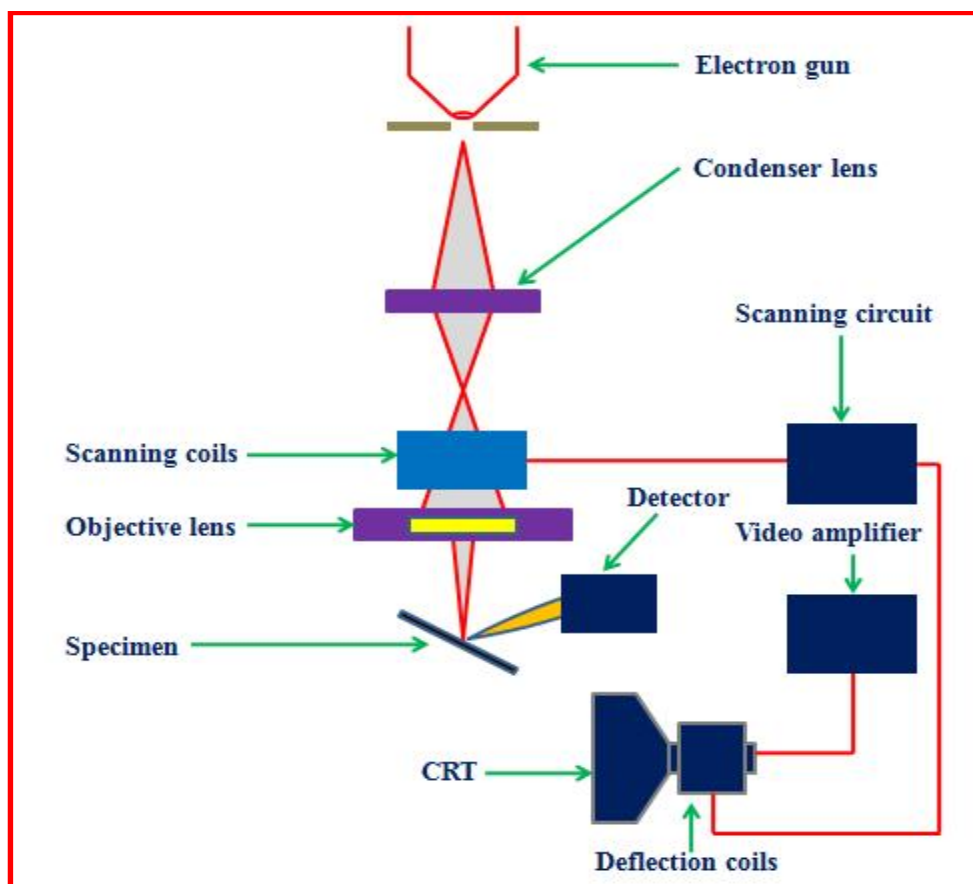


Fig. 3.10 Schematic representation of FESEM

3.3.5 Transmission electron microscopy (TEM)

The particle measurement and physical properties of material is measured by using TEM. It also provides details about particle size distribution. In TEM, a high powered beam generated from electron source is used and it is passed across coherent lens for focusing the beam of object. The transmitted portion is concentrated by coherent lens produce the image. TEM instrument contains sample chamber, electron gun, condenser, projector lenses, objective and vaccum [16, 17]. In the conventional instrument of TEM for the construction or production of image it uses transmitted or scattered beam. The specification of instrument used for our investigation is HRTEM (TEM, JEM–2100F Model, Japan).

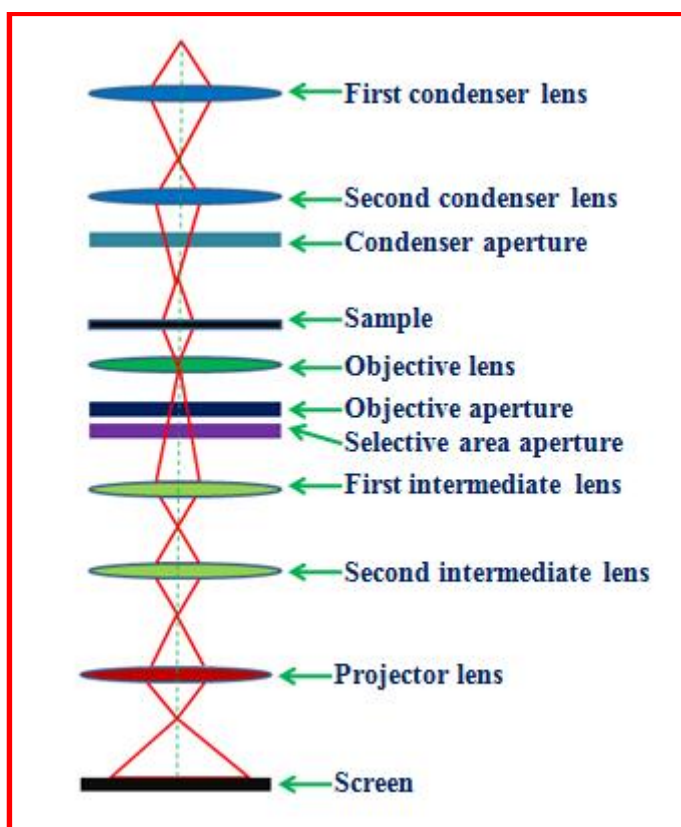


Fig. 3.11 Schematic representation of TEM

The separation of material in water solvent is required to form colloidal solution in TEM technique. Drop can be located on dried and conducting grid is used for analysis. Material to be analyzed must be thin and in between range of 0.1 and 1.9 μm .



Fig. 3.12 TEM instrument

3.3.6 Vibrating sample magnetometer (VSM)

Magnetic field, time and temperature are studied as function of magnetic characteristics using VSM. VSM technique follows Faraday's law i.e. electric field will be produced by varying magnetic flux and this can be expressed as in equation (3.3).

$$\varepsilon = -N \frac{d}{dt}(BA \cos \vartheta) \dots \dots 3.3$$

Where, N is number related with turns in coil, the A represents area under coil turn and θ is an angle between direction normal to a coil surface and B field. [18].

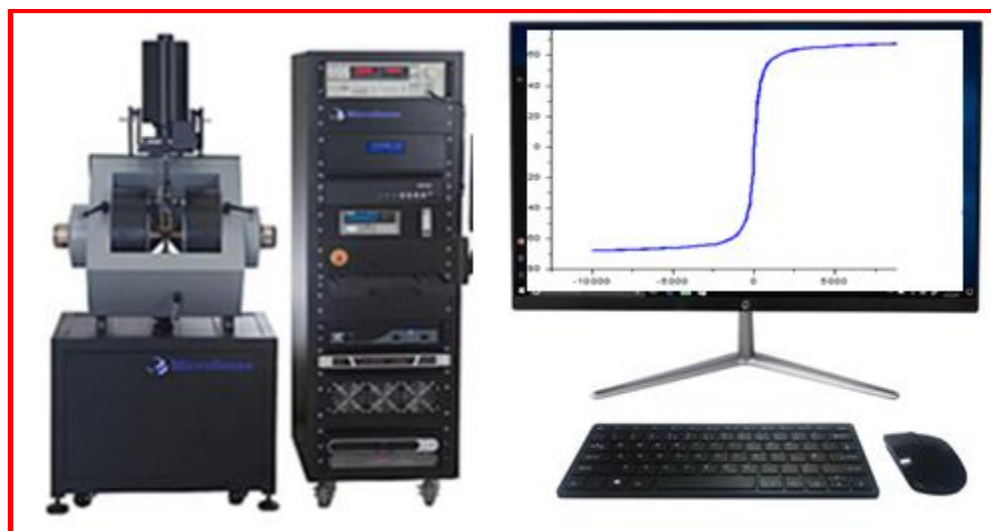


Fig. 3.13 Vibrating sample magnetometer instrument

Material to be studied is located on long rod in steady magnetic field and applied external magnetic field magnetizes the material. Magnetic field around the material is generated by magnetic dipole-dipole moment and it is called as magnetic stray field. Magnetic stray field changes as set up of pick up coils to sense same and function of time. The detection coils voltage can be induced by oscillatory motion of magnetized material. A trans-impedance amplifier amplifies an induced current. The magnetization of material can be showed using software and magnetization can be depended on the strength of magnetic field.

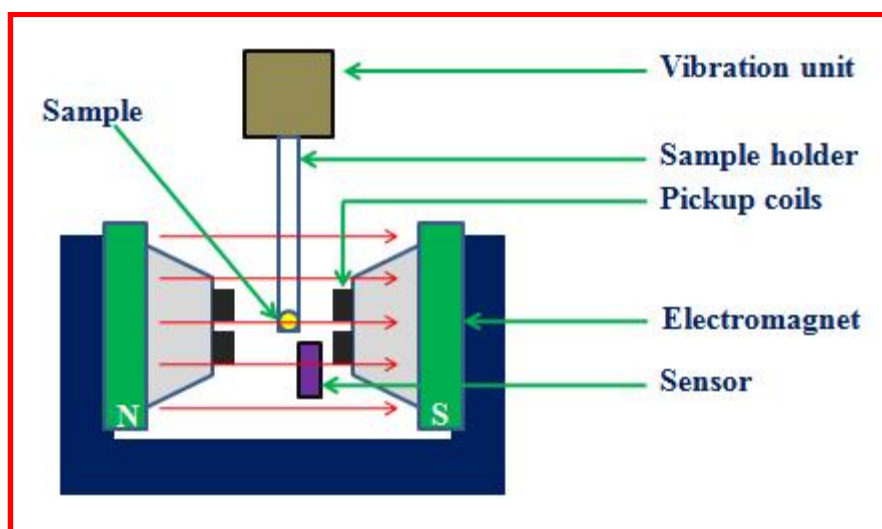


Fig. 3.14 Schematic representation of VSM**SQUID-VSM**

Magnetic properties of tiny material over range of temperatures and magnetic fields are being studied using analytical instrument called quantum design magnetic property measurement system (MPMS). It provides computerized control and data collection. There are few analytical techniques used in SQUID-VSM over standard VSM to optimize a speed and sensitivity. Material vibration takes place at known frequency and sensitive detection is employed for data collection and rejection of factitious signals. The strength of signal produced by a material is independent on the vibration frequency unlike conventional non-superconducting VSM technique. It depends only on magnetic moment of material, sensitive design of SQUID detection circuit and vibration amplitude. In SQUID-VSM, a superconducting magnet is used to subject the material to magnetic fields up to 70 kOe. Material chamber, SQUID and liquid helium is used to cool magnet by giving temperature control of sample in between range of 400 to 1.8 K. System operates properly only if liquid helium and liquid nitrogen cryogenics are in use [19].

**Fig. 3.14** SQUID-VSM instrument

3.3.7 Dynamic light scattering (DLS)

The DLS is a very valuable technique and having too much weightage in the field of biomedical. The use of this DLS technique gives information about colloidal stability and aggregation of nanoparticles. The size of nanoparticles in solution can be characterized by using DLS technique. It is mostly suitable to capture tiny changes in mean diameter because of adsorbed layers on surface of MNPs. DLS measures the Brownian motion. Brownian motion states that the hydrodynamic diameter of the particles and hydrodynamic diameter includes physical particles as well as coating on the surface and shell of solvent strongly anchored to surface. The particles which are small in size less than 1 μm can be characterized by DLS technique [20-22].

Brownian motion is responsible for the suspension of macromolecules in a liquid media undergo because of random collisions with solvent 4π molecules. Here, probability density function can be expressed by equation (3.4) [23].

$$P(r, t|0,0) = (4\pi Dt)^{-\frac{3}{2}} \exp(-r^2 / 4Dt) \dots \dots 3.4$$

where, D is the diffusion constant.

The size of particle is measured in manner with Stokes-Einstein formula as expressed in equation (3.5) [24].

$$D = k_B \frac{T}{6\pi\eta a} \dots \dots 3.5$$

where, k_B is the Boltzmann constant, a is the radius, T represents the temperature (Kelvin degrees) and η represents viscosity of solvent.

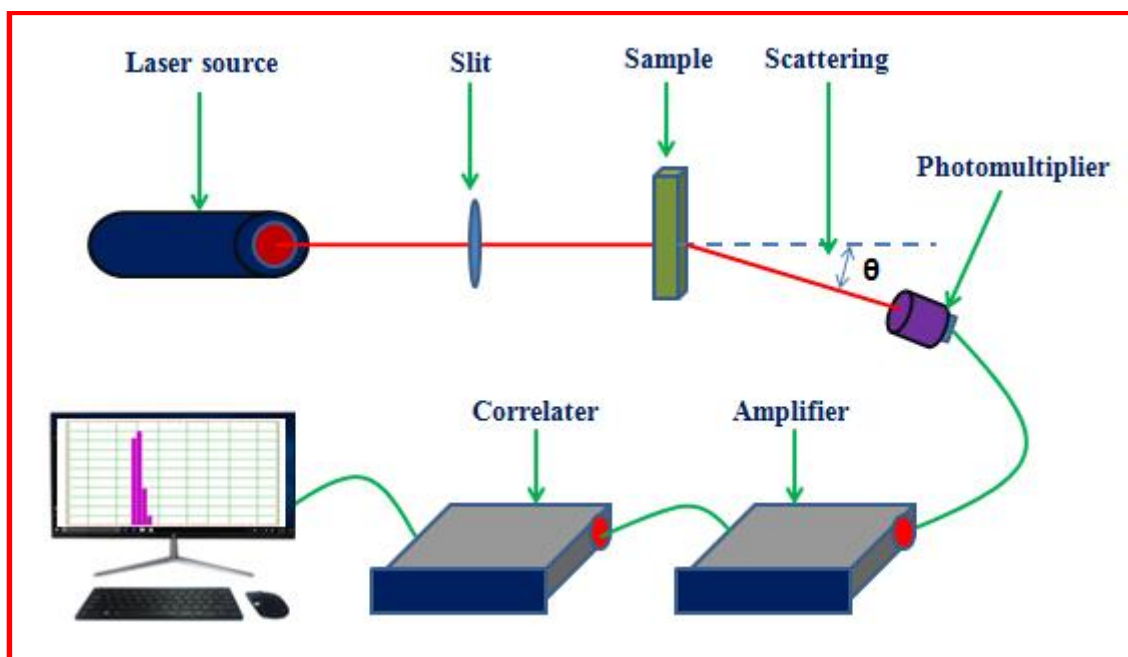


Fig. 3.15 Schematic representation of DLS

In present investigation, a DLS instrument PSS/NICOMP 380 ZLS is used. Electric field of the light induces an oscillating polarization of electrons in the molecules, when light impinges on matter.



Fig. 3.16 DLS instrument

3.3.8 Induction heating system

There are many therapies available for cancer treatment but magnetic induction hyperthermia is very popular and effective therapy among other therapies. Magnetic

induction hyperthermia is most encouraging therapy for cancer treatment and it has generated lot of interest in medical field. Infectious tumor tissues are extra responsive to induced heat compared to usual cell. It is controllable and localized heating method, which does not expose with to be heated parts. Induction heating method is used in thermal therapy to produce exterior magnetic fields and to control temperature of fluid *in vivo* or *in vitro* applications [25, 26].

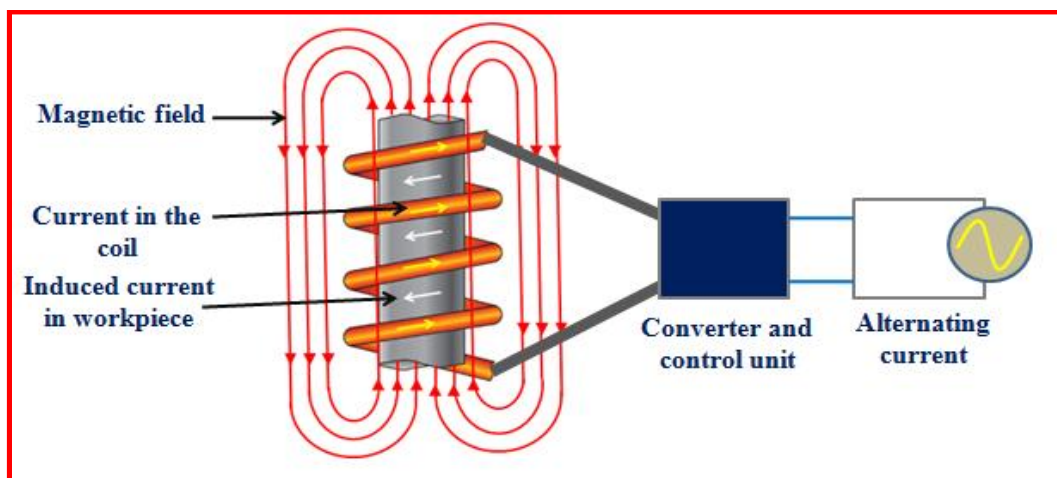


Fig. 3.17 Schematic representation of induction heating system

Induction heating system is depended on Faraday's law [27]: "The amount of voltage created is equal to the change in magnetic flux divided by the change in time". A large AC can be carried out through a coil at high frequency electricity source and this is work coil. The intense and high speed changing magnetic are generated in space into work coil. This alternating magnetic field frequently demagnetizes and magnetizes iron crystals. The material having vast area into their B-H curve will have greatest loss for that material [28, 29].



Fig. 3.18 Induction heating system instrument

To study potential of material for hyperthermia application, induction heating was performed in a plastic micro centrifuge 1.5 mL tube using an induction heating unit (Easy Heat 8310, Ambrell; UK) with a 6 cm diameter and 4 turns heating coil. The MNPs are suspended in 1 mL of distilled water was placed at the center of the coil and the applied frequency was 265 kHz. The heat dissipation by magnetic fluid with field is measured in terms of specific absorption rate (W/g), defined as in equation (3.6):

$$\text{SAR} = C \left(\frac{dT}{dt} \right) \left(\frac{m_s}{m_m} \right) \dots \dots \dots 3.6$$

Where, C is specific heat capacity of suspension ($4.186 \text{ J/ (g } ^\circ\text{C)}$), (dT/dt) denote an initial slope of temperature versus time graph, m_s represents mass of suspension and m_m is the mass of the magnetic material in suspension.

3.3.9 Biocompatibility study:Cytotoxicity assay

For biomedical applications, MNPs are enhanced to study interaction with cell and it is required to ensure absence of any adverse effect on cell. The biocompatibility of MNPs is a significant factor in biological applications. In depth study of biocompatibility is required as there is possibility of toxic effects of nanoparticles on human health. Toxicity of MNPs is controlled by particle shape, size, surface charge, composition and stability [30]. In biocompatibility study, cytotoxic assay is used to select MNPs which can be used in redox active and adsorb dyes. Multiple tests need to be conducted to ensure valid conclusion. The material samples can be forwarded for doing *in vivo* tests only after biocompatibility study display no or minimum effects in used concentrations. Assays like LDH (lactate dehydrogenase), MTT assay, Trypan blue and identification of cytokine [31]. All potential interferences should be considered while choosing the correct assay to stay way from obtaining false negative and false positive results. Assay used to discover cytotoxicity should be valid for to be tested materials. For example, neutral red test depends on adsorption of dye to discover living cells [32, 33]. In this work, MTT assay has been used to reduce the errors and to attain the quality data. It is simple, inexpensive with ease of analyse.

Type of cell and organ can be responsible for toxic effect of nanoparticles. This may be due to variation in physiology of cell, proliferation state and membrane characteristics. MNPs are generally initiated into a body through intravenous, subcutaneous, intra-muscular or intraocular pathway in biomedical applications. Several cell types based on variety of affected organs ranging from liver, nervous system, blood and kidney can be selected for MNPs cytotoxicity study. The conditions of cells and number optimization are important factors in appropriate selection of cell type process for cytotoxic study. In this study, L929 mouse fibroblast

cell lines and MCF7 (adenocarcinoma cell line of human breast) cell lines have been selected for cytotoxicity evaluation for nanoparticles [34, 35].

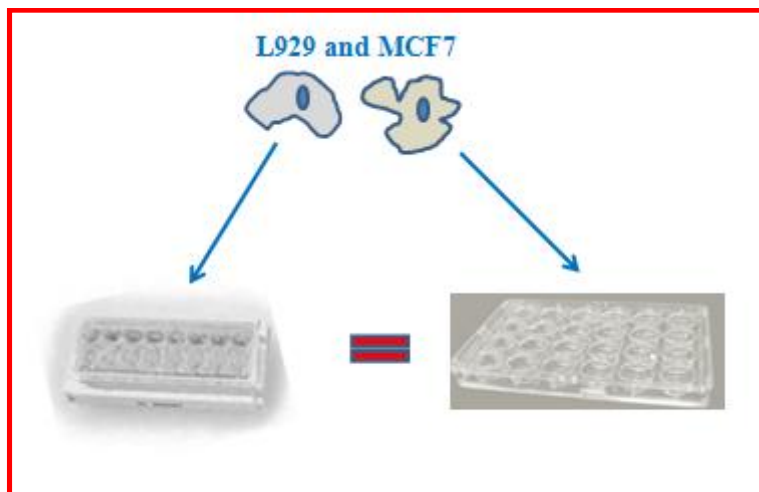


Fig. 3.18 Biocompatibility study on L929 mouse fibroblast cell lines

It is necessary to develop a standard for appropriate dose metrics for cytotoxicity studies. *In vitro*, the dose for MNPs is defined at several levels respected to mode of action and site of action. These dose metrics can have the advantage of particle dependent dissimilarity in cellular uptake. Dispersion state of nanoparticles is vital factor for nanotoxicological studies. Therefore, appropriate dose of nanoparticles should be selected for cytotoxicity assay to understand toxic effects of MNPs [36, 37].

References

1. H. Pardoe, W. Chua-anusorn, T. Pierre and J. Dobson, *J. Magn. Magn. Mater.*, 2001, 225, 41-45.
2. S. Son, J. Reichel, B. He, M. Schuchman and S. Lee, *J. Am. Chem. Soc.*, 2005, 127, 7316-7317.
3. Y. Jun, Y. Huh, J. Choi, J. Lee, H. Song, S. Kim, S. Yoon, K. Kim, J. Shin, J. Suh and J. Cheon, *J. Am. Chem. Soc.*, 2005, 127, 5732-5733.
4. E. Allard, C. Passirani and J. Benoit, *Biomaterials*, 2009, 30, 2302-2318.
5. X. Lasheras, M. Insausti, I. Muro, E. Garaio, F. Plazaola, M. Moros, L. Matteis, J. Fuente and L. Lezama, *J. Phys. Chem. C*, 2016, 120, 3492-3500.
6. S. Shah, A. Majeed, K. Rashid, S. Awan, *Materials Chem. and Phy.*, 2013, 138, 703-708.
7. W. Wu, Q. He and C. Jiang, *Nanoscale Res. Lett.*, 2008, 3, 397-415.
8. L. Zhao, H. Yang, L. Yu, Y. Cui, X. Zhao, B. Zou and S. Feng, *J. Magn. Magn. Mater.*, 2006, 301, 445-451.
9. S. Pillai, *Solid State Physics*, 2009, 429-431, 6th Edition, New Age Science Publishing.
10. B. Sharma, *Instrumental method for chemical analysis*, 2005, 494-536, 24th Edition, Goel Publishing house, Meerut.
11. A. Goldstein, *Handbook of Nanophase Materials*, 1997, 317-336, Marcel Dekker, Inc, New York.
12. R. Khandpur, *Handbook of Analytical Instruments*, 2006, 344-363, 2nd Edition, Tata McGraw-Hill Publishing Company Limited, New Delhi.

13. G. Socrates, Infrared and Raman Characteristic Group Frequencies: Tables and Charts, 2001, 68-87, 3rd Edition, Wiley, John Wiley & Sons, New York.
14. B. Smith, Chemical Infra-red Fourier Transform Spectroscopy, 2001, 19-53, 2nd Edition, CRC Press, Taylor and Francis Group.
15. A. Ul-Hamid, A Beginners' Guide to Scanning Electron Microscopy, 2018, 15-75, Springer, Springer Nature, Switzerland.
16. M. De Graef, Introduction to conventional transmission electron Microscopy, 2003, 136-233, Cambridge University Press Publishing.
17. <http://www.ammrf.org.au/myscope/tem/introduction>
18. A. Niazi, P. Poddar and A. Rastogi, A precision low-cost vibrating sample magnetometer, 2000, Current Science, 79, 99-109.
19. J. Clarke, A. Braginski, The SQUID Handbook: Fundamentals and Technology of SQUIDs and SQUID Systems, Vol. I, 2004, 29-87, Wiley, Wiley-VCH Verlag, GmbH & Co. KGaA, New York.
20. B. Berne, R. Pecora, Dynamic Light Scattering, 1976, 24-53, Dover Publications Inc, New York.
21. S. Thomas, R. Thomas, A. Zachariah and R. Mishra, Vol. 3, 2017, 37-50, Thermal and Rheological Measurement Techniques for Nanomaterials Characterization, Elsevier, Mathew Deans.
22. R. De Palma, S. Peeters, M. Van Bael, H. Van den Rul, K. Bonroy, W. Laureyn, J. Mullens, G. Borghs and G. Maes, Chem. Mater. 2007, 19, 1821-1831.
23. P. Hiemenz, R. Rjagopalan, Principles of Colloid and Surface Chemistry, 1997, 26-85, 3rd Edition, CRC Press, Taylor and Francis Group, New York.

24. F. Caruso, *Colloids and Colloid Assemblies: Synthesis, Modification, Organization and Utilization of Colloid Particles*, 2004, 175-210, Wiley-VCH, Wiley-VCH Verlag, GmbH & Co. KGaA, New York.
25. S. Laurent and M. Mahmoudi, *Adv. Colloid Interface Sci.*, 2011, 166, 8-23.
26. R. Hergt, S. Dutz, R. Müller, M. Zeisberger, *J. Phys.: Condens. Matter.*, 2006, 18, 2919-2934.
27. J. Fortin, C. Wilhelm, J. Servais, C. Me'nager, J. Bacri and F. Gazeau, *J. Am. Chem. Soc.*, 2007, 129, 2628-2635.
28. C. Lemarchand, R. Grefa and P. Couvreur, *Eur. J. Pharm. Biopharm.*, 2004, 58, 327-341.
29. H. Cao, J. Deng and X. Gao, *App. Surf. Sci.*, 2009, 255, 7974-7980.
30. R. Weissleder, D. Stark, B. Engelstad, B. Bacon, C. Compton, D. White, P. Jacobs and J. Lewis, *Am. J. Roentgenol.* 1989, 152, 167-173.
31. D. Richards and A. Ivanisevic, *Chem. Soc. Rev.*, 2012, 41, 2052–2060.
32. T. Neubergera, B. Schöpfa, H. Hofmann, M. Hofmann and B. Rechenberg, *J. Magn. Mater.*, 2005, 293, 483-496.
33. W. Schütt, C. Grüttner, U. Häfeli, M. Zborowski, J. Teller, H. Putzar and C. Schümichen, *Hybridoma.*, 1997, 16, 109-117.
34. A. Nemmar, M. Hoylaerts and P. Hoet, *Am. J. Respir. Crit. Care Med.*, 2002, 166, 998-1004.
35. N. Lewinski, V. Colvin and R. Drezek, *Small.*, 2008, 4, 26-49.
36. B. Díaz, C. Sánchez-Espinel and M. Arruebo, *Small.*, 2008, 4, 2025-2034.
37. Z. Lacava, R. Azevedo, E. Martins, L. Lacava, M. Freitas, V. Garcia, C. Rébula,

A. Lemos, M. Sousa, F. Tourinho, M. Da Silva and P. Morais, *J. Magn. Magn. Mater.*, 1999, 201, 431-434.

Synthesis and Characterization of MnFe_2O_4 Nanoparticles

International Journal of Nanoscience
Vol. 18, No. 1 (2019) 1950003 (8 pages)
© World Scientific Publishing Company
DOI: 10.1142/S0219581X19500030



Structural, Morphological, Magnetic and Self-Heating Studies of One-Step Polyol Synthesized Manganese Ferrite (MnFe_2O_4) Nanoparticles

P. R. Ghutepatil^{*,‡} and S. H. Pawar^{*,†,§}

^{*}Center for Interdisciplinary Research, D. Y. Patil University
Kolhapur 416006, Maharashtra, India

[†]Center for Research and Technology Developments Sinhgad Institutes
Solapur 413255, Maharashtra, India

The parts of this chapter have been published as reserach article.

In thinking about nanotechnology today, what's most important is understanding where it leads, what nanotechnology will look like after we reach the assembler breakthrough.

-K. Eric Drexler

4.1 Introduction

The iron oxide MNPs are fascinating the many researchers and scientists these days because of their magnificent physical, chemical properties and possible use in biomedical applications such as delivery of drug, magnetic resonance imaging, isolation of DNA of cell, tissue repairing and hyperthermia [1-8]. In nature, an iron oxide MNPs have been discovered in different forms and Fe₃O₄ (magnetite), γ -Fe₂O₃ (maghemite) and α -Fe₂O₃ (hematite) are most typical among them [9-11]. A synthesis of nanoparticles is required to improve chemical and physical traits to utilize nanoparticles appropriate for biomedical applications [12, 13].

The MNPs are synthesized by using physical and chemical processes. Chemical synthesis processes provide an appropriate route for size control composition modulation [14-17]. The different properties of nanoparticles like size, morphology, surface chemistry and composition will be regulated using proper synthesis process because physical and chemical properties of MNPs can be influenced by synthesis methods hence it is important research area to develop useful properties of nanoparticles [18-20].

4.2 Synthesis methods of MNPs

There are two approaches for the synthesis of nanoparticles shown in Fig.4.1 and they are top down and bottom up. In top down approach, the nanomaterials are fabricated from big entities or bulk materials without atomic level control. In bottom up approach, materials are synthesized from molecular components, which are based on principle of molecular recognition [21]. Synthesis approach should produce the nanoparticles that satisfy the following criteria:

- Controlled particle size, shape, distribution, crystal structure.
- Stabilization of physical properties.
- Lower impurities or purity improvement.

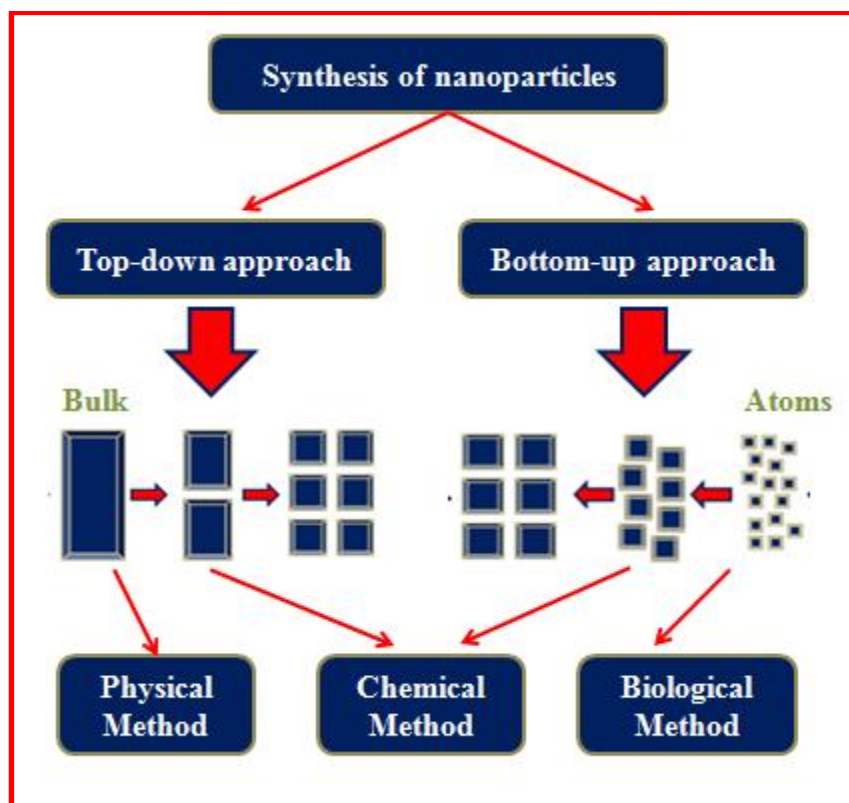


Fig. 4.1 Synthesis of nanoparticles

Chemical method supports the manipulation of sample particle at atomic and molecular scale [22]. In this chapter, different chemical synthesis methods have been discussed. Chemical methods provide the flexibility in synthesizing and designing new material, which can be purified into endmost product. The main advantage of chemical process over other processes is superior chemical homogeneity [23]. Several chemical methods including co-precipitation, polyol, hydrothermal, combustion, sol-gel, microemulsion and thermal decomposition are available to synthesize of magnetic material for biomedical applications. These approaches are being used to synthesize nanoparticles with invariable composition and narrow size distribution.

4.3 Chemical methods

The various synthesis methods of MNPs have been reviewed and discussed which is shown in Fig. 4.2. Synthesis of MNPs has become important research area as

chemical and physical properties of MNPs can be influenced by synthesis methods. Researchers and scientists have dedicated a lot of efforts in last decade to produce the monodispersed, size controlled and highly stable MNPs. The MNPs have been synthesized chemically as shown in below pictorial diagram.

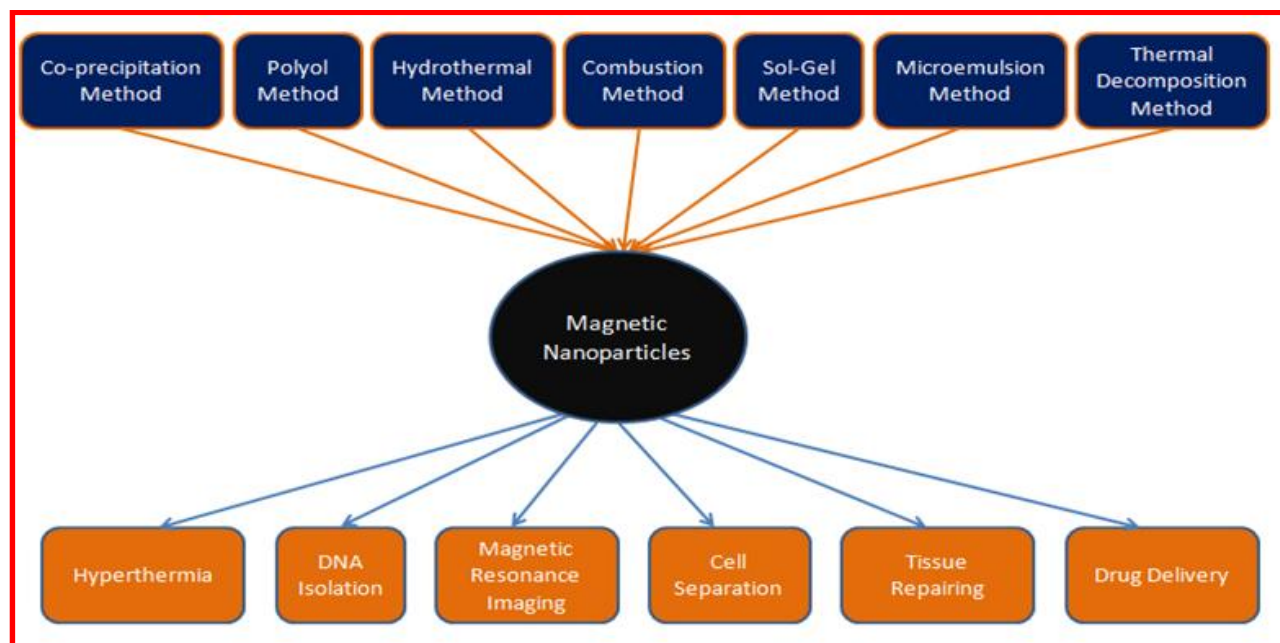


Fig. 4.2 Multi synthesis chemical routes of MNPs for variety of biomedical application

4.3.1 Co-precipitation method

Co-precipitation method is promising and most used synthesis method for biomedical applications due to its simplicity, procedures and requirement of less harmful materials in biomedical applications [24]. Iron oxides (Fe_3O_4 or $\gamma\text{Fe}_2\text{O}_3$) can be synthesized in aqueous medium by ferric salts and aging stoichiometric mixture of ferrous. The Fe_3O_4 formulation is defined as shown in Fig.4.3.

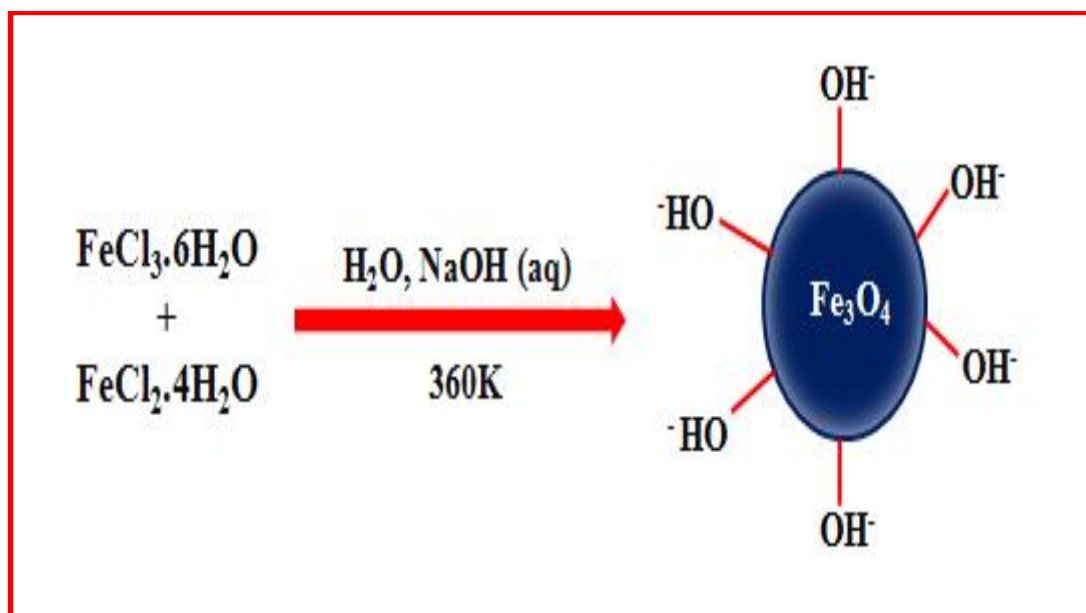


Fig. 4.3 Synthesis of MNPs using co-precipitation method

The precipitation of Fe₃O₄ is anticipated at a range of pH value between 8 and 14 in accordance with thermodynamics of reaction with a stoichiometric ratio (Fe³⁺/Fe²⁺) of 2:1 ratio in non oxidizing environment. The Fe₃O₄ (magnetite) gets transferred into γFe₂O₃ (maghemite) in an existence of oxygen as it is very sensitive to oxygen. Not only oxidation transforms magnetite to maghemite but also several electron/ions also transfers based on the pH value. The morphology as well as composition varied with type of used chlorides, nitrates or sulfates salts, reaction, pH value, ionic strength of media and Fe³⁺/M²⁺ ratio (M = Fe, Co, Ni, Mn, Cu, Mg, Ba, Sr, etc) [25-27]. Low reaction temperature, environmental friendly solvent high production, relatively narrow size distribution and simplicity are the advantages of this approach. The disadvantage of this approach is that size of particle cannot be controlled.

4.3.2 Polyol method

Polyol method is very powerful approach for preparation of non agglomerated nanoparticles with required size and shape, which can be obtained by controlling

kinetic of precipitation. The mechanism behind this synthesis process is as: solid metal precursor dissolution dissolved metallic species reduction by the polyol, extension of nuclei and metallic phase nucleation. The nanoparticles with distribution can be obtained by achieving complete separation of nucleation and avoiding aggregation of metal particles during nucleation. Non aggregated magnetite nanoparticles can be directly produced by using polyols including ethylene glycol (EG), temperature using modified polyol process. Here, only reaction with DEG yields non agglomerated magnetite nanoparticles with invariable shape and this can be corresponded with the suitable number of coordinating groups. Transmission electron microscopy (TEM) analysis confirms that MNPs prepared by polyol methods are monodispersed in nature [28, 29]. The Fe₃O₄ formulation by polyol method is shown in Fig.4.4.

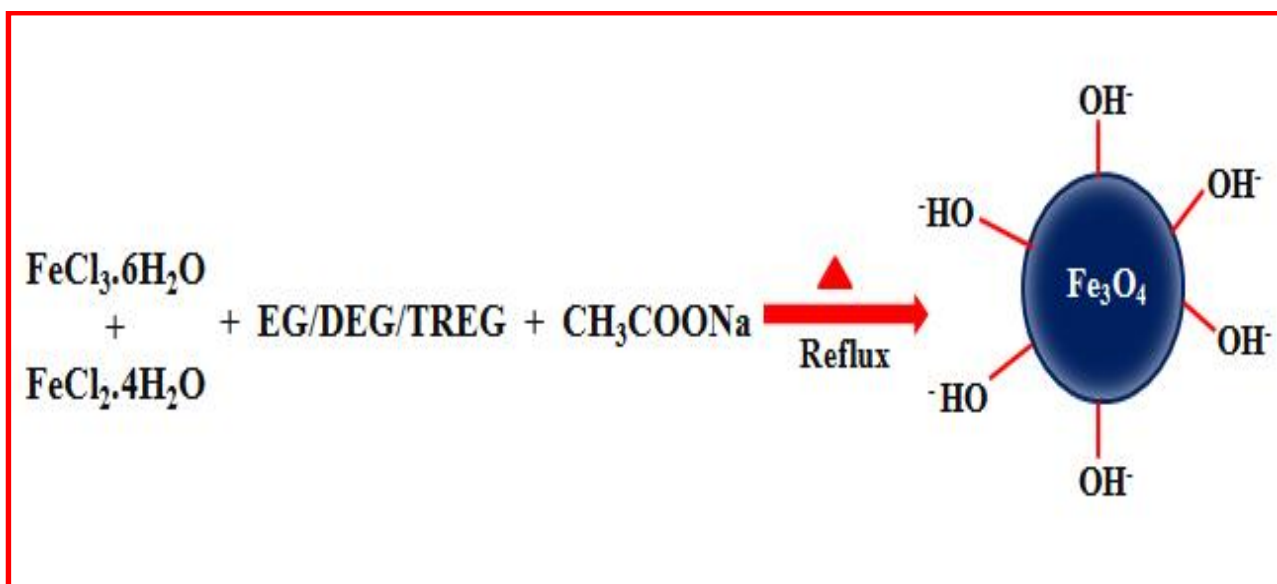


Fig. 4.4 Synthesis of MNPs using polyol method

In advanced polyol, Sun *et al.* [30] have prepared uniform size magnetite particles by high temperature reduction of Fe(acac)₃ (acac=acetylacetonate) by 1, 2-hexadecanediol in the existence of oleylamine and oleic acid. The particle diameter is adjusted up to 20 nm by changing reaction conditions. The advantages of polyol

synthesis method are that the uniform shape and narrow size distributed nanoparticles can be obtained.

4.3.3 Hydrothermal method

In hydrothermal process, synthesis is being carried out in water media in autoclaves or reactors where temperature and pressure could be more than 2000 psi and 200°C respectively. Ferrite particles can be formed by hydrolysis, oxidation as well as neutralization of mixed metal hydroxides in hydrothermal method. The solvent temperature and time affected crucially on quality of products in this process [31-33]. Many researchers are using this method to synthesize the nanoparticles.

Wang et al.[34] prepared well crystallized Fe₃O₄ particles using ferrous chloride and di-amine hydrate by one step process. The synthesized material exhibited saturation magnetization of 85.8 emu/g and 12.3 emu/g at 140 °C and 100 °C respectively. Zheng et al. [35] have used a hydrothermal method to prepare nanoparticles in existence of sodium bis (2-ethylhexyl) sulfosuccinate as a surfactant. The magnetic properties of yielded nanoparticles exhibited a superparamagnetism at room temperature. The main advantages of this method are that crystallization of nanoparticles can be improved and high saturation magnetization is obtained by increasing temperature. Fig. 4.5 shows synthesis of MNPs using hydrothermal method.

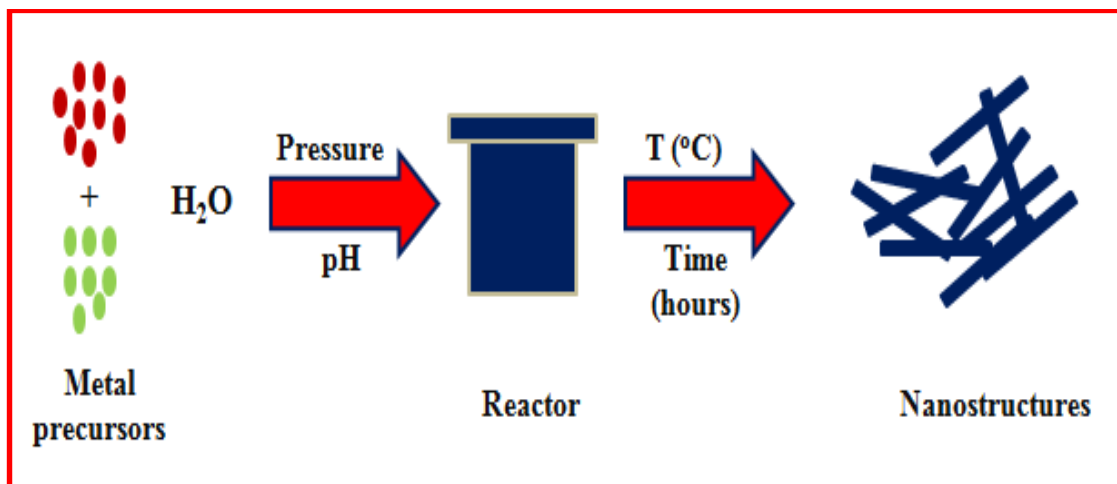


Fig. 4.5 Synthesis of MNPs using hydrothermal method

4.3.4 Combustion method

In combustion method, an oxidizer, right temperature and fuel are required to generate a fire. This process is based on highly redox chemical reactions between fuel and oxidizer. In Redox reaction oxidation process is defined as the addition of oxygen or electronegative element and reduction is defined addition of hydrogen or electropositive element [36]. The Fe₃O₄ formulation by combustion method is shown in Fig.4.6.

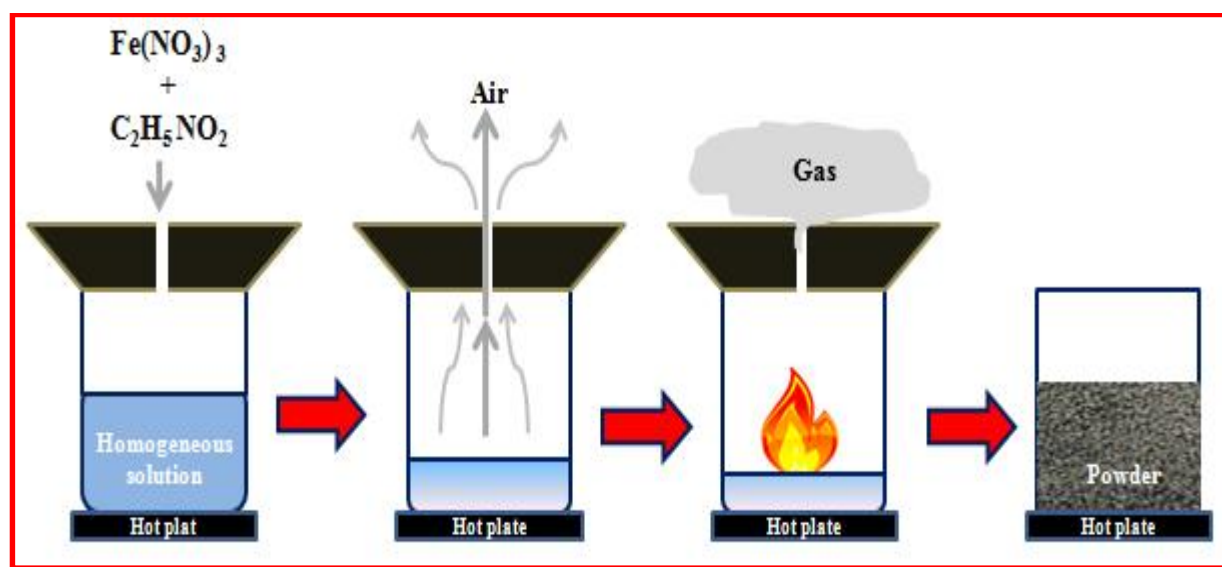


Fig. 4.6 Synthesis of MNPs using combustion method

Merzhanov [37] has explored this method first time to synthesize number of oxide materials and nonoxide materials. The process was required fine precursors, which were ignited at temperatures $>1000^{\circ}\text{C}$. Martirosyan et al. [38] yielded crystalline ferrite nanoparticles with size range of 50-100 nm by using combustion synthesis of oxides and explained that the porosity of product had increased by extensive emission of CO_2 . In combustion process, the magnetic properties of product and size of particle are depended on content in oxygen concentrations and reactants mixture.

4.3.5 Sol-Gel method

Sol-Gel method is based on molecular precursors condensation and hydroxylation in solution, which derives a Sol of particles. Inorganic polymerization and condensation generate 3-dimensional metal oxide, denominated soak Gel. Hence, the name of method is Sol-Gel. In sol-gel method, water solution of metal salts is co-precipitated and then followed by treatment to form inorganic or metallo-organic precursor. Then, this can be concentrated to a gel and eventually fired to produce the fine grained polycrystalline particles. The reaction is performed at room temperature so more temperature is required to get final crystalline state. The properties of gel are largely depending on upon structure formed during the sol stage of sol-gel process [39-42]. The magnetite formulation by sol-gel method is shown in Fig. 4.7.

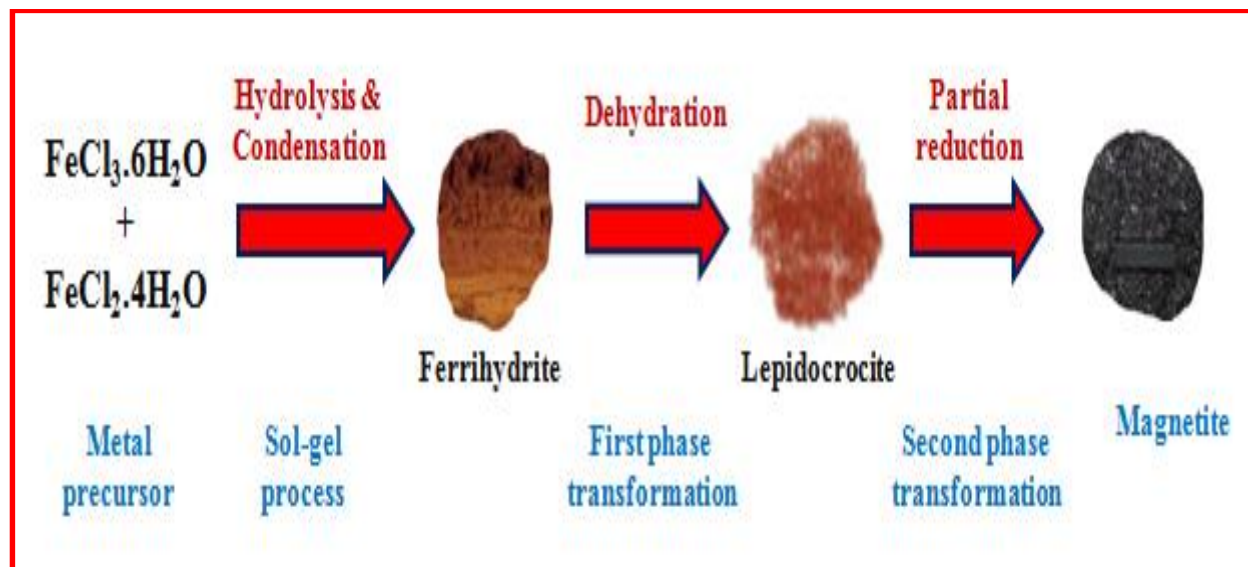


Fig. 4.7 Synthesis of MNPs using sol-gel method

Solinas et al. [43] have produced $\text{Fe}_2\text{O}_3\text{-SiO}_2$ nanoparticles with a Fe/Si molar concentration between 0.24 and 0.56 by using sol-gel process. In this work, they investigated surface of evaporation and volume (S/V) ratio of the sol and the temperature on the gelation process. The result showed that the gelation process determines the phase and size of MNPs formed in silica. The main benefits of this method are that it gives good stoichiometric control and produces ultrafine particles with narrow size distribution in short time at lower temperature. The disadvantage of this method is that it produces 3-dimensional oxide networks so it restricts its efficiency regarding formation of disconnected and independent nanosized particles.

4.3.6 Microemulsion method

In disseminate process, the w/o (water in oil) microemulsion containing of nano-sized droplets of water disseminated in oil phase and stabilized by suitable surfactant molecules at the water/oil interface [44, 45]. Salazar-Alvarez has synthesized MNPs by using reverse emulsions. They used nanoemulsion system containing AOT-BuOH/cHex/H₂O with surfactant/cosurfactant molar ratio of 1 and surfactant/water molar ratio of 2.85. First nano emulsion holding iron source and

second holding solution of sodium hydroxide have been mixed to prepare magnetite nanoparticles. The nano emulsion was encountered with acetone to detach the particles and then washed with various times with ethanol. The nanoparticles exhibited superparamagnetic behavior with high magnetization values [46]. The metal oxide formulation by microemulsion method is shown in Fig. 4.8.

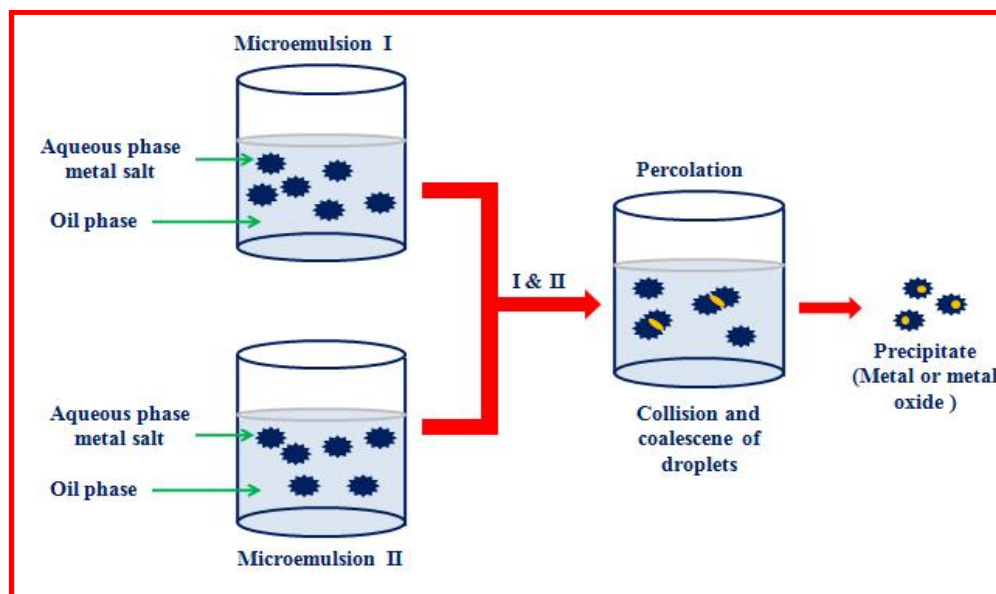


Fig. 4.8 Synthesis of MNPs using microemulsion method

The water and oil phases generally contain various dissolved components, hence selection of the surfactant relies on the physicochemical characteristics of the system such as cationic, anionic, or non-ionic surfactants can be used [47]. The main advantage of microemulsion process is the heterogeneity of nanoparticles, which can be procured by amount of surfactant, oil phase and reacting conditions.

4.3.7 Thermal decomposition method



Fig. 4.9 Synthesis of MNPs using thermal decomposition method

The iron oxide nanoparticles formulation by thermal decomposition method is shown in Fig. 4.9. A uniform size iron oxide MNPs size can be synthesized using thermal decomposition of metallic precursor in which metal acetylacetonates like [M(acac)_n] (M=Fe, Mn, Ni, Cr; n=2 or 3, acac= acetylacetonate), cupferronates, [MxCup_x] (M=metal ion; Cup=Nnitrosophenyl hydroxylamine, C₆H₅N(NO)O⁻) [11], and carbonyls are generally used as organo metallic precursor. A fatty acids, oleic acid and hexadecylamine can be used as surfactants. In this method, the organo metallic compounds, surfactants and solvents are conclusive factors for size morphology and controlling of MNPs [48, 49].

4.4 Experimental

4.4.1 Synthesis of MnFe₂O₄ nanoparticles by polyol method

Polyol method is best method for preparation of non agglomerated nanoparticles precise size, which follows kinetic precipitation method for formation nanoparticles. This method avoids aggregation of metal particles. Synthesis steps of MnFe₂O₄ nanoparticles are as below. A mixture of Mn (CH₃COO)₂ (6 mmol), FeCl₃ (12 mmol) was dissolved in 40 mL diethylene glycol with vigorous stirring for 20 min

followed by addition of sodium acetate. The mixture was then refluxed for 3 h at 210 °C. Then MNPs were repeatedly washed with a mixture of ethanol and ethyl acetate in the ratio 1:2 and separated by using a magnetic decantation process and dried at room temperature [50, 51]. Fig 4.10 represents the setup used for the synthesis of manganese ferrite nanoparticles and Fig.4.11 shows reaction mechanism of MnFe₂O₄ nanoparticles synthesis.



Fig. 4.10 Reflux setup used for polyol synthesis of MnFe₂O₄ nanoparticles

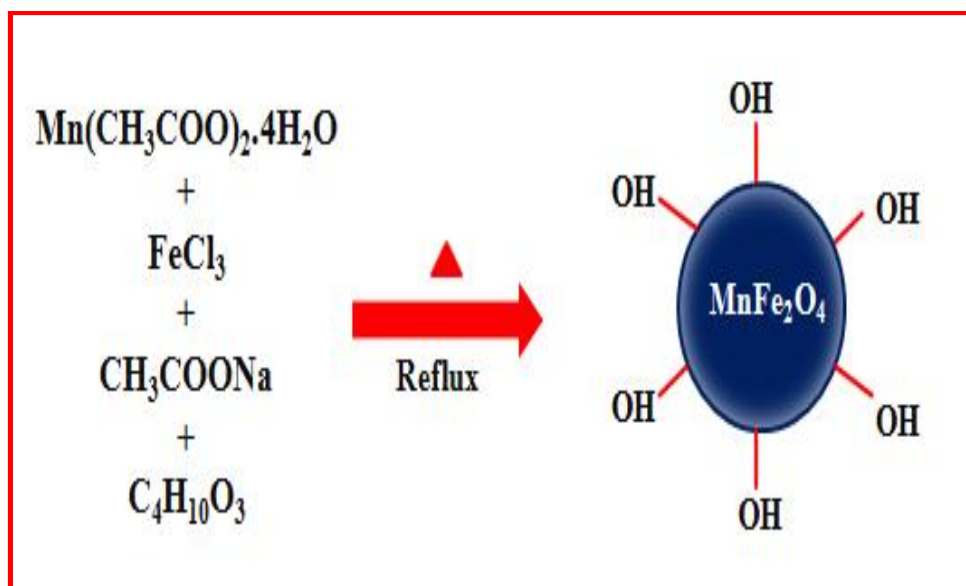


Fig. 4.11 Reaction mechanism of MnFe₂O₄ nanoparticles synthesis

4.4.2 Characterization of MnFe₂O₄ nanoparticles

XRD (RigakuMiniFlex 600) was used for structural analysis and phase identification of obtained MNPs by using Cu-K_α (λ=1.5406 Å) in the 2θ range from 20° to 80°. FESEM (Hitachi S-4800) and HRTEM (TEM, JEM-2100F Model, Japan) were used to determine the morphology and size of the nanoparticles. Presence of magnetic core as well as coating of the MNPs was confirmed by FTIR spectroscopy (Alpha ATR Bruker Eco Model). The size distribution of MNPs was determined by DLS measurements using a PSS/NICOMP 380 ZLS (Particle Sizing System, Santa Barbara, CA, USA). TGA was performed for thermal study of MNPs using transanalytical instrument mode (SDT 2960). MNPs were heated from room temperature to 900 °C with a heating rate 10 °C min⁻¹ under nitrogen (N₂) flow to measure a weight loss. Magnetic characterization was done with SQUID-VSM using the applied magnetic field of ±40 at room temperature.

4.5 Results and discussion

4.5.1 Structural analysis

X-ray diffraction analysis

The crystal structure and phase analysis of synthesized MNPs is determined using X-ray diffraction analysis (XRD) technique. Synthesized MnFe₂O₄ nanoparticles were structurally investigated using XRD as shown in Fig. 4.12. The patterns of XRD were obtained in the 2θ range of 20-80°. The diffraction peaks values (220), (311), (400), (422), (511) and (440) were obtained with (hkl) and then all peaks were matched with the JCPDS file number 38-0430. The strongest reflection comes from the (311) plane and it is corresponding to the cubic spinel structure. The most intense peak in Gaussian fit (311) was used to calculate a full width at half maxima (FWHM) is used to determine crystallite size (D) by using equation (3.1). An inverse spinel cubic structure (Fd3m) of the sample is affirmed from obtained diffractograms. The Lattice constant (a) was calculated using the d value and with their respective (hkl) parameters using equation (4.1) by considering single phase of sample. The Lattice constant value was ~8.346 Å. The calculated lattice constant (a), identified the samples to be cubic spinel [52]. The crystallite size of MnFe₂O₄ nanoparticles estimated by Scherrer's formula is 10 nm. The intensities and position of lines in diffraction pattern confirm the spinel structure.

$$a = d\sqrt{h^2 + k^2 + l^2} \dots \dots \dots 4.1$$

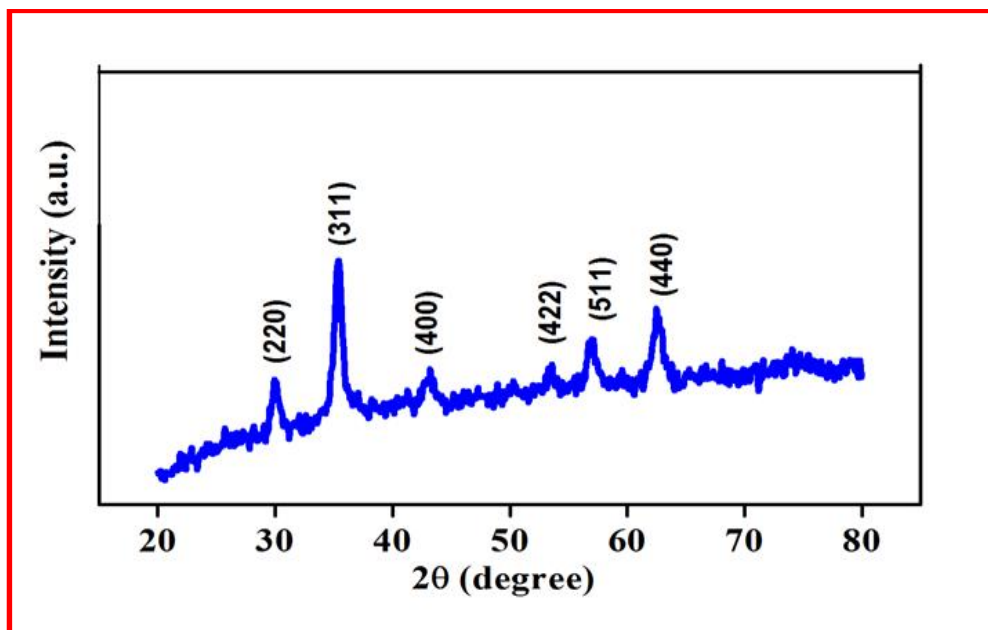


Fig. 4.12 XRD pattern of MnFe₂O₄ nanoparticles

4.5.2 Microstructural analysis

SEM analysis

A surface morphology MnFe₂O₄ nanoparticle was analyzed by FE-SEM and which is shown in Fig. 4.13. The morphology shows that particles are conglomerated in nature and most of them are roughly spherical. It is dependent on the intermolecular force between nanoparticles and cumulative behavior of nanoparticles. The elastic and inelastic scattering is generated when a beam of electrons interacts with atoms of the material. FE-SEM image of MnFe₂O₄ shows agglomerated form of nanoparticles, which are approximately 1 μm in size as shown in Fig.4.13 (a). Fig.4.13 (b) shows that the nanoparticles are separated from each other and approximately ~ 13 nm in size. This is confirmed by TEM [53].

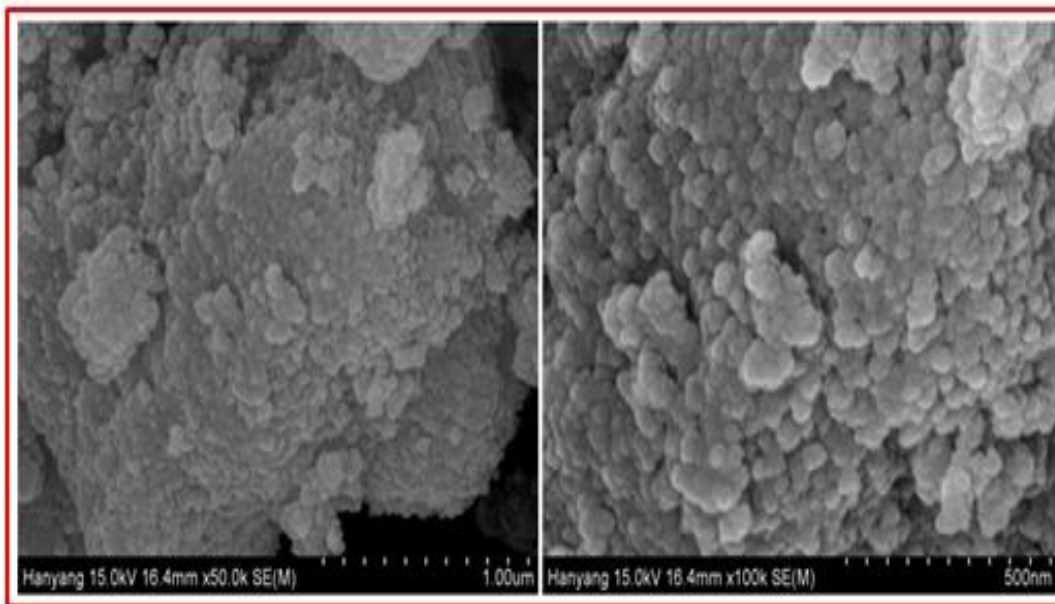


Fig. 4.13 FE-SEM images of MnFe₂O₄ nanoparticles

TEM analysis

Fig. 4.14 (a and b) shows TEM image of MnFe₂O₄ nanoparticles and it shows the formation of roughly spherical nanoparticles with some conglomeration. The obtained nanoparticles show average particle size ~13 nm. The particle size matches with crystallite size calculated from XRD analysis. Fig. 4.14 (c) represents the selected area electron diffraction (SAED) patterns and it shows bright rings indicating crystalline nature of nanoparticles as specified in XRD patterns. The pattern of ring is (220), (311), (400), (511) and (440) planes, which can be clearly seen in XRD results.

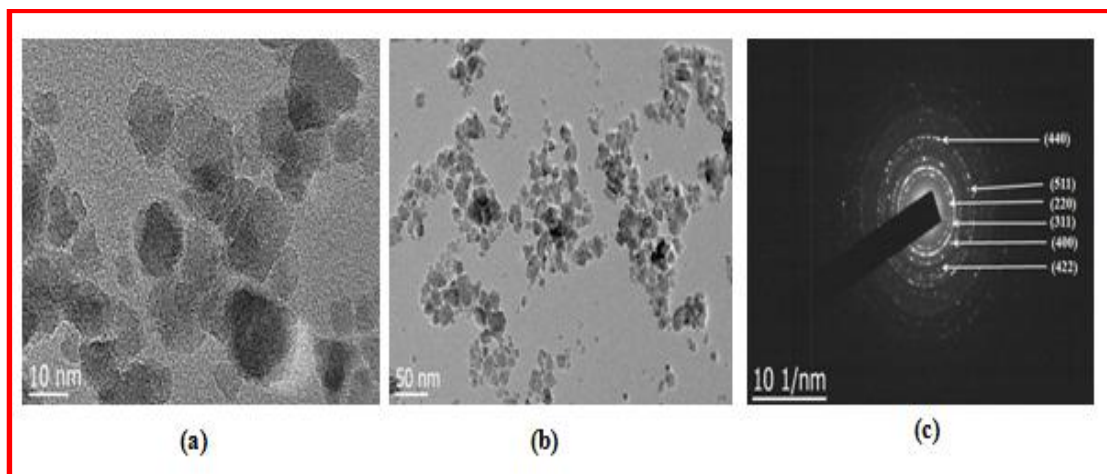


Fig. 4.14 TEM images of MnFe₂O₄ nanoparticles

4.5.3 Chemical bonding study

FTIR analysis

FTIR is a very useful technique to determine functional group of molecule, which is used during the synthesis process. Fig. 4.15 shows the FTIR spectrum of MnFe₂O₄ over the range of 450 to 4000 cm⁻¹. FTIR gives details about stretching frequencies. The band observed for sample at around ~590 cm⁻¹ is attributed to the Fe-O which attributed to intrinsic stretching vibrations of metal oxygen at tetrahedral and octahedral sites. The peak at about 2959 cm⁻¹ correspond to the C-H stretching. The other peaks at about 1580 cm⁻¹, 1258 cm⁻¹, 1430 cm⁻¹ and 1057 cm⁻¹ are due to O-H stretching, C-H bending, C-O bending and O-H bending vibrations, respectively, of diethylene molecules adsorbed [54, 55].

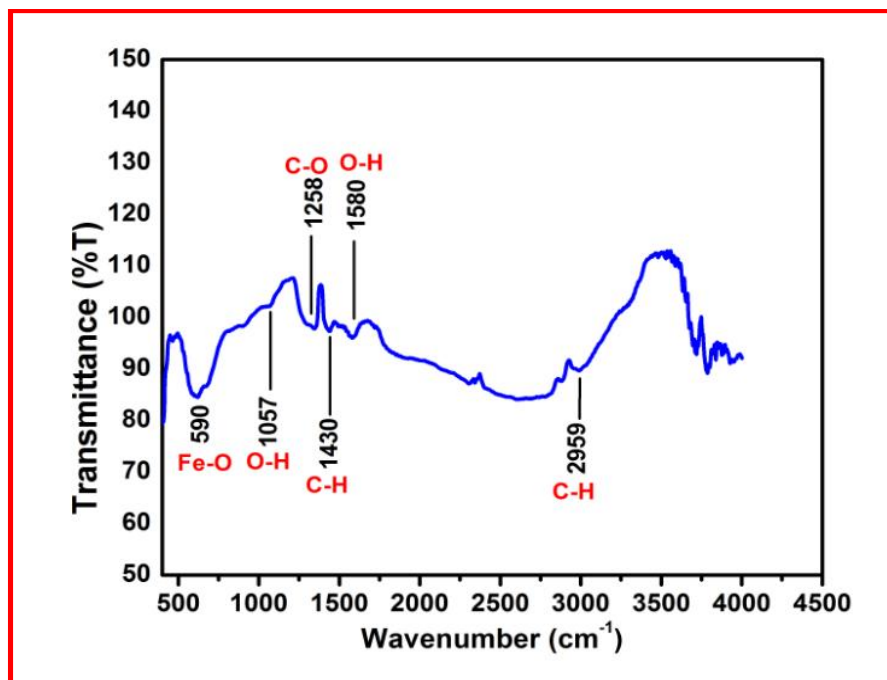


Fig. 4.15 FTIR spectrum of MnFe₂O₄ nanoparticles

4.5.4 Magnetization study

VSM analysis

VSM technique is useful to study the magnetic properties of the material as function of temperature, time and magnetic field. The magnetic properties of MnFe₂O₄ nanoparticles measured by VSM and measurements carried out at 300 K carried out as presented in Fig. 4.16. It can be seen from hysteresis curve of MnFe₂O₄ MNPs at 300 K that there is no coercivity or remanence exists, indicating the superparamagnetic behavior. The saturation magnetization observed for MnFe₂O₄ is found to be 60 emu/g at an applied field of ± 40 kOe. The observed value of saturation magnetization is less in compare to bulk value (80 emu/g) but large in compare to other values [56]. The smaller value of saturation magnetization is because of lattice defects and existence of magnetically inert layer at the surface of nanoparticles.

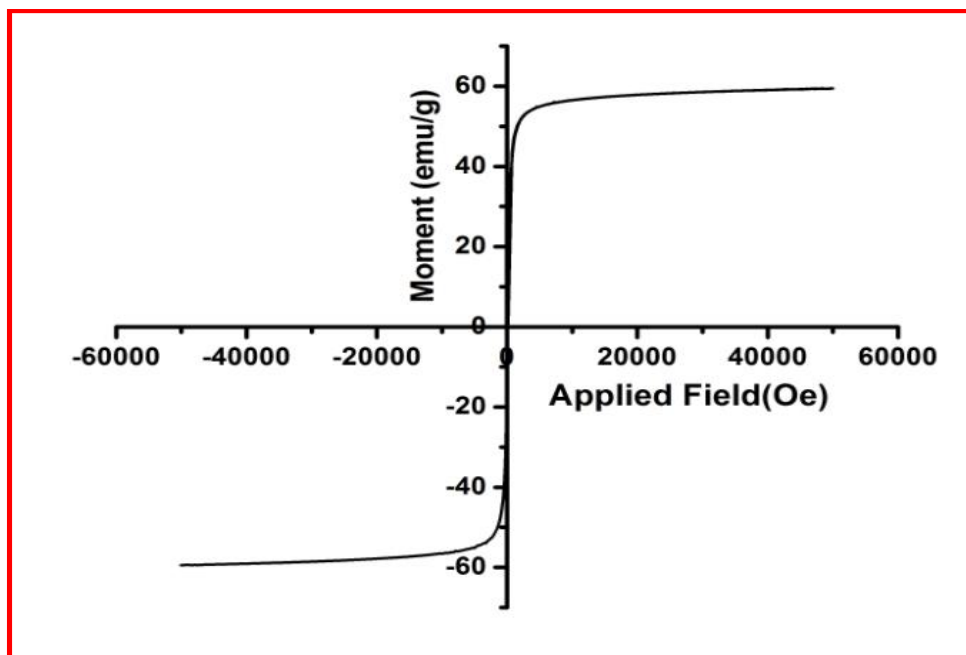


Fig. 4.16 M-H curve of MnFe₂O₄ nanoparticles

4.5.5 Thermogravimetric analysis

TGA analysis

The bonding strength and thermal stability of MNPs is determined using TGA analysis. Ligands bound more strongly desorb at a higher temperature. Thermogravimetry curve for MnFe₂O₄ nanoparticles were recorded in the temperature range in between 25 to 900 °C with a heating rate of 10 °C min⁻¹ in nitrogen atmosphere. Fig. 4.17 shows weight loss in three steps for MnFe₂O₄ nanoparticles in the temperature ranges of room temperature to 200 °C, 200-400 °C and 600-800 °C. The initial weight loss corresponds to the evaporation of adsorbed water, the weight loss in second step represents the decomposition of diethylene glycol from the surface of sample. Weight loss in third from 600-800 °C is quite slow step due to the further decomposition of sample to form pure MnFe₂O₄ [29, 57].

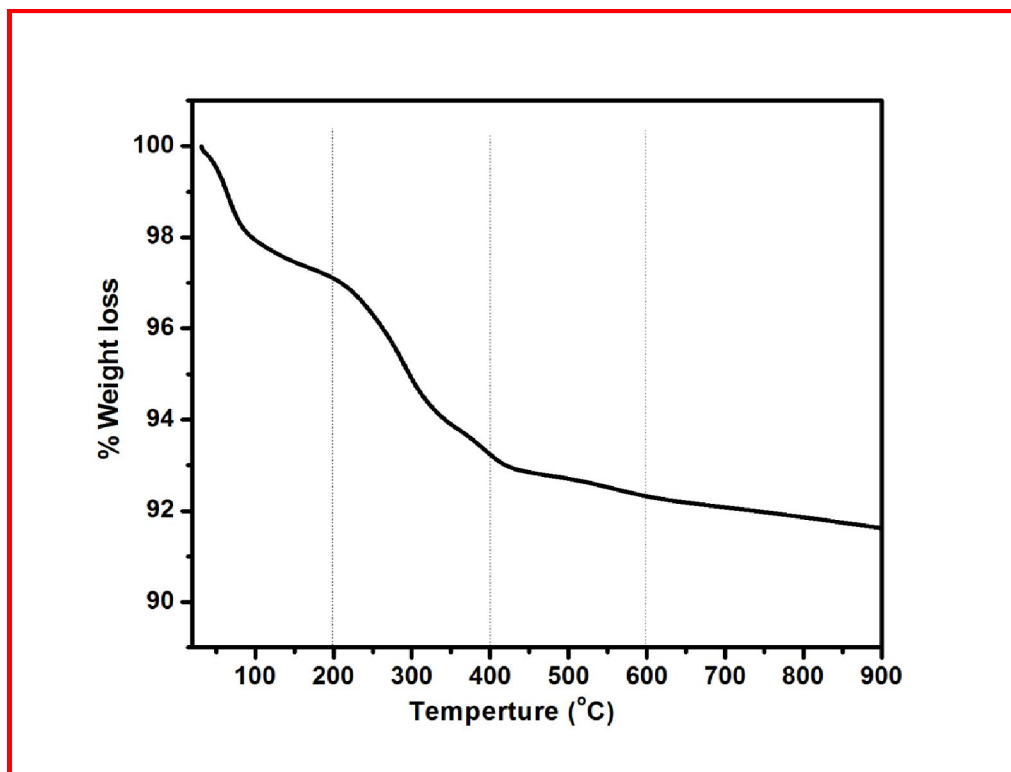


Fig. 4.17 Thermogravimetric pattern of MnFe₂O₄ nanoparticles

4.5.6 Colloidal stability study

DLS analysis

DLS measurements have been performed to find out the hydrodynamic size in aqueous state. The particles which are small in size less than 1 μm can be characterized by DLS technique. Fig.4.18 illustrates the hydrodynamic size of MnFe₂O₄ nanoparticles in distilled water at pH \sim 7. The hydrodynamic size of MnFe₂O₄ nanoparticles is found to be \sim 104.5 (\pm 13.0) nm. DLS shows large size of nanoparticles as compared XRD and TEM. Discrepant result in TEM and DLS techniques is the main reason that we cannot exclude for the samples where aggregation of two to three nanocrystals capped together within the same polymer shell. The MnFe₂O₄ nanoparticles in present case exhibit hydrodynamic size close to the mentioned values there by having potential application in biomedical field [58].

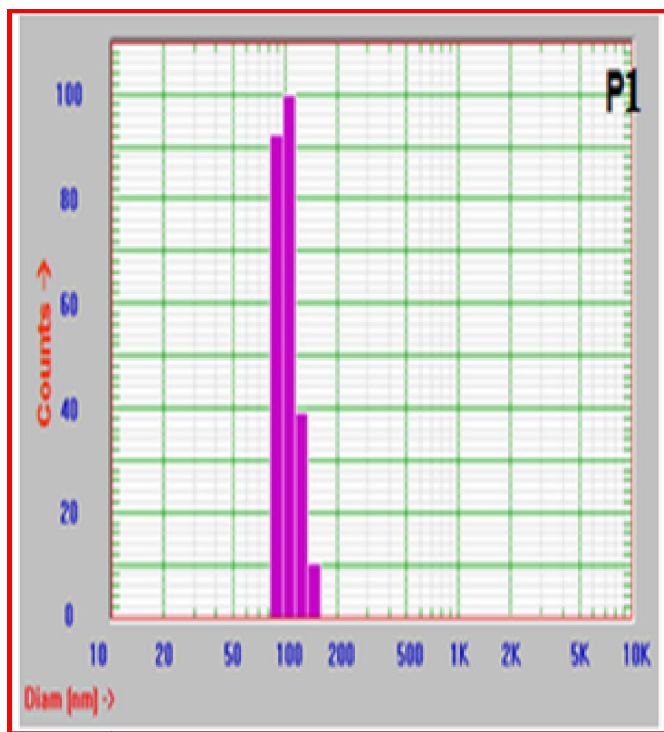


Fig. 4.18 HDD at pH~7 in water for MnFe₂O₄ nanoparticles

4.6 Conclusions

This chapter gives brief account on various chemical methods used for synthesis of MNPs. MnFe₂O₄ nanoparticles synthesized using polyol synthesis method. The structural, magnetic and morphological properties of MnFe₂O₄ nanoparticles have been studied in detail. An experimental result revealed that exhibition of superparamagnetic behavior and at room temperature high saturation magnetization i.e. 60 emu/g. Surface morphology of MnFe₂O₄ nanoparticles shows that particles are conglomerated in nature and most of them are roughly spherical. The nanoparticles size 13 nm is obtained by this polyol method and will useful in biomedical application.

References

1. S. Fazal, B. Paul-Prasanth, S. Nair and D. Menon, *ACS Appl. Mater. Interfaces*, 2017, 9, 28260-28272.
2. Z. Beji, A. Hanini, L. Smiri, J. Gavard, K. Kacem, F. Villain, J. Greneche, F. Chau and S. Ammar, *Chem. Mater.*, 2010, 22, 5420-5429.
3. L. Lartigue, C. Innocenti, T. Kalaivani, A. Awwad, M. Duque, Y. Guari, J. Larionova, C. Guerin, J. Montero, V. Barragan-Montero, P. Arosio, A. Lascialfari, D. Gatteschi and C. Sangregorio, *J. Am. Chem. Soc.*, 2011, 133, 10459-10472.
4. S. Patra, E. Roy, P. Karfa, S. Kumar, R. Madhuri and P. Sharma, *ACS Appl. Mater. Interfaces*, 2015, 7, 9235-9246.
5. S. Laurent, D. Forge, M. Port, A. Roch, C. Robic, L. Elst and R. Muller, *Chem. Rev.*, 2008, 108, 2064-2110.
6. X. Lasheras, M. Insausti, I. Muro, E. Garaio, F. Plazaola, M. Moros, L. De Matteis, J. M. de la Fuente and L. Lezama, *J. Phys. Chem. C*, 2016, 120, 3492-3500.
7. S. Shah, A. Majeed, K. Rashid and S. Awan, *Materials Chem. and Phy.*, 2013, 138, 703-708.
8. I. Sharifi, H. Shokrollahi and S. Amiri, *J. Magn. Magn. Mater.*, 2012, 324, 903-915.
9. C. Bean and J. Livingston, *J. Appl. Phys.*, 1959, 30, 120-129.
10. L. Babes, B. Denizot, G. Tanguy, J. Le Jeune and P. Jallet, *J. Coll. Int. Sci.*, 1999, 212, 474-482.

11. W. Wu, Q. He and C. Jiang, *Nanoscale Res. Lett.*, 2008, 3, 397-415.
12. L. Zhao, H. Yang, L. Yu, Y. Cui, X. Zhao, B. Zou and S. Feng, *J. Magn. Magn. Mater.*, 2006, 301, 445-451.
13. M. Phadatare, A. Salunkhe, V. Khot, C. Sathish, D. Dhawale and S. Pawar, *J. Alloys Comp.*, 2013, 546, 314-319.
14. A. Gupta and M. Gupta, *Biomaterials*, 2005, 26, 3995-4021.
15. C. Lee, H. Lee and R. Westervelt, *Appl. Phys. Lett.*, 2001, 79, 3308-3310.
16. A. Gupta and A. Curtis, *Biomaterials*, 2004, 25, 3029-3040.
17. A. Gupta and S. Wells, *IEEE T. Nanobiosci.*, 2004, 25, 66-73.
18. D. Kim, Y. Zhang, J. Kehr, T. Klason, B. Bjelke and M. Muhammed, *J. Magn. Magn. Mater.*, 2001, 225, 256-261.
19. S. Sun, C. Murry, D. Welle, L. Folk and A. Moser, *Science*, 2002, 287, 1989-1992.
20. M. Chen and D. Nikles, *Nano Lett.*, 2002, 2, 211-214.
21. P. Rogders, *Nat. Nanotechnol.*, 2006, 10, 1038.
22. L. Liz, *J. Mater. Sci.*, 1994, 29, 3797-3801.
23. M. Ferrick, J. Murtagh and J. Thomas, *Macromolecules*, 1989, 22, 1515-1517
24. C. Pereira, A. Pereira, C. Fernandes, M. Rocha, R. Mendes, M. Fernandez–García, A. Guedes, P. Tavares, J. Greneche, J. Araujo and C. Freire, *Chem. Mater.*, 2012, 24, 1496-1504.
25. S. Doh, E. Kim, B. Lee and J. Oh, *J. Magn. Magn. Mater.*, 2004, 276, 2238-2240.

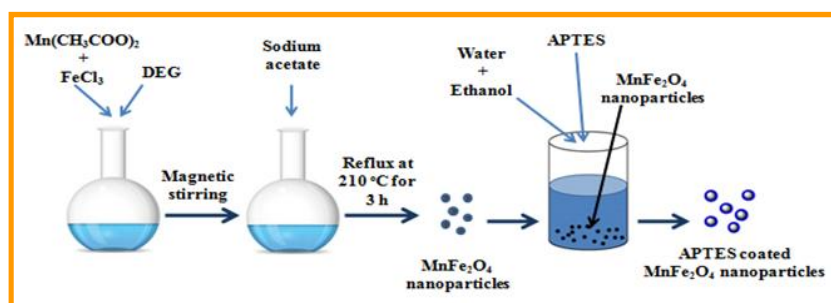
26. Y. Meng, Z. Liu, H. Dai, H. Hu and D. Zeng, *Powder Technol.*, 2012, 229, 270-275.
27. J. Jolivet and C. Chaneac, *E. Chem. Commun.*, 2004, 5, 481-483.
28. R. Joseyphus, D. Kodama, T. Matsumoto, Y. Sato, B. Jeyadevan and K. Tohji, *J. Magn. Magn. Mater.*, 2007, 310, 2393-2395.
29. W. Cai and J. Wan, *Colloid Interface Sci.*, 2007, 305, 366-370.
30. S. Sun, H. Zeng, D. Robinson, S. Raoux, P. Rice, S. Wang and G. Li, *J. Am. Chem. Soc.*, 2004, 126, 273-279.
31. Y. Hao and A. Teja, *J. Mater. Sci.*, 2003, 18, 415-422.
32. J. Osunam, D. De Caro, C. Amiens, B. Chaudret, E. Snoeck, M. Respaud, J. Broto, and A. Fert, *J. Phys. Chem.*, 1996, 100, 14571-14574.
33. C. Xu, J. Lee and A. Teja, *J. Supercrit. Fluid.*, 2008, 44, 92-97.
34. J. Wang, J. Sun, Q. Sun and W. Chen, *Mater. Res. Bull.*, 2003, 38, 1113-1118.
35. Y. Zheng, Y. Cheng, F. Bao and Y. Wang, *Mater. Res. Bull.*, 2006, 41, 525-529.
36. V. Khot, A. Salunkhe, N. Thorat, R. Ningthoujam and S. Pawar, *Dalton Trans.*, 2013, 42, 1249-1258.
37. A. Merzhanov, *Chemistry Of Advance Materials*, 1993, 19-39, Blackwell Scienific, Oxford.
38. K. Martirosyan and D. Luss, *Ind. Eng. Chem. Res.*, 2007, 46, 1492-1499.
39. A. Raghavender, K. Zadro, D. Pajic, Z. Skoko and N. Biliskov, *Mater. Lett.*, 2010, 64, 1144-1146.
40. C. Cannas, D. Gatteschi, A. Musinu, G. Piccaluga and C. Sangregorio, *J. Phys.*

- Chem.,1998, 102, 7721-7726.
41. A. Ismail, *Appl. Catal.*, 2005, 58, 115-121.
 42. X. Liu, Q. Tao, S. Shen and Y. Sens, *Actuators*, 1997, 40, 161-165.
 43. S. Solinas, G. Piccaluga, M. Morales and C. Serna, *Acta. Mater.*, 2001, 49, 2805-2811.
 44. Y. Li, M. Afzaal and P. O'Brien, *J. Mater. Chem.*, 2006, 22, 2175-2180.
 45. Y. Pang, X. Bao, *J. Mater. Chem.*, 2002, 12, 3699-3704.
 46. E. Kim, H. Lee, B. Kwak and B. Kim, *J. Magn. Magn. Mater.*, 2005, 289, 328-330.
 47. V. Pillai, P. Kumar, M. Hou, P. Ayyub and D. Shah, *Adv. Colloid Interface Sci.*, 1995, 55, 241-269.
 48. D. Farrell, S. Majetich and J. Wilcoxon, *J. Phys. Chem. B*, 2003, 107, 11022-11030.
 49. A. Samia, K. Hyzer, J. Schlueter, C. Qin and J. Jiang, *J. Am. Chem. Soc.*, 2005, 127, 4126-4127.
 50. L. Zhao, H. Yang, L. Yu, Y. Cui, X. Zhao, B. Zou and S. Feng, *J. Magn. Magn. Mater.*, 2006, 301, 445-451.
 51. M. Mahmoudi, A. Simchi, M. Imani and U. Hafeli, *J. Phys. Chem. C*, 2009, 113, 8124–8131.
 52. R. Hachani, M. Lowdell, M. Birchall, A. Hervault, D. Mertz, S. Begin-Colin and N.Thanh, *Nanoscale*, 2016, 8, 3278-3287.
 53. J. Bramhill, S. Ross and G. Ross, *Int. J. Environ. Res. Public Health*, 2017, 14,

66-71.

54. B. Rittich, A. Spanova, D. Horak, M. Benes, L. Klesnilova, K. Petrova and A. Rybnika, *Colloids Surf. B*, 2006, 52, 143-148.
55. M. Zborowski, J. Chalmers and W. Lowrie, *Magnetic Cell Manipulation and Sorting, Microsystems and Nanosystems*, 2017, 15-55.
56. K. Zipare, J. Dhumal, S. Bandgar, V. Mathe, G. Shahane, *J. Nanosci. Nanoeng.*, 2015, 3, 178-182.
57. P. Guo, G. Zhang, J. Yu, H. Li, X. S. Zhao, *Colloids Surf. A*, 2012, 395, 168-174.
58. E. Cho, H. Holback, K. Liu, S. Abouelmagd, J. Park, Y. Yeo, *Mol. Pharmaceutics*, 2013, 10, 2093-2110.

Studies on Functionalization of MnFe_2O_4 Nanoparticles with APTES



Chemical Papers
<https://doi.org/10.1007/s11696-019-00768-z>

ORIGINAL PAPER



APTES (3-aminopropyltriethoxy silane) functionalized MnFe_2O_4 nanoparticles: a potential material for magnetic fluid hyperthermia

P. R. Ghutepatil¹ · A. B. Salunkhe² · V. M. Khot³ · S. H. Pawar^{1,4}

The parts of this chapter have been published as research article.

Nanotechnology will eventually apply to all cancers. However, this grant is focusing on breast and prostate cancers because they represent a number of compelling challenges and opportunities in cancer research.

-Sean Murdock

5.1 Introduction

For the application of nanotechnology in biology and medicine, nanomaterial should satisfy below criteria:

- Nanoparticles must be outlined to interconnect cells and proteins without disconcerting the biological activities.
- Nanoparticle should conserve colloidal stability.
- Nano-material should be biocompatible and non-toxic.

The above criteria are obtained by selective fabrication of nanoparticle's surface using molecules. The remarkable properties and usefulness of nanoparticles can arise from their anomaly including size, superparamagnetism, surface to volume ratio and biocompatibility [1]. MNPs are being used in various biomedical implementations like magnetic hyperthermia, MRI, drug delivery, cell labeling [2-7]. Different techniques can be used for surface modification by using different surfactants like polymers, lipids and fatty acids. Due to the capping of nanoparticles their surface functionality, charge, reactivity, storage life and dimensions may changes. Variety of functional groups has been used to modification of surface of MNPs. Stability of nanoparticles can be improved by absorbing various surfactants on the surface of nanoparticles. The absorbed surfactant layer generates repulsive force between nanoparticles and restricts flocculation there, which improves the stability in water or other media [8-11].

MNPs can be coated by different types of surfactants to minimize toxicity, avert cluster formation, extend storage life and escalate the compatibility between nanoparticles and aqueous medium [12, 13]. Here, (3-Aminopropyl) triethoxysilane (APTES) is used as coating material due to its biocompatibility, existence of amino functional groups for bonding of different bioactive molecules and less toxicity. APTES is amine silane normally used in the functionalization of surfaces and process of silanization with alkoxysilane molecules. Silanization is the covering of a surface

with organo functional alkoxy silane molecules. The surface of MNPs can be anchored by silane coupling agent by directly silanizing with APTES [14]. APTES compound is an important coupling agent has found its applications in surface-decoration in which they form monolayer of amino-silane and is a widely used grafting agent [15]. Active amino groups (-NH₂) enhance surface functionalization and it covalently bonds with other active groups such as carboxyl (COOH), which can bond with other functional groups or antibodies [16].

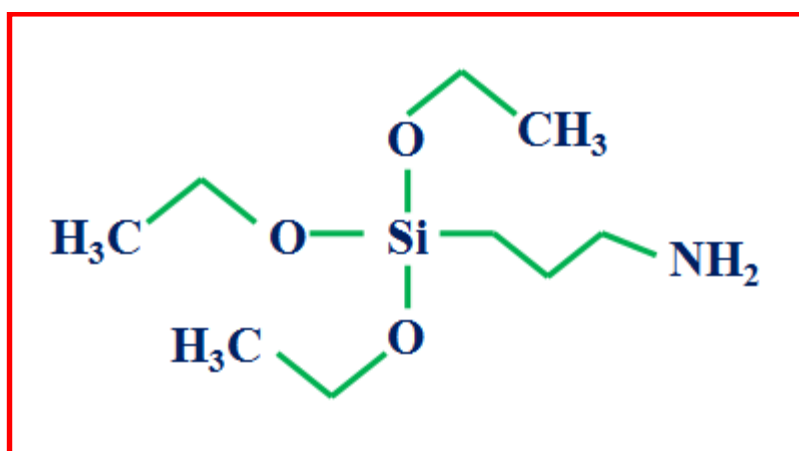


Fig.5.1 Structure of 3-aminopropyltriethoxysilane (APTES)

In present investigation, polyol method is used to synthesize MnFe₂O₄ MNPs and functionalized with APTES to enhance the colloidal stability for along with the structural, morphological and magnetic characteristics. The prime objective of this work is to study the functionalization of the nanoparticles. Coated and uncoated nanoparticles are abbreviated as P1 and P2 through out the chapter.

5.2 Experimental

5.2.1 Synthesis of APTES coated MnFe₂O₄ nanoparticles

The synthesis of bare MnFe₂O₄ nanoparticles has been explained in section 4.4.1 of Chapter 4. Fig.5.2 represents procedure for synthesis of APTES coated MnFe₂O₄ nanoparticles. The surface of MnFe₂O₄ was coated with 3-

aminopropyltriethoxysilane (APTES) by silanization reaction. The MnFe₂O₄ nanoparticles obtained by above polyol method were dispersed in an ethanol and water and sonicated to get uniform dispersion. The 2 mL APTES was added, while bath temperature at 40 °C and stirred for 2 h. The formed product was separated by magnetic decantation process and dried at room temperature [31]. This sample denoted as 'P2'.

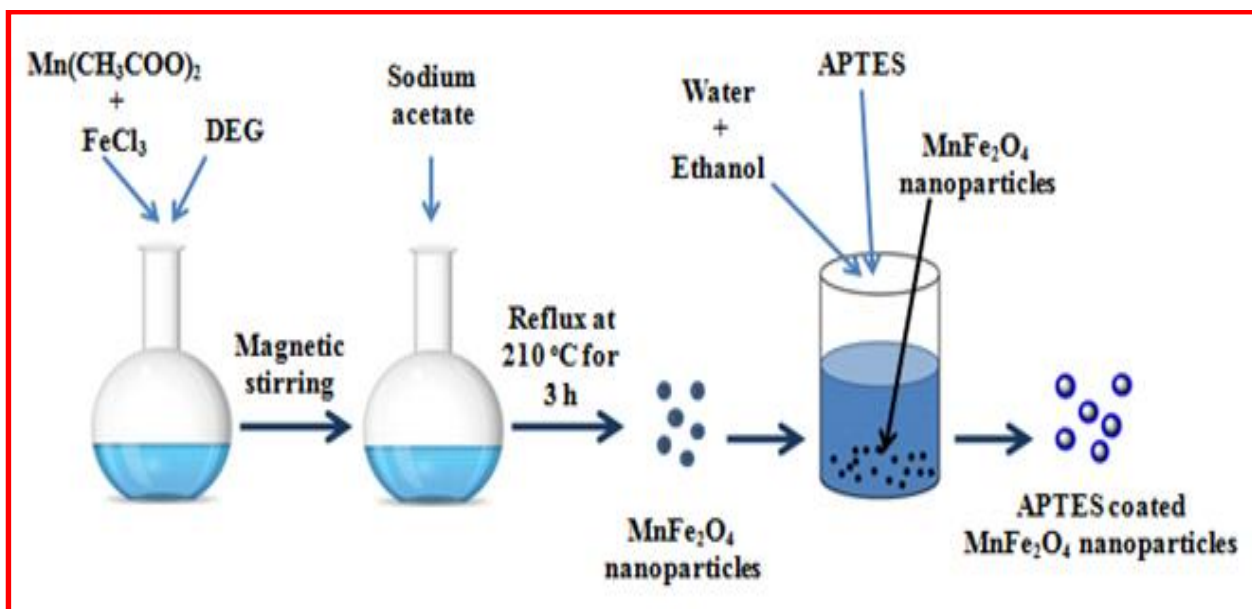


Fig. 5.2 Graphical representation of synthesis of APTES coated MnFe₂O₄ nanoparticles

After that, the coated MnFe₂O₄ nanoparticles were washed several times with double distilled water, to remove excess amount of chemicals. After purification, NPs dried naturally and are subjected to characterize using various techniques. Fig. 5.3 represents procedure for synthesis of APTES coated MnFe₂O₄ nanoparticles.

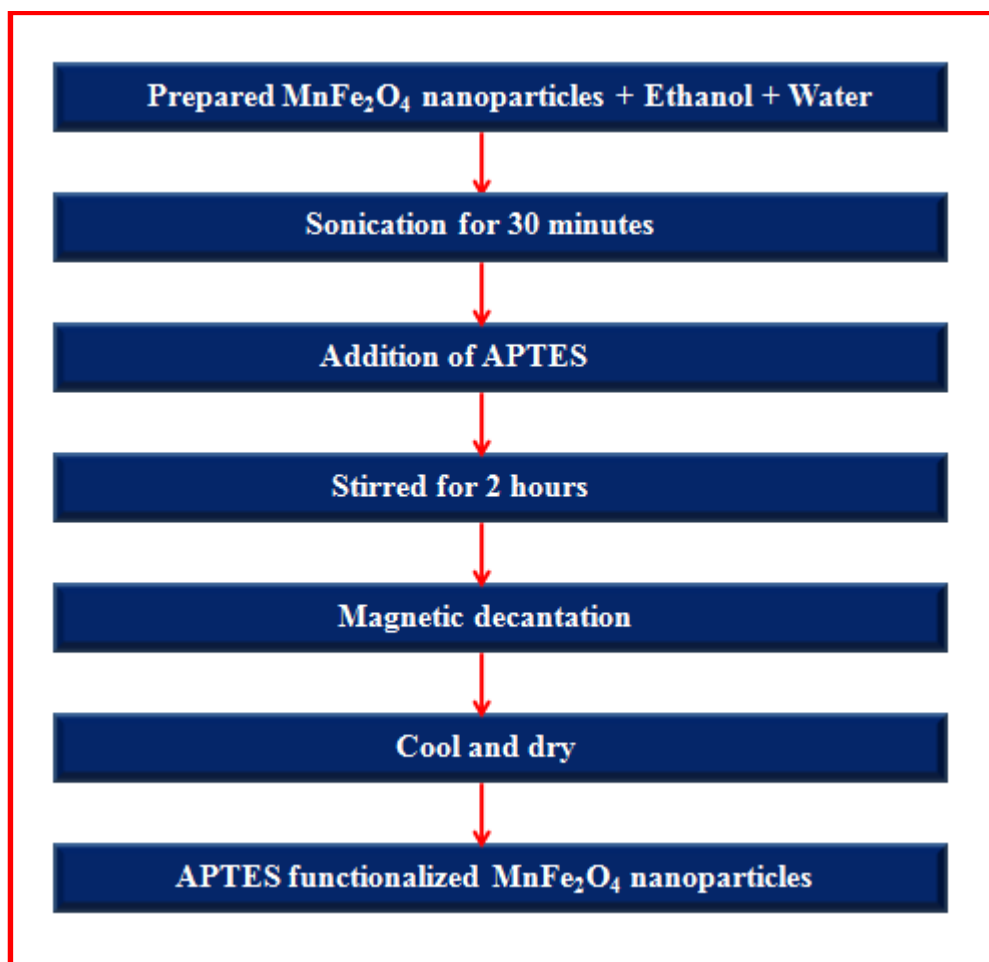


Fig. 5.3 Procedure for synthesis of APTES coated MnFe₂O₄ nanoparticles

5.2.2 Characterization

The XRD (Rigaku MiniFlex 600) was used for structural analysis and phase identification of obtained MNPs by using Cu-K_α ($\lambda=1.5406 \text{ \AA}$) in the 2θ range from 20° to 80° . FESEM (Hitachi S-4800) and HRTEM (TEM, JEM-2100F Model, Japan) were used to determine the morphology and size of the nanoparticles. Presence of magnetic core and coating of the MNPs were confirmed by FTIR spectroscopy (Alpha ATR Bruker Eco Model). The size distribution of MNPs was determined by DLS measurements using a PSS/NICOMP 380 ZLS (Particle Sizing System, Santa Barbara, CA, USA). Transanalytical instrument mode (SDT 2960) was used for thermal study of coated and uncoated MNPs. MNPs were heated from room temperature to 900°C with a heating rate $10^\circ\text{C min}^{-1}$ under nitrogen (N₂) flow to

measure a weight loss. Magnetic characterization was carried out with SQUID-VSM under the applied magnetic field of ± 40 at room temperature.

5.3 Results and discussion

5.3.1 Structural analysis

XRD analysis

Structural analysis and phase identification of obtained MNPs were performed using XRD technique. Diffraction patterns of P1 and P2 samples are showed in Fig. 5.4 The diffraction peaks are indexed at (220), (311), (400), (422), (511) and (440) planes and all the peaks are matched with the cubic spinel structure of MnFe₂O₄ (JCPDS Card No. 73-1964). The full-width at half maximum (FWHM) of the most intense peak (311) is used to calculate crystallite size of MNPs by Scherrer's formula (3.1). An inverse spinel cubic structure (Fd3m) of both samples is affirmed from obtained diffractograms. The Lattice constant value was ~ 8.346 Å and it was calculated considering single phase for both samples. It can be concluded from XRD pattern that coating with APTES does not influence the crystal structure of MnFe₂O₄. It is observed that after APTES coating peak broadening increased and intensity is slight decreased. The crystallite size calculated by Scherrer's formula is 8~10 nm [33].

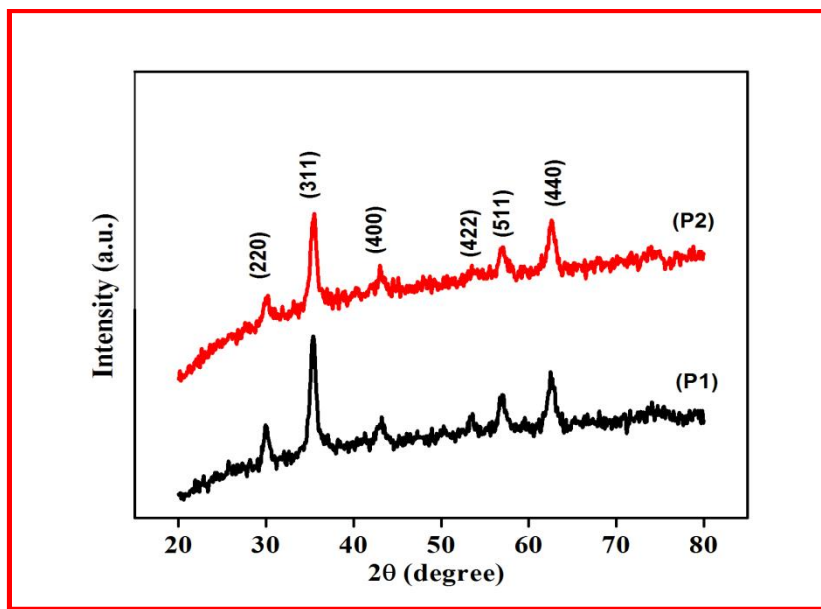


Fig. 5.4 XRD patterns of uncoated MnFe₂O₄ (P1) and APTES coated MnFe₂O₄ (P2)

5.3.2 Microstructural analysis

SEM analysis

SEM is used to determine morphology of the prepared samples as shown in Fig. 5.5. (a and b) The uncoated nanoparticles have shown more agglomeration in comparison with coated one due to the dipole-dipole interaction. Both the nanoparticles are spherical in shape. The coated nanoparticles formed clusters due to the magnetic nature of nanoparticles [34]. Fig.5.5 (a) shows complicated morphology due to high agglomeration while Fig.5.5 (b) shows distinct nanoclusters which are roughly spherical in shape. After coating, morphology of MnFe₂O₄ is observed in uniform crystal size.

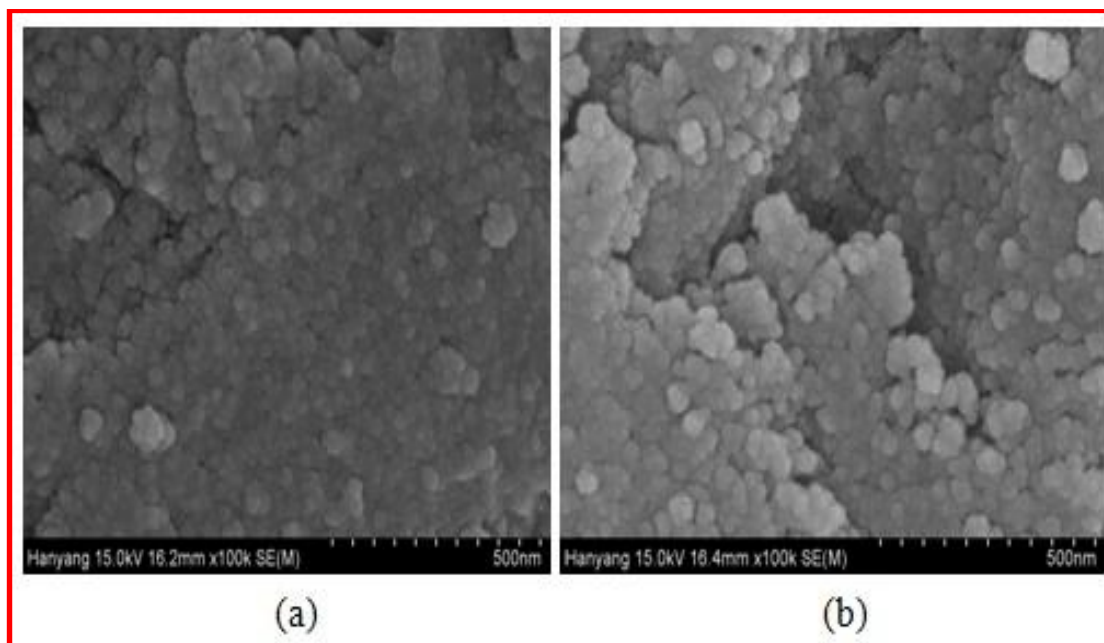


Fig. 5.5 FE-SEM images of (a) uncoated MnFe₂O₄ (P1), (b) APTES coated MnFe₂O₄ (P2)

TEM analysis

The particle size and morphology of uncoated and coated MNPs were studied with the help of TEM, which are shown in Fig. 5.6 (a, b) TEM images show roughly spherical nanoparticles having some irregularities, with slightly wide size distribution. However, sample (P2) i.e. APTES coated MNPs shows slight conglomeration. This is probably due to the oriented attachment growth mechanism leading the minimization of surface energy. It depends on the collective behaviour of nanoparticles and intermolecular force existing between them [35]. The average particle size is within the range 11-13 nm, which is in well accordance with the particle diameters obtained from XRD data. The corresponding selected area electron diffraction (SAED) patterns of coated sample (P2) in Fig. 5.5(c) show glowing ring patterns indicating crystalline nature of sample.

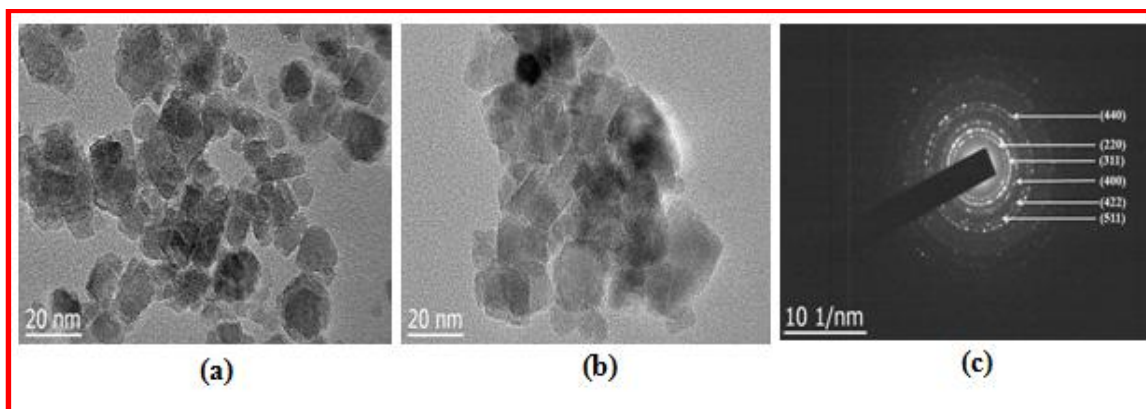


Fig. 5.6 TEM images of (a) uncoated MnFe₂O₄ (P1), (b) APTES coated MnFe₂O₄ (P2) and (c) SAED pattern

5.3.3 Chemical bonding study

FTIR analysis

The existence of APTES on the surface of MNPs was confirmed by FTIR spectroscopy. FTIR spectra of uncoated and coated nanoparticles are shown in Fig. 5.7. The band observed for sample (P1) at around $\sim 590\text{ cm}^{-1}$ is attributed to the Fe-O and peaks at about 2870-2959, 1580, 1430 and 1057 cm^{-1} are due to C-H stretching, O-H stretching, C-H bending, C-O bending and O-H bending vibrations respectively [37, 38]. The bands noticed for sample (P2) at 584 correspond to Fe-O-Si. However, these bands cannot be seen in FTIR spectrum due to overlapping with Fe-O vibration of nanoparticles. The adsorption of silane onto the surface of nanoparticles was confirmed by peaks at 1066 cm^{-1} , 1561 cm^{-1} , 3343 cm^{-1} , 1483 cm^{-1} corresponds to Si-O-Si, N-H bending, N-H stretching and C-N stretching vibrations, respectively. The presence of anchored propyl group was confirmed by C-H stretching vibrations that appeared at 2936 and 2887 cm^{-1} [39, 40]. Therefore FTIR spectrum confirms the presence of APTES on the surface of MnFe₂O₄ nanoparticles.

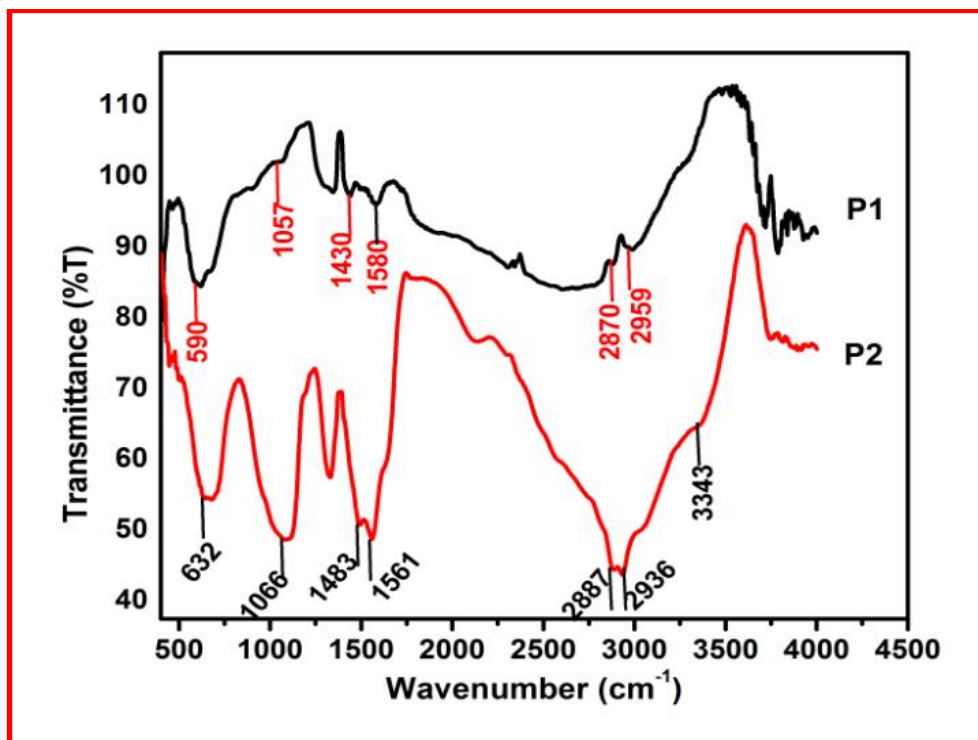


Fig. 5.7 FTIR spectra of uncoated MnFe₂O₄ (P1) and APTES coated MnFe₂O₄ (P2)

5.3.4 Magnetization study

VSM analysis

The M versus H measurement is taken at 300 K to understand the effect of functionalization on the magnetic behavior of MnFe₂O₄ and results have been displayed in Fig.5.8. A hysteresis curve of uncoated (P1) and APTES coated (P2) MnFe₂O₄ nanoparticles at 300 K show that coercivity and remanence are negligible for both the samples. It indicates the superparamagnetic behavior of MnFe₂O₄ nanoparticles before and after coating. The M_s values of APTES coated MnFe₂O₄ (53 emu/g) which is smaller than the M_s values of uncoated MnFe₂O₄ (60 emu/g) at an applied field of ± 40 kOe. The reduction in magnetization for sample (P2) is due to the coating, which reduces the magnetization value because of magnetic dipolar interaction [41, 42].

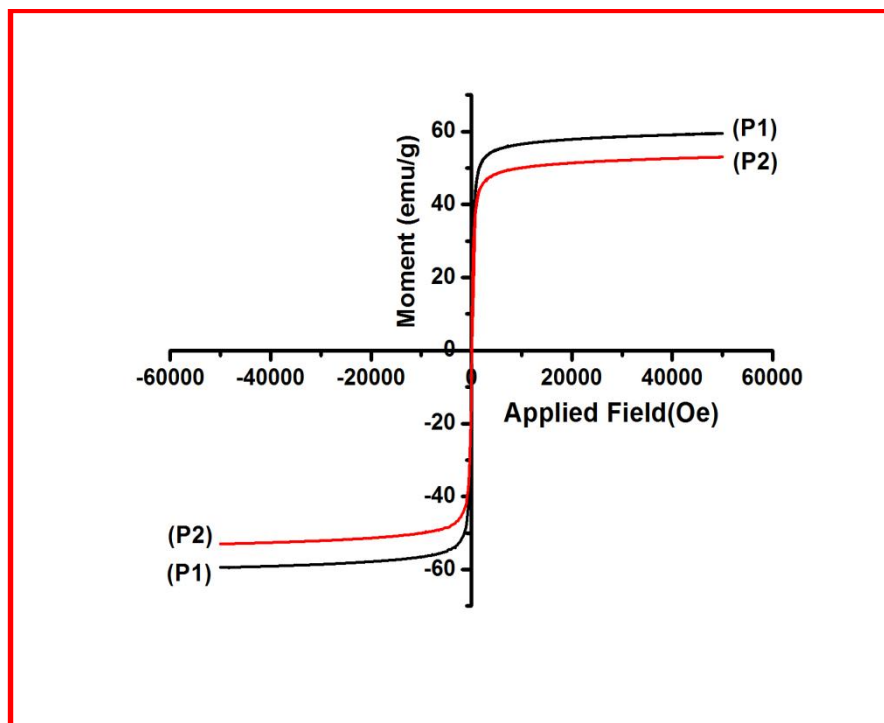


Fig. 5.8 M-H curve of uncoated MnFe₂O₄ (P1) and APTES coated MnFe₂O₄ (P2)

5.3.5 Thermogravimetric analysis

TGA analysis

TGA provides further confirmation on structure of coating on surface of nanoparticles. TGA analysis of uncoated and coated MnFe₂O₄ nanoparticles is shown in Fig. 5.9. Thermogravimetric (TG) study of uncoated and coated MnFe₂O₄ nanoparticles is carried out in nitrogen atmosphere in temperature range from room temperature to 900 °C with a heating rate of 10 °C min⁻¹. The uncoated MnFe₂O₄ nanoparticles exhibit lower weight loss as compared to coated nanoparticles. The sample (P1) in Fig. 5.9 shows weight loss in three stages in the temperature ranges of room temperature to 200 °C, 200-400 °C and 600-800 °C. The weight loss in initial step corresponding to the evaporation of adsorbed water and moisture, the weight loss in second step represents the decomposition of diethylene glycol from the surface of sample and weight loss in third step from 600-800 °C, it is quite slow step due to the further decomposition of sample to form pure MnFe₂O₄ [43]. The Sample

(P2) shows TGA curve of APTES coated nanoparticles. A drastic drop can be seen in the range 150-400 °C and it is contributed from the thermal decomposition of the 3-aminopropyl groups [44]. TGA analysis has confirmed that APTES get anchored on the surface of MnFe₂O₄.

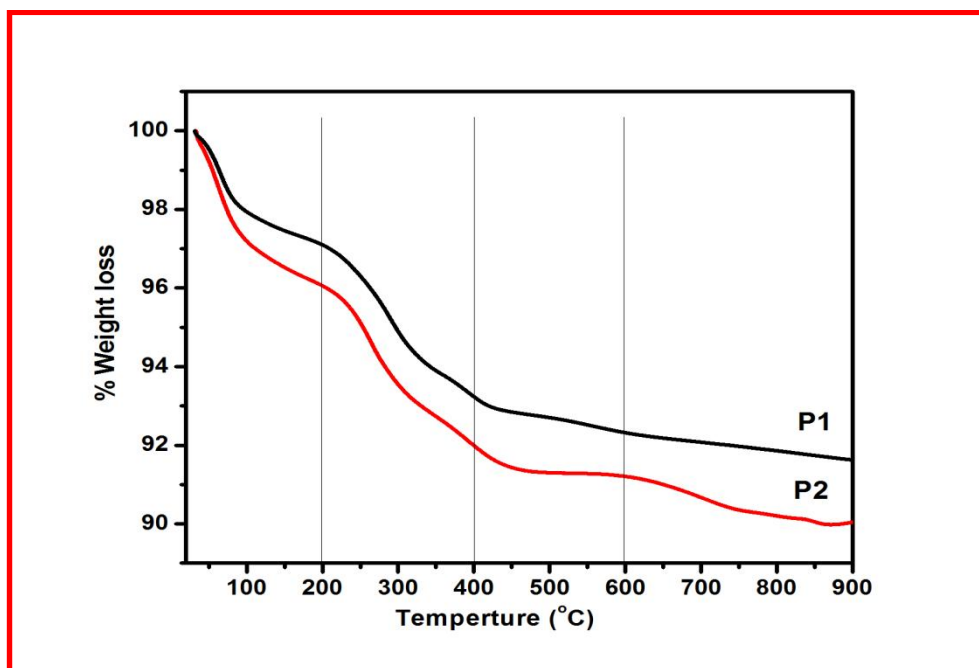


Fig. 5.9 Thermogravimetric pattern of uncoated MnFe₂O₄ (P1) and coated MnFe₂O₄ (P2)

5.3.6 Colloidal stability study

DLS analysis

DLS measurements have been performed to study the effect of functionalization on the overall size of the MNPs when dispersed in double distilled water. Fig. 5.10 illustrates the hydrodynamic size of the uncoated (P1) and APTES coated (P2) MnFe₂O₄ in distilled water at pH ~7. The hydrodynamic size of uncoated and APTES coated MnFe₂O₄ nanoparticles is found to be ~104.5 (±13.0) and ~50.2 (±9.7) nm, respectively. DLS show large size of nanoparticles as compared XRD and TEM due to their accumulation in absence of exterior magnetic field caused by

magnetic dipole–dipole interactions between nanoparticles and it leads to larger hydrodynamic size. There is discrepancy in size measurements from TEM and DLS techniques. This is readily due to the reason that we cannot exclude for the samples where small aggregates of two to three nanocrystals capped together within the same polymer shell. Hydrodynamic size of MNPs is one of the key characteristic for biomedical applications [36]. The MnFe₂O₄ nanoparticles in present case exhibit hydrodynamic size close to the mentioned values there by having potential application in biomedical field.

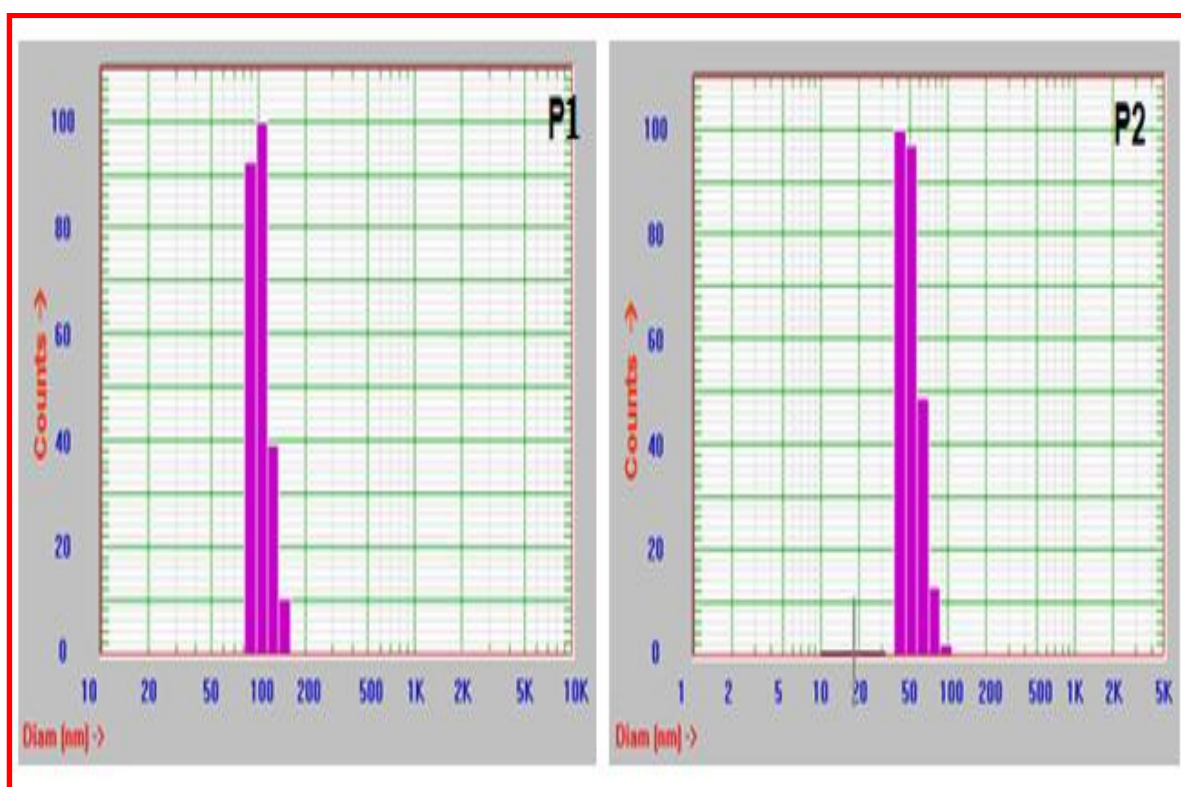


Fig. 5.10 DLS histogram of uncoated MnFe₂O₄ (P1) and APTES coated MnFe₂O₄ (P2)

5.4 Conclusions

Monodispersed MnFe₂O₄ nanoparticles were synthesized by a polyol method successfully and surface of MnFe₂O₄ was coated with 3-aminopropyltriethoxy silane (APTES) in order to obtain well-dispersed surface functionalized biocompatible MNPs. This study demonstrated the effect of APTES coating on the surface behavior of MnFe₂O₄ MNPs. A simple ultrasonication method can be used for coating of APTES on the surface of MnFe₂O₄ MNPs. The APTES is anchored on the surface of MnFe₂O₄ via silanization reaction and it is confirmed from FTIR as well as TGA study. From the SEM and TEM analysis it is observed that MNPs are roughly spherical or ellipsoidal-shaped and were around 11-13 nm in size. Experimental results showed that nanoparticles exhibited superparamagnetic behavior and high saturation magnetization at room temperature.

References

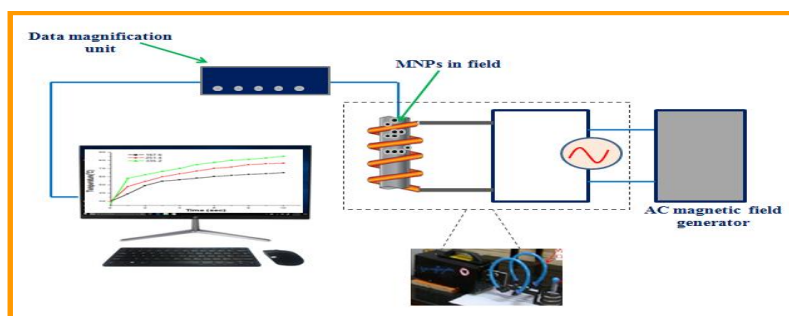
1. M. Mahmoudi, A. Simchi, M. Imani and U. Hafeli, *J. Phys. Chem. C*, 2009, 113, 8124-8131.
2. R. Hachani, M. Lowdell, M. Birchall, A Hervault, D Mertz, S. Begin-Colin and N. Thanh, *Nanoscale*, 2016, 8, 3278-3287.
3. B. Rittich, A. Spanova, D. Horak, M. Benes, L. Klesnilova, K. Petrova and A. Rybnika, *Colloids Surf. B*, 2006, 52, 143-148.
4. L. Zhao, H. Yang, L. Yu, Y. Cui, X. Zhao, B. Zou and S. Feng, *J. Magn. Magn. Mater.*, 2006, 301, 445-451.
5. M. Zborowski, J. Chalmers and W. Lowrie, *Microtechnology for Cell Manipulation and Sorting, Microsystems and Nanosystems*, 2017, 15-55.
6. J. Bramhill, S. Ross and G. Ross, *Int. J. Environ. Res. Public Health*, 2017, 14, 66-73.
7. A. Muela, D. Munoz, R. Martin-Rodriguez, I. Orue, E. Garaio, A. Diaz de Cerio, J. Alonso, J. Garcia and M. Luisa Fdez-Gubieda, *J. Phys. Chem. C*, 2016, 120, 24437-24448.
8. A. Gupta and M. Gupta, *Biomaterials*, 2005, 26, 3995-4021.
9. D. Kim, M. Amin, S. Elborai, S. Lee, Y. Koseoglu, M. Zahn and M. Muhammed, *J. Appl. Phys.*, 2005, 97, 10J510.
10. M. Phadatare, J. Meshram, K. Gurav, J. Kim and S. Pawar, *J. Phys. D: Appl. Phys*, 2016, 49, 095004-095013.
11. P. Presa, Y. Luengo, M. Multigner, R. Costo, M. Morales and A. Rivero, *J. Phys. Chem. C*, 2012, 116, 25602–25610.

12. B. Sahoo, S. Sahu, S. Nayak, D. Dhara and P. Pramanik, *Catal. Sci. Technol.*, 2012, 2, 1367-1374.
13. E. Smith and W. Chen, *Langmuir.*, 2008, 24, 12405-12409.
14. W. Cai and J. Wan, *J. Colloid Interface Sci.*, 2007, 305, 366-370.
15. Z. Beji, A. Hanini, L. Smiri, J. Gavard, K. Kacem, F. Villain, J. Greneche, F. Chau and S. Ammar, *Chem. Mater.*, 2010, 22, 5420-5429.
16. R. Hergt, W. Andra and H. Nowak, *Magnetic hyperthermia and thermoablation, Magnetism in Medicine*, 2nd Edition, Berlin: Wiley-VCH, 2006.
17. P. Moroz, S. Jones and B. Gray, *Int. J. Hyperthermia*, 2002, 18, 267-284.
18. B. Thiesen and A. Jordan, *Inter. J. Hyperthermia*, 2008, 24, 467-474.
19. P. Wust, B. Hildebrandt, G. Sreenivasa, B. Rau, J. Gellermann, H. Riess, R. Felix and P. Schlag, *Lancet. Oncol.*, 2002, 3, 487-497.
20. R. Weissleder, D. Stark, B. Engelstad, B. Bacon, C. Compton, D. White, P. Jacobs and J. Lewis, *Am. J. Roentgenol.*, 1989, 152, 167.
21. R. Rand, H. Snow, D. Elliott and G. Haskins, *U. S. Patent specification* 4, 1985, 545, 368.
22. I. Brigger, C. Dubernet and P. Couvreur, *Adv. Drug. Deli. Rev.*, 2002, 54, 631-651.
23. R. Rosensweig, *J. Magn. Magn. Mater.*, 2002, 252, 370-374.
24. A. Salunkhe, V. Khot and S. Pawar, *Curr. Top. Med. Chem.*, 2014, 14, 572-594.
25. N. Shetake, M. Balla, A. Kumar and B. Pandey, *J. Radiat. Cancer. Res.*, 2016, 7, 13-17.

26. A. Hervault and N.Thanh, *Nanoscale.*, 2014, 6(20), 11553-11573.
27. S. Rovers, L. Poel, C. Dietz, J. Noijen, R. Hoogenboom, M. Kemmere, K. Kopinga and J. Keurentjes, *J. Phys. Chem. C*, 2009,113,14638-14643.
28. V. Khot, A. Salunkhe, N. Thorat, R. Ningthoujam and S. Pawar, *Dalton Trans.*, 2013, 42, 1249-1258.
29. R. Ghosh, Y. Pradhan, S. Devi, M. Tewari, A. Kumar, S.Sharma, N. Gajbhiye, R.Vatsa, B. Pandey and R. Ningthoujam, *J. Mater. Chem.*, 2011, 21, 13388-13398.
30. Q. Pankhurst, J. Connolly, S. Jones and J. Dobson, *J. Phys. D: Appl. Phys.*, 2003, 36, R167-R181.
31. S. Xuan, F. Wang, Y. Wang, J. Yu and K. Leung, *J. Mater. Chem.*, 2010, 20, 5086-5094
32. X. Li, G. Zhu, Y. Luo, B. Yuan and Y. Feng, *Trends Anal. Chem.*, 2013, 45, 233-247.
33. S. Waje, M. Hashim, W. Yusoff and Z. Abb, *Appl. Surf. Sci.*, 2010, 256, 3122-3127.
34. A. Ebrahiminezhad, Y. Ghasemib, S. Rasoul–Amini, J. Barar and S. Davarana, *Colloids Surf. B*, 2013, 102, 534-539.
35. K. Barick, M. Aslam, P. Prasad, V. Dravid and D. Bhadur, *J. Magn. Magn. Mater.*, 2009, 321, 1529-1532.
36. Y. Li, X. Li and T. He, *Langmuir*, 2013, 29, 15275-15282.
37. M. Mashhadizadeh and M. Amoli-Diva, *J. Nanomed. Nanotechol.*, 2012, 3, 1000139.

38. D. Maity, S. Kale, R. Ghanekar, J. Xue and J. Ding, *J. Magn. Magn. Mater.*, 2009, 321, 3093-3098.
39. D. Keerthana, K. Namratha, K. Byrappa and H. Yathirajan, *J. Magn. Magn. Mater.* 2015, 378 551-557.
40. B. Feng, R. Hong, L. Wang, L. Guo, H. Li, J. Ding, Y. Zheng and D. Wei, *Colloids Surf. A*, 2008, 328, 52-59.
41. P. Guo, G. Zhang, J. Yu, H. Li and X. Zhao, *Colloids Surf. A*, 2012, 395, 168-174.
42. H. Cao, J. He, L. Deng and X. Gao, *App. Surf. Sci.*, 2009, 255, 7974-7980.
43. M. Yamaura, L. Sampaio, M. Macedo, M. Nakamura and H. Toma, *J. Magn. Magn. Mater.*, 2004, 279, 210-217.
44. S. Laurent, S. Dutz, U. Hafeli and M. Mahmoudi, *Adv. Colloid Interface Sci.*, 2011, 166, 8-23.

Magnetic hyperthermia study of APTES Functionalized MnFe_2O_4 Nanoparticles



Chemical Papers
<https://doi.org/10.1007/s11696-019-00768-z>

ORIGINAL PAPER

APTES (3-aminopropyltriethoxy silane) functionalized MnFe_2O_4 nanoparticles: a potential material for magnetic fluid hyperthermia

P. R. Ghutepatil¹ · A. B. Salunkhe² · V. M. Khot³ · S. H. Pawar^{1,4}

Check for updates

The parts of this chapter have been published as research article.

The impact of nanotechnology is likely to exceed the impact that the electronics revolution has had on our lives.

-Steve Jurvetson

6.1 Introduction

In the beginning of 21st century, the foremost communal health issue problem is restriction of cancer disease. Cancer has continued as leading reason for deaths in the world despite intensive attempts taken to restrict the cancer. In cancer, the unusual tissues or cells grow with likely to conquer parts of the body and eventually they harm the body. The unusual tissues or cells form a subset of (neoplasm) tumor. These unusual tissues or cells can penetrate into normal body tissues. These unusual tissues or cells can be furthermore recognized by breast cancer, lung cancer, colon cancer etc. In 1957, Gilchrist et al. had first evinced the use of nanoparticles for cancer therapy using magnetic hyperthermia. Normally, cancer therapies are categorized into radiotherapy chemotherapy and surgery treatments but these treatments are not always adequate to assassinate the disease from bottom or root. Radiation therapy and chemotherapy may be used along with surgery. But these types of treatments show some side effects. To overcome from these side effects, an efficient treatment is required and this can be done by magnetic hyperthermia without any side effects [1].

In hyperthermia treatment, the cancer tissues or cells are killed in temperature range of 43-47 °C with minimal injury to normal cells. Healthy cells can survive up to temperature 46 °C but not cancerous cells [2, 3]. Magnetic hyperthermia is also known as thermotherapy which is relatively new method for cancer therapy. In this treatment, alternate magnetic field and MNPs integrates and used as a heating source for cancer cell treatment. MNPs are injected in tumor cells and exterior magnetic field is applied in hyperthermia therapy. After the injection of MNPs, they enter in affected area and cancer cell can be destroyed by reaching temperature around 42-46 °C without influencing normal cells [4].

6.2 Magnetic hyperthermia of MNPs

There are many therapies available for cancer treatment but some are costly and some have side effects. Hyperthermia therapy is most encouraging therapy for

cancer treatment. The concept of applying heat to treat certain condition or tumor is not a new, it has long history. In ancient history, Greeks, Romans and Indians used to apply a heat to treat various tumors. In 1988, Westermarck intentionally used hyperthermia to treat cancer with temperature of 42 to 44°C. In 1950s decade, hyperthermia therapy using magnetic field and nanoparticles has been started. There are 2 types of heating treatments renowned i.e. hyperthermia and thermoablation. Hyperthermia therapy can be performed between 41 to 46° C, where as thermoablation can be performed between 46 to 56 °C to destruct the tumors. In thermal therapy, the applied heat should be appropriate and should be applied to correct site or part of body. Also, cancer cells get damaged or killed only when applied temperature is high enough and sustains long enough [5, 6].

There are many ways by which heat is induced for hyperthermia therapy. The most usual ways are direct application of heat, microwave heating, focused ultrasound, induction heating and magnetic hyperthermia. Magnetic hyperthermia is very popular and effective therapy among hyperthermia therapies. Magnetic hyperthermia produces controllable heat inside patient's body and temperature distribution can be controlled by size of MNPs [7]. In 1999, Jorden et al. [8] was first instigated the magnetic fluid hyperthermia technique. A fluid containing MNPs can be injected into cancer tissues or cells and exterior alternating magnetic field is being applied with frequencies. The MNPs generate heat and destroy tumor cells or tissues.

The most challenging issue is to heat only cancerous cells without destroying healthy cells. There are different techniques like radiofrequency, infrared radiations etc and tubes with hot water bath available for induction of hyperthermia. However, these are not so beneficial or suitable techniques due to its various side effects. Therefore magnetic hyperthermia is propitious therapy which imply on dispersion of MNPs throughout the affected tissue by applying an exterior AC magnetic field. A fluid containing MNPs can be injected into cancer tissues or cells and exterior alternating magnetic field is being applied with frequencies in hyperthermia therapy

using MNPs. The fluid must be biocompatible and well dispersed [9]. When a mixture of MNPs and water or hydrocarbon fluid is infused or suffused in a tumor or cell and exposed to an exterior alternating magnetic field with different frequencies which generate heat, it can become a source of heat to raise a temperature which can weaken or destroy unusual cancer-affected tissues or cells [10].

Magnetic hyperthermia has received huge recognition because of various following reasons:

- Targeted, homogenous and controlled heat generation capacity.
- Ability to access deep-rooted tumors.
- Ability to specifically target the tumor vasculature or hypoxic tumor.

6.3 Magnetic induction heating

Local hyperthermia using MNPs has become a potential therapeutic modality of cancer therapy in the area of medicine. The main principle of MNP-based hyperthermia is a distribution of nanoparticles through a targeted tumor area or site accompanied by heat generation using an exterior alternating magnetic field. Heat generation efficiency due to an applied magnetic field of any particle is measured by SAR. Heating mechanism of MNPs includes three types of heat losses, i.e. hysteresis losses, Neel and Brownian relaxation losses. The Brownian and Neel diffusion of MNPs magnetic moment govern magnetization relaxation with very less hysteresis loss [11, 12].

Magnetic heat induction of MNPs provides following advantages over traditional hyperthermia treatment:

- MNPs can have sizes from few nm to tens of nm. Therefore, tumor cells absorb them easily. It increases the effectiveness of delivering heat to targeted tissue.
- MNPs can efficiently pass the brain barrier and blood.

- MNPs can be easily engineered into colloidal form with different drug delivery approaches.
- Magnetic fields within armless range can be applied to human body.

6.3.1 Mechanism of magnetic induction heating

In magnetic induction, sample can be exposed to higher frequency magnetic field, which originates electric field causing in Joule heating by conduction current law. Spinel ferrites are promising candidates for hyperthermia therapy because of their higher frequency response, higher resistivity property and higher heating ability. In magnetic induction heating system, the MNPs are subjected to an exterior AC magnetic field and due to their losses during their magnetization turnaround process [13, 14]. Principle mechanism of cancer hyperthermia therapy using MNPs is shown in Fig. 6.1

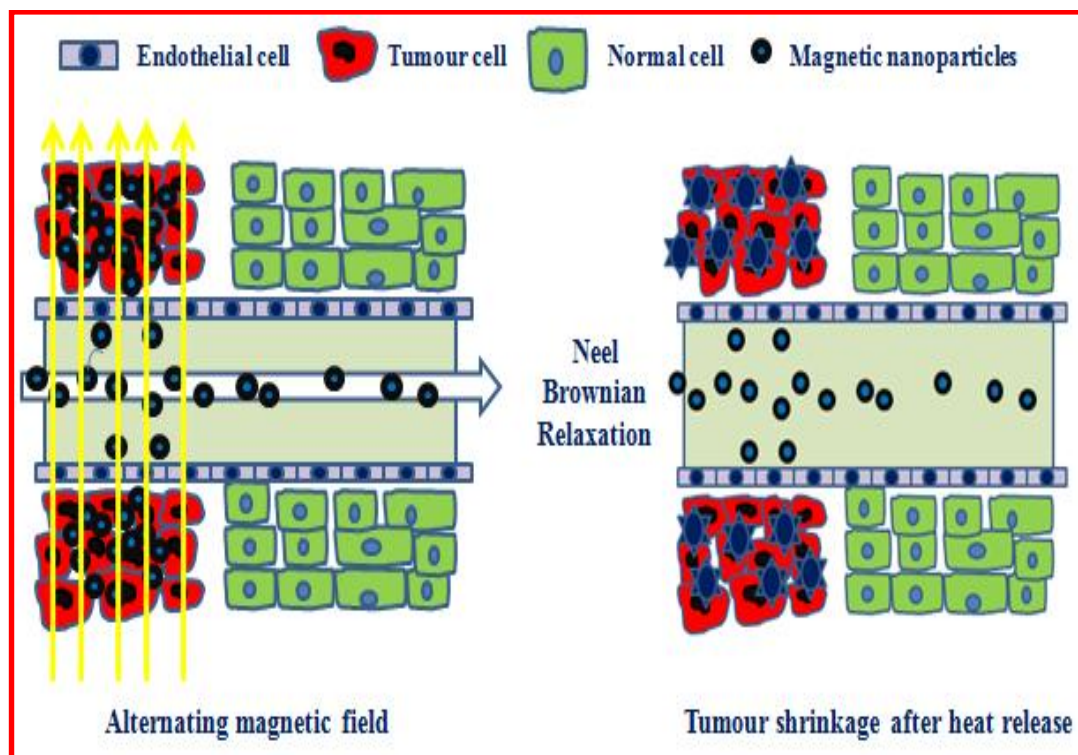


Fig. 6.1 Mechanism of magnetic fluid hyperthermia

6.3.2 Heat dissipation processes by MNPs

In induction heating, when MNPs are attributed to an exterior AC magnetic field it generates heat, which diminishes the cancer cells at 42-46 °C without affecting normal cells. MNPs having core diameter < 20 nm can be used in magnetic hyperthermia. The nanoparticles should be well-dispersed in the fluid superparamagnetic. The magnetization relaxation is ruled by collaboration of two rotations i.e. external rotation and internal rotation. It means Brownian and Neel diffusion of magnetic moment of particles with less contribution by hysteresis loss. The mechanism of relaxation is not only depends on the size of MNPs but also on the magnetic material. There are three different processes by which MNPs can generate heat in exterior alternating field i.e. eddy current losses, hysteresis losses and Néel and Brownian relaxation losses [15-17].

Hysteresis losses

Magnetic structure of MNPs is voluntarily breaks into domains. Domains are regions collecting magnetic moments of particle with same orientation. Magnetization exhibits nonlinear behavior when the sample is subjected to the cycle of positive/negative fields, which can be described by singular representation called hysteresis loop. This normally happens at high field magnitudes. Magnetization and demagnetization of magnetic core causes the hysteresis loss when current flow in reverse and forward direction. Magnetic flux increases as magnetization force increases whereas magnetic flux doesn't get decreased at matching rate when magnetization force decreases. It decreases slowly. Flux density can have positive (+) value when magnetization force reaches to 0 (zero). Magnetization force should be applied in -ve direction to reach flux density at zero. The heat freed by MNP through hysteresis loss is given by,

$$A = \int_{-H_{max}}^{+H_{max}} \mu_o M(H)dH \dots \dots 6.1$$

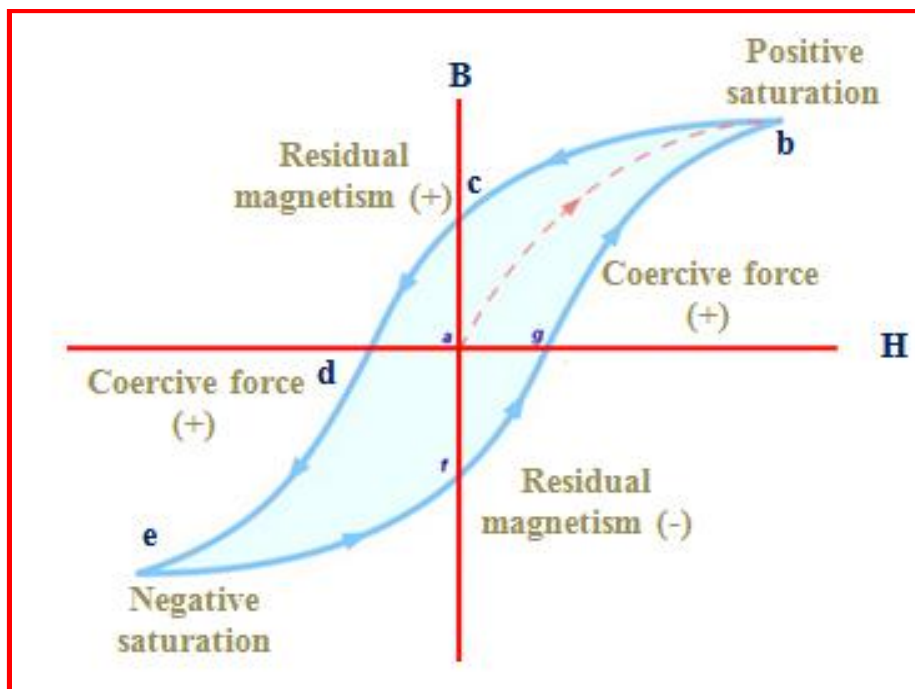


Fig. 6.2 Hysteresis loop

Relaxation Losses

Heating of magnetic nanoparticles is caused by magnetic relaxation loss. Relaxation losses can be categorized as Néel relaxation loss and Brownian relaxation loss.

Néel relaxation loss

The Néel relaxation loss can be demonstrated by magnetic moment's rotation. In this case, the magnetic moment of MNPs normally has two steady orientations anti parallel to each other due to magnetic anisotropy of MNPs and can be unconnected by energy barrier. There is limited possibility for magnetization to forward and reverse direction at finite temperature. The shape and surface of material, volume of the superparamagnetic MNPs can influence the Néel relaxation time so the heating efficiency MNPs.

The formula for the Néel relaxation time constant is defined as:

$$\tau_N = \tau_0 e^{\frac{KV_m}{K_B T}} \dots\dots 6.2$$

where τ_0 represents relaxation factor, K represents magnetic anisotropy energy density, V_m denotes mean particle volume, K_B is the Boltzmann constant, and T represents absolute temperature, $\tau_0 = 10^{-9}$ s.

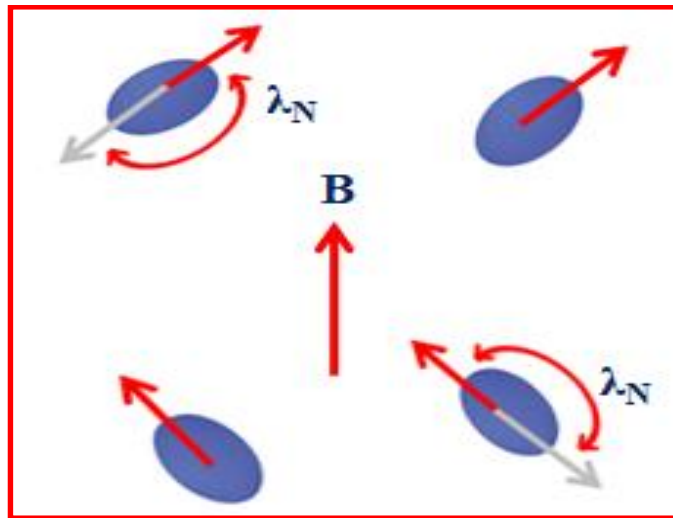


Fig. 6.3 Neel relaxation loss

Brownian relaxation loss

The magnetic moment gets aligned with magnetic field (H) and particle gets rotated under an AC magnetic field in Brownian rotational relaxation (τ_B). Heat can be produced during rotation and heat dissipation can be occurred after strike with adjacent medium and it is because of Brownian motion within carrier liquid. This corresponds to magnetic nanoparticles rotation as torque. This is attributed to the rotation of the magnetic particle as a whole because of the torque employed on magnetic moment by exterior AC magnetic field. The energy freed during relaxation is called Brownian relaxation. Brownian relaxation at the temperature (T) is expressed by:

$$\tau_B = \left(\frac{3\eta V_H}{K_B T} \right) \dots \dots 6.3$$

Where, η represents dynamic viscosity of liquid carrier and V_H denotes hydrodynamic radius, K_B is Boltzmann constant.

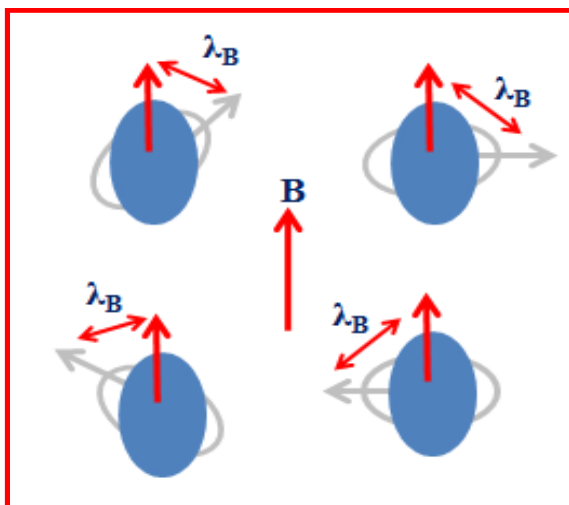


Fig 6.4 Brownian relaxation loss

Eddy current loss

Following the Faraday-Lenz's law [18] of electromagnetic induction, when an AC field penetrates a conducting the sample, the associated time-varying magnetic flux can be induced the evolution of eddy currents opposing to the applied field (Fig. 6.5). The reduction in field is depended on electrical conductivity of material and field frequency and permeability. The loss of heat occurred because of the eddy currents (ED) is calculated by:

$$ED = \frac{(\mu\pi d f H)^2}{20\rho} \dots \dots 6.4$$

Where, μ represents the permeability, d represents diameter and ρ represents material's resistivity.

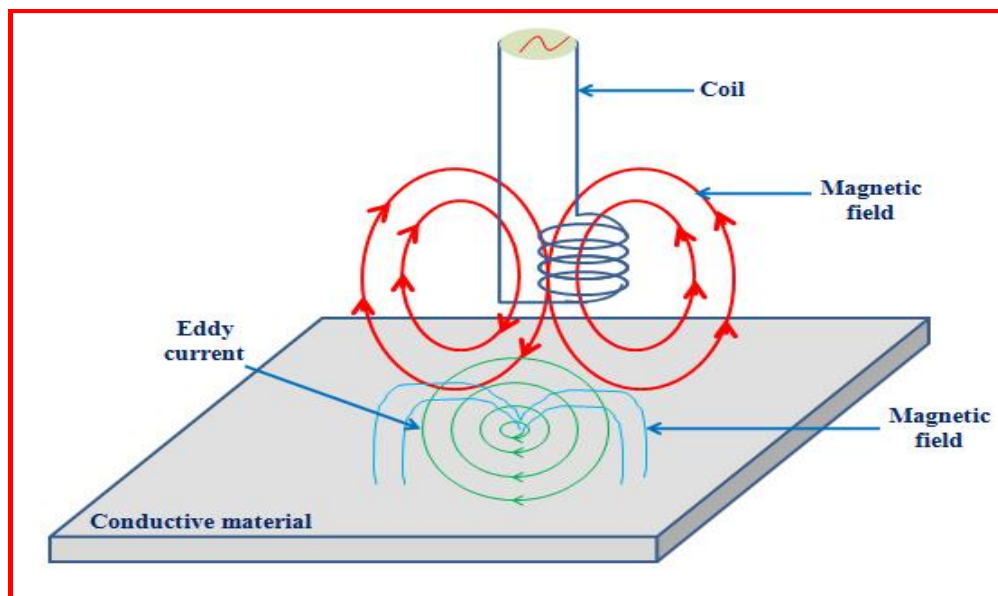


Fig. 6.5 Eddy current loss mechanism

Magnetic induction heating of MNPs is normally occurred by hysteresis loss and relaxation loss in alternating magnetic field because of eddy current generated heating is very small as compare to magnetic losses [5].

6.3.3 Specific absorption rate

The capacity of heating of MNPs is measured by SAR value and SAR value is defined as heat quantity generated per unit gram of the magnetic material per unit of time. SAR value for magnetic nanoparticles can be calculated by:

$$SAR = C \left(\frac{dT}{dt} \right) \left(\frac{m_s}{m_m} \right) \dots \dots 6.5$$

where, C represents specific heat capacity of the water ($4.18 \text{ Jg}^{-1}\text{K}^{-1}$). The $\frac{dT}{dt}$ represents initial slope and m_s is mass of suspension and m_m is mass of the magnetic material in suspension. SAR value must as highest as possible in the case of hyperthermia application [5, 19].

The SAR value controlled by following factors:

- Amplitude of magnetic field(H)
- Used frequency (f)
- Permeability of particle (μ)
- Size and shape of particle

6.4 Experimental

Experiment of induction heating of polyol synthesized bare MnFe₂O₄ and APTES functionalized MnFe₂O₄ MNPs was carried out in a plastic micro centrifuge 1.5 mL tube using an induction heating unit (Easy Heat 8310, Ambrell; UK) with a 6 cm diameter and 4 turns heating coil. The MNPs are suspended in 1 mL of distilled water was placed at the center of the coil and the applied frequency was 265 kHz. The heat dissipation by magnetic fluid with field is measured in terms of specific absorption rate (W/g).

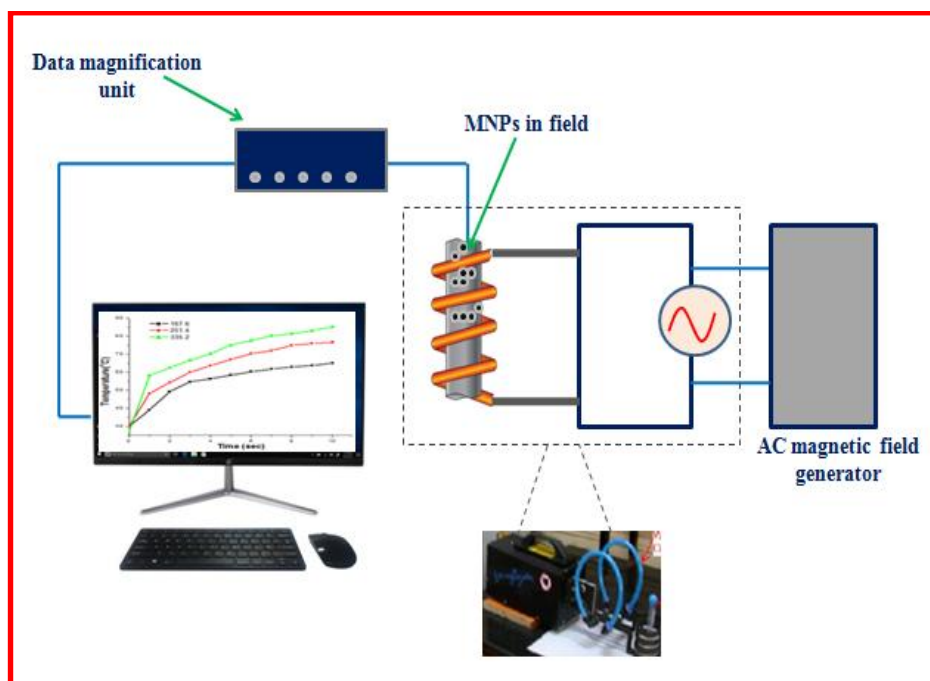


Fig. 6.6 Induction heating experiment representation

To keep the temperature of the coil at ambient temperature, water circulation in coils was provided. Concentrations 5 mg mL⁻¹ and 10 mg mL⁻¹ in water were taken to study the heating characteristics for hyperthermia applications. Samples were sonicated for 10 min for homogenization to obtain reliable mensuration. The AC magnetic fields 167.6, 251.4 and 335.2 Oe were applied to measure temperature rise of APTES coated MnFe₂O₄ nanoparticles at 265 kHz frequency.

For the conducted experiments, the magnetic field was calculated from the relationship:

$$H = 1.257 \frac{ni}{L} \dots \dots \dots 6.6$$

Where, n, i and L denote the number of turn, applied current and diameter of turn in centimeters respectively. Calculated values of magnetic field (H) at 200, 300 and 400A were 167.6, 251.4 and 335.2 Oe which is equivalent to 13.3, 20.0 and 26.7 kAm⁻¹ respectively. The rise in temperature was measured using an optical fiber probe having accuracy 0.1 °C.

6.5 Results and discussion

6.5.1 Hyperthermia properties of MnFe₂O₄ nanoparticles

Self heating temperature rise properties of bare MnFe₂O₄ nanoparticles have been studied for different concentrations and field amplitude. The concentrations 5 mg mL⁻¹ and 10 mg mL⁻¹ in water were taken to study the heating characteristics for hyperthermia applications. The samples were sonicated for 30 min for homogenization for reliable mensuration. The AC magnetic fields 167.6, 251.4 and 335.2 Oe were applied to measure temperature rise of MnFe₂O₄ nanoparticles at 265 kHz frequency.

Fig. 6.7 shows the temperature vs time curve for MnFe₂O₄ nanoparticles (5 mg mL⁻¹) at different fields 167.6, 251.4 and 335.2 Oe at 265 kHz frequency. It is clearly

observed that both samples attained hyperthermia temperature range at all field amplitudes within short period of time.

It is observed that the threshold hyperthermia temperature is achieved by both (5 mg mL⁻¹ and 10 mg mL⁻¹) at all fields (167.6, 251.4 and 335.2 Oe) at 265 kHz frequency. Fig. 6.7 shows the time required to achieve hyperthermia temperature for 5 mg mL⁻¹ concentration.

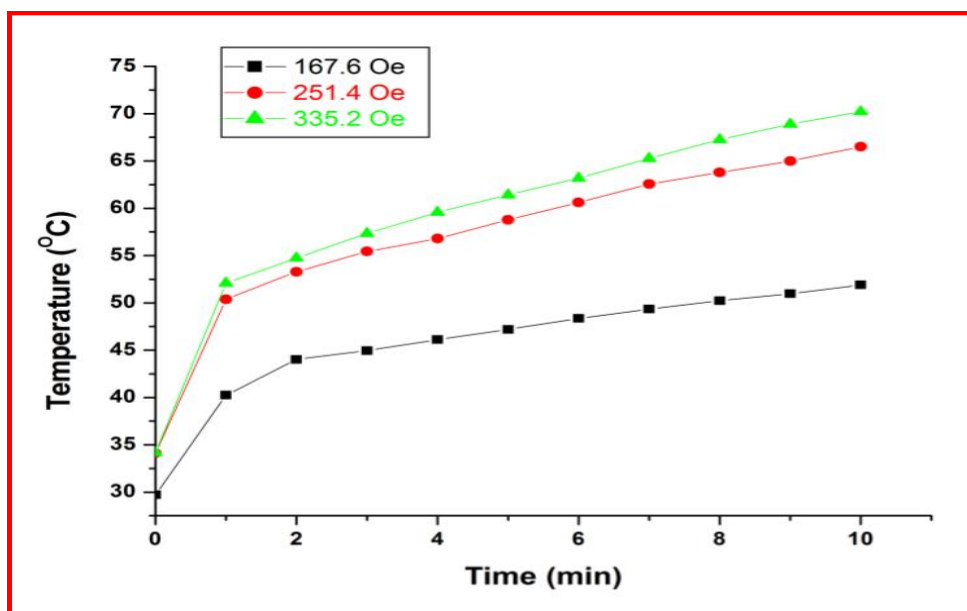


Fig. 6.7 Temperature kinetic curve for MnFe₂O₄ nanoparticles (5 mg mL⁻¹) at different applied AC magnetic fields (167.6, 251.4 and 335.2 Oe)

There is expeditious temperature expanding in initial stages is because of the magnetic hysteresis loss, Neel and Brownian relaxations of each ferromagnetic nanoparticles activated by exterior AC magnetic field [20]. For 10 mg mL⁻¹ sample, time required to reach the appropriate hyperthermia temperature is less as compared to 5 mg mL⁻¹. Fig. 6.7 and 6.8 represent rise in temperature and Fig. 6.9 shows the hyperthermia efficiency i.e. SAR value. The SAR values of MnFe₂O₄ nanoparticles are calculated using equation 6.7. SAR of 5 mg mL⁻¹ concentration is increased from 147.80 to 251.44 W/g⁻¹ with increase in the field from field from 167.6 to 335.2 Oe

respectively, where as SAR of 10 mg mL⁻¹ concentration is increases from 108.3 to 165.88 W/g⁻¹ with increase in the field from field from 167.6 to 335.2 Oe at 265 kHz frequency.

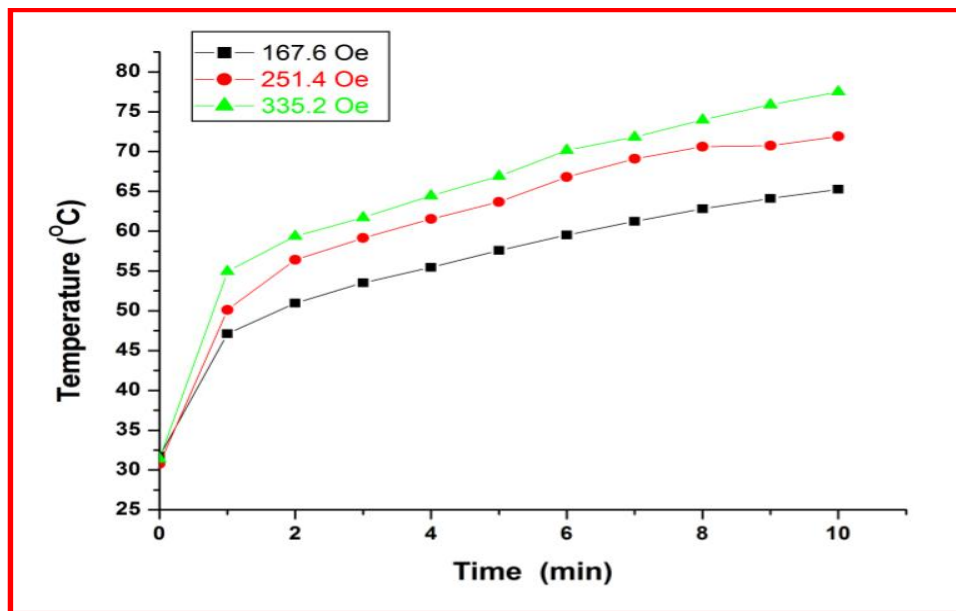


Fig. 6.8 Temperature kinetic curve for MnFe₂O₄ nanoparticles (10 mg mL⁻¹) at different applied AC magnetic fields (167.6, 251.4 and 335.2 Oe)

The SAR value is high for 5 mg mL⁻¹ compared to 10 mg mL⁻¹ concentration even though there is high temperature rise in the case of sample 10 mg mL⁻¹ compared to 5 mg mL⁻¹.

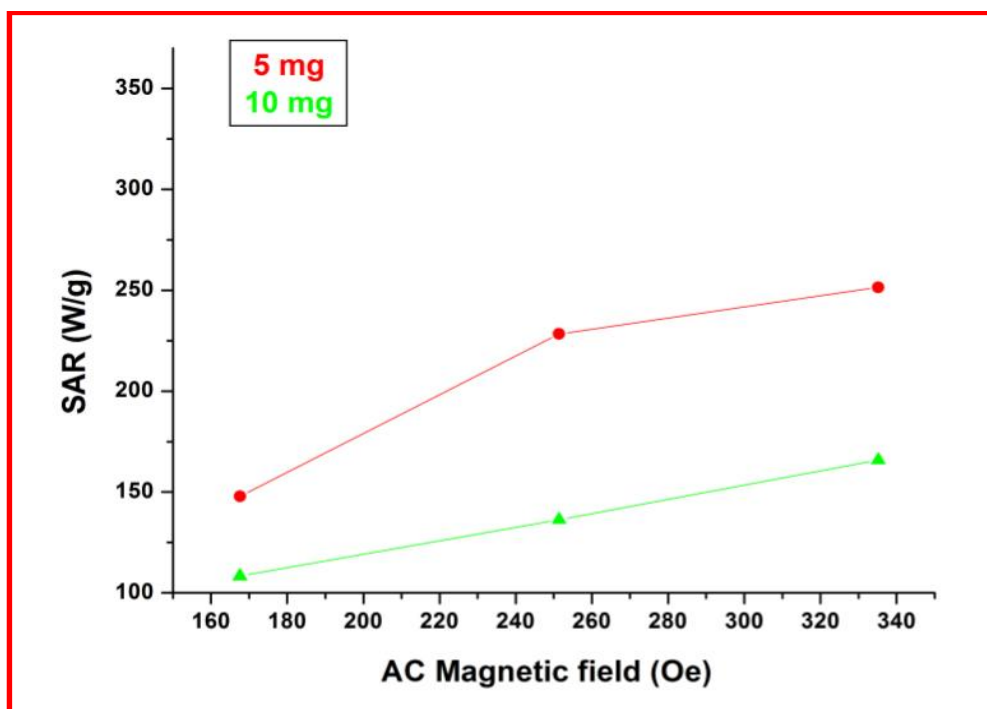


Fig. 6.9 SAR values for MnFe₂O₄ nanoparticles (5mg/mL and 10 mg/mL) at different applied AC magnetic fields (167.6, 251.4 and 335.2 Oe)

This may be due to particle conglomeration in high particle concentration, which leads to extreme rise in dipole-dipole interaction in particles. Higher the SAR value, superior is the candidate material to be used for hyperthermia therapy [20-22]. The SAR value for MnFe₂O₄ nanoparticles which are prepared by polyol method is the higher than MnFe₂O₄ nanoparticles prepared by other methods. Therefore, it can be concluded that MnFe₂O₄ nanoparticles prepared by polyol method with high SAR value can be considered as great potential material for hyperthermia applications.

6.5.2 Hyperthermia properties of APTES functionalized MnFe₂O₄ nanoparticles

Temperature kinetics and SAR of APTES coated MnFe₂O₄ nanoparticles are shown in Fig. 6.10. The concentrations 5 mg mL⁻¹ and 10 mg mL⁻¹ in water were taken to study the heating characteristics for hyperthermia applications. The samples were sonicated for 10 min for homogenization for reliable mensuration. The AC

magnetic fields 167.6, 251.4 and 335.2 Oe were applied to measure temperature rise of APTES coated MnFe₂O₄ nanoparticles at 265 kHz frequency. Fig. 6.10 and 6.11 represent rise in temperature and Fig. 6.12 shows the hyperthermia efficiency i.e. SAR value. A heat is dissipated to the surrounding due to interaction of MNPs with applied field and delay in the relaxation of the magnetic moment. From VSM study, it is already clear that APTES coated MnFe₂O₄ nanoparticles are superparamagnetic in nature. For superparamagnetic nanoparticles, heat losses are due to friction occurring from particle oscillations and rotation of magnetic moments with each field, which are Néel and Brownian relaxation modes. Temperature was increased with increase in applied magnetic field with time for both concentrations. Magnetic field 167.6 Oe is sufficient to reach the hyperthermia temperature within short time at a frequency of 265 kHz [20-22].

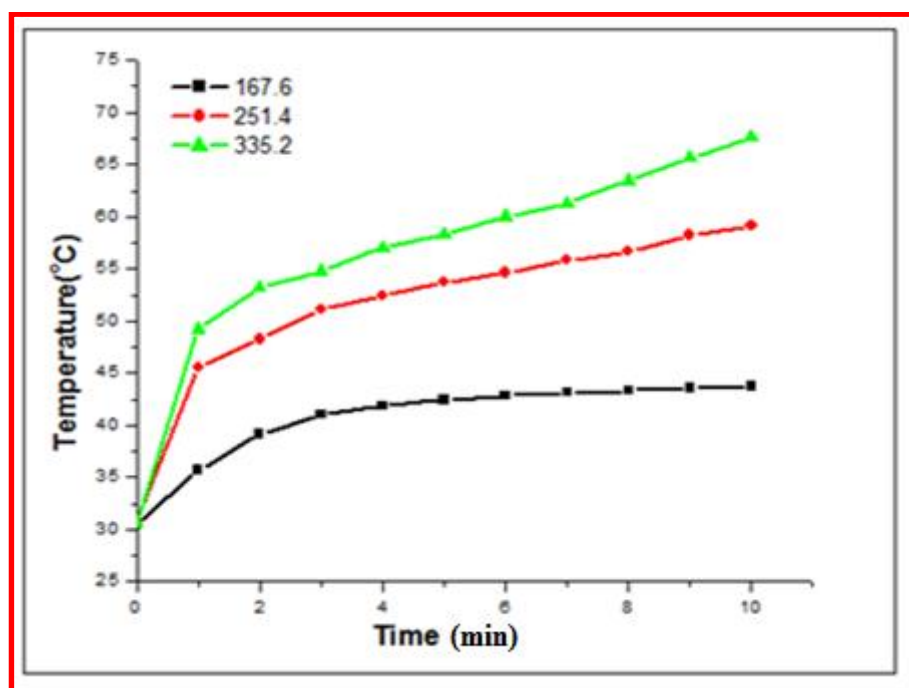


Fig. 6.10 Temperature kinetic curve for APTES coated MnFe₂O₄ nanoparticles for 5 mg mL⁻¹ concentration at different magnetic fields (167.6, 251.4 and 335.2 Oe)

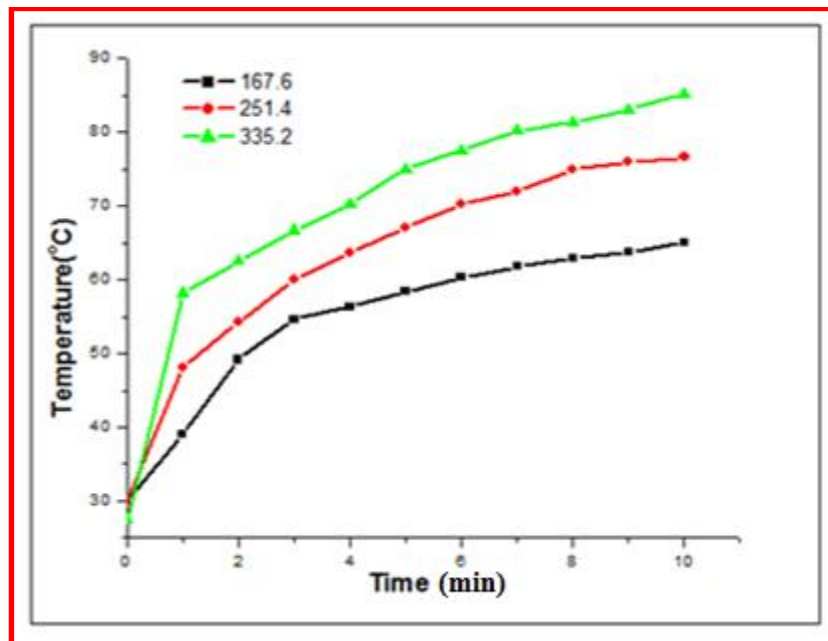


Fig. 6.11 Temperature kinetic curve for APTES coated MnFe₂O₄ nanoparticles for 10 mg mL⁻¹ concentration at different magnetic fields (167.6, 251.4 and 335.2 Oe)

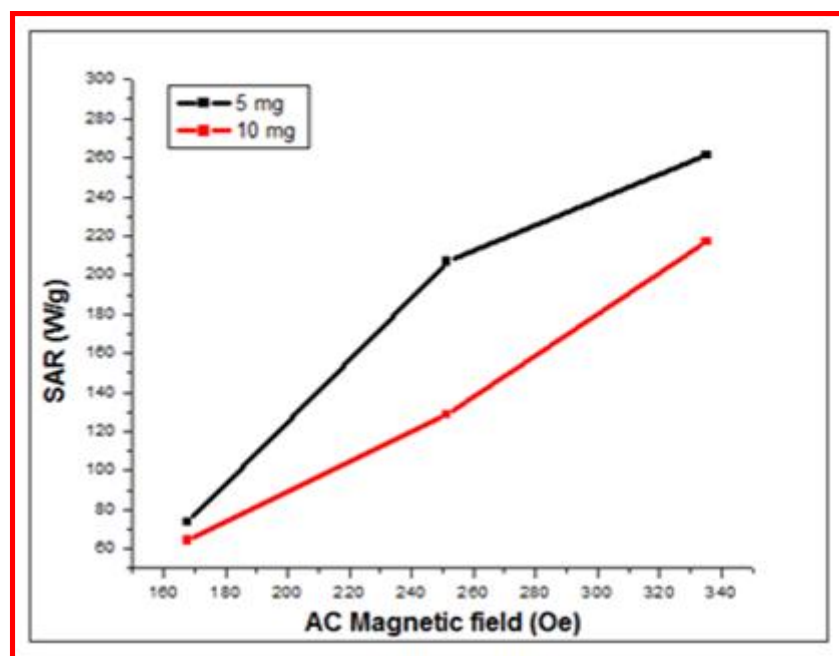


Fig. 6.12 SAR value of APTES coated MnFe₂O₄ nanoparticles

The SAR values of APTES coated MnFe₂O₄ nanoparticles are calculated using eq. 6.5 and which are increased from 73.90 to 261.53 W g⁻¹ for 5 mg mL⁻¹ and 64.20

to 216.98 W g⁻¹ for 10 mg mL⁻¹ with increasing field strength and these values are very astonishing. The SAR value is high for 5 mg mL⁻¹ compared to 10 mg mL⁻¹ concentration despite there is higher temperature rise in the case of sample 10 mg mL⁻¹ compared to 5 mg mL⁻¹. This may be due to particle conglomeration in high particle concentration, which leads to extreme rise in dipole-dipole interaction in particles. However the SAR Value is decreased when concentration of nanoparticles is increased. This clearly suggest that increasing the nanoparticles to attain high value of SAR is not the solution for hyperthermia application as SAR is also dependant on number of factors such as filed strength, amplitude, anisotropy of the nanoparticles and interparticle interactions [23]. It is observed that heating efficiency for APTES coated MnFe₂O₄ nanoparticles is higher than for uncoated one. It could be due to the APTES coating that the SPM fraction of the MnFe₂O₄ retained much better than the uncoated MnFe₂O₄.

Excellent chemical properties, high biocompatibility, ease of synthesis and superparamagnetic properties are the main requisite to stimulate interest in MNPs [24]. However MNPs have drawbacks like improper instrumentation, lack of core knowledge and in exact thermotherapy. Those drawbacks overcome by using complex magnetic oxide by modifying instrinsic or extrinsic properties of nanoparticles [25]. Kim et al. [26] have performed synthesis of chitosan functionalized MnFe₂O₄ nanoparticles for use in hyperthermia therapy using magnetic field. They have used EDS concentrations to control the size of chitosan coated MnFe₂O₄ nanoparticles and AC field has been induced to demonstrate nanoparticles for hyperthermia application. The MnFe₂O₄ nanoparticles under the field 653 Oe at 266 kHz shows values of SAR is found to be 1.45 W g⁻¹. Pradhan et al. [27] have prepared and characterized manganese ferrite which relies on magnetic liposome's for hyperthermia treatment. They have found that (TFH) is better method of grafting and SAR value for MnFe₂O₄ magnetic observed was 145 W/g of iron at 15 kA/m AC field. Doaga et al. [28] have synthesized MnFe₂O₄ nanoparticles via co-precipitation method which gives

controllable size and shape. The SAR value was measured at 1.95 MHz frequency and observed value of SAR was 148.4 W g⁻¹ an AC field of 4500 A m⁻¹. Pradhan et al. [29] have prepared lauric acid coated Fe₃O₄, MnFe₂O₄, and CoFe₂O₄ and compared regarding heating ability. They have studied their induction heating properties in at an AC magnetic field (H) of 15 kA/m and a frequency (f) of 300 kHz and they concluded that Fe₃O₄ and MnFe₂O₄ showed higher SAR (120 and 97 W/g) than CoFe₂O₄ (37 W/g). Cruz et al. [30] have obtained MnFe₂O₄ nanoparticles within range 4.4 to 17 nm by hydrothermal synthesis method. Ability to use nanoparticles for hyperthermia was assessed by determining heating efficiency in aqueous media. They were concluded that obtained nanoparticles have better heat efficiency and they got 168 Wg⁻¹ SAR value. Sabale et al. [31] were prepared superparamagnetic MFe₂O₄ by polyol method. They have taken sample with concentration of 10 and 20 mg and frequency 276 kHz was applied. They have noticed that the field 419.0 Oe is not sufficient to reach threshold hyperthermia temperature. i.e. 41°C for NiFe₂O₄ and MnFe₂O₄. Mendo et al. [32] have synthesized MFe₂O₄ (M = Co, Fe, Mn) compounds using a hydrothermal treatment in presence of medicinal cotton. SAR was determined by induction heating measurements and value of SAR for MnFe₂O₄ is (90 W/g). Khot et al. [20] have prepared Dextran coated MgFe₂O₄ nanoparticles by combustion method and studied their induction heating properties in the same range of field amplitudes and concentrations. Value of SAR obtained is around ~85.5 W g⁻¹. Nikam et al. [33] have studied the AC magnetic heating properties of Co_{0.5}Zn_{0.5}Fe₂O₄ nanoparticles for their applications in hyperthermia therapy and values of SAR is found to be 107.82 W g⁻¹. SAR values observed in our case are high as compared to MgFe₂O₄ and Co_{0.5}Zn_{0.5}Fe₂O₄ nanoparticles.

The SAR value observed for APTES coated nanoparticles was higher at lowest possible particle concentration than above listed prepared nanoparticles [17]. The increase in SAR value and low cytotoxicity made the APTES functionalized MNPs more suitable for hyperthermia therapy application than the bare nanoparticles.

APTES coated MnFe₂O₄ nanoparticles with high SAR can be potential heating mediator for cancer hyperthermia therapy subjected to thorough investigation of their biocompatibility and optimized nanoparticles concentration for induction heating studies, which is a present scope of further research.

6.6 Conclusions

The magnetic induction heating studies of MnFe₂O₄ and APTES coated MnFe₂O₄ MNPs are studied for their biomedical implementations such as magnetic hyperthermia. Both, specific absorption rate and the actual temperature rise are maximum in case of APTES coated MnFe₂O₄ nanoparticles compare to bare MnFe₂O₄ nanoparticles. The APTES coated MnFe₂O₄ MNPs generated SAR value of about 261.53 w/g where as SAR value of bare MnFe₂O₄ is 251.44 w/g at sample concentration of 5 mg mL⁻¹. Such high value of SAR could be due to increased hysteresis losses under AC magnetic field due to increased interaction between the particles. Interaction between the particles influences exchange coupling energy and anisotropy energy, which affects heating abilities. Thus APTES coated MnFe₂O₄ nanoparticles with large enough SAR at low particle concentration can be a promising heating agent for magnetic particle hyperthermia.

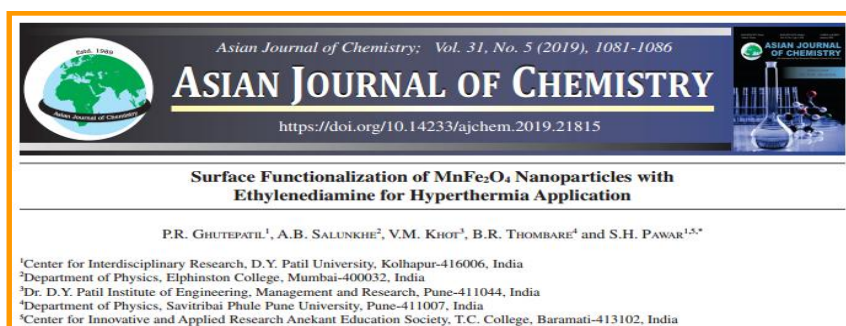
References

1. Q. Pankhurst, J. Connolly, S. Jones and J. Dobson, *J. Phys. D:Appl. Phys.*, 2003, 36, 167-181.
2. S. Jha, P. Sharma and R. Malviya, *Achiev. Life Sci.*, 2016, 10, 161-167.
3. M. Latorre and C. Rinaldi, *P R Health Sci J.*, 2009, 28, 227-238.
4. A. Muela, D. Munoz, R. Martín-Rodríguez, I. Orue, E. Garaio, A. Diaz de Cerio, J. Alonso, J. Garcia, and M. Luisa Fdez-Gubieda, *J. Phys. Chem. C*, 2016, 120, 24437-24448.
5. R. Hergt, W. Andra and H. Nowak, *Magnetism in Medicine*, 2006, 550-570, 2nd Edition, Berlin: Wiley-VCH.
6. P. Moroz, S. Jones and B. Gray, *Int. J. Hyperthermia*, 2002, 18, 267-284.
7. B. Thiesen and A. Jordan, *Inter. J. Hyperthermia* 2008, 24, 467-474.
8. A. Jordan, R. Scholz, P. Wust, H. Fahling, R. Felix, *J. Magn. Magn. Mater.*, 1999, 201, 413-419.
9. R. Weissleder, D. Stark, B. Engelstad, B. Bacon, C. Compton, D. White, P. Jacobs and J. Lewis, *Am. J. Roentgenol.* 1989, 152, 167-173.
10. R. Rand, H. Snow, D. Elliott and G. Haskins, *U. S. Patent specification*, 1985, 4, 368.
11. I. Brigger, C. Dubernet and P. Couvreur, *Adv. Drug Deli. Rev.*, 2002, 54, 631-651.
12. R. Rosensweig, *J. Magn. Magn. Mater.*, 2002, 252, 370-374.
13. A. Salunkhe, V. Khot and S. Pawar, *Curr. Top. Med. Chem.*, 2014, 14, 572-594.

14. N. Shetake, M. Balla, A. Kumar and B. Pandey, *Journal of Radiation and Cancer Research*, 2016, 7, 13-17.
15. A. Hervault and N. Thanh, *Nanoscale*, 2014, 6, 11553-11573.
16. S. Rovers, L. Poel, C. Dietz, J. Noijen, R. Hoogenboom, M. Kemmere, K. Kopinga and J. Keurentjes, *J. Phys. Chem. C*, 2009, 113, 14638-14643.
17. R. Ghosh, Y. Pradhan, S. Devi, M. Tewari, A. Kumar, S. Sharma, N. Gajbhiye, R. Vatsa, B. Pandey and R. Ningthoujam, *J. Mater. Chem.*, 2011, 21, 13388-13398.
18. Q. Pankhurst, J. Connolly, S. Jones and J. Dobson, *J. Phys. D: Appl. Phys.*, 2003, 36, 167-181.
19. S. Laurent, S. Dutz, U. Hafeli and M. Mahmoudi, *Adv. Colloid Interface Sci.*, 2011, 166, 8-23.
20. V. Khot, A. Salunkhe, N. Thorat, R. Ningthoujam and S. Pawar, *Dalton Trans.*, 2013, 42, 1249-1258.
21. R. Hergt, S. Dutz and M. Zeisberger, *Nanotechnology*, 2010, 21, 015706.
22. S. Jadhav, D. Nikam, V. Khot, S. Mali, C. Hong and S. Pawar, *Mater. Charact.*, 2015, 102, 209–220.
23. S. Bae and S. Lee, *Appl. Phys. Lett.*, 2006, 89, 252503.
24. A. Nemmar, M. Hoylaerts and P. Hoet, *Am. J. Respir. Crit. Care Med.*, 2002, 166, 998-1004.
25. A. K. Gupta and M. Gupta, *Biomaterials*, 2005, 26, 3995-4021.
26. D. Kim, D. Nikles and B. Christopher, *Materials*, 2010, 3, 4051-4065.

27. P. Pradhan, J. Giri, R. Banerjee, J. Bellare and D. Bahadur, *J. Magn. Magn. Mater.*, 2007, 311, 208-215.
28. A. Doaga, A. Cojocariu, W. Amin, F. Heib, P. Bender, R. Hempelmann and O. Caltun, *Mater. Chem. Phys.*, 2013, 143, 305-310.
29. P. Pradhan, J. Giri, G. Samanta, H. Sarma, K. Mishra, J. Bellare, R. Banerjee and D. Bahadur, *J. Biomed. Mater. Res. B*, 2007, 81B, 12-22.
30. M. Cruz, L. Ferreira, J. Ramos, S. Mendo, A. Alves, M. Godinho and M. Carvalho, *J. Alloys Compd*, 2017, 703, 370-380
31. S. Sabale, V. Jadhav, V. Khot, X. Zhu, M. Xin and H. Chen, *J. Mater. Sci: Mater Med.*, 2015, 26(3), 127-136.
32. S. Mendo, A. Alves, L. Ferreira, M. Cruz, M. Mendonça, M. Godinho and M. Carvalho, *New J. Chem.*, 2015, 39, 7182-7193.
33. D. Nikam, S. Jadhav, V. Khot, M. Phadtare and S. Pawar, *J. Magn. Magn. Mater.*, 2014, 349, 208-213.

In Situ Surface Functionalization of MnFe₂O₄ Nanoparticles and Their Potential Application in Cancer Hyperthermia Therapy



The parts of this chapter have been published in reserach article.

Nano LIFE

Synthesis of monodispersed polyvinylpyrrolidone functionalized biocompatible manganese ferrite nanoparticles for hyperthermia application
 --Manuscript Draft--

Manuscript Number:	
Full Title:	Synthesis of monodispersed polyvinylpyrrolidone functionalized biocompatible manganese ferrite nanoparticles for hyperthermia application
Article Type:	Research Paper

The parts of this chapter have been submitted in reserach article for publication.

People might be negotiating now but five years from today, should nanotechnology go into full swing, and those deals will be rendered useless.

-Thomas Scott

7.1 Introduction

Among the nanomaterials, MNPs have emerged as an important material for implementation in area of biomedicine as well as technology. Spinel ferrites are the influential magnetic materials for directing elementary relationships between the magnetic properties and their structure. In recent years, spinel ferrites have been explored with great interest because of their excellent properties, ease of synthesis, superparamagnetic properties in order to use them in biomedical implementation. Powerful crystal structure of spinel ferrites provide excellent options for fine tuning and understanding the superparamagnetic properties of MNPs by chemical fabrication. Manganese ferrites (MnFe₂O₄) are largely studied due to their capability to form an ideal magnetic system towards controlling and understanding the magnetic properties at the atomic level through alteration [1-4].

Precisely, MNPs are injected into affected tumor tissues by exposing them to external AC magnetic field in hyperthermia therapy. Magnetic hyperthermia therapy works on the principle that MNPs dissipate heat when corresponded to an exterior AC magnetic field of appropriate frequency and amplitude. Here, MNPs are being used as heating source for cancer cell treatment and heat is being generated by MNPs due to three different losses i.e. hysteresis, Ne'el and Brownian. However, only Ne'el and Brownian losses are observed in case of superparamagnetic nanoparticles [5, 6]. For hyperthermia therapy, the MNPs should have high SAR and this value of MNPs is controlled by particle size, shape, distribution, dipole–dipole interactions, density, magnetic anisotropy and magnetic field amplitude [7].

Mostly MNPs are toxic in nature, so surface modification is required to use them in implementation in the field of biomedical. MNPs can be coated by different types of surfactants to minimize toxicity, prevent agglomeration and extend storage life [8]. The different biocompatible materials including Polyvinylpyrrolidone (PVP),

3-aminopropyltriethoxy silane (APTES), silica, polyethylene glycol (PEG), chitosan, dextran, acrypol etc can be used for surface modification of MNPs.

In situ functionalization

For biomedical applications, MNPs should be monodispersed, water dispersible, biocompatible and provide functional moiety which act as adjunctant between of various biomolecules and surface of MNPs. Synthesis and functionalization processes can be performed into two steps. Two step synthesis and functionalization processes are always time consuming, tedious and not applicable for fabrication on large scale. During one pot synthesis, once the coating reaction starts the process of nucleation immediately happen and stops further particle growth. In one pot functionalization method, the carboxyl group, phosphonates, amino group, thiol and hydroxyl groups are used, which helps to conjugate with various biomolecules like drug molecule and Nucleic acid. Chemical fabrication of MNPs is important factor for specific interactions such as multistep post synthetic grafting process, organosilane, phosphonates and other polymeric molecules. In post synthetic grafting, use of costly chemicals make process ineffective for large scale production and contineous exposing of MNPs to hard conditions of reactions could influence magnetic properties [9, 10].

In the literature many methods are reported to synthesize using several chemicals and observed that MNPs synthesis by chemically gives malleable designing and polishing new final product. Mixing take places at molecular level, which offers best chemical homogeneity. Polyol synthesis method is widely used synthesis method among other methods like sol-gel, hydrothermal synthesis, co-precipitation, microemulsion, combustion etc. There has been various chemical materials used for the fixation of moieties on MNPs surface to obtain functionalized MNPs for variety of biomedical applications. The synthesis methods used for the fixation of these groups on functionalized nanoparticles are too expensive and complicated [11]. Barick et al.

[12] have prepared amino functionalized water soluble Fe₃O₄ nanoparticles for application in MRI. Sun and Zeng et al. [13] have prepared controllable monodispersed MNPs by thermal decomposition method. However, hydrophilic as well as monodispersed formation remains big problem.

In the present investigation, the ethylenediamine (EDA) and polyvinylpyrrolidone (PVP) functionalized MnFe₂O₄ nanoparticles were prepared by polyol method as it is simple, gives smaller size and provides best route for tailoring the characteristics of the MNPs. The several investigations have been carried out on the synthesis and characterization of MnFe₂O₄ nanoparticles, which were dispersible in aqueous media and superparamagnetic behaviour. The synthesis method involves heating of chloride precursor in diethylene glycol and in presence of both functionalized material separately. The EDA functionalized and PVP functionalized nanoparticles were characterized further to evaluate their properties. The rise in temperature and SAR of EDA as well as PVP functionalized nanoparticles have been investigated under AC magnetic field at appropriate field amplitudes and frequency to study their efficacy as heating mediator in magnetic hyperthermia anticancer therapy.

7.2 Experimental

7.2.1 Synthesis of EDA functionalized MnFe₂O₄ nanoparticles

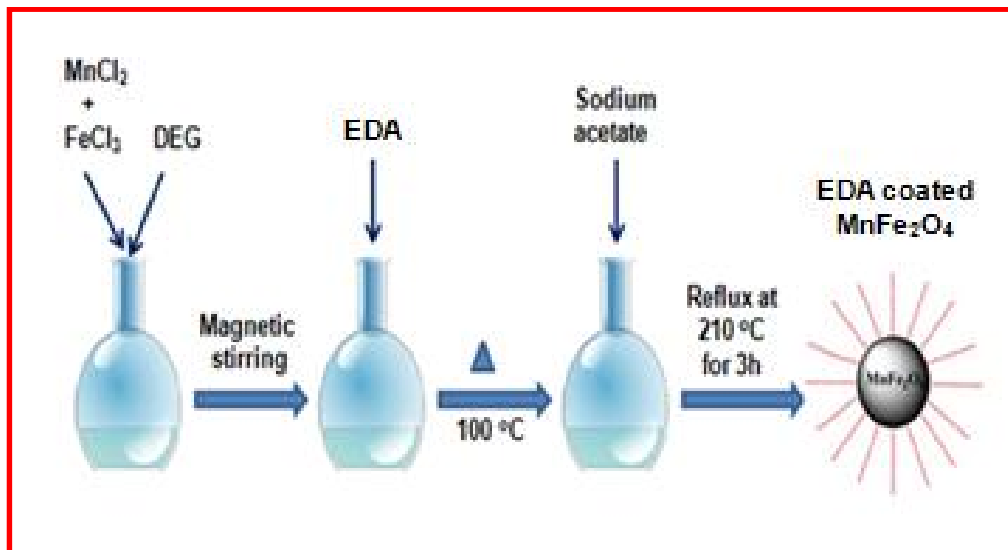


Fig. 7.1 Graphical representation of preparation of EDA functionalization MnFe₂O₄

The EDA functionalized MnFe₂O₄ MNPs were prepared using polyol method. A mixture of MnCl₂ (6 mmol), FeCl₃ (12 mmol) was dissolved in 30 mL diethylene glycol to form clear solution followed by addition of sodium acetate and 15 mL of EDA solution. The reaction mixture is stirred vigorously and refluxed for 3 h at 210 °C. The obtained particles show black colour which is colloidal particles synthesized in round bottom flask, and then cooled at room temperature. Here ethanol is used for number of washing, then these particles were separated by magnetic decantation and dried at room temperature [12]. Fig. 7.2 represents the procedure in the form of flow chart for synthesis of EDA coated MnFe₂O₄ nanoparticles.

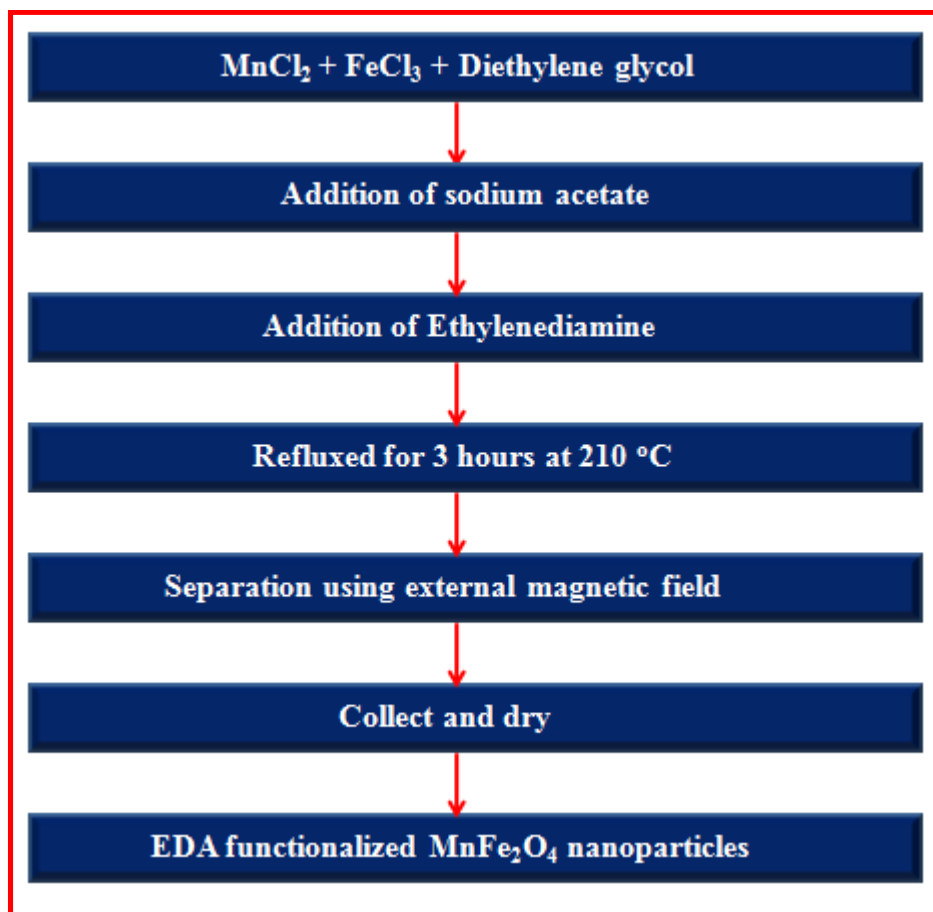


Fig 7.2 Procedure for synthesis of EDA coated MnFe₂O₄ nanoparticles

7.2.2 Synthesis of PVP functionalized MnFe₂O₄ nanoparticles

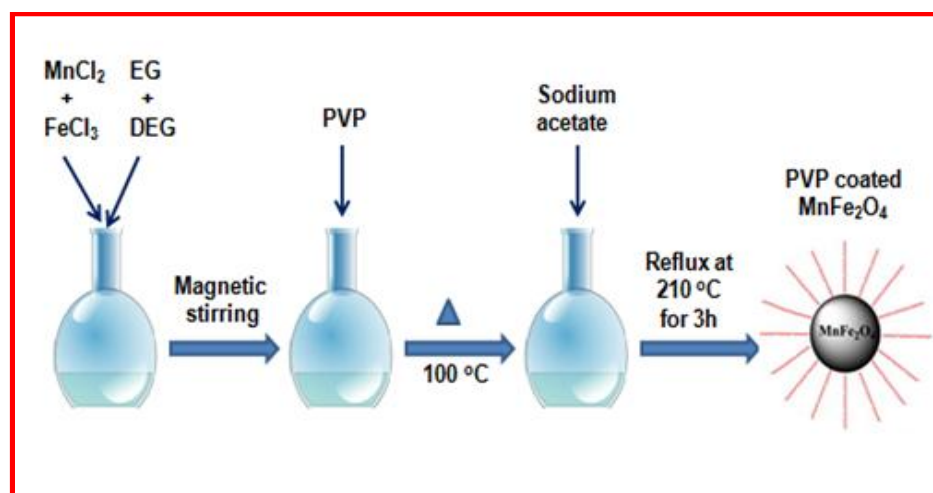


Fig. 7.3 Graphical representation of preparation of PVP coated MnFe₂O₄

MnFe₂O₄ MNPs were prepared by using polyol method. The 10 mmol of FeCl₃ and 5 mmol of MnCl₂ were dissolved in 40 mL of diethylene glycol in a round bottom flask under magnetic stirring. After 30 min, 2 g of PVP was added to the above solution and the solution was heated at 100 °C to give a transparent solution. The 1.5 g sodium acetate was added into the solution and reaction mixture was refluxed for 3 h at 210 °C. The color of the reaction mixture was changed to black during heating process and black solid was separated from the mixture by magnetic decantation. Finally, particles were washed many times with ethanol and dried at room temperature [14]. Flow-chart of the procedure for synthesis of PVP coated MnFe₂O₄ nanoparticles is shown in Fig. 7.4.

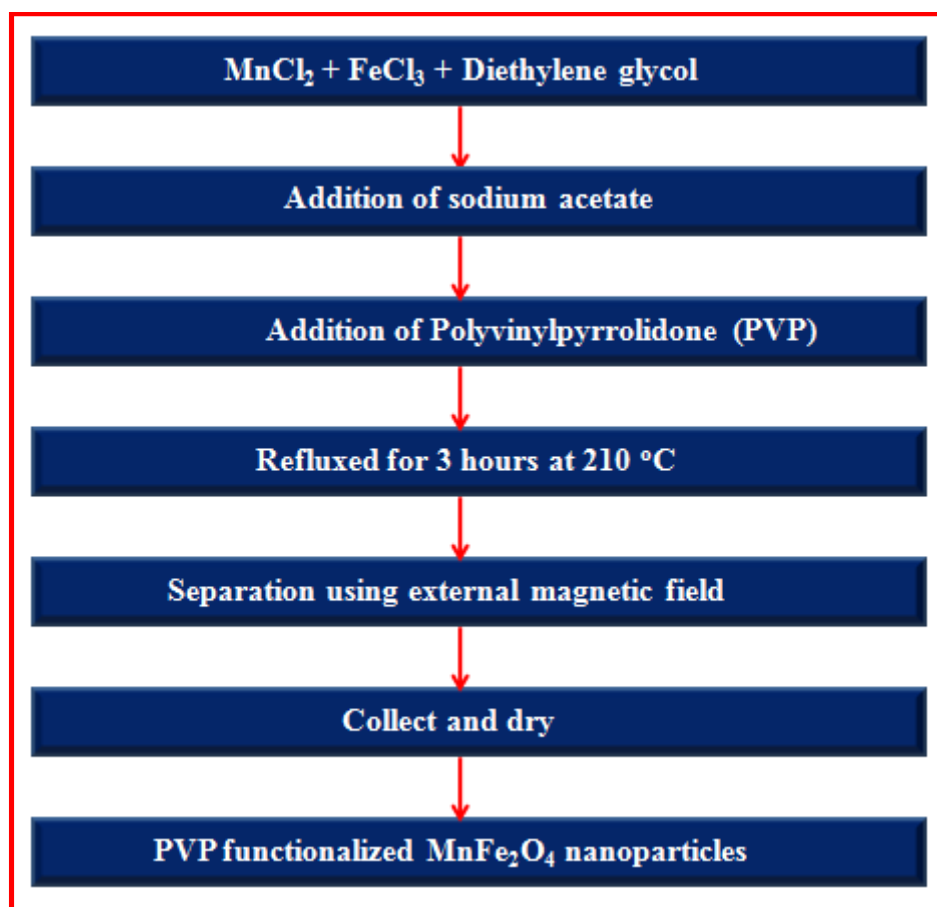


Fig. 7.4 Procedure for synthesis of PVP coated MnFe₂O₄ nanoparticles

7.2.3 Characterization

Phase purity and structural analysis of EDA and PVP functionalized MNPs were studied using XRD (Philip-3710) with Cr-K α radiation ($\lambda = 1.5418 \text{ \AA}$) in the 2θ range from 20° to 80° . MNPs were used to get FTIR spectra by using spectroscopy (Alpha ATR Bruker Eco Model) in the range 450 to 4000 cm^{-1} . Study of thermal properties of functionalized MNPs was brought out using transanalytical instrument mode (SDT 2960). The experiment of thermal study carried out in nitrogen atmosphere. The range of temperature 25 – 700°C with heating rate $10^\circ\text{C min}^{-1}$ used here. The SEM and TEM images were used to study the particle size and morphology of MNPs. The particle size of MnFe₂O₄ nanoparticles was measured with TEM (TEM, JEM-2100F Model, Japan). The morphology of EDA and PVP functionalized MNPs was confirmed by SEM (JEOL JSM 6360). Coercivity and saturation magnetization was calculated by VSM at room temperature from M-H curve.

An experiment of induction heating of MNPs was carried out for hyperthermia applications using induction heating unit (Easy heat 8310, Ambrell, UK). For this experiment, the samples 5 mg mL^{-1} and 10 mg mL^{-1} of distilled water were taken in a plastic micro centrifuge tube (1.5 ml), heating coil having 6 cm diameter with four turns and the applied frequency was 265 kHz . The MNPs were dispersed in water and sonicated to attain a good dispersion in water. Samples were heated for 10 min with the desired current (200 to 400A , i.e. 167.6 , 251.4 to 335.2 Oe) and optical fiber probe with accuracy 0.1°C was being used to measure temperature.

7.3 Result and Discussion

7.3.1 Role of ethylenediamine

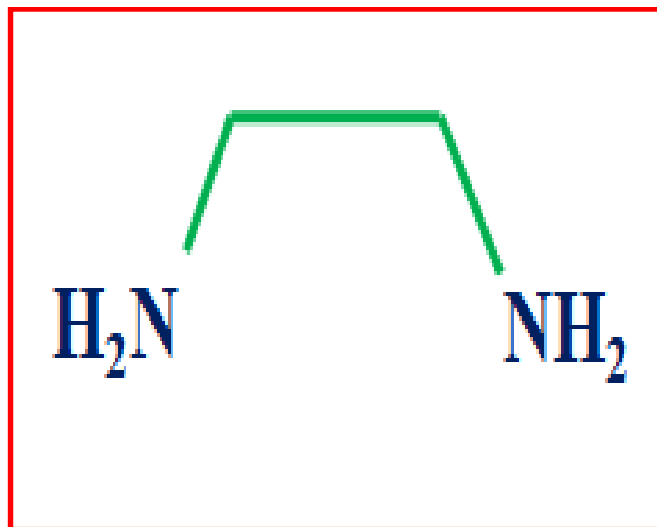


Fig. 7.5 Structure of EDA

Synthesis of MNPs can be performed using polyol like diethylene glycol, diethylene to minimize the metal salts and particles of metal to prepare various inorganic compounds with non-aggregated particles. Ethylenediamine can be used as reducing agent along with diethylene glycol. Ethylenediamine is viscous and hygroscopic liquid. It is having odor of ammonia and it is extensively dispensed in biological tissue and component of lecithin. EDA is also used as surfactant and helpful for the removing CO₂ and H₂S from gas. In biomedical field, ethylenediamine is used as sclerosing agent for treatment of Sclerotherapy. To overcome the disadvantages like aggregation between the particles diethylene, glycol can be used because it gives less degree of aggregation. Ethylenediamine execute role of reducing agent while amino group present on EDA surface protects the MNPs from unwanted growth and aggregation by providing chance to conjugate with different biomolecules like enzyme, DNA, drug etc [15,16].

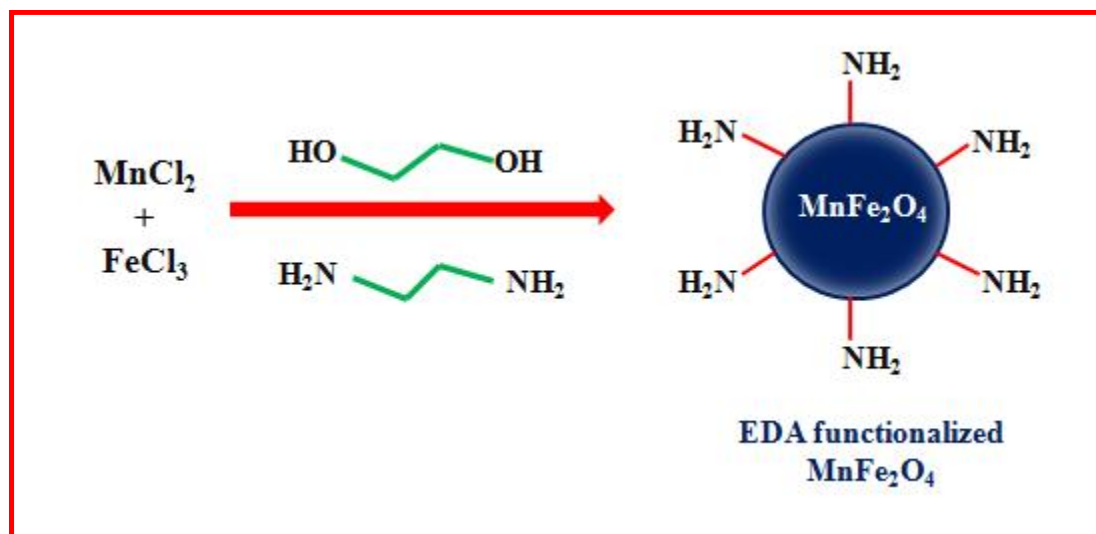


Fig. 7.6 Reaction of EDA coated MnFe₂O₄ nanoparticles

7.3.2 Role of PVP

PVP is a non-toxic, bulky and non-ionic polymer with C=O, C-N and CH₂ functional groups, which is broadly utilized for synthesis of MNPs. PVP prevents aggregation of MNPs due to repulsive forces, which appear from its hydrophobic carbon chains extended into solvents interacting with each other. The polar groups of PVP have a stronger affinity for iron and cobalt ions. Negative end of polar groups attracts the positive end (Mn & Fe) of ferrite particles. The number of polar groups gets increased due to increase in concentration of PVP. Particle aggregation is controlled due to electrostatic attraction resulting in separation of metallic ions. PVP molecule holds a hydrophilic component and a considerable hydrophobic group. PVP is excellent solvent in water and most of non-aqueous liquids.

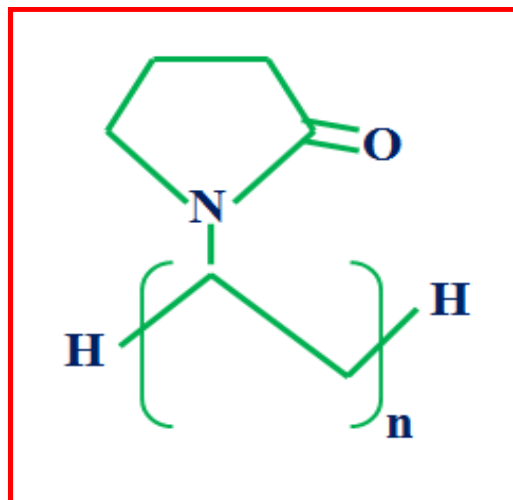


Fig. 7.7 Structure of PVP

Depending on certain synthetic conditions and material system, PVP can perform as a surface stabilizer, nanoparticle dispersant, growth modifier and reducing agent. PVP adopts role based on the specific material class and reaction conditions. Solubility of PVP renders PVP as outstanding phase transfer agent and its biocompatibility enables application of PVP functionalized nanomaterials for biomedical applications.

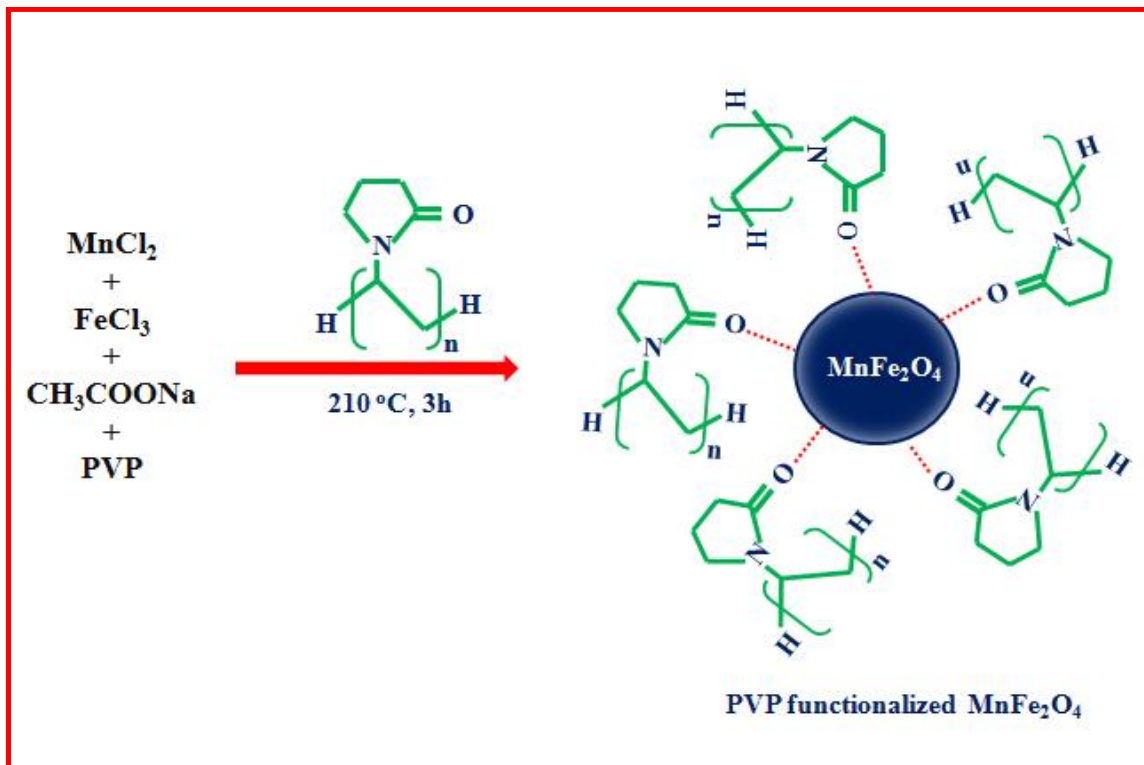


Fig. 7.8 Reaction of PVP coated MnFe₂O₄ nanoparticles

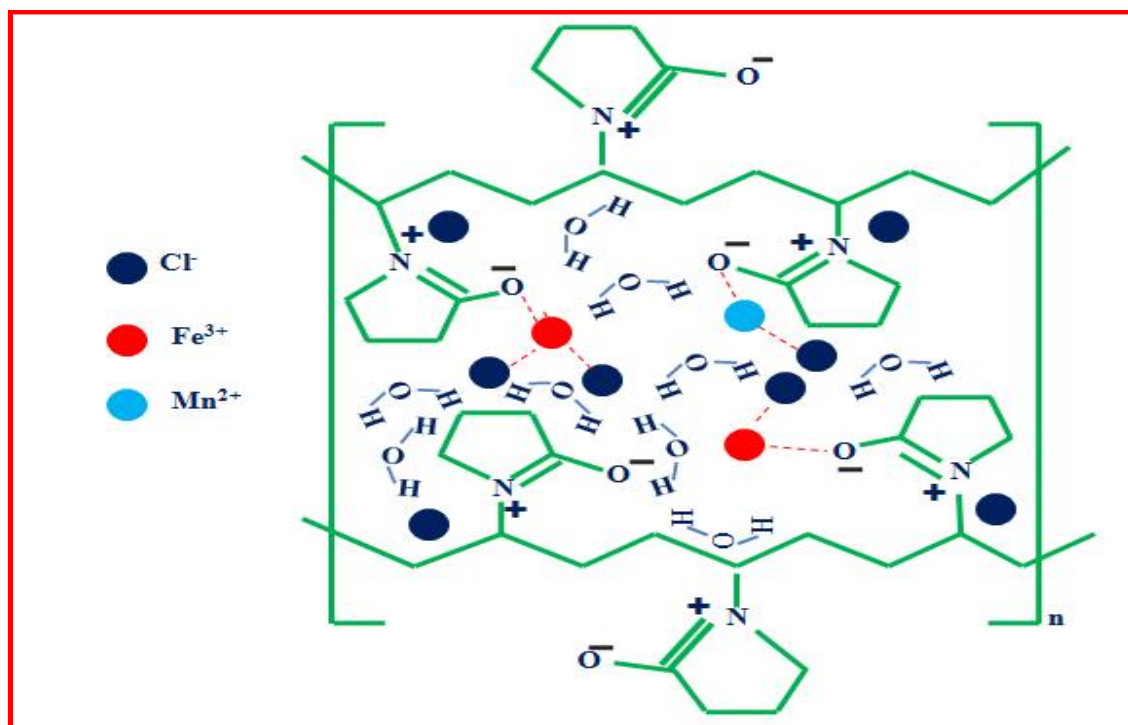


Fig. 7.9 Interaction between PVP and metal ions

7.3.3 Structural analysis

XRD analysis

The synthesized EDA functionalized MnFe₂O₄ was structurally investigated using XRD which is shown in Fig. 7.10. The diffraction peaks values (220), (311), (400), (440) and (511) obtained with (hkl) and then all peaks were matched with the JCPDS file number 38-0430. The Gaussian fit of a most intense peak (311) was used to calculate FWHM for calculation of crystallite size (D) [17]. Crystallite size of EDA functionalized MnFe₂O₄ nanoparticles estimated by Scherrer's formula is about 7 nm.

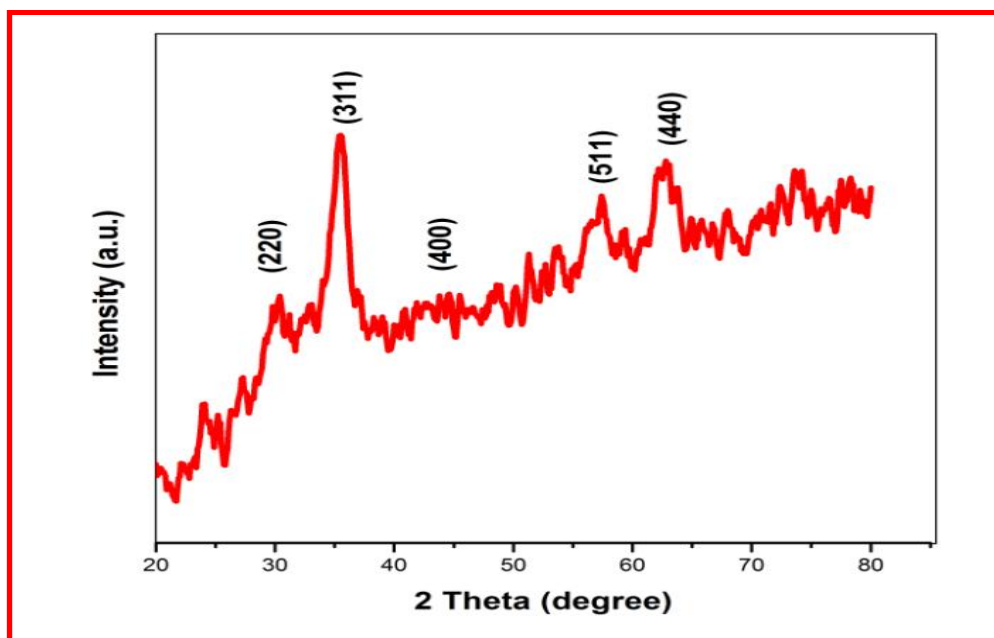


Fig. 7.10 XRD pattern of EDA functionalized MnFe₂O₄ MNPs.

The phase characteristics and crystalline structure analysis of PVP functionalized MnFe₂O₄ nanoparticles were studied using XRD. Fig.7.11 shows the XRD diffraction peaks and all diffraction peaks equally matched with cubic spinel structure of MnFe₂O₄ (JCPDS Card No.73-1964). This confirms formation of spinel phase of MnFe₂O₄ nanoparticles [15]. From the Scherrer's formula average crystallite size of nanoparticles is found to be 9 nm.

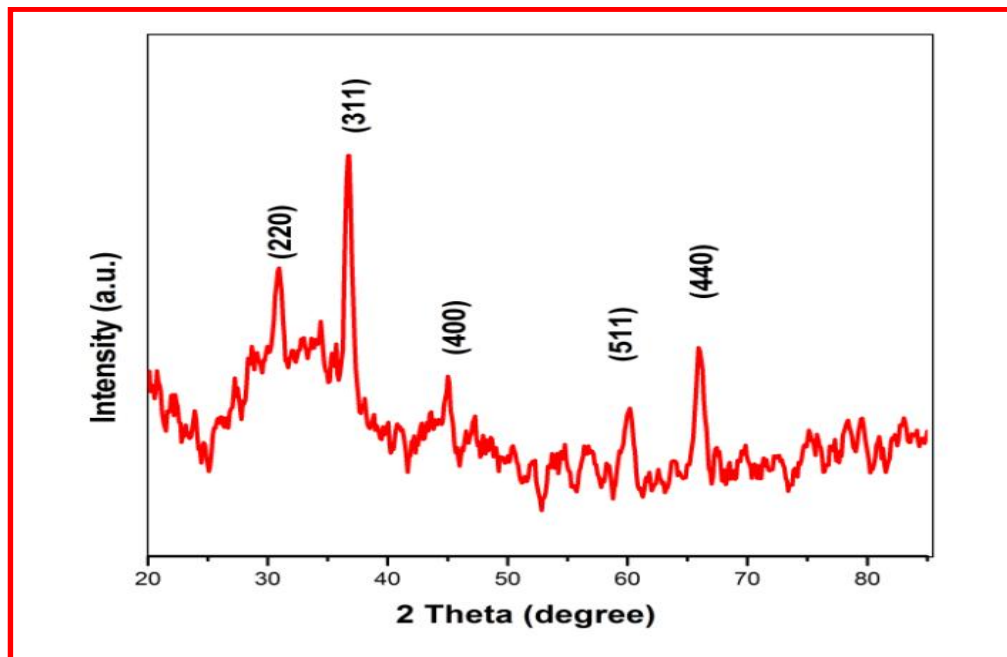


Fig. 7.11 XRD pattern of PVP coated MnFe₂O₄ nanoparticles

7.3.4 Microstructural analysis

SEM analysis

The surface morphology of EDA functionalized MnFe₂O₄ MNPs were analyzed by SEM and which is shown in Fig. 7.12. The morphology of EDA functionalized nanoparticles shows conglomerated in nature and this is due to presence of ethylenediamine on the surface or it may be caused by the orientation in attachment growth mechanism which assists to the minimization of surface energy. This phenomenon based on the collective behaviour and intermolecular force among the particles.

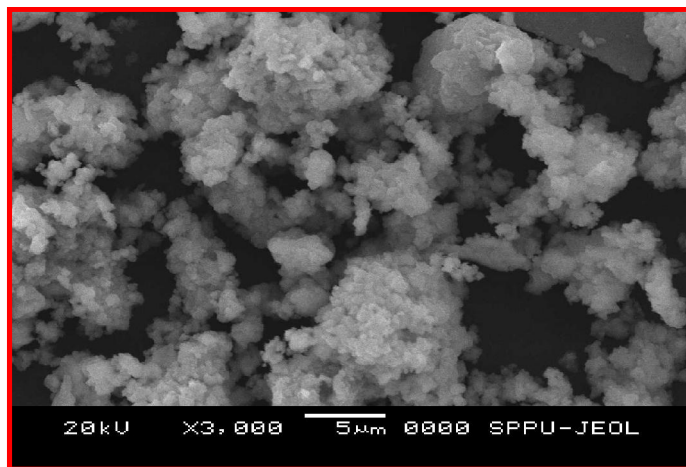


Fig. 7.12 SEM image of EDA functionalized MnFe₂O₄ MNPs

The surface morphology of PVP functionalized MnFe₂O₄ nanoparticles were analyzed by SEM and which is shown in Fig. 7.13. The morphology shows that particles are conglomerated in nature and most of them are quasi spherical. It is dependent on the intermolecular force between nanoparticles and cumulative behavior of nanoparticles.

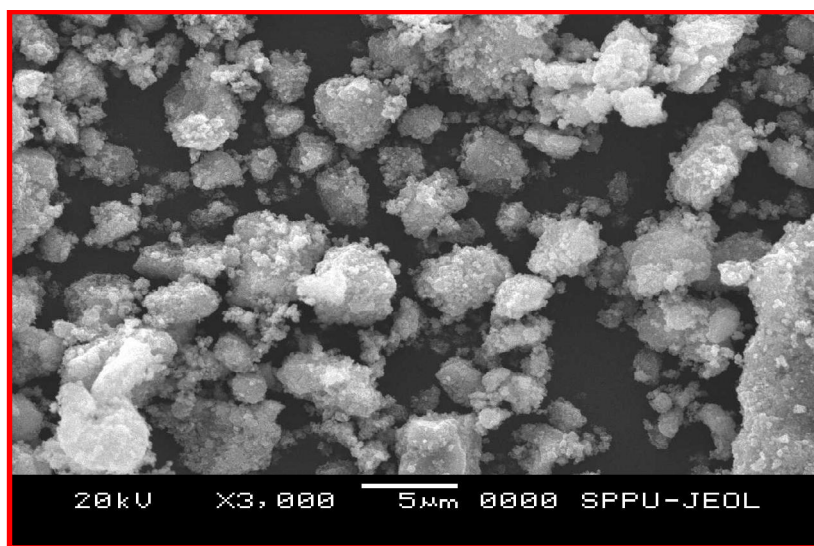


Fig. 7.13 SEM image of PVP coated MnFe₂O₄ nanoparticles

TEM analysis

Fig. 7.14 (a) shows TEM image of EDA functionalized MnFe₂O₄ MNPs and it shows the formation of roughly spherical nanoparticles with average particle size about 8 nm. The particle size calculated from TEM matches with crystallite size calculated from XRD analysis. Fig. 7.14 (b) represents the selected area electron diffraction (SAED) patterns and it shows bright ring patterns which indicates crystalline nature of nanoparticles as specified by XRD patterns. The ring patterns correspond to (220), (311), (400), (511) and (440) planes, which is clearly seen in graph of XRD.

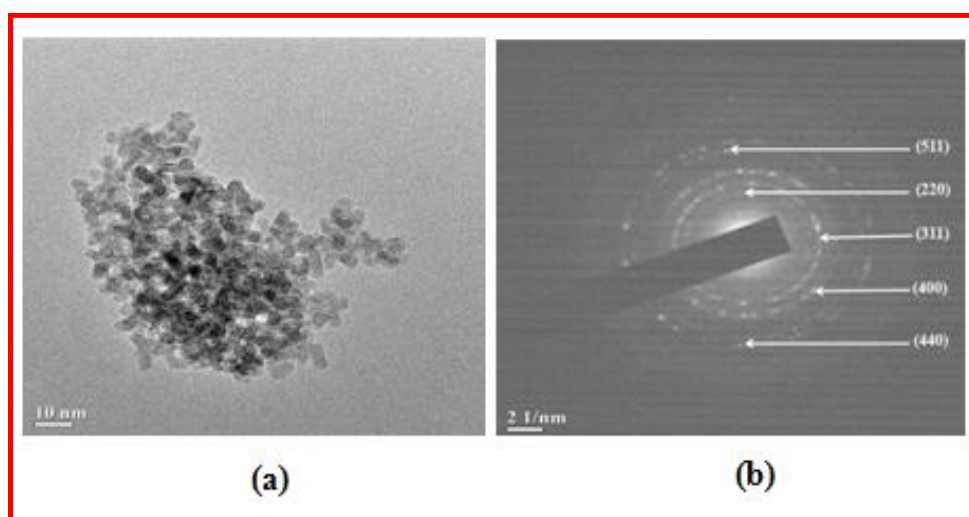


Fig.7.14 (a) TEM image and (b) SAED pattern of EDA functionalized MnFe₂O₄

TEM analysis was used to study the size and morphology of PVP coated nanoparticles. Fig. 7.15 shows the TEM images of MnFe₂O₄ nanoparticles. The MNPs were roughly spherical in shape and had good dispersibility. The dispersibility of nanoparticles was increased due to PVP functionalization and it can be ascribed as existence of non-magnetic layer of PVP. The average particle size was approximately 13 nm, which is in line with size obtained from XRD analysis. The selected area electron diffraction (SAED) patterns of PVP functionalized nanoparticles show glowing ring patterns specifying crystalline behaviour (Fig. 7.15 inset).

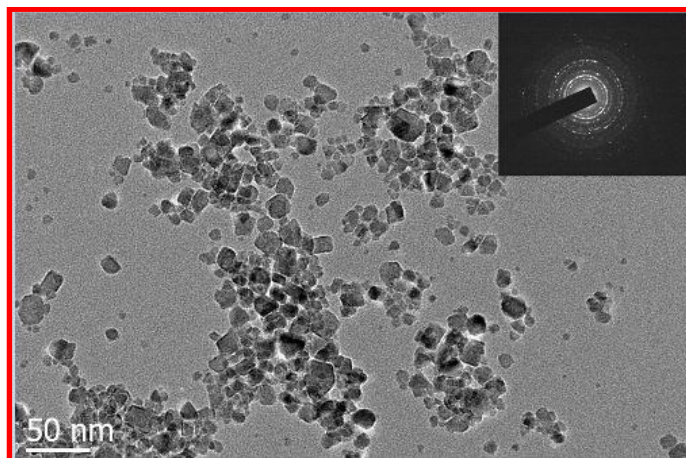


Fig. 7.15 TEM image of PVP functionalized MnFe₂O₄ (inset: SAED pattern)

7.3.5 Chemical bonding study

FTIR analysis

Fig. 7.16 is of FTIR spectrum of EDA functionalized MnFe₂O₄ over the range of 450 to 4000 cm⁻¹. The attachment of functional group to surface of MNPs was analyzed by FTIR technique. FTIR gives details about ions position in crystal through vibrational bands. A characteristic band near 600 cm⁻¹ is due to stretching vibrations of Fe³⁺-O²⁻ and it is observed for all ferrites. The peaks at approximately 1631 and 3400 cm⁻¹ of EDA functionalized MnFe₂O₄ match with ethylenediamine peaks [16, 17]. This observation shows an existence of EDA molecules on MnFe₂O₄ nanoparticles surface.

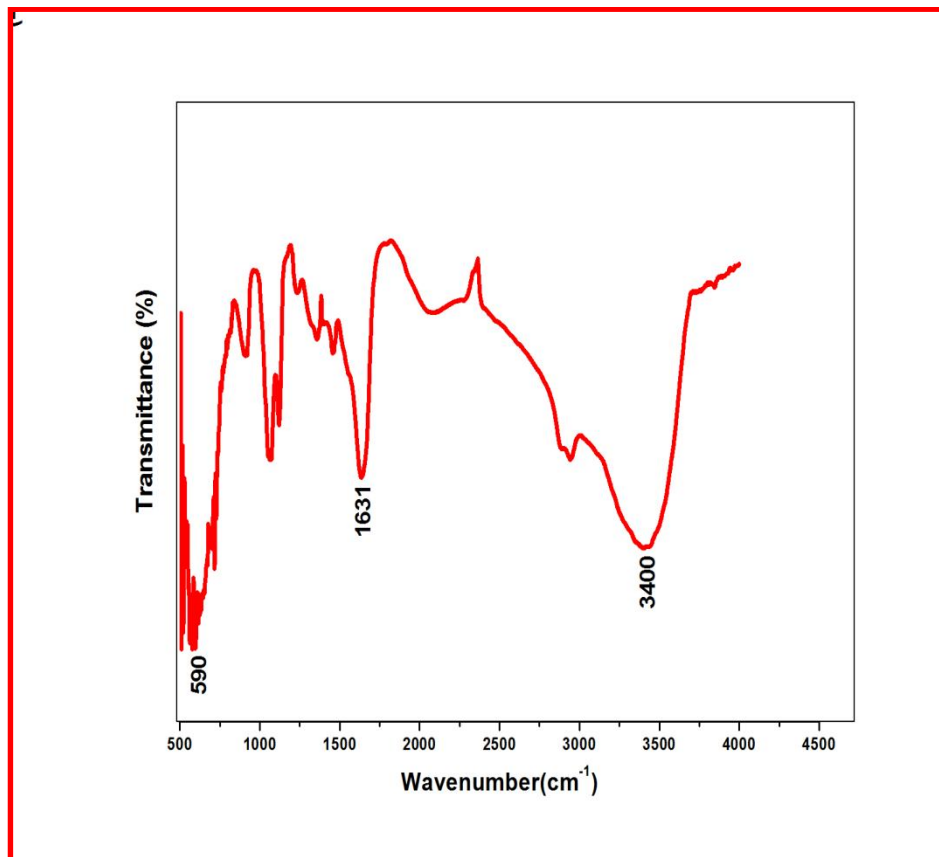


Fig. 7.16 FTIR spectrum of EDA functionalized MnFe₂O₄ MNPs

The existence of PVP on the surface of the MNPs was confirmed by FTIR spectroscopy. Fig. 7.17 displays the FTIR spectrum of PVP functionalized nanoparticles. From the IR spectrum presented in this figure, the absorption peak at 580 cm⁻¹ belongs to metal oxygen bonding. The peak at 1663 cm⁻¹ belongs to C=O group of N-vinyl pyrrolidone. Asymmetric scissoring bending vibrations of CH₂ group of N-vinyl pyrrolidone are appeared at 1440 cm⁻¹. The absorbent peak centered at 1276 cm⁻¹ is due to C–N stretching vibration of Nvinyl pyrrolidone. Also, the spectrum of the sample consists of bands at 2964 cm⁻¹ and 1455 cm⁻¹ corresponding to –CH₂ symmetric and asymmetric vibrations respectively [16, 17].

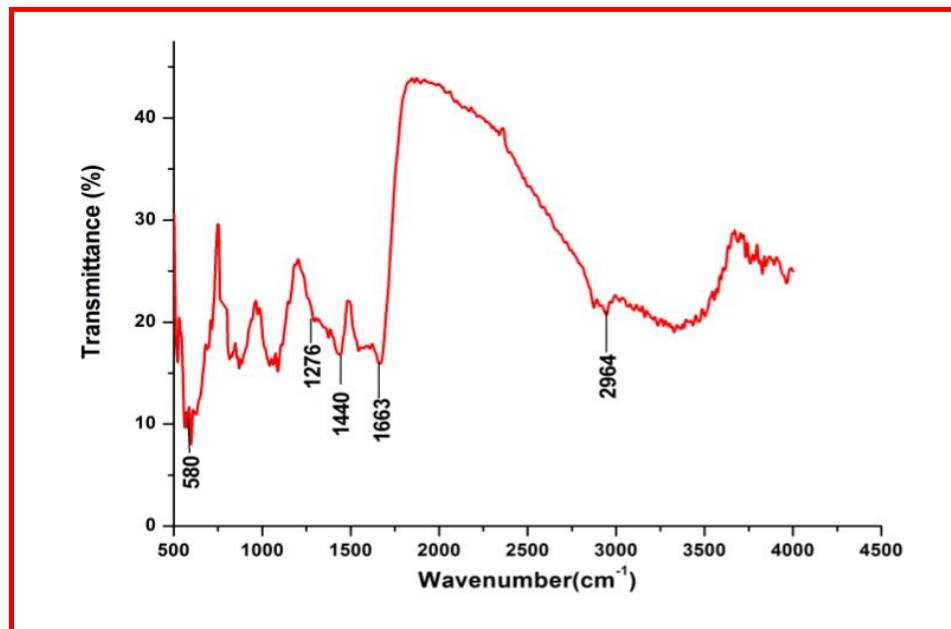


Fig. 7.17 FTIR spectrum of PVP coated MnFe₂O₄ nanoparticles

7.3.6 Magnetization study

VSM analysis

The magnetic properties of EDA functionalized MnFe₂O₄ nanoparticles measured by VSM and M versus H measurements at 300 K were carried out as presented in Fig. 7.18. It can be seen from hysteresis curve of functionalized MnFe₂O₄ MNPs at 300 K that there is no coercivity or remanence existed, indicating the superparamagnetic behavior. The saturation magnetization observed for EDA functionalized MnFe₂O₄ is found to be 53 emu/g and which is smaller than the bulk ferrite and reason behind this is the lattice defects, weak magnetic super-exchange interactions and existence of a magnetically stationary layer on the surface of the nanoparticles [18].

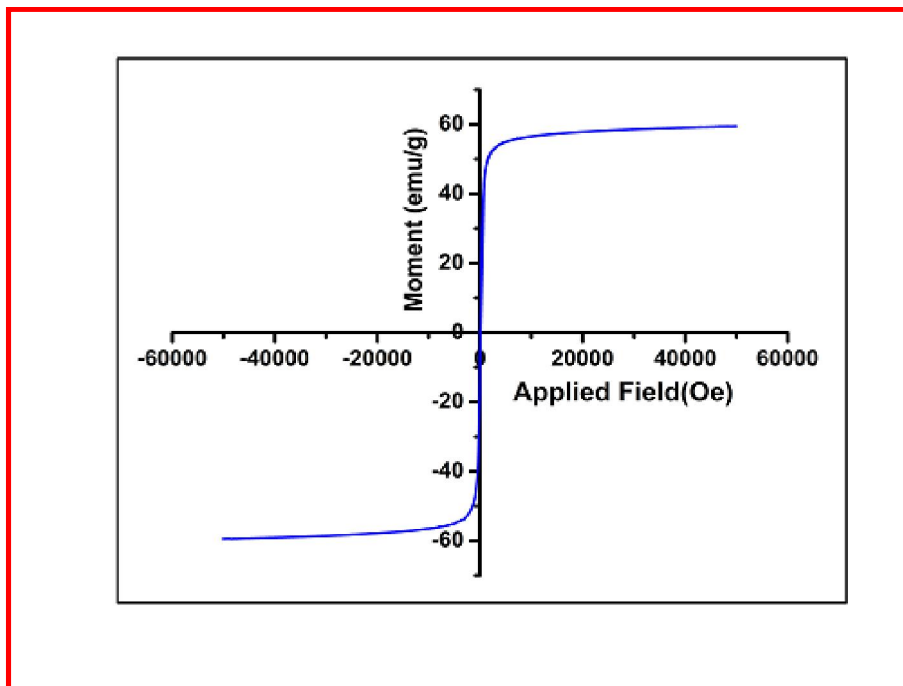


Fig. 7.18 M–H curve of EDA functionalized MnFe₂O₄ nanoparticles

The M versus H measurements have been taken at temperature 300K to understand the effect of temperature on magnetic behavior of MnFe₂O₄ and results have been displayed in Fig. 7.19. From the figure, it can be observed that magnetization of PVP functionalized MnFe₂O₄ is 64 emu g⁻¹ at 300K. This increase in magnetization at lower temperature was due to frustration effects in ferrites below the blocking temperature of the materials. A hysteresis curve of PVP coated MnFe₂O₄ nanoparticles at 300 K shows that there are negligible coercivity and remanence found, which indicates superparamagnetic behavior [18].

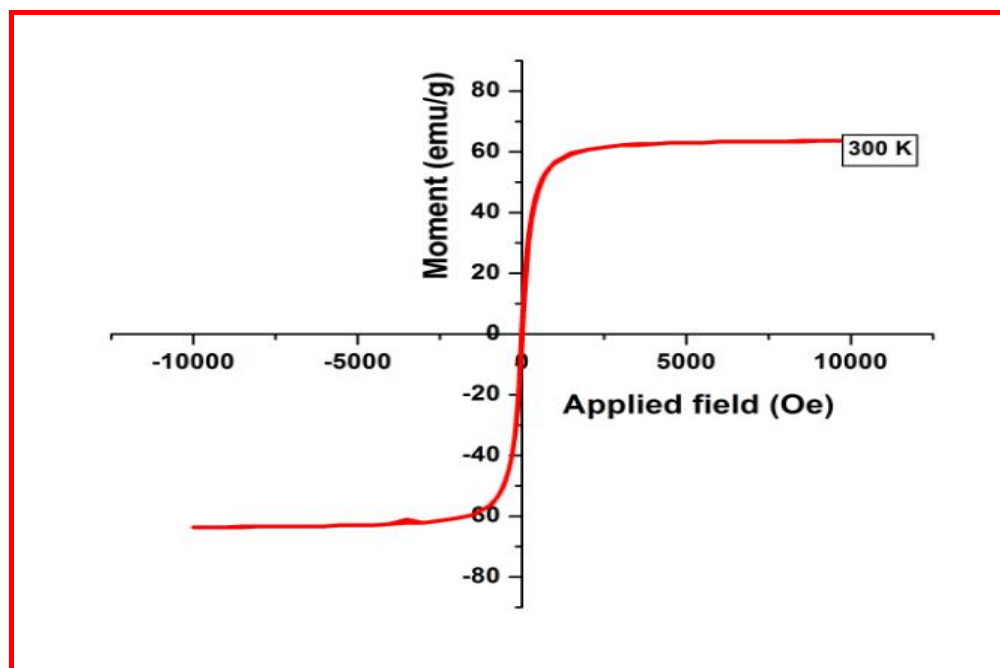


Fig. 7.19 M-H curve of PVP coated MnFe₂O₄ nanoparticles

7.3.7 Thermogravimetric analysis

TGA analysis

Thermogravimetry curves for the EDA functionalized MnFe₂O₄ nanoparticles were recorded in the temperature range from 25 to 700 °C with a heating rate of 10 °C in nitrogen atmosphere. Fig. 7.20 shows weight loss in three steps for EDA functionalized MnFe₂O₄. Weight loss in initial stage was due to water and moisture removed from surface. Weight loss in second stage was noticed because of the decomposition of diethylene glycol, which was modified with ethylenediamine. Third weight loss was seen due to the surface bonded ethylenediamine molecules, which was above 400 °C [19].

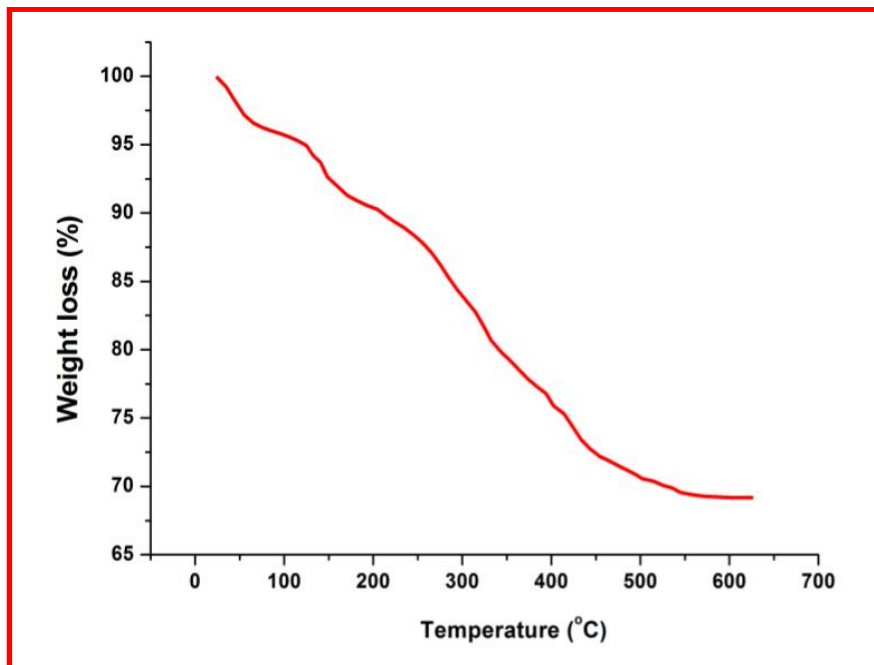


Fig. 7.20 Thermogravimetry curve of EDA functionalized MnFe₂O₄

TGA provides further confirmation of coating on surface of nanoparticles. Fig. 7.21 shows TGA study of PVP coated MnFe₂O₄ nanoparticles. In this experiment, the sample was heated from ambient temperature to 700 °C with a heating rate of 10 °C / min under the flow of nitrogen (N₂) and measured the change in the weight of sample due to the loss of coating material. A weight loss of about 2% can be attributing to the removal of PVP modified glycol molecules anchored to the surface of MNPs below 200 °C [19]. The second variation starts at 230 °C is owing to the decomposition of PVP. TGA analysis has confirmed that PVP get anchored on the surface of MnFe₂O₄.

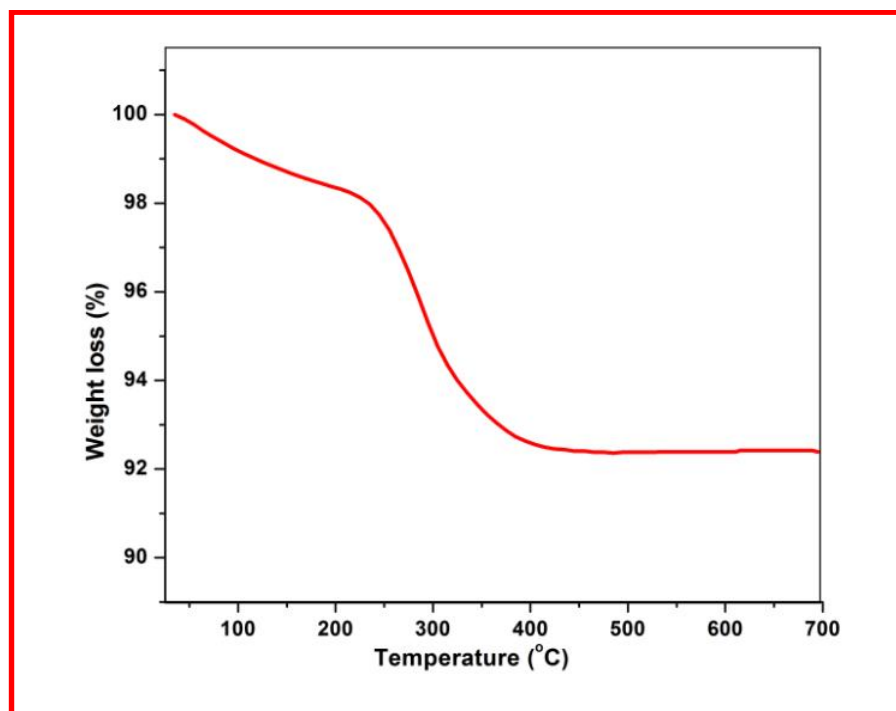


Fig. 7.21 Thermogravimetric pattern of PVP functionalized MnFe₂O₄

7.3.8 Hyperthermia properties

Hyperthermia properties of EDA functionalized MnFe₂O₄

The temperature rise of EDA functionalized MNPs with time evaluated under different magnetic fields from 167.6, 251.4 and 335.2 Oe for 10 min with a concentration of 5 mg mL⁻¹ and 10 mg mL⁻¹ is shown in Fig. 7.22 and 7.23. From temperature curve, it is observed that EDA functionalized nanoparticles gain the hyperthermia temperature within a short time span and at a lower AC magnetic field. Time required to reach the hyperthermia temperature is less for suspension of 10 mg mL⁻¹ in comparison with 5 mg mL⁻¹ and this may be due to the increase in exchange coupling energy. It is observed that for particle concentration of 5 mg mL⁻¹, the field 167.6 Oe is not sufficient to reach hyperthermia temperature while for concentration 10 mg mL⁻¹, hyperthermia temperature is reached for all values of applied fields. In initial stage, the rapid temperature rise is due to the Neel relaxations and Brownian relaxations as eddy current losses are negligible for high resistivity ferrites [20, 21].

The SAR value for 5 mg mL⁻¹ and 10 mg mL⁻¹ increases from 40.66 to 94.65 W g⁻¹ and 33.33 to 73.00 W g⁻¹ with increase in field from 167.6 to 335.2 Oe respectively. In case of sample 10 mg mL⁻¹, there is a higher temperature rise compared to sample 5 mg mL⁻¹ but the SAR is higher in the case of 5 mg mL⁻¹. The highest SAR value 94.65 W g⁻¹ was found at 5 mg mL⁻¹ concentration. The material to be used for hyperthermia therapy is superior when SAR value is high and high SAR value minimizes the amount of magnetic material applied for hyperthermia [22].

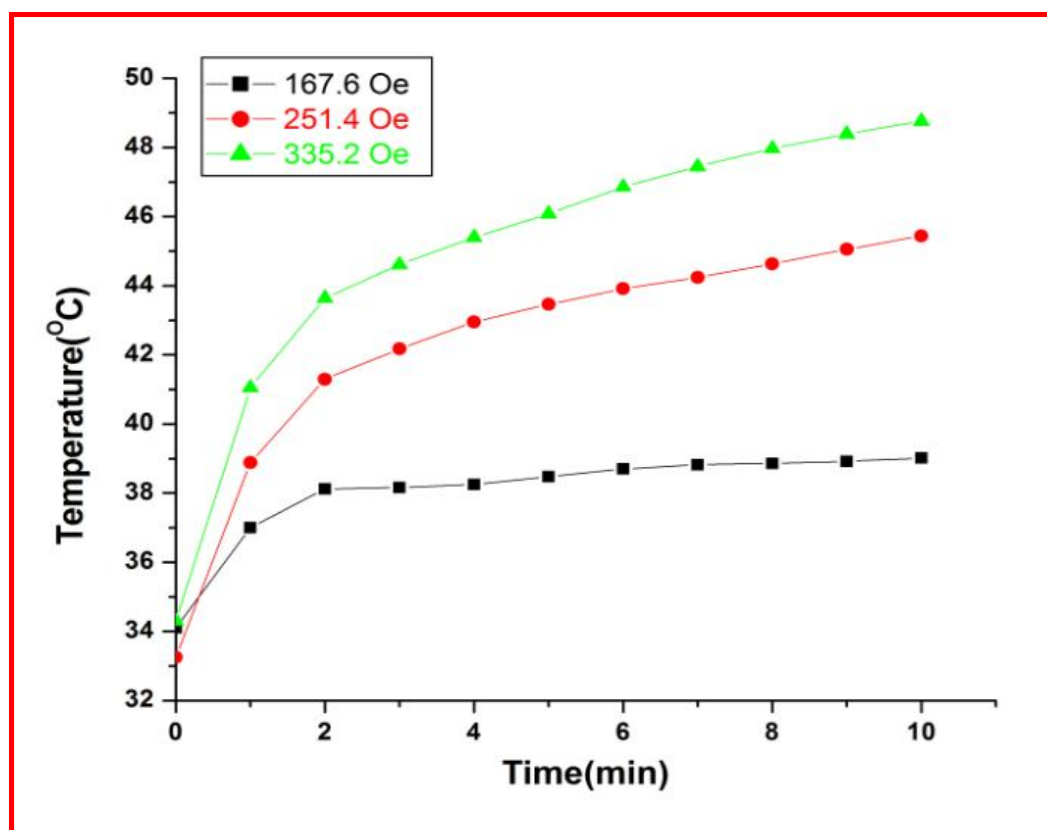


Fig. 7.22 Temperature versus time curve of EDA functionalized MnFe₂O₄ for 5 mg mL⁻¹ concentration at different fields

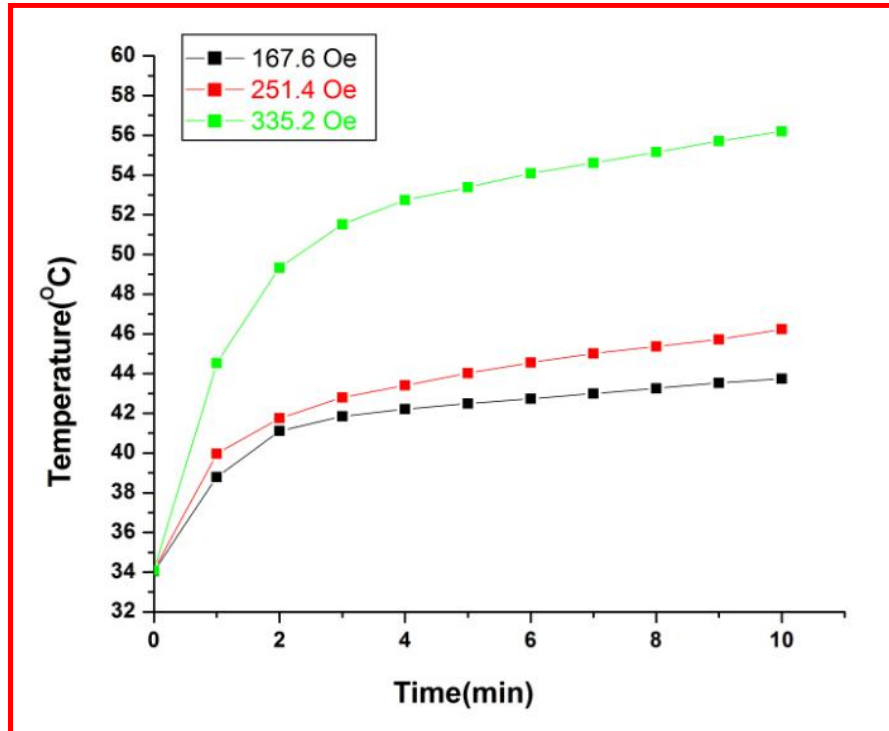


Fig. 7.23 Temperature versus time curve of EDA functionalized MnFe₂O₄ for 10 mg mL⁻¹ concentration at different fields.

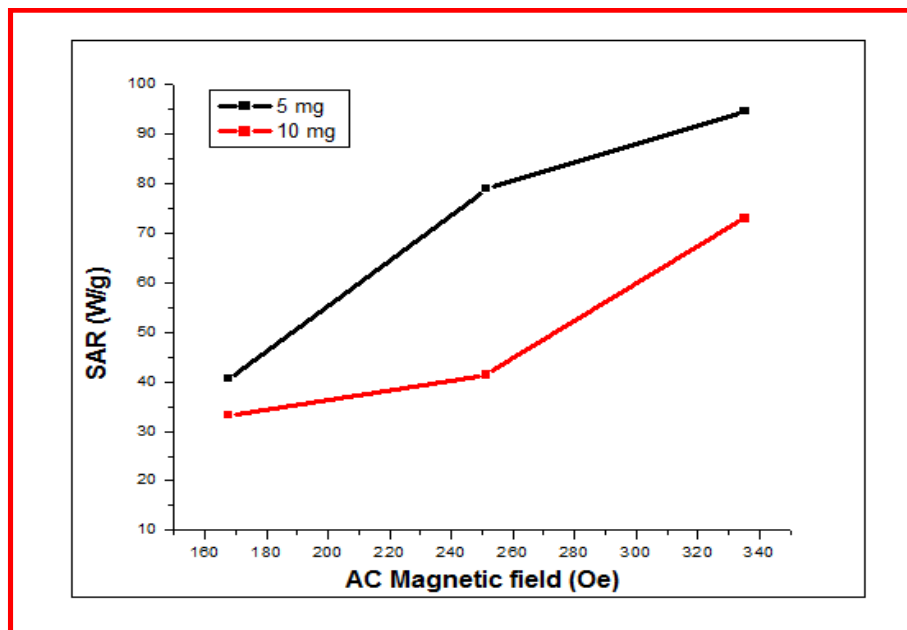


Fig. 7.24 SAR of EDA functionalized MnFe₂O₄

Hyperthermia properties of PVP functionalized MnFe₂O₄

Temperature kinetics of PVP functionalized MnFe₂O₄ nanoparticles are shown in Fig. 7.25 and 7.26. The concentrations 5 mg mL⁻¹ and 10 mg mL⁻¹ in water were taken to study the heating characteristics for hyperthermia applications. The samples were sonicated for 10 min for homogenization for reliable mensuration. The AC magnetic fields 167.6, 251.4 and 335.2 Oe were applied to measure temperature rise of PVP functionalized nanoparticles at 265 kHz frequency. Fig. 7.27 shows the hyperthermia efficiency i.e. SAR value. A heat is dissipated to the surrounding due to interaction of MNPs with applied field and delay in the relaxation of the magnetic moment. For superparamagnetic nanoparticles, heat losses are caused because of friction occurring from oscillations of particle and rotation of magnetic moments with each field, which are Neel and Brownian relaxation modes [22, 23]. Temperature was increased with increase in applied magnetic field with time for both concentrations. Magnetic 167.6 Oe is sufficient to reach the hyperthermia temperature within short time at a frequency of 265 kHz. Time required to reach the appropriate hyperthermia temperature for 10 mg mL⁻¹ sample is less as compared to 5 mg mL⁻¹.

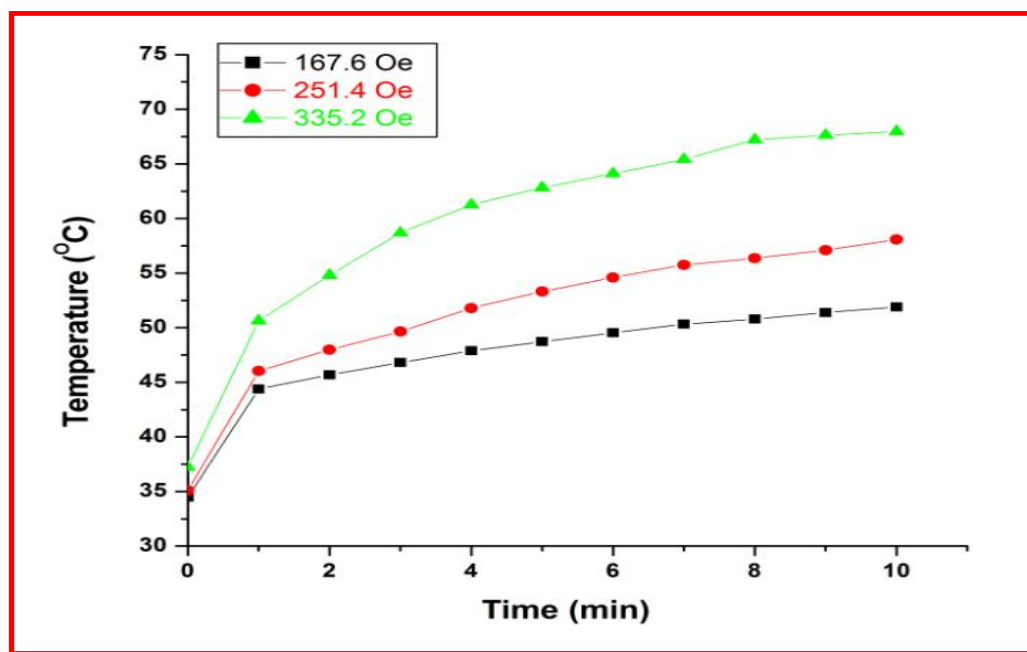


Fig. 7.25 Temperature versus time curve for 5 mg mL⁻¹ concentration of PVP coated MnFe₂O₄ nanoparticles at different magnetic fields

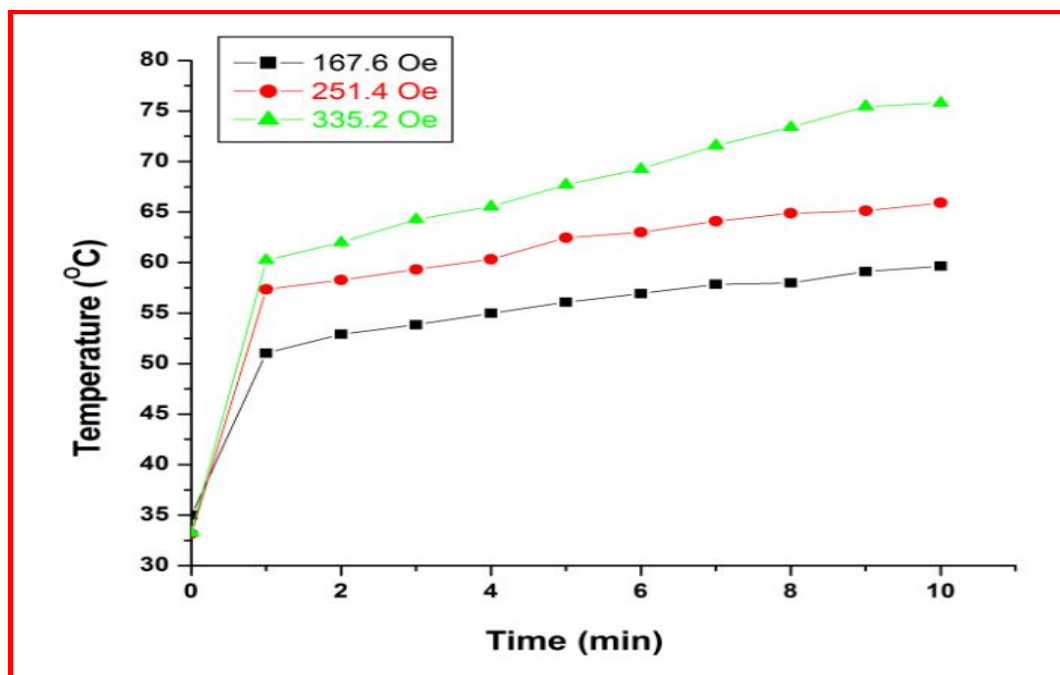


Fig. 7.26 Temperature versus time curve for 10 mg mL⁻¹ concentration of PVP coated MnFe₂O₄ nanoparticles at different magnetic fields

The SAR values are increased from 346.73 to 468.37 W g⁻¹ for 5 mg mL⁻¹ and 225.07 to 378 W g⁻¹ for 10 mg mL⁻¹ with increasing field strength. The SAR value is high for 5 mg mL⁻¹ than 10 mg mL⁻¹ concentration despite there is a high temperature rise in the case of sample 10 mg mL⁻¹ compared to 5 mg mL⁻¹. This may be due to particle conglomeration in high particle concentration, which leads to extreme rise in dipole-dipole interaction in particles. If the SAR value is higher, then we can say that material is superior candidate to be used for hyperthermia therapy [24]. Therefore, it can be concluded that PVP functionalized MnFe₂O₄ nanoparticles with high SAR value can be considered as great potential material for hyperthermia applications.

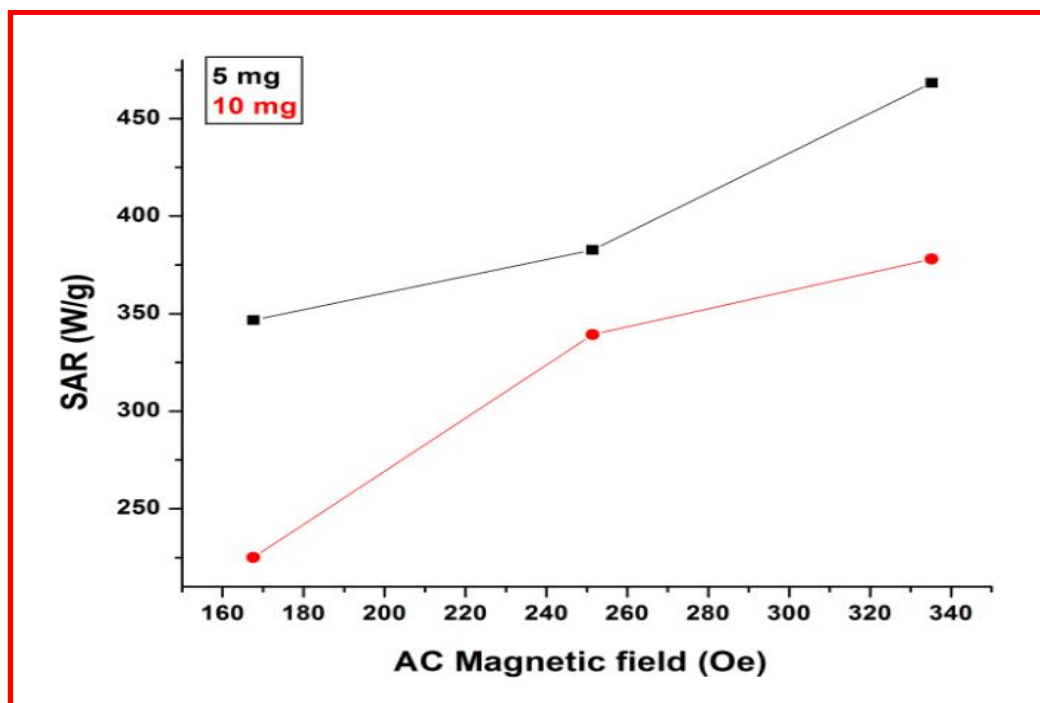


Fig. 7.27 SAR value of PVP coated MnFe₂O₄ nanoparticles at different magnetic fields

7.3.9 Potential of nanoparticles in cancer therapy

In recent years, there is huge advancement in medicine field but cancer still remains major source of death in world. Cancer is the second leading cause of human deaths. Inappropriate diagnosis and disease detection at later stages are the most common reasons behind deaths. Risk of cancer is getting increased significantly day by day and many cancers cases occur more commonly in developed countries. Diagnosis of the cancer at early stage and to cure it without side effects remains challenge to scientific community. Hyperthermia therapy can reduce serious side effects compare to other therapies. In hyperthermia therapy, the affected cancer tissues are heated to temperature range of 41°C to 46°C by exposing MNPs to external AC magnetic field. Manganese ferrite (MnFe₂O₄) among spinel ferrites is a remarkable magnetic material for biomedical applications due to their high resistivity and high saturation magnetization. Thermal conductivity of manganese ferrite

nanoparticles is lower than NiFe₂O₄, CoFe₂O₄. Relaxivity of manganese ferrite nanoparticles is large due to their large magnetic spin magnitude, which improves heating in AC magnetic field. Therefore, manganese ferrite nanoparticles over other spinel ferrites have been selected for magnetic hyperthermia cancer therapy.

The main emphasis of the present work is to develop functionalized MnFe₂O₄ nanoparticles for advanced magnetic particle hyperthermia for treatment of cancer in one step that is *in situ* functionalization. Here, we have synthesized EDA and PVP functionalized modispersed and superparamagnetic MnFe₂O₄ nanoparticles using one pot synthesis method. These synthesized nanoparticles shows highest SAR value and take less time to reach threshold hyperthermia temperature. Among these materials PVP functionalized MnFe₂O₄ sample shows high SAR as well as required less time to reach threshold hyperthermia temperature.

7.4 Conclusions

The ethylenediamine (EDA) functionalized MnFe₂O₄ nanoparticles with around 8 nm size were synthesized by polyol method. The structural, morphological and magnetic properties of EDA functionalized MNPs were studied using XRD, FTIR, TGA, SEM, TEM and SQUID. The induction heating ability of MNPs was studied in order to use them for magnetic hyperthermia anticancer therapy. Magnetic particle hyperthermia study was performed for these functionalized nanoparticles at 167.6, 251.4 and 335.2 Oe, which showed self-heating temperature rise up to 48.76 °C to 56.34 °C at 5 mg mL⁻¹ and 10 mg mL⁻¹ concentrations in water respectively. The highest SAR value 94.65 W g⁻¹ of EDA functionalized MnFe₂O₄ was calculated at 5 mg mL⁻¹ concentration.

The monodispersed manganese iron oxide (MnFe₂O₄) nanoparticles coated with PVP were synthesized in diethylene glycol by using polyol reflux method. The nanoparticles were roughly spherical and were about 13 nm in size. The FTIR and TGA results show the existence of PVP on surface of MnFe₂O₄ nanoparticles. The

obtained nanoparticles exhibited superparamagnetism and high saturation magnetization at room temperature. The induction heating study of these nanoparticles was performed at 167.6, 251.4 and 335.2 Oe use them in hyperthermia applications. From the results it is observed that self-heating temperature rise up to 68.18 °C to 75.82 °C at 5 mg mL⁻¹ and 10 mg mL⁻¹ concentrations in water respectively. PVP coated nanoparticles show high temperature rise characteristics in less time when exposed to an external AC magnetic field and highest SAR value 468.37 W g⁻¹ was found at an applied field of 335.2 Oe with a particle concentration of 5 mg mL⁻¹ compared to EDA functionalized MnFe₂O₄. The MnFe₂O₄ nanoparticles coated with PVP had a high SAR value at low particle concentration. Therefore, PVP coated MnFe₂O₄ nanoparticles can be a potential heating agent for efficient cancer hyperthermia therapy application.

References

1. C. Sun, J. Lee and M. Zhang, *Adv. Drug Deliv. Rev.*, 2008, 60, 1252-1265.
2. B. Rittich, A. Spanova, D. Horak, M. Benes, L. Klesnilova, K. Petrova and A. Rybnika, *Colloids Surf. B*, 2006, 52, 143-148.
3. Z. Beji, A. Hanini, L. Smiri, J. Gavard, K. Kacem, F. Villain, J. Greneche, F. Chau and S. Ammar, *Chem. Mater.*, 2010, 22, 5420-5429.
4. R. Ghosh, L. Pradhan, Y. Devi, S. Meena, R. Tewari, A. Kumar, S. Sharma, N. Gajbhiye, R. Vatsa, B. Pandey and R. Ningthoujam, *J. Mater. Chem.*, 2011, 21, 13388-13398.
5. B. Cullity and D. Graham, *Introduction to Magnetic Materials*, 1972, 1-66, 2nd Edition, Wiley, John Wiley and Sons Group. 1972.
6. R. Hiergeist, W. Andra, N. Buske, R. Hergt, I. Hilger, U. Richter and W. Kaiser, *J. Magn. Magn. Mater.*, 1999, 201, 420-422.
7. I. Sharifi, H. Shokrollahi, M. Doroodmand and R. Safi, *J. Magn. Magn. Mater.*, 2012, 324, 1854-1861.
8. A. Raghavender, K. Zadro, D. Pajic, Z. Skoko and N. Biliskov, *Mater. Lett.*, 2010, 64, 1144-1146.
9. K. Sapsford, W. Algar, L. Berti, K. Gemmill, B. Casey, E. Oh, M. Stewart and I. Medintz., *Chem. Rev.*, 2013, 113, 1904-2074.
10. S. Mohapatra, S. Rout, S. Maiti, T. Maiti and A. Panda, *J. Mater. Chem.*, 2011, 21, 9185-9193.
11. Y. Huang, Y. Wang and X. Yan, *Environ. Sci. Technol.*, 2010, 44, 7908-7913.
12. K. Barick, M. Aslam, P. Prasad, V. Dravid and D. Bhadur, *J. Magn. Magn.*

- Mater., 2009, 321, 1529-1532.
13. S. Sun and H. Zheng, *J. Am. Chem. Soc.*, 2002, 124, 8204-8205.
 14. D. Maity, S. Choo, J. Yi, J. Ding and J. Xue, *J. Magn. Magn. Mater.*, 2009, 321, 1256-1259.
 15. F. Fievet, J. Lagier, B. Blin, B. Beaudoin, M. Figlarz, *Solid. State. Ion.*, 1989, 198, 32-33.
 16. H. Zaki and H. Dawoud, *Physica. B*, 2010, 405, 4476-4479.
 17. H. Ni, X. Sun, Y. Li and C. Li, *J. Mater. Sci.*, 2015, 50, 4270-4279.
 18. R. Cornell and U. Schwertmann, *The Iron Oxides*, 1996, 111-136, 2nd Edition, Willey-VCH; New York.
 19. H. Yuan, Y. Wang, S. Zhou and S. Lou, *Chem. Eng. J.*, 2011, 175, 555-560.
 20. R. Rosensweig, *J. Magn. Magn. Mater.*, 2002, 252, 370-374.
 21. S. Bae and S. Lee, *Appl. Phys. Lett.*, 2006, 89, 252503.
 22. R. Hergt, S. Dutz and M. Zeisberger, *Nanotechnology*, 2010, 21, 015706.
 23. S. Jadhav, D. Nikam, V. Khot, S. Mali, C. Hong and S. Pawar, *Mater. Charact.*, 2015, 102, 209–220.
 24. E. Strable, J. Bulte, B. Moskowitz, K. Vivekanandan, M. Allen and T. Douglas, *Chem. Mater.*, 2001, 13, 2201-2209.

Biocompatibility Study of Functionalized MnFe_2O_4 Nanoparticles

Chemical Papers
<https://doi.org/10.1007/s11696-019-00768-z>

ORIGINAL PAPER

Check for updates

APTES (3-aminopropyltriethoxy silane) functionalized MnFe_2O_4 nanoparticles: a potential material for magnetic fluid hyperthermia

P. R. Ghutepatil¹ · A. B. Salunkhe² · V. M. Khot³ · S. H. Pawar^{1,4}

Asian Journal of Chemistry: Vol. 31, No. 5 (2019), 1081-1086
ASIAN JOURNAL OF CHEMISTRY
<https://doi.org/10.14233/ajchem.2019.21815>

Surface Functionalization of MnFe_2O_4 Nanoparticles with Ethylenediamine for Hyperthermia Application

P. R. GHUTEPATIL¹, A. B. SALUNKHE², V. M. KHOT³, B. R. THOMBARE⁴ and S. H. PAWAR^{1,5*}

¹Center for Interdisciplinary Research, D.Y. Patil University, Kolhapur-416006, India
²Department of Physics, Elphinstone College, Mumbai-400032, India
³Dr. D.Y. Patil Institute of Engineering, Management and Research, Pune-411044, India
⁴Department of Physics, Savitribai Phule Pune University, Pune-411007, India
⁵Center for Innovative and Applied Research Anekant Education Society, T.C. College, Baramati-413102, India

The parts of this chapter have been published in reserach article.

Nano LIFE

Synthesis of monodispersed polyvinylpyrrolidone functionalized biocompatible manganese ferrite nanoparticles for hyperthermia application
 --Manuscript Draft--

Manuscript Number:	
Full Title:	Synthesis of monodispersed polyvinylpyrrolidone functionalized biocompatible manganese ferrite nanoparticles for hyperthermia application
Article Type:	Research Paper

The parts of this chapter have been submitted in reserach article for publication.

We're very optimistic that nanotechnology can markedly improve cancer therapy.

-Jim Thomas

8.1 Introduction

Biocompatibility of nanoparticles is a foremost topic in the field of medicine. Biocompatibility study of nanomaterials is most important indicators of the biological evaluation system *in vitro* and it is a censorious part for successful applications of biomedical materials. Biocompatible material should not create toxicity when reacted with organs of body. Biocompatible material is also called as biomaterial. Surface biocompatibility and structural biocompatibility these are the two types of biocompatibility. A rudimentary conception toxicity of MNPs is tremendously necessary for biological system. Adverse effects of physical or chemical agents on living organisms are studied using toxicology. It is required to not only discuss about nanoparticles in general terms but also to identify them in the context of their possible biological interactions [1, 2].

The estimation of toxicity of *in vitro* toxicological assessment of nanomaterials is significant for use in area of nanomedicine. The relevant choice of concentration, selection of cell line and option of viability assay are required while performing the experiment of toxicity [3].

The toxicity of MNPs can be decided by following features:

- Chemical constituent of the material
- Surface charge on the material
- Surface area to volume ratio of material
- Hydrophobic, hydrophilic groups of the material

8.2 Experimental

8.2.1 Selection and procurement of cell culture

The assessment of cytotoxicity of bare MnFe₂O₄, APTES, EDA and PVP functionalized MnFe₂O₄ were carried out on MCF7 (adenocarcinoma cell line of human breast) and L929 (mouse fibroblast) cell lines for *in vitro* application. These

cell lines are procured from National Centre for Cell Sciences, Pune, India and assay used for the toxicity study is MTT assay.

The cell viability was determined with the equation,

$$\text{Cell viability} = A_{\text{tested}} / A_{\text{control}} * 100$$

Where, A_{tested} and A_{control} are the test sample and control sample respectively.

8.2.2 The MTT assay experimental procedure

- The cell line was cultured in DMEM media and it was boosted with 10% heat inactivated fetal calf serum (FBS) as well as 1% Antibiotic – Antimycotic solution.
- The cells were seeded at a density of approximately 5×10^3 cells/well in a 96-well micro plate and conserved at 37°C in 95% humidity and 5% CO₂ overnight.
- The concentrations (0.2, 0.4, 0.6, 0.8, 1, 1.2 mg/mL) of samples were treated for incubation period of 1 day.
- After that cells are washed with PBS two times and then MTT staining solution (5mg/ml in PBS) was added and incubated at 37°C.
- After 4h, addition of 100 μ L of di-methyl sulfoxide was added to each well for the dissolution the formazan crystals. After that, absorbance was measured by using microplate reader.

8.3 Results and discussion

8.3.1 Choice of cell type

Organs and type of cell encountered control the toxic effect of MNPs due to the variation in cell physiology, membrane characteristics, phagocyte characteristics and proliferation state. The important factor in cytotoxicity assay is the selection of suitable cell lines. In addition, it is also needed to give priority to the conditions of cells. Among the commonly used cell lines, fibroblast cells are conducive for the trial. In addition, cancer cells are also a better choice than normal cells owing enhanced rate of growth, metabolic activity and easy to use [4-6].

In present study, L929 and MCF7 cell lines are selected for confirmation of biocompatibility of the prepared MnFe₂O₄, APTES, EDA and PVP functionalized MnFe₂O₄. For the evaluation of compatibility of the materials above cell lines are generally used.

8.3.2 Choice of cytotoxicity assay

Selection of the proper assay to the evaluation of cytotoxicity is crucial to the precise evaluation of cytotoxicity study. How external agents are act in the body can be studied by this method. In comparison with this method to the animal study cell culture study is trouble free to control as well as less expensive. The different assay can be employed to study the toxicity of nanoparticles on cell cultures. There are variety of assay used for the evaluation of toxicity and these are lactate dehydrogenase (LDH), (3-(4,5-dimethyl thiazol-2yl)-2,5 diphenyltetrazolium bromide (MTT), Dye exclusion assay (Trypan blue) including recognition of cytokine/chemokine fabrication etc. Choice of accurate toxicity assay is a key to the accurate assessment of toxicity of nanoparticles. The nanoparticles absorb dye, be redox energetic and significant for the cytotoxicity study is suitable. Among different assays, MTT assay is commonly used assay and easy to use. Therefore in the present investigation, the cytotoxicity has been evaluated by means of MTT assay to reduce the error and to get the calibre results. This assay is very simple and easy to evaluate [6-9].

8.3.3 Physicochemical properties of nanoparticles

The retention time and exocytosis process of the particles in cells can be influenced by size, shape, surface properties, absence or presence of surface bound biomolecules and surface smoothness or roughness of MNPs [10]. The quantity and rate of nanoparticle uptakes can be determined by size of MNPs. The increase in surface area can determine potential number of reactive group on MNPs surface. Toxicological effects can be influenced by physicochemical and structural properties of MNPs with a decrease in size [11, 12].

Reproducible data can be obtained only when MNPs are monodispersed in nature. Monodispersed MNPs can be produced by controlled synthesis protocols only. To avoid the conglomeration between the particles characteristics of nanoparticles can be fitted very cautiously. Particle clustering is avoided thoroughly by tailoring the MNPs carefully. MNPs surface becomes reactive toward biological environment after decreasing the size. The cellular uptake and efficiency of MNPs are dependent on size of MNPs. The size of MNPs plays an important role in distribution, elimination of materials and physiological response [13-15].

8.3.4 *In vitro* cytotoxicity study of bare MnFe₂O₄ nanoparticles

Plasma membrane can be influenced by existence of nanoparticles on surface of cell after the treatment of normal cells and it can lead to breaking down of cells. When nanoparticles are detached from surface of cell, cells can be stained with MTT (3-(4,5-dimethyl thiazol-2yl)-2,5 diphenyltetrazolium bromide). The MTT invades into cell and proceed to mitochondria, where it is reduced to colored (dark purple) and insoluble formazan product because of viable cells reduce the yellow tetrazolium salt to purple dye [16-19].

The cytotoxicity study of bare MnFe₂O₄ MNPs prepared by polyol method is performed on L929 and MCF cell lines with concentrations (0.2,0.4,0.6,0.8,1.0 and 1.2 mg/ml) and for this incubation time period is 24 h by using MTT assay. Fig. 8.1 (a and b) shows the obtained data.

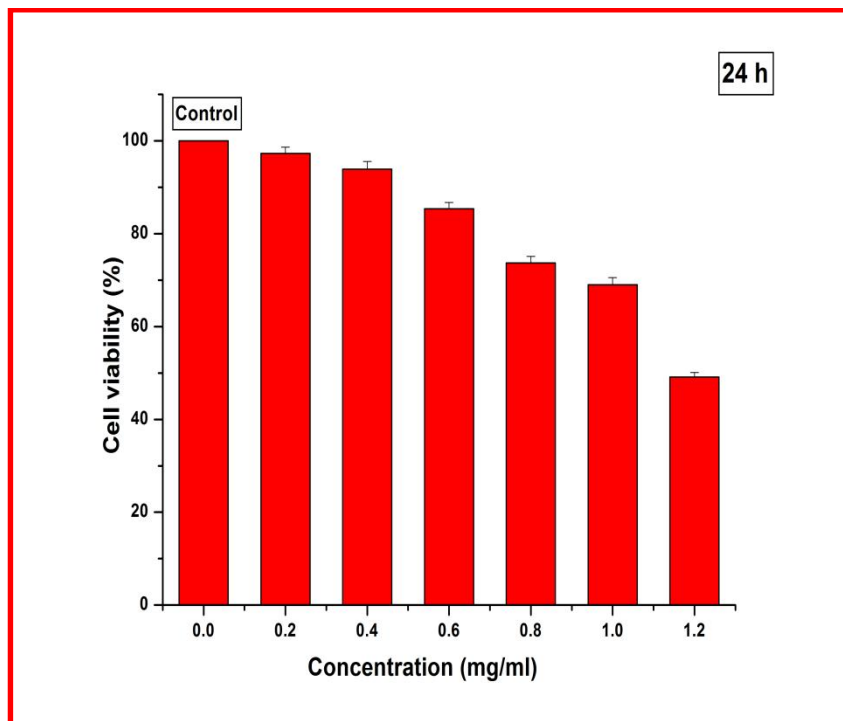


Fig.8.1 (a) Cell viability of bare MnFe₂O₄ nanoparticles on L929 cell line at different concentrations (0.2, 0.4, 0.6, 0.8, 1.0 and 1.2 mgmL⁻¹)

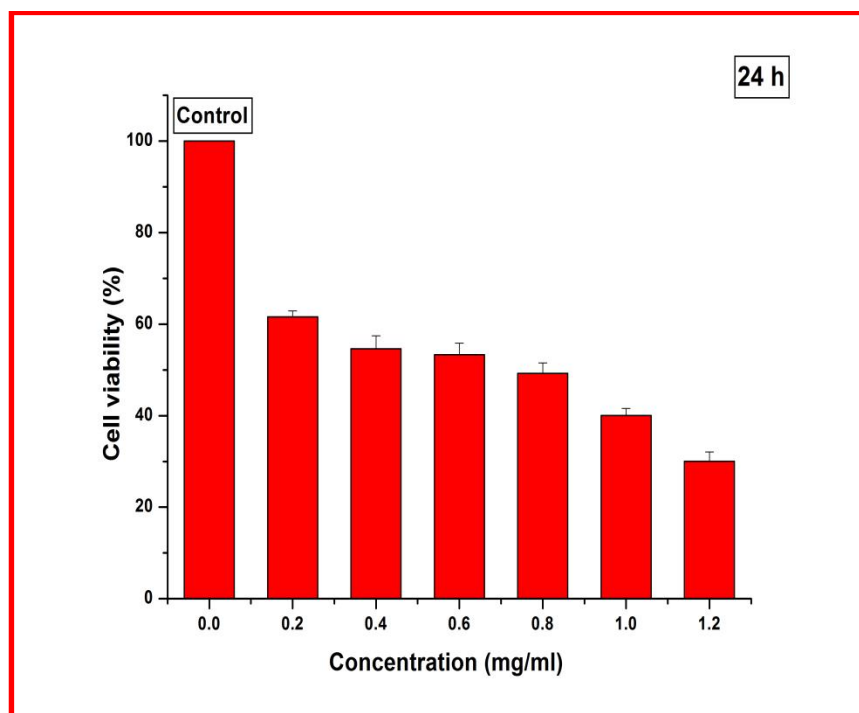


Fig.8.1 (b) Cell viability of bare MnFe₂O₄ on MCF7 cell line at different concentrations (0.2, 0.4, 0.6, 0.8, 1.0 and 1.2 mgmL⁻¹)

Fig. 8.1 (a) and 8.1 (b) shows the graph of cell viability vs concentration of bare MnFe₂O₄ MNPs on L929 cell line and MCF7 cell line for 24 h. Values are expressed as mean \pm SD, n=3. It is observed that cell viability decreases when concentration of nanoparticles increases. This study shows that dose and time relying nature as the viability is decreasing with increase in concentration of NPs. From Fig. 8.1 (a) and 8.1 (b), it is clearly observed that bare MnFe₂O₄ MNPs prepared by polyol method exhibit low toxicity to L929 cells compare to MCF cells. The cell viability of bare MnFe₂O₄ nanoparticles on L929 cells up to concentration 1.2 mg/mL by MTT assay is 49.1 % and 30.4 % on MCF cells for 24 h, respectively. From fig it is shown that these nanoparticles are less toxic up to 1 mg/ml concentration for L929 cells. Therefore, it can be concluded that these MnFe₂O₄ nanoparticles can be used for biomedical implementations up to NPs concentration of about 1mg/mL.

8.3.5 *In vitro* cytotoxicity study of APTES functionalized MnFe₂O₄ nanoparticles

The cytotoxicity study of APTES functionalized MnFe₂O₄ MNPs were done on L929 and MCF7 cell lines with various concentrations like (0.2,0.4,0.6,0.8,1.0 and 1.2 mg/ml) at incubation time of 24 h by MTT assay.The procured data is shown in Fig. 8.2 (a) and 8.2 (b).

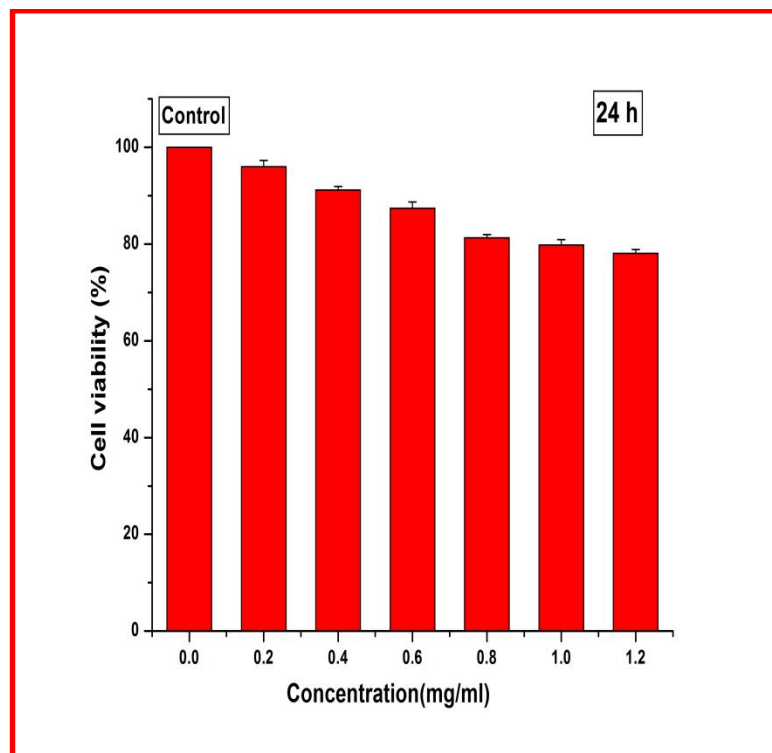


Fig. 8.2(a) Cell viability of APTES functionalized MnFe₂O₄ nanoparticles on L929 cell line at different concentrations (0.2, 0.4, 0.6, 0.8, 1.0 and 1.2 mgmL⁻¹)

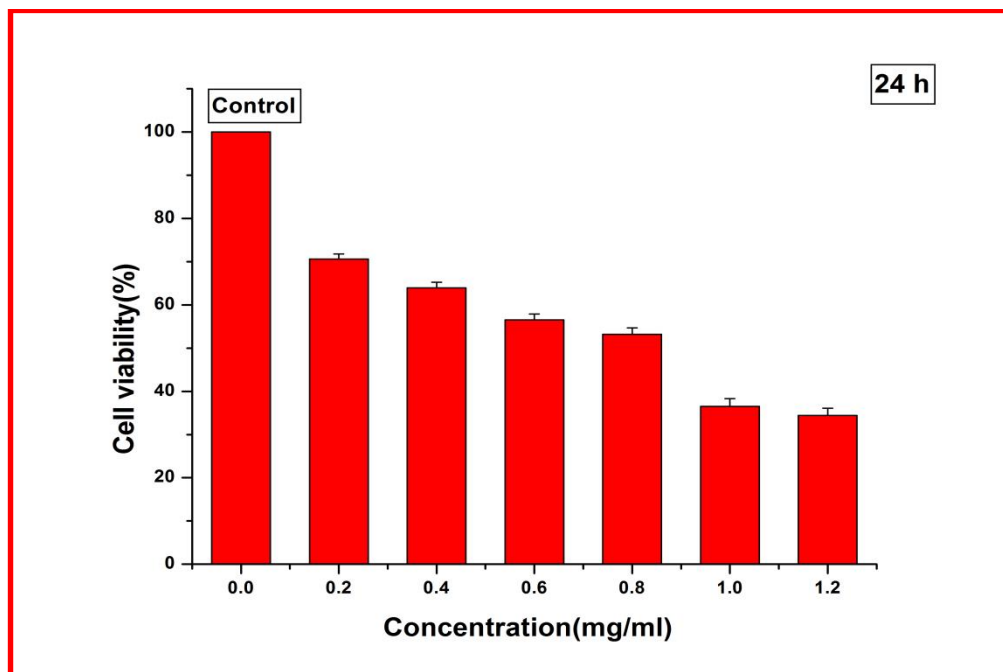


Fig. 8.2 (b) Cell viability of APTES functionalized MnFe₂O₄ nanoparticles on MCF7 cell line at different concentrations (0.2, 0.4, 0.6, 0.8, 1.0 and 1.2 mgmL⁻¹)

Cell viability of APTES coated MnFe₂O₄ NPs on L929 cells and MCF cells with concentration 1.2mg/ml by MTT assay is 78.1 and 34.39 % for 24 h respectively. From the results, it is clear that these nanoparticles are not toxic (biocompatible) for L929 cell line and not toxic for MCF cells up to 0.2 mg/ml concentration. Cell viability was significantly reduced for MCF7 cells when the concentration of nanoparticles is more than 0.2 mg/mL. Therefore, this study proves dose dependant nature as the viability goes on decreases when concentration of nanoparticles increases. The procured results confirm that functionalization of MnFe₂O₄ surface with APTES is superior material to use it in the biomedical implementation, especially for MFH.

8.3.6 *In vitro* cytotoxicity study of EDA functionalized MnFe₂O₄ nanoparticles

Cell viability against the concentration of EDA functionalized MnFe₂O₄ on L929 cell lines and MCF7 cell lines for 24 h, is shown in Fig. 8.3 (a) and 8.3 (b).

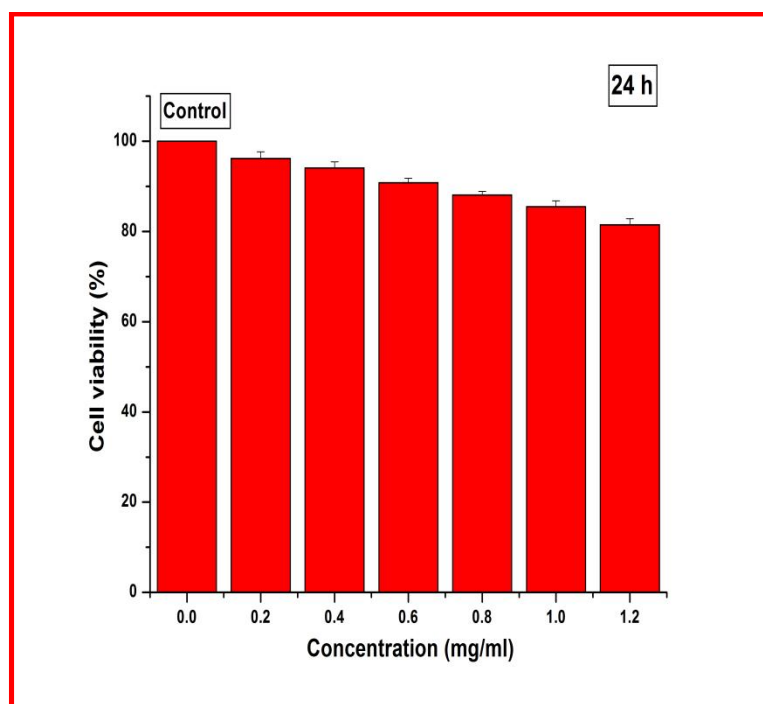


Fig. 8.3 (a) Cell viability of EDA functionalized MnFe₂O₄ nanoparticles on L929 cell line at different concentrations (0.2, 0.4, 0.6, 0.8, 1.0 and 1.2 mg mL⁻¹)

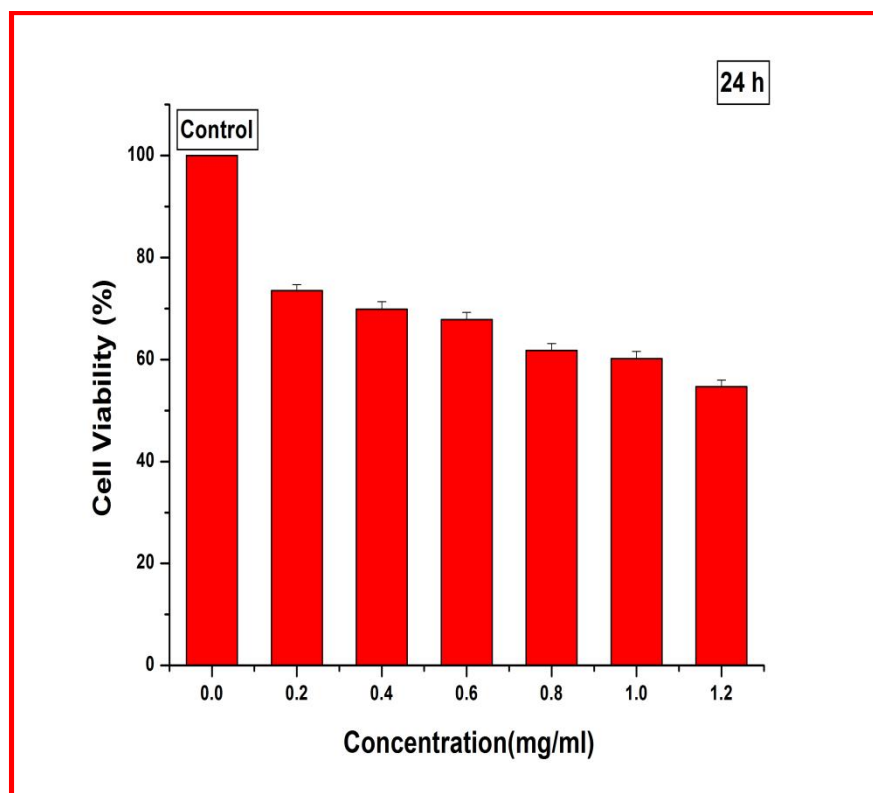


Fig. 8.3 (b) Cell viability of EDA functionalized MnFe₂O₄ on MCF7 cell line at different concentrations (0.2, 0.4, 0.6, 0.8, 1.0 and 1.2 mg mL⁻¹)

The cell viability of EDA functionalized MnFe₂O₄ MNPs on L929 cells and MCF7 cells with up to concentration 1.2 mg/mL by MTT assay is 81.5 and 54.65 % for 24 h incubation period. It can be observed that these nanoparticles are less toxic for L929 and not toxic or less toxic for MCF cells up to 0.6 mg/ml concentration. From the Fig.8.3 (a) and 8.3 (b), it is observed that the EDA functionalized MnFe₂O₄ nanoparticles are less toxic or non toxic than the bare MnFe₂O₄ sample. The reason for low toxicity of MNPs coated with EDA than bare MnFe₂O₄ is that it protects surfaces from interaction with cells or proteins. It has been showed that EDA functionalized NPs can interact with membranes of cell and which enhances cellular response because of biocompatible coating on surface.

8.3.7 *In vitro* cytotoxicity study of PVP functionalized MnFe₂O₄ nanoparticles

Cell viability vs concentration of PVP functionalized MnFe₂O₄ MNPs on L929 cell lines and MCF cell lines for 24 h, is shown in Fig.8.4 (a) and 8.4 (b).

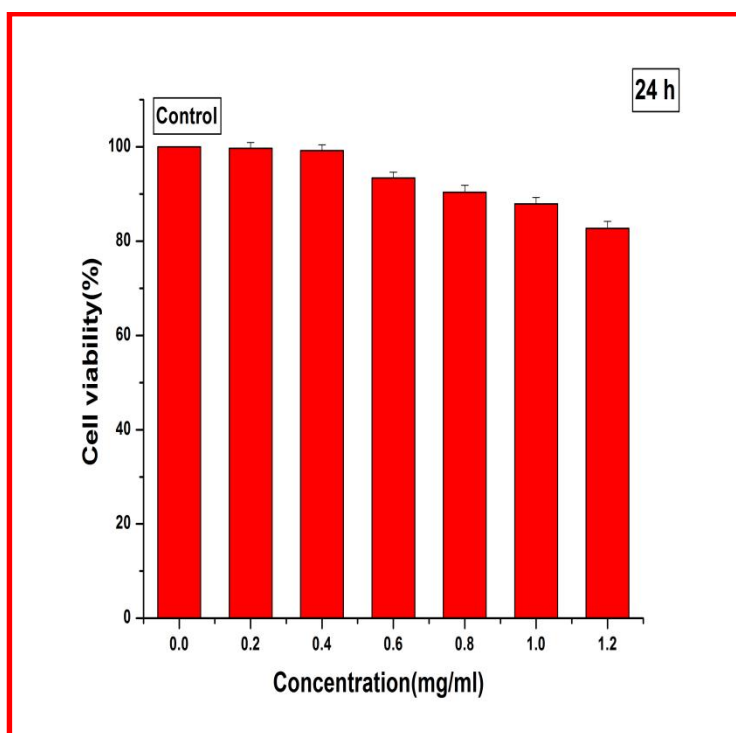


Fig.8.4 (a) Cell viability of PVP functionalized MnFe₂O₄ nanoparticles on L929 cell line at different concentrations (0.2, 0.4, 0.6, 0.8, 1.0 and 1.2 mg mL⁻¹)

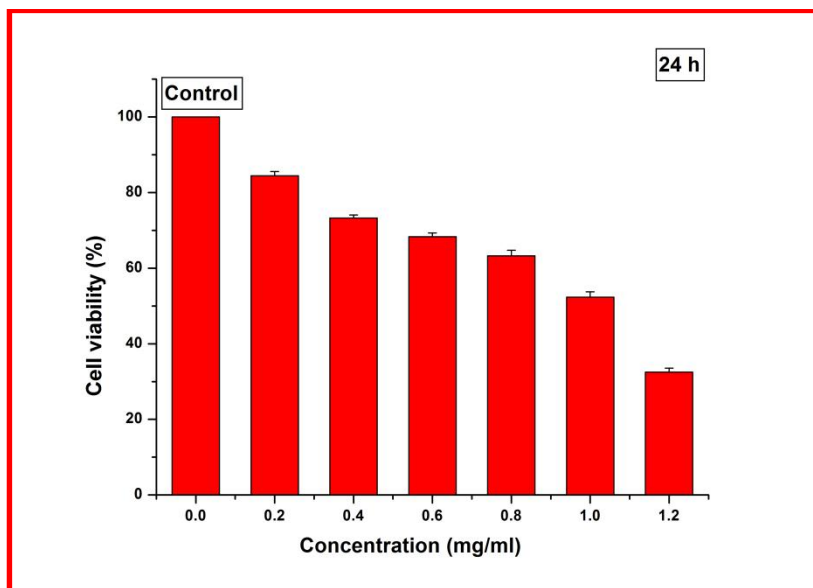


Fig.8.4 (b) Cell viability of PVP functionalized MnFe₂O₄ nanoparticles on MCF7 cell line at different concentrations (0.2, 0.4, 0.6, 0.8, 1.0 and 1.2 mg mL⁻¹)

The cell viability of PVP functionalized MnFe₂O₄ MNPs on L929 cells and MCF cells with concentration 1.2 mg/mL by MTT assay is 83 and 32.48 % for 24 h respectively. It is observed that the nanoparticles are not toxic for L929 and less toxic for MCF cells up to 0.8 mg/ml concentration. Hence, to improve the biocompatibility uncoated MnFe₂O₄ MNPs biocompatible functionalization with PVP is a crucial for *in vivo* applications.

8.4 Mechanisms of nanoparticles cytotoxicity

There are various substances that are known to cause toxicity at their nano size while being relatively inert in their bulk form. However, knowing the types of cell death that may occur can give insight into the affect nanoparticles may have on cells. There are two main types of cell death processes i.e. apoptosis and necrosis.

The cells which are not needed longer perform suicide by triggering an intracellular death program in Apoptosis process. Apoptosis is also called as programmed cell death (PCD). In Apoptosis process, cellular components break down

and condense causing reduction in cell's size. Release of specific proteins within the cell causes the breakdown of cellular components. When the cells break down into small fragment then it is called as apoptotic bodies. These broken fragments are surrounded in membranes so that nearby cells not get harmed. The dying cells then send indication to another type of cells and to these cells are called as phagocytic cells. Without doing any harm to neighbouring cells phagocytic cells demolish the apoptotic bodies.

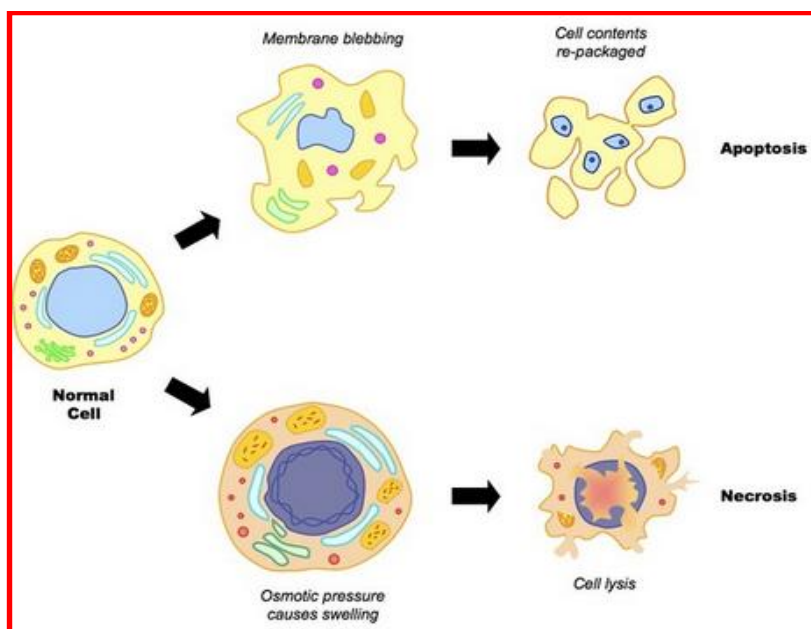


Fig 8.5 Schematic representation of apoptosis and necrosis [21]

The external factors of cell like infection, trauma or toxins could result into uncontrolled digestion of cell causes Necrosis. It is considered as unprogrammed cell death and is less orderly than apoptosis. Special enzymes are released with necrosis by keeping the lysosomes. The injuries received by the cell may begin disorganized chain reaction causing the release in enzymes. The cells which are died due to necrosis can liberate toxic chemicals, which destroy other cells. Necrosis caused by the exposure of living cells to nanoparticles may go through various types of internal or cell organelle damage that attributes to eventual death [20-22].

There are several different mechanisms which can cause cytotoxicity. However, most intracellular and *in vitro* toxicities emerge from creation of excess ROS and disturbance of actin cytoskeleton.

Reactive oxygen species (ROS) formation induced by nanoparticles

Reactive oxygen species (ROS) includes oxygen like peroxides having ability of unwanted reactions with cellular components. DNA can be damaged or apoptosis can be occurred due to high levels of ROS within the cell. Many studies have proved that ROS are responsible for cytotoxicity, which cause death of cell. MNPs can increase reactive oxygen species formation after taking to cells's interior. ROS are considered accountable for cytotoxicity in many studies that investigate the mechanism by which functionalization cause cell death [23].

Cytoskeleton disruption induced by nanoparticles

The cell cytoskeleton can be damaged by nanoparticles after MNPs endocytosis. The cell shape can be retained by active structured cytoskeleton, which allows cellular motion. Eukaryotic cells contain 3 types of cytoskeletal filaments i.e. microfilaments, microtubules and intermediate filaments. Microfilaments can have diameter of approximately 5-8 nm and they are created of 2 tangled actin chains. Microfilaments are mostly focused under the membrane of cell. Microfilaments are important to mechano-transduction in relation with these roles. Microfilaments are essential for cell moment and along with myosin, muscular contraction. The examination of microfilaments changes is very significant in understanding toxicity caused by nanoparticles endocytosis [24-26]. Recently the effects of nanoparticles on cellular morphology as well as cytoskeleton received more attention recently.

8.5 Conclusions

The biocompatibility of MNPs is a significant part in order to use them for biological applications such as drug delivery, MRI, bioseparation, tissue engineering

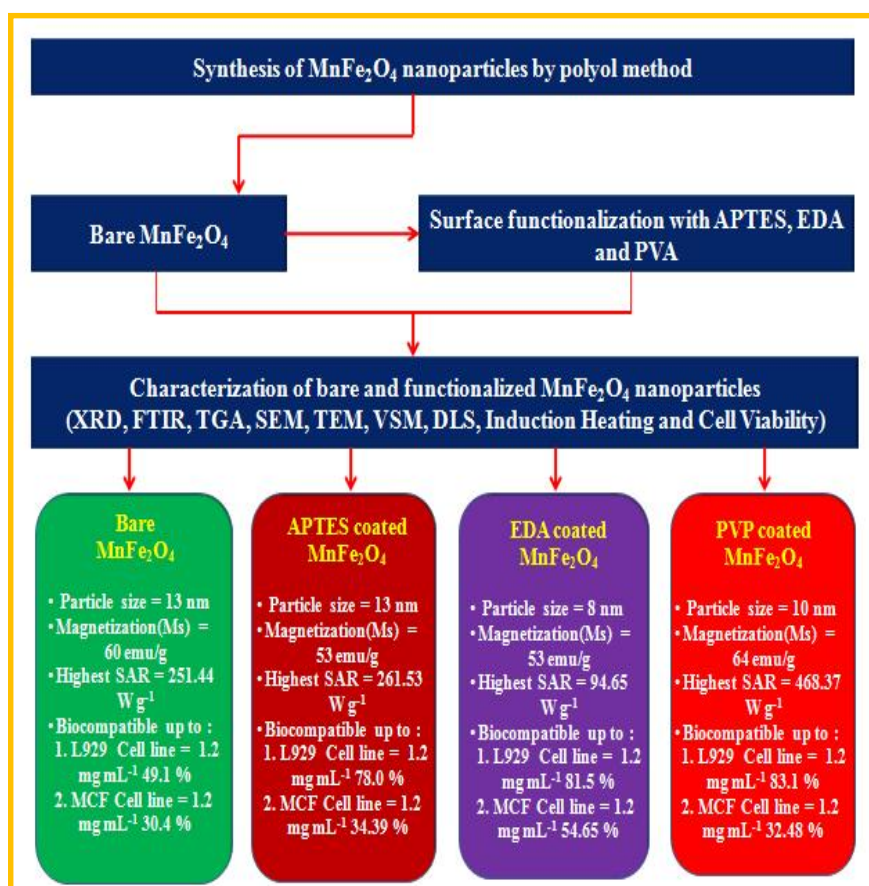
and magnetic hyperthermia. For biomedical applications, MNPs are purposely enhanced to interact with cell and it is essential to certify that this engineering is not causing any inauspicious effect. Toxicity of nanoparticles can be controlled by several factors such as chemical composition, synthesis process, size, shape, crystallinity and surface reactivity. In this chapter, the cell viability study of synthesized MnFe₂O₄, APTES functionalized, EDA functionalized, PVP functionalized MnFe₂O₄ nanoparticles is evaluated by means of simple and cost effective MTT assay on L929 cell line and MCF7 cell line. From the cytotoxicity data of all samples, it is clear that all the samples are non toxic to L929 cell line up to 0.6 mg/ml. For MCF7 cell line, all samples are toxic except PVP functionalized MnFe₂O₄ nanoparticles as it shows non toxicity up to 0.2 mg/ml. It can be concluded that PVP functionalized MnFe₂O₄ nanoparticles are more compatible to both cell line in comparison with bare MnFe₂O₄, APTES and EDA functionalized MnFe₂O₄.

References

1. B. Viswanath and S. Kim, *Rev. Environ. Contam. Toxicol.*, 2016, 242, 61-104.
2. K. Donaldson, V. Stone, C. Tran, W. Kreyling and P. Borm, *Occup. Environ. Med.*, 2004, 61, 727-728.
3. A. Kunzmann, B. Andersson, T. Thurnherr, H. Krug, A. Scheynius and B. Fadeel *Biochim Biophys Acta.*, 2011, 1810, 361-373.
4. M. Mahmoudi, S. Sant, B. Wang, S. Laurent and T. Sen, *Adv. Drug. Deliv. Rev.*, 2011, 63, 24-46.
5. S. Laurent, C. Burtea, C. Thirifays, F. Rezaee and M. Mahmoudi, *J. Colloid Interface Sci.*, 2013, 392, 431-445.
6. D. Richardsa and A. Ivanisevic, *Chem. Soc. Rev.*, 2012, 41, 2052-2060.
7. N. Lewinski, V. Colvin, and R. Drezek, *Small.*, 2008, 4, 26-49.
8. M. Mahmoudi, S. Saeedi-Eslami, M. Shokrgozar, K. Azadmanesh, M. Hassanlou and H. Kalhor, *Nanoscale*, 2012, 4, 5461-5468.
9. B. Díaz, C. Sánchez-Espinel and M. Arruebo, *Small.*, 2008, 4, 2025-2034.
10. B. Kong, J. Seog, L. Graham and S. Lee, *Nanomedicine.*, 2011, 6, 929-941.
11. S. Sharifi, S. Behzadi, S. Laurent, M. Forrest, P. Stroeve and M. Mahmoudi, *Chem. Soc. Rev.*, 2012, 41, 2323-2343.
12. A. Nel, T. Xia, L. Mäder and N. Li, *Science.*, 2006, 311, 622-627.
13. J. West and N. Halas, *Annu. Rev. Biomed. Eng.*, 2003, 5, 285-292.
14. R. Yanes, D. Tarn, A. Hwang, D. Ferris, S. Sherman, C. Thomas, et al., *Small.*, 2013, 9, 697-704.

15. L. Wu, L. Chu, L. Lo, Y. Liao, Y. Wang and C. Yang, *ACS Nano.*, 2012, 7, 365-375.
16. N. Bhattarai, F. Masten and M. Zhang, *Macromol. Biosci.*, 2005, 5, 107-115.
17. P. Chang, M. Kurisawa, J. Chung and Y. Yang, *Biomaterials.*, 2007, 28, 540-549.
18. G. Baldi, D. Bonacchi, M. Franchini, D. Gentili, G. Lorenzi, A. Ricci and C. Ravagli, *Langmuir.*, 2007,23, 4026-4028.
19. N. Thorat, R. Patil, V. Khot, A. Salunkhe, A. Prasad, K. Barick, R. Ningthoujam and S. Pawar, *New J. Chem.*, 2013, 37, 2733-2742.
20. Y. Huang, M. Cambre and H. Lee, *Int. J. Mol. Sci.*, 2017, 18, 2702-2712.
21. J. Fard, S. Jafari and M. Eghbal, *Adv Pharm Bull.*, 2015, 5, 447-454.
22. S. Soenena, P. Rivera-Gil, J. Montenegro, W. Parak, S. De Smedta and K. Braeckmans, *Nano Today*, 2011, 6, 446-465.
23. U. Patil, S. Adireddy, A. Jaiswal, S. Mandava , B. Lee and D. Chrisey, *Int. J. Mol. Sci.*, 2015, 16, 24417-24450.
24. K. Donaldson, V. Stone, P. Borm, L. Jimenez, P. Gilmour, R. Schins, A. Knaapen, I. Rahman, S. Faux, D. Brown and W. MacNee, *Free Radic Biol. Med.*, 2003,34, 1369-1382.
25. S. Soenen, E. Illyes, D. Vercauteren, K. Braeckmans, Z. Majer, S. De Smedt, M. De Cuyper, *Biomaterials*, 2009, 30, 6803-6813.
26. S. Soenen, N. Nuytten, S. De Meyer, S. De Smedt and M. De Cuyper, *Small.*, 2010, 6, 832-842.

Summary and Conclusions



We believe that nanotechnology will have a transformative effect on cancer diagnosis and treatment. In fact, its impact is already visible in the research being conducted through many of the centres we are announcing today. Through the applications of nanotechnology, we will increase the rate of progress towards eliminating the suffering and death due to cancer.

-Jim Thomas

9.1 Introduction

Nanotechnology is at forefront of speedily developing new diagnostic and therapeutic facilities in medicine area mainly in cancer. In 21st century, cancer is one of major disease that is causing millions of deaths and still remains a difficult to treat. Different methods are being expanded to ameliorate the detection and treatment of cancer chemotherapy, radiotherapy, biopsies etc. However, these methods have various side effects. They cause a major harm to normal cell along with affected cancer cell as they are not operated locally. The nano-biotechnology is combination of nanotechnology and biology, which is emerged as research area for researchers. Magnetic nanoparticles give controllable size and capability for engineering exteriorly. Due to this, magnetic nanoparticles used in various biomedical applications like protein purification, drug delivery, hyperthermia therapy and medical imaging.

Magnetic hyperthermia is type of cancer therapy which reduces severe side effects caused to normal tissues in comparison to conventional cancer therapies. In hyperthermia treatment, cells of cancer get destroyed when exposed to 42-45 °C temperature. The cancer affected cells or tissues are usually discovered to be more heat responsive in comparison with healthy cells or tissues. The reason behind this is that tumor tissues are poorly oxygenated while normal tissues are well oxygenated. Heat can be applied locally during hyperthermia treatment so side effects are further reduced. This is major advantage of hyperthermia over other treatments. Heat is dissipated from the magnetic nanoparticles when exposed to exterior magnetic field.

In recent days, research on spinel ferrites has been increased due to their potential in biomedical field. Spinel ferrites are the most widely used and investigated ferrites. The simple ferrites (MFe_2O_4 , $M = Fe, Mn, Co, Zn$, etc), perovskites ($La_{1-x}Sr_xMnO_{3-\delta}$) and mixed ferrites (Co-Zn, Mn-Zn, Ni-Zn, Mg-Cu etc) can be used for magnetic hyperthermia. Among these ferrites, manganese ferrite ($MnFe_2O_4$) has received great attention because of its remarkable properties such as coercivity,

moderate saturation magnetization, superparamagnetism, good chemical stability and mechanical hardness. Characteristics properties of manganese ferrite can be controlled by constitution, morphology and size of nanoparticles. Due to this, MnFe_2O_4 is considered most suitable magnetic material for hyperthermia.

Therefore, efforts have been taken to synthesize APTES, EDA, PVP coated MnFe_2O_4 nanoparticles for hyperthermia in present thesis. The obtained nanoparticles are subjected for biocompatibility and consequently studied their induction heating properties for hyperthermia therapy application.

9.2 Competent components of the thesis

The primary objective of this thesis is to prepare magnetic nanoparticles by using polyol method to apply them for magnetic hyperthermia. Polyol synthesis method was used to prepare bare MnFe_2O_4 nanoparticles and then functionalized with 3-aminopropyltriethoxy silane (APTES) by silanization reaction. The ethylenediamine (EDA) and polyvinylpyrrolidone (PVP) functionalized MnFe_2O_4 nanoparticles were prepared using *in situ* functionalization. The main advantages of polyol synthesis method are that the uniform shape and narrow size distributed nanoparticles can be obtained. Experimental results showed that nanoparticles exhibited superparamagnetism and high magnetization at room temperature. Nanoparticles also showed high temperature rise phenomenon when is exposed to an exterior AC magnetic field.

The MnFe_2O_4 MNPs were synthesized and functionalized with APTES, which were quasi spherical and around 13 nm in size. Functionalized MNPs have shown greater colloidal stability than that of bare MNPs. FTIR and TGA results have shown existence of APTES on the MnFe_2O_4 surface. Induction heating study was performed at 167.6, 251.4 and 335.2 Oe to use these MNPs for hyperthermia therapy applications. The increase in SAR value (261.53 W g^{-1}) and low cytotoxicity made the

APTES functionalized MNPs more suitable for hyperthermia therapy application than the bare nanoparticles.

EDA functionalized MnFe_2O_4 nanoparticles were around 8 nm in size. The structural, magnetic and morphological properties of MnFe_2O_4 nanoparticles have been studied in detail. Magnetic particle hyperthermia (MPH) study was performed for these functionalized nanoparticles at 167.6, 251.4 and 335.2 Oe. The highest SAR value 94.65 W g^{-1} was to be calculated by using 335.2 Oe applied field for EDA functionalized nanoparticles. It has shown lower cytotoxicity than the bare nanoparticles.

PVP functionalized nanoparticles were spherical and about 10 nm in size. The FTIR and TGA results have confirmed the existence of PVP on the surface of MnFe_2O_4 nanoparticles. The induction heating study of prepared material was performed at equivalent to 167.6, 251.4 and 335.2 Oe to use it in hyperthermia applications. The highest SAR value 468.37 W g^{-1} was found at an applied field of 335.2 Oe for PVP functionalized nanoparticles. Increased SAR and lowered cytotoxicity made MNPs more suitable for hyperthermia therapy application. It was seen that the survival rate of cell relies on the nanoparticles concentration in the culture media and coating concentration. Result showed that cell viability of PVP functionalized nanoparticles is 83% for L929 and 32.48 for MCF7 cell line upto concentrations 1.2 mg/mL and it suggests that nanoparticles are less toxic to L929 but toxic to MCF7 cell line.

Hence, the study proved that the bare as well as APTES, EDA and PVP functionalized MnFe_2O_4 nanoparticles have a great potential to be used for hyperthermia therapy application due to high magnetization, SAR values, superparamagnetic behavior, nano size, negligible cytotoxicity and high colloidal stabilities. But in comparison with all materials, PVP functionalized MnFe_2O_4

nanoparticles can be promising material for hyperthermia applications due to high SAR as well as low toxicity.

Magnetic nanoparticles should show below features for successful administration of magnetic hyperthermia.

- Magnetic nanoparticles should produce high temperature rise characteristics in AC magnetic field.
- Magnetic nanoparticles must provide highest (SAR) at lowest particle concentration.
- Magnetic nanoparticles should be biocompatible.

The prepared nanoparticles have shown all above properties so that these nanoparticles can be a potential material for Hyperthermia therapy application.

9.3 Summary of thesis

The presented work is divided into the 9 chapters. Summary of each chapter is mentioned below:

Chapter 1 This chapter explains brief introduction of nanotechnology and nanoparticles. The chapter begins with the concept of nanotechnology. Magnetic nanoparticles are one of sub classes of nanoparticles. The different types of magnetic nanoparticles and synthesis approaches are explained. From various spinel ferrites, MnFe_2O_4 nanoparticles reviewed as most probable contestant which can potentially accomplishes the needs of the cancer diagnosis and therapy. Finally, first chapter ends with the well definition of problem.

Chapter 2 This chapter covers theory of surface functionalization. Surface functionalization allows them to coat with various biomolecules and this makes them astonishing candidate for biomedical applications.

Chapter 3 This chapter includes several characterization techniques of magnetic nanoparticles with their working principle. The characterization of synthesized magnetic nanoparticles is necessary to study the effect of synthesis and usability of nanoparticles for biomedical applications depending on their characteristics.

Chapter 4 This chapter focuses various synthesis methods used for MNPs and preparation MnFe_2O_4 MNPs using polyol method. The synthesized nanoparticles were analysed by using XRD, FTIR, SEM, TEM and VSM for structural, morphological and magnetic analysis.

Chapter 5 This chapter covers the synthesis of monodispersed MnFe_2O_4 nanoparticles and functionalization of MnFe_2O_4 nanoparticles with 3-aminopropyltriethoxy silane (APTES) in order to obtain well-dispersed surface functionalized biocompatible magnetic nanoparticles to use them for hyperthermia therapy application application.

Chapter 6 This chapter includes an induction heating studies of bare MnFe_2O_4 and APTES functionalized MnFe_2O_4 nanoparticles. Induction heating study was performed at 167.6, 251.4 and 335.2 Oe to use these nanoparticles for hyperthermia therapy applications

Chapter 7 This chapter focuses on the synthesis of monodispersed MnFe_2O_4 MNPs in situ functionalization of MnFe_2O_4 nanoparticles with ethylenediamine (EDA) and polyvinylpyrrolidone (PVP). Functionalized nanoparticles were characterized by using XRD, FTIR, SEM, TEM and VSM for structural, morphological and magnetic analysis. Heating ability was studied to assess the feasibility to use them in hyperthermia applications.

Chapter 8 This chapter focuses on the theory of biocompatibility and detailed study of functionalized MnFe_2O_4 nanoparticles. The different parameters influencing the biocompatibility of magnetic nanoparticles are explained in this chapter.

9.4 Major conclusions

- MnFe_2O_4 nanoparticles having uniform size were synthesized by low temperature polyol synthesis method. Silanization reaction is used to modify the surface of NPs with the help of 3-aminopropyltriethoxy silane (APTES).
- Monodispersed EDA and PVP functionalized MnFe_2O_4 nanoparticles were synthesized by using simple one step polyol method.
- Induction heating study was performed at 167.6, 251.4 and 335.2 Oe to use these nanoparticles for hyperthermia therapy applications.
- PVP functionalized MnFe_2O_4 nanoparticles have provided highest SAR value 468.37 W g⁻¹ at an applied field of 335.2 Oe with 5mg mL⁻¹ particle concentration in comparison with APTES and EDA functionalized MnFe_2O_4 nanoparticles.
- The cell viability of PVP functionalized MnFe_2O_4 nanoparticles was above 83% at concentration upto 1.2 mg mL⁻¹ on L929 cell line and at this concentration this material show 32.48% cell viability to MCF7 cell line.
- Study revealed that the PVP coated MnFe_2O_4 nanoparticles are potential material for hyperthermia therapy application.

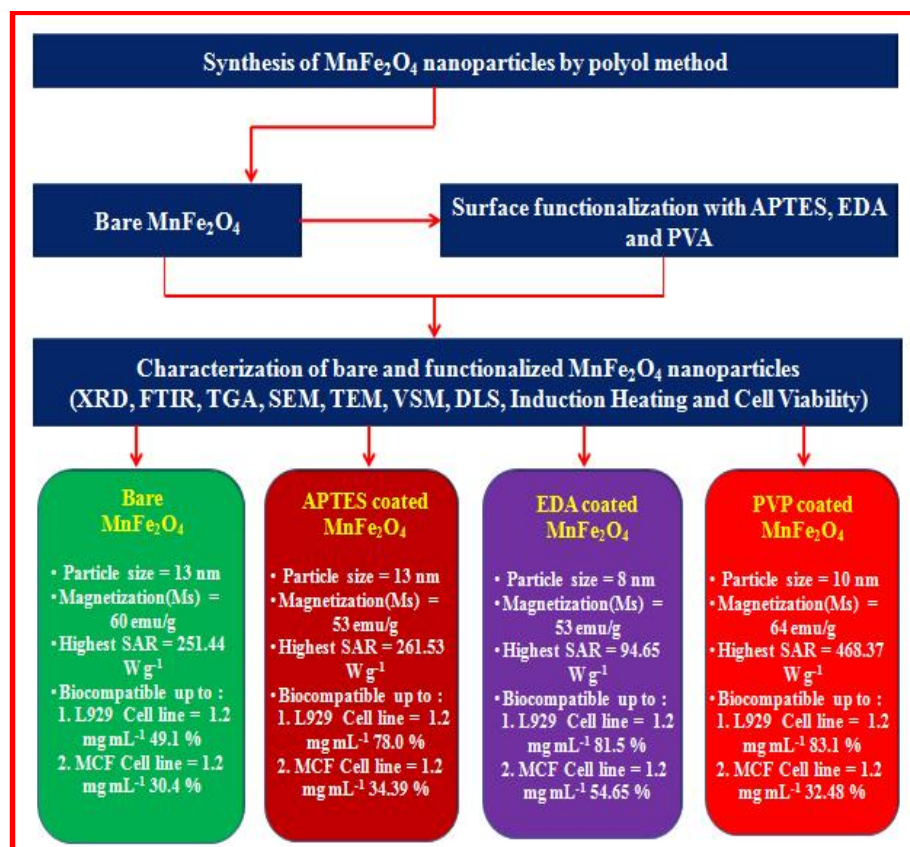


Fig 9.1 Effective formulation of bare, APTES, EDA and PVP functionalized nanoparticles

9.5 Future scope of the thesis

The next important step will be the investigation and assessment biological performance of the nanoparticles for *in vivo* applications. We will focus on evaluation of effect of physical parameters like temperature rise which is responsible for cell death. The higher SAR value can be obtained by rearrangement of magnetocrystalline anisotropy. The functionalized magnetic nanoparticles can be employed for hyperthermia applications subject to biocompatibility studies which is the future scope of present work.

CURRICULUM VITAE

Mrs. Priti Ghutepatil

Research Scholar,
Centre for Interdisciplinary Research,
D. Y. Patil Education Society,
Kolhapur-416 006 (MS), India.



Academic Profile

Ph. D. in Chemistry,

Submitted thesis on May 2019.
Centre for Interdisciplinary Research,
D. Y. Patil Education Society,
Kolhapur-416 006 (MS), India.

Title of thesis:

“Studies on synthesis and characterization of MnFe₂O₄ Nanoparticles & their Hyperthermia Therapy application”

M. Sc. in Organic Chemistry, 2011

First class with distinction
Swami Ramanand Teerth Marathwada University,
Nanded – 431 606 (MS), India.

B. Sc. in Chemistry, 2009

First class with distinction
Solapur University,
Solapur – 413 255 (MS), India.

Professional Experience

1. Worked as an **Assistant Professor** for D. Y. Patil College of Engineering and Technology, kolhapur from **Jan 2012** to **Jan 2014**.
2. Worked as an **Assistant Professor** for Pad. Dr. D.Y.Patil Institute of Engineering, Management & Research, pune from **July 2014** to **Feb 2016**.

Experimental Skills

1. Expertise in synthesis and functionalization of Magnetic Nanoparticles (MNPs).
2. Characterization Instruments handled: X-ray diffractometer, Zeta potential and particle size analyzer, Induction heating instrument for hyperthermia, Vibrating sample magnetometer, Fourier transform infrared spectrometer, Scanning electron microscope, Chromatography (Paper Chromatography, TLC, Column Chromatography, Ion Exchange), UV Spectrophotometer, Colorimetry, Reaction assisted on Microwave, Atomic Absorption Spectrophotometer for soil and water Testing
3. Other known techniques: Transmission electron microscopy (TEM) and High resolution transmission electron microscopy (HRTEM), X-ray photoelectron spectroscopy (XPS), Atomic force microscopy, SQUID analysis etc.

Research Experience

1. Ph.D. Thesis entitled "**Studies on synthesis and characterization of MnFe₂O₄ Nanoparticles & their Hyperthermia Therapy application**" under the supervision of **Prof. Dr. S. H. Pawar**, Center for Interdisciplinary Research, D. Y. Patil Education Society, Kolhapur, India (2012-2019).
2. Successfully completed the project **Microwave Assisted Facile Synthesis of Tetra substituted Imidazoles (2010-2011)**.

List of Publications

1. P. R. Ghutepatil and S. H. Pawar, Structural, Morphological, Magnetic and Self-Heating Studies of One-Step Polyol Synthesized Manganese Ferrite (MnFe_2O_4) Nanoparticles, **International Journal of Nanoscience** (2019).
<https://doi.org/10.1142/S0219581X19500030>
2. P. R. Ghutepatil, A. B. Salunkhe, V. M. Khot and S. H. Pawar, APTES (3-aminopropyltriethoxy silane) functionalized MnFe_2O_4 nanoparticles: a potential material for magnetic fluid hyperthermia, **Chemical papers** (2019).
<https://doi.org/10.1007/s11696-019-00768-z>
3. A. Tiwari, R. Satvekar, S. Rohiwal, V. Karande, A. Raut, P. Ghuteatil, P. Shete, S. Ghosh and S. H. Pawar, Magneto-separation of genomic deoxyribose nucleic acid using pH responsive Fe_3O_4 @silica@chitosan nanoparticles in biological samples, **RSC Advances** (2015).
4. P. R. Ghutepatil, A. B. Salunkhe, V. M. Khot, B. R. Thombare and S. H. Pawar, Surface Functionalization of MnFe_2O_4 Nanoparticles with Ethylenediamine for Hyperthermia Application, **Asian Journal of Chemistry** (2019).
<https://doi.org/10.14233/ajchem.2019.21815>
5. P. R. Ghutepatil and S. H. Pawar, Multisynthesis chemical routes of magnetic nanoparticles for variety of biomedical applications (Review), **Journal of Frontiers and International Research Technology Development** (2018).
6. P. R. Ghutepatil, A. B. Salunkhe, V. M. Khot and S. H. Pawar, Synthesis of monodispersed polyvinylpyrrolidone functionalized biocompatible manganese ferrite nanoparticles for hyperthermia application, **Nano LIFE** (2019) (Submitted).

International and National Conferences/Workshops

1. International Conference on Nanotechnology Addressing the Convergence of Materials Science, Biotechnology and Medical Science **(IC-NACMBM-2017)**.
2. International Conference on Nanomaterials and Nanotechnology **(NANO-2015)**.
3. International Conference on Nannomaterials: Synthesis, Characterization and Applications **(ICN-2018)**.
4. International Conference Empowering Society with Microbial Technology **(2019)**.
5. International Workshop on Ph. D. Program for Medical Innovations **(IWPPMI-2014)**.
6. National Conference on New and Emerging Technologies for Water Resources **(NETWAR-2018)**.
7. National Symposium on Medical Biophysics **(2015)**.
8. National Conference on Emerging Trend in Nanomaterials and Their Applications **(ETNA-2017)**.
9. National Webinar on Nanobiotechnology **(NWN- 2018)**.

Date: 16-05-2019

Place: Kolhapur

Gadil P. R.

Mrs. Priti Ghutepatil